



**UNIVERSITY OF  
BIRMINGHAM**

**QUANTIFYING THE IMPACT OF HEAT AND CLIMATE  
CHANGE ON LONDON UNDERGROUND'S  
INFRASTRUCTURE**

by

**SARAH VICTORIA GREENHAM**

A thesis submitted to the University of Birmingham for the degree of

**DOCTOR OF PHILOSOPHY**

School of Engineering  
College of Engineering and Physical Sciences  
University of Birmingham  
June 2023

UNIVERSITY OF  
BIRMINGHAM

**University of Birmingham Research Archive**

**e-theses repository**

This unpublished thesis/dissertation is copyright of the author and/or third parties. The intellectual property rights of the author or third parties in respect of this work are as defined by The Copyright Designs and Patents Act 1988 or as modified by any successor legislation.

Any use made of information contained in this thesis/dissertation must be in accordance with that legislation and must be properly acknowledged. Further distribution or reproduction in any format is prohibited without the permission of the copyright holder.



# Abstract

Transport for London (TfL) own and operate the world's oldest metro network, the London Underground (LU). As the climate is changing, TfL is faced with operational challenges during periods of extreme weather, particularly regarding heat. TfL has short- and medium-term extreme weather plans in place, but it is uncertain whether these will be sufficient to withstand future climate change on the LU network in the long-term, and the potential degree of preparedness required. The challenges TfL face are further complicated by the complexity of LU's infrastructure and operational legacy, resulting in three different environments (surface, sub-surface tunnels, and deep tube tunnels) with major disparities in station platform temperatures across the network.

The research presented in this thesis quantifies the impact of heat and climate change across the LU network. By critically reviewing current techniques, this study consolidates and develops several methodological approaches through the analysis. Firstly, it addresses the differing thermal environments across the three parts of the LU network. Then, it develops spatially led fault exposure rates for point-related assets, which have known vulnerabilities to temperature. Finally, the fault exposure rates are utilised to help estimate the change in point-related failures according to different climate change projection scenarios for London. A systematic, data-driven approach synthesising weather and climate information with asset faults provides an unbiased view of asset risk to temperature, in a sector that is usually highly dependent on the tacit knowledge of those who operate the network.

The results of this study suggest ways TfL could increase its capacity to deliver a more climate-resilient LU network for the future and provide strategic direction on climate change adaptation, primarily via data and stakeholder engagement. Although the data-driven approach utilised was valuable in identifying potential failure thresholds in the context of future climate change, its limitations highlighted the importance of a collaborative approach to climate resilience and adaptation for the LU network. Moreover, the approach and subsequent findings of this study demonstrated the wider applicability of its methods, with the potential scope to extend analysis to further LU assets and other railway and metro operators.

Keywords: extreme heat, London Underground, climate resilience, climate change adaptation

# Dedication

What started off as a very normal entry and introduction to life as a PhD student in October 2018 took a very unusual turn on 11<sup>th</sup> March 2020, when the COVID-19 outbreak was declared a global pandemic. I was studying abroad at the time, worrying about the implications, as I witnessed everything unfold from a place closer to the epicentre of the outbreak than all my loved ones back home in the UK. The lockdown that followed upon my return home transformed our way of life, as well as the way I worked through my PhD.

I therefore dedicate my thesis to every student who made it through their studies during the pandemic, arguably in the most difficult period of my generation's lives to date. I also dedicate it to those who lost a loved one to COVID-19 and had to navigate the grief in a time with so many rules, barriers, and restrictions in place. Finally, I dedicate my thesis to the memory of my dear Grandfather, who we lost at the height of the pandemic in January 2021.

These last few years have nevertheless demonstrated the tenacity and resolve of humans in the wake of a global crisis. We showed adaptability and resilience. What we have learnt from the COVID-19 pandemic in terms of our human capabilities gives me hope that we can work together to tackle the climate emergency.

# Acknowledgements

This PhD was funded by a scholarship at the University of Birmingham via the Engineering and Physical Sciences Research Council (EPSRC). Further funding was awarded for two research trips to Tokyo under the Japan Society for the Promotion of Science (JSPS) Summer Program in 2019 and the European Union Horizon 2020 Research and Innovation Programme through the Marie Skłodowska-Curie Grant under Agreement 691135.

Firstly, I must acknowledge the unwavering support of my supervisors, Professor Andrew Quinn and Dr Emma Ferranti. I am extremely grateful for their advice and guidance, as well as the knowledge they have imparted to me. It has been a pleasure and I sincerely thank you both.

Thank you to TfL and the stakeholders within who provided significant inputs in data, time, and resources so I could conduct this research. Special thanks to Dr Katherine Drayson, for all the encouragement from start to finish; to Rebecca Powell, for helping and accompanying me in Palestra; and to Charles Snead, without whom, none of this would have materialised.

I am also grateful for the kindness and hospitality of my hosts while studying in Japan. Many thanks to Kato Sensei of the University of Tokyo, and Saito-san of the Railway Technical Research Institute, who warmly welcomed me into their labs for my 5-6 months spent in Tokyo.

Finally, I must thank my loved ones, who have been my biggest advocates through this journey. My family, especially my parents and my brother Mike, I'm sorry for what I've put you through. Charlene, Jenny, Hannah, and Steph, thank you for the coffee stops, dinner dates, weekend trips, and all the other fun times in between. Dr Rachel Fisher, you've done so much to help me as a colleague and friend, and I will always remember it. Darragh – who has been most patient of all – you are my rock and miraculously kept me grounded through all my academic and personal (mis)adventures. Thank you for waiting for me, I'm hoping it was worth it.

# Preface

The following research articles, publications and reports were produced throughout the undertaking of this PhD. The work from these publications is incorporated into this thesis as included material. Co-authors have given permission for these publications to be included in this thesis.

## Peer-reviewed research articles

**Greenham, S.**, Ferranti, E., Quinn, A. 2023. “A review of the industry ‘rule of thumb’ to estimate rail temperature under a changing climate” (in draft).

**Greenham, S.**, Ferranti, E., & Quinn, A. 2023. “Validation of a simple tunnel temperature estimation model on the London Underground network to project the impact of future climate change” (in draft).

**Greenham, S.**, Ferranti, E., Powell, R., Drayson, K., Quinn, A. 2023. “The impact of heat and climate change on London Underground’s infrastructure” (accepted, in press), *Weather*.

**Greenham, S.**, Workman, R., McPherson, K., Ferranti, E., Fisher, R., Mills, S., Street, R., Dora, J., Quinn, A. 2023. “Are transport networks in low-income countries prepared for climate change? Barriers to preparing for climate change in Africa and South Asia” (submitted, in revision). *Mitigation and Adaptation Strategies for Global Change*.

**Greenham, S.**, Ferranti, E.J.S., Quinn, A., & Drayson, K. 2020. “The impact of high temperatures and extreme heat to delays on the London Underground rail network: An empirical study” *Meteorological Applications* **27**(3).

## Policy-focused publications and reports

**Greenham, S.**, Workman, R., Ferranti, E., McPherson, K., Quinn, A., Street, R., Dora, J., Fisher, R., Mills, S., Packham, K., Baxter, W., Roberts, C. 2022. *Climate-Resilient Transport: A policy guide for low-income countries in Africa and South Asia*. Prepared by the University of Birmingham and TRL, UK. May 2022. <https://transport-links.com/download/climate-resilient-transport-a-policy-guide/>

**Greenham, S.**, Ferranti, E., Workman, R., McPherson, K., Quinn, A., Fisher, R., Mills, S., Street, R., Packham, K., Baxter, W., Dora, J., Roberts, C. 2022. *State of Knowledge report: Adaptation for Transport Resilience to Climate Change (AfTR-CC) for LICs in Africa and South Asia*. University of Birmingham, Transport Research Laboratory (TRL), January 2022. <https://transport-links.com/download/state-of-knowledge-report-adaptation-for-transport-resilience-to-climate-change-aftr-cc-for-lics-in-africa-and-south-asia/>

Ferranti, E.J.S., **Greenham, S.V.**, & Wood, R. 2022. *Adaptation Pathways for Infrastructure Operators and Policymakers. A Briefing Note produced for the Tyndall Centre for Climate Change Research*.

**Greenham, S.**, Ferranti, E., Jaroszweski, D., Chapman, L., Quinn, A., Wood, R. 2021. *The implications of net zero ambitions for infrastructure resilience to climate change*. Addressing the Climate Challenge, Forum for Global Challenges, University of Birmingham, September 2021. <https://blog.bham.ac.uk/publicaffairs/wp-content/uploads/sites/89/2021/09/Addressing-the-climate-challenge-comp.pdf>

Ferranti, E.J.S., **Greenham, S.V.**, Dora, J. Pyatt, N., Quinn, A.D., Reeder, T. 2021. *Review of Network Rail's Weather Resilience and Climate Change Adaptation Plans. A report for the Office of Rail and Road*. Climate Sense Ltd and Birmingham Centre for Railway Research & Education (BCRRE), University of Birmingham. March 2021. <https://www.orr.gov.uk/media/22602>

**Greenham, S.V.**, Ferranti, E.J.S, and Wood, R. 2020. *Climate change risks to UK infrastructure by achieving net zero. A Briefing Note for Policymakers*. Prepared for the Climate Change Risk Assessment Steering Group. May 2020.



# Table of contents

Abstract .....	i
Dedication .....	ii
Acknowledgements .....	iii
Preface.....	iv
Table of contents .....	vi
List of figures .....	xv
List of tables.....	xxii
List of definitions .....	xxv
Chapter One   Introduction .....	1
1.1. Background .....	1
1.1.1. The London Underground: a brief history.....	2
1.1.2. Heat on the London Underground.....	6
1.2. Signals of climate change and its impact on observed temperature.....	10
1.2.1. Mean surface temperature change .....	11
1.2.2. Temperature extremes .....	12
1.2.3. Diurnal temperature range .....	14
1.3. Contributing factors to thermal environments across the LU network .....	15
1.3.1. On the surface: the urban heat island effect .....	15
1.3.2. In the tunnels: infrastructure and operations .....	17
1.4. The concept of climate risk .....	19

1.5. Policy context .....	21
1.6. Future climate change .....	23
1.6.1. UK climate projection scenarios .....	24
1.6.2. Adapting to future climate change .....	27
1.7. Research context: A climate-resilient London Underground network .....	28
1.8. Thesis structure .....	29
Chapter Two   Literature review .....	31
2.1. Overview of literature review .....	31
2.2. Impact of heat and climate change on railway infrastructure .....	31
2.2.1. Surface assets .....	32
2.2.2. Tunnel assets .....	36
2.3. Quantifying the extent of climate risk on railway assets .....	37
2.4. Weather and climate risk management on the LU network.....	40
2.4.1. Seasonal planning .....	40
2.4.2. Response to extreme temperature events .....	43
2.5. Measuring operational performance .....	44
2.5.1. Lost customer hours .....	46
2.5.2. Delay minutes .....	47
2.5.3. Average delay length .....	48
2.5.4. Excess journey time .....	49
2.5.5. Delay or fault frequency .....	50

2.5.6. Fragility curves .....	52
2.5.7. Quantifying resilience .....	54
2.6. Temperature thresholds .....	56
2.6.1. LU network thresholds .....	57
2.6.2. Changing thresholds under future climate change .....	57
2.7. Chapter summary and research justification .....	58
Chapter Three   Methodology.....	60
3.1. Chapter overview .....	60
3.2. Data acquisition and parameters.....	61
3.2.1. Key study parameters and boundaries .....	64
3.2.1.1. Network type.....	64
3.2.1.2. LU line .....	65
3.2.1.3. Direction of travel .....	66
3.2.2. Temperature observation data .....	67
3.2.2.1. Surface temperature observations .....	67
3.2.2.2. Spatial extrapolation of surface temperature using the urban heat island index .....	69
3.2.2.3. Tunnel platform temperature observations .....	71
3.2.3. LU asset fault data .....	72
3.2.3.1. Study asset group .....	73
3.2.3.2. Pre-processing and quality assurance .....	75

3.2.4. Climate projections .....	76
3.2.4.1. Climate variables and time slices .....	77
3.2.4.2. Baseline scenario .....	77
3.2.4.3. RCPs and probabilistic scenarios .....	78
3.2.4.4. Projection data sampling .....	79
3.2.4.5. Selected projection data .....	80
3.3. Analysis of thermal environment.....	82
3.3.1. Descriptive statistics .....	82
3.3.1.1. Key temperature variables .....	83
3.3.1.2. Climate thresholds .....	83
3.3.2. Tunnel temperature estimation model.....	84
3.3.2.1. The model .....	85
3.3.2.2. Applying the model .....	87
3.3.2.3. Model validation.....	89
3.4. Fault exposure rate analysis .....	90
3.4.1. Calculating the fault exposure rate.....	90
3.4.2. Identifying trends in the fault exposure rates .....	91
3.4.3. Determining temperature thresholds .....	91
3.5. Analysis of climate projections.....	92
3.5.1. Projected change in thermal environment.....	92
3.5.1.1. Future surface temperatures.....	93

3.5.1.2. Future sub-surface and deep tube tunnel temperatures .....	94
3.5.2. Calculating change in work orders under future climate change scenarios .....	94
3.6. Chapter summary .....	95
Chapter Four   Thermal environment .....	96
4.1. Chapter overview .....	96
4.2. Descriptive statistics.....	96
4.2.1. Temperature variables .....	97
4.2.1.1. Distribution of surface temperature variables .....	99
4.2.1.2. Distribution of sub-surface temperature variables .....	101
4.2.1.3. Distribution of deep tube tunnel temperature variables .....	103
4.2.2. Climate thresholds .....	105
4.3. Estimating tunnel temperatures .....	106
4.3.1.1. Mean daily temperature ( $t_{mean}$ ) .....	107
4.3.1.2. Maximum daily temperature ( $t_{max}$ ) .....	115
4.3.1.3. Minimum daily temperature ( $t_{min}$ ).....	118
4.3.1.4. Diurnal temperature range ( $\Delta t$ ).....	120
4.4. Chapter summary .....	121
Chapter Five   Fault exposure rates .....	124
5.1. Chapter overview .....	124
5.2. Work orders .....	124
5.2.1. Work order data overview .....	125

5.2.2. Temperature variables.....	127
5.3. Fault exposure rates: surface.....	128
5.3.1. Daily mean temperature ( $t_{mean}$ ).....	128
5.3.2. Daily maximum temperature ( $t_{max}$ ).....	134
5.3.3. Daily minimum temperature ( $t_{min}$ ).....	141
5.3.4. Diurnal temperature range ( $\Delta t$ ).....	143
5.4. Fault exposure rates: sub-surface.....	145
5.4.1. Daily mean temperature ( $t_{mean}$ ).....	145
5.4.2. Daily maximum temperature ( $t_{max}$ ).....	149
5.4.3. Daily minimum temperature ( $t_{min}$ ).....	153
5.4.4. Diurnal temperature range ( $\Delta t$ ).....	156
5.5. Fault exposure rates: deep tube tunnels.....	158
5.5.1. Daily mean temperature ( $t_{mean}$ ).....	160
5.5.2. Daily maximum temperature ( $t_{max}$ ).....	162
5.5.3. Daily minimum temperature ( $t_{min}$ ).....	167
5.5.4. Diurnal temperature range ( $\Delta t$ ).....	170
5.6. Chapter summary.....	172
Chapter Six   Future climate change.....	174
6.1. Chapter overview.....	174
6.2. Change in thermal environment across the LU network.....	174
6.2.1. Change in surface temperature.....	175

6.2.2. Change in sub-surface temperature .....	179
6.2.3. Change in tunnel temperature.....	181
6.3. Change in work orders across the LU network .....	184
6.3.1. Change in surface work orders .....	186
6.3.2. Change in sub-surface work orders .....	188
6.3.3. Change in deep tube tunnel work orders .....	189
6.3.4. Total change in work orders across the LU network.....	190
6.4. Chapter summary .....	191
Chapter Seven   Discussion.....	194
7.1. Chapter overview .....	194
7.2. Discussion of results chapters .....	194
7.2.1. Thermal environment .....	195
7.2.1.1. Temperature variables.....	195
7.2.1.2. Climate thresholds.....	196
7.2.1.3. Tunnel temperature estimation model.....	199
7.2.2. Fault exposure rates .....	200
7.2.2.1. Fault thresholds .....	201
7.2.2.2. Failure harvesting.....	206
7.2.3. Future climate change.....	207
7.2.3.1. Change in thermal environment.....	207
7.2.3.2. Change in future work orders.....	209

7.3. Increasing TfL’s capacity to adapt to heat and climate change across the LU network	210
7.3.1. Data	210
7.3.1.1. Weather observations	211
7.3.1.2. LU platform temperature observations	211
7.3.1.3. Weather forecasts	212
7.3.1.4. Fault data	213
7.3.1.5. Climate data	216
7.3.2. Stakeholder engagement	218
7.3.2.1. Internal stakeholder engagement	219
7.3.2.2. External stakeholder engagement	219
7.3.3. The adaptation direction	221
7.4. Critique of methodology and further development	225
7.4.1. Joining temperature and work order data	225
7.4.2. Prediction capabilities	226
7.4.3. Considerations in interpreting results	227
7.5. Looking ahead towards more climate-resilient transport networks	228
7.5.1. Mapping climate risk	229
7.5.2. Linking fault exposure rates with delay data	230
7.5.3. Progressing the analysis of extreme weather events	231
7.5.4. The international perspective	232



7.6. Next steps for TfL in delivering more climate-resilient transport.....	232
7.7. Chapter summary .....	233
Chapter Eight   Conclusion.....	235
8.1. Conclusion overview.....	235
8.2. Achievement of aims and objectives.....	235
8.2.1. Justifying a data-driven approach.....	235
8.2.2. Demonstrating the spatial variability of temperature across metro networks .....	236
8.2.3. Quantification of the effect of temperature on infrastructure.....	236
8.2.4. Quantification of the effect of future climate change on infrastructure .....	237
8.2.5. Future research development and direction.....	237
8.2.6. Practical application of the research and implications .....	238
8.3. Concluding remarks .....	239
References.....	240
Appendices.....	256

# List of figures

Figure 1.1 The LU network in the context of the Greater London administrative boundary.....	5
Figure 1.2 The central part of the LU network, showing examples of parallel/shared track sections across the LU lines.....	5
Figure 1.3 Passenger ridership on the LU network <i>per</i> 4-weekly reporting period from April 2010 to October 2022. The steep drop in ridership represents the impact of the coronavirus pandemic, which has since begun to recover (Data: TfL, 2022g).....	6
Figure 1.4 The location of London Clay bedrock across London and in the context of the LU network (Data: BGS, 2020).....	8
Figure 1.5 Advertisements for travelling on the LU network in the summer months (left) and the winter months (right), from almost a century ago. LU tunnel temperatures were lower than the present day and considered more comfortable for travel compared to surface temperatures, emphasised here as a key selling point (Source: Herrick, 1926, 1927).....	9
Figure 1.6 Trends in global atmospheric CO <sub>2</sub> since 1958, showing the continued increase in concentration. The red line shows the monthly global mean concentration, and the black line shows the monthly mean concentration after correction for the average seasonal cycle (Source: NOAA, 2022) .....	11
Figure 1.7 Timeline of high temperature events reported in the UK during the summer, 1990-2022. Each bar represents one high temperature event. The dark points differentiate high temperature events that occurred close together, as some of the bars overlap in the timeline. (Data: Met Office, 2022c) .....	13
Figure 1.8 Timeline of low temperature events (including frost and snow) reported in the UK, 1990-2022. Each bar represents one low temperature event. The dark points differentiate low temperature events that occurred close together, as some of the bars overlap in the timeline. (Data: Met Office, 2022c) .....	14
Figure 1.9 UHI intensity for the Greater London Area for an example summer, with altitude-corrected midnight temperatures according to the UrbClim model (Lauwaet <i>et al.</i> , 2015) (Source: VITO, n.d.).....	16
Figure 1.10 Modelled peak time heat source distribution in the LU tunnels for 2013 on the Central Line (Data: Mortada <i>et al.</i> , 2015) .....	18

Figure 1.11 Risk Propeller conceptualising the interactions among the determinants of risk. It illustrates that risk comprises the magnitude of hazard, vulnerability, and exposure (Source: IPCC, 2022) ..... 19

Figure 1.12 UKCP18 mean temperature change trajectories for the lowest (RCP 2.6, blue) and highest (RCP 8.5, red) future emissions scenarios, up to 2100. The shaded areas outside the lines represent different percentile values of the scenario, with the solid line representing the median (50<sup>th</sup> percentile). Past temperature observations are shown in the solid black line (Source: Lowe *et al.*, 2019)..... 25

Figure 2.1 Examples of the relationships between temperature hazards, the impacts on railway assets, and direct/indirect consequences for the railway network. It shows how the environmental condition can impact an asset, that can lead to operational consequences for the railway network owner or operator (Adapted from: Palin *et al.*, 2021)..... 33

Figure 2.2 A buckled rail due to thermal expansion (Source: Skarova *et al.*, 2022) ..... 34

Figure 2.3 Schematic of a switch, where track in one direction converges with another. A set of points is shown in orange, showing how the asset is connected to track (Source: RailSystem, n.d.) ..... 35

Figure 2.4 Total annual Schedule 8 compensation payments attributed to weather across Network Rail’s infrastructure. Note that these costs are not inflation adjusted but include an increase in the cost of a delay minute from around 2015 (Network Rail, 2021b) ..... 38

Figure 2.5 Total number of risks *per* climate hazard across TfL’s infrastructure, as identified by TfL based on best available professional judgement (Source: TfL, 2021b) ..... 39

Figure 2.6 Key defined weather thresholds across the LU network according to the Hot Weather Plan and Winter Weather Contingency Plan (Adapted from: TfL, 2022f, 2022e) ..... 57

Figure 3.1 Linkages between stages of methodology for this study. Key results are emphasised in bold. .... 60

Figure 3.2 Division of LU network by network type..... 65

Figure 3.3 Axonometric drawing of Manor House station, Piccadilly line, showing the deep tube tunnels separated by direction of travel (Source: TfL, 2017a)..... 66

Figure 3.4 Met Office weather stations within the Greater London administrative boundary 68

Figure 3.5 The UrbClim UHI index for London used in this study, in the context of the LU network and all stations..... 70

Figure 3.6 Temperature observation accuracy of the Tinytag loggers used across the LU tunnel station platforms (Source: Tinytag, 2019).....	72
Figure 3.7 Hierarchy structure of point and train stop asset groups by asset management system analysed in this study.....	74
Figure 3.8 Estimated mean global surface temperature change according to each emissions scenario. RCP 8.5 is in red and RCP 6.0 is in orange, showing the divergence in temperature change between the scenarios during the 21 <sup>st</sup> Century (Source: IPCC, 2013).....	79
Figure 3.9 Distribution of climate projection data of temperature anomalies for minimum monthly temperature (top), mean monthly temperature (middle), and maximum monthly temperature (bottom) for RCPs 6.0 (left) and 8.5 (right) (Data: Met Office, 2018c).....	81
Figure 3.10 Parameters of the tunnel temperature estimation model equation (Adapted from: Kimura <i>et al.</i> , 2018).....	87
Figure 3.11 Examples of the differences in cross correlation trends by platform. A typical cross correlation for this study is on the left, whereas an anomalous cross correlation is on the right. The red arrow indicates the value of $t_d$ with the highest cross correlation coefficient reported by the code script used for this analysis, whereas the green arrow indicates the peak closest to $t_d = 0$ ; the value selected for this platform upon further investigation.....	88
Figure 3.12 Scatterplot of sample data (Covent Garden station, Piccadilly line, westbound platform, 2015-2016) showing how to identify $a$ and $b$ values of the tunnel model.....	89
Figure 4.1 7-day rolling average of $t_{mean}$ observations for each network type of the LU network .....	97
Figure 4.2 7-day rolling average of $t_{min}$ observations for each network type of the LU network .....	98
Figure 4.3 7-day rolling average of $t_{max}$ observations for each network type of the LU network .....	98
Figure 4.4 7-day rolling average of $\Delta t$ observations for each network type of the LU network .....	99
Figure 4.5 Distribution of surface temperature by daily temperature variable based on the observations at St. James’s Park weather station for the study period.....	100
Figure 4.6 Distribution of $\Delta t$ outliers throughout the year.....	101

Figure 4.7 Distribution of sub-surface temperature by temperature variable based all sub-surface station platform observations for the study period. Plots from left to right for each variable: EB, WB, IR, OR.....	102
Figure 4.8 Paddington sub-surface station platform for the District and Circle lines (Source: McKenna, 2005) CC BY-SA 4.0 .....	103
Figure 4.9 Distribution of tunnel temperature by $t_{min}$ (a), $t_{mean}$ (b), $t_{max}$ (c) and $\Delta t$ (d) based all tunnel station platform observations for the study period. The left plot of each LU line is the NB/EB tunnel, and the right plot is the SB/WB tunnel .....	104
Figure 4.10 Mean value of $t_{mean} t_d$ per LU station platform for the study period, grouped by LU line and direction of travel. Error bars indicate one standard deviation.....	108
Figure 4.11 Locations of instances across the LU tunnel network where $t_{mean} t_d \geq 5$ days in one or both directions of travel .....	108
Figure 4.12 Axonometric drawings of Hampstead station (left) and Belsize Park station (right) (Source: TfL, 2017a).....	109
Figure 4.13 Mean value of $t_{mean} a$ per LU station platform for the study period, grouped by LU line and direction of travel. Error bars indicate one standard deviation.....	110
Figure 4.14 Mean value of $t_{mean} b$ per LU station platform for the study period, grouped by LU tunnel. Error bars indicate one standard deviation .....	110
Figure 4.15 Regression residual density plots of $t_{mean}$ per LU sub-surface direction of travel .....	113
Figure 4.16 Regression residual density plots of $t_{mean}$ per LU deep tube tunnel .....	114
Figure 4.17 Mean value of $t_{max} t_d$ per LU station platform for the study period, grouped by LU tunnel. Error bars indicate one standard deviation .....	115
Figure 4.18 Mean value of $t_{max} a$ per LU station platform for the study period, grouped by LU tunnel. Error bars indicate one standard deviation.....	116
Figure 4.19 Mean value of $t_{max} b$ per LU station platform for the study period, grouped by LU tunnel. Error bars indicate one standard deviation.....	116
Figure 4.20 Mean value of $t_{min} t_d$ per LU station platform for the study period, grouped by LU tunnel. Error bars indicate one standard deviation.....	119
Figure 4.21 Mean value of $t_{min} a$ per LU station platform for the study period, grouped by LU tunnel. Error bars indicate one standard deviation.....	119

Figure 4.22 Mean value of $t_{min}$ <i>b per</i> LU station platform for the study period, grouped by LU tunnel. Error bars indicate one standard deviation .....	119
Figure 5.1 Type of WOs raised in the study period.....	125
Figure 5.2 Status of WOs raised upon closure .....	126
Figure 5.3 Relative proportion of days and WOs occurring during days that exceeded each climate threshold .....	127
Figure 5.4 Fault exposure rates of $t_{mean}$ <i>per</i> LU line for the surface part of the LU network .....	130
Figure 5.5 Difference in fault exposure rate trends of surface $t_{mean}$ for all lines by WO type .....	131
Figure 5.6 Daily count of surface corrective and reactive WOs in the days before and after the hottest two days of the study period. Days that fall into the hot day climate threshold are highlighted in yellow. The dotted line denotes the hottest day of that time interval, 01/07/2015 (left) and 26/07/2018 (right).....	133
Figure 5.7 Fault exposure rates of $t_{max}$ <i>per</i> LU line for the surface part of the LU network	135
Figure 5.8 WOs raised on 28/02/2018 across the surface part of the LU network .....	136
Figure 5.9 Mean percentage of climate threshold days <i>per</i> year that occurred before the annual peak surface $t_{max}$ was reported for the whole study period. Error bars denote one standard deviation .....	139
Figure 5.10 Fault exposure rates for all surface $t_{max}$ , grouped by WO type; pre- and post-annual peak surface $t_{max}$ .....	140
Figure 5.11 Fault exposure rates of $t_{min}$ <i>per</i> LU line for the surface part of the LU network .....	142
Figure 5.12 Fault exposure rates of $\Delta t$ <i>per</i> LU line for the surface part of the LU network .	144
Figure 5.13 Fault exposure rates of $t_{mean}$ <i>per</i> LU line for the sub-surface part of the LU network.....	146
Figure 5.14 Difference in fault exposure rate trends of sub-surface $t_{mean}$ for all lines by WO type .....	148
Figure 5.15 Fault exposure rates of $t_{max}$ <i>per</i> LU line for the sub-surface part of the LU network .....	150

Figure 5.16 Fault exposure rates for all sub-surface $t_{max}$ , grouped by WO type; pre- and post-annual peak surface $t_{max}$ .....	151
Figure 5.17 Total fault exposure rates for sub-surface $t_{max}$ by station, which is the sum of all fault exposure rates <i>per</i> $t_{max}$ temperature bin and therefore combines rates for high and low temperature observations but does not differentiate between them .....	152
Figure 5.18 Fault exposure rates of $t_{min}$ <i>per</i> LU line for the sub-surface part of the LU network .....	154
Figure 5.19 Differences in sub-surface fault exposure rates by station for $t_{min}$ , $t_{mean}$ and $t_{max}$ .....	155
Figure 5.20 Fault exposure rates of $\Delta t$ <i>per</i> LU line for the sub-surface part of the LU network .....	157
Figure 5.21 Mean monthly corrective and reactive WOs raised in the tunnel section for the entire study period. Error bars indicate one standard deviation of the mean. Note differing y-axis scales.....	159
Figure 5.22 Fault exposure rates of $t_{mean}$ <i>per</i> LU line for the tunnel part of the LU network .....	161
Figure 5.23 Fault exposure rates of $t_{max}$ <i>per</i> LU line for the tunnel part of the LU network	163
Figure 5.24 Total fault exposure rates for tunnel $t_{max}$ by station, which is the sum of all fault exposure rates <i>per</i> $t_{max}$ temperature bin and therefore combines rates for high and low temperature observations but does not differentiate between them.....	165
Figure 5.25 Fault exposure rates for all tunnel $t_{max}$ , grouped by WO type; pre- and post- annual peak surface $t_{max}$ .....	167
Figure 5.26 Fault exposure rates of $t_{min}$ <i>per</i> LU line for the tunnel part of the LU network	168
Figure 5.27 Fault exposure rates of $\Delta t$ <i>per</i> LU line for the tunnel part of the LU network...	171
Figure 6.1 Box plot showing the spatial distribution of UHI index by surface stations across the LU network .....	176
Figure 6.2 Estimated annual distributions of surface $t_{max}$ for observed and future climate scenarios.....	178
Figure 6.3 Estimated mean annual distribution of days <i>per</i> month exceeding the summer day climate threshold (top) and hot day climate threshold (bottom).....	179

Figure 6.4 Distribution of past and projected monthly sub-surface $t_{max}$ across each direction of travel, as calculated using station level data with the tunnel temperature estimation model .....	180
Figure 6.5 Estimated annual exposure frequency distributions of daily sub-surface $t_{max}$ for observed and future climate scenarios.....	181
Figure 6.6 Distribution of past and projected monthly tunnel $t_{max}$ across each LU tunnel, as calculated using station platform data with the tunnel temperature estimation model .....	183
Figure 6.7 Estimated annual exposure frequency distributions of daily tunnel $t_{max}$ for observed and future climate scenarios .....	184
Figure 6.8 Estimated annual surface WOs for observed (2006-2018) $t_{max}$ compared with the four selected 90 <sup>th</sup> percentile climate projection scenarios.....	187
Figure 6.9 Estimated annual surface WOs, including WO estimates for upper $t_{max}$ values outside of observations .....	187
Figure 6.10 Estimated annual sub-surface WOs for observed (2006-2018) $t_{max}$ compared with the four selected 90 <sup>th</sup> percentile climate projection scenarios .....	188
Figure 6.11 Estimated annual sub-surface WOs, including WO estimates for upper $t_{max}$ values outside of observations .....	189
Figure 6.12 Estimated annual sub-surface WOs for observed (2006-2018) $t_{max}$ compared with the four selected 90 <sup>th</sup> percentile climate projection scenarios .....	190
Figure 6.13 Estimated annual tunnel WOs, including WO estimates for upper $t_{max}$ values outside of observations .....	190
Figure 6.14. Total estimated annual WOs by network type for observed and estimated climate projection scenarios .....	191
Figure 7.1. Some examples of external stakeholders relevant to TfL from a climate change adaptation perspective .....	221
Figure 7.2. A conceptual diagram of potential adaptation outcomes over time (Source: Schipper, 2020).....	223



# List of tables

Table 1.1 Key data on each LU line (Data: TfL, 2021a) .....	4
Table 1.2 Centennial averages for the CET series (°C), 1659-2021 (Data: Kendon <i>et al.</i> , 2022) .....	12
Table 1.3 Examples of cross-risk connections, emphasising the complexity of risk and how one risk or determinant of risk can be linked to another (Adapted from: Pescaroli and Alexander, 2018) .....	20
Table 1.4 Current priority climate risk areas for the UK according to the 2022 CCRA (Source: HM Government, 2022; CCC, 2021a) .....	22
Table 1.5 Summary of each AR5 future emissions scenario, with each scenarios' likely range of estimated mean global surface temperature increase for 2081-2100 relative to 1850-1900 (Data: IPCC, 2013) .....	24
Table 1.6 Estimated present and future return periods of high maximum daily temperatures in the UK, showing how future return periods are expected to reduce substantially, especially the occurrence of a maximum daily temperature of 40°C even in the medium-low scenario of RCP 4.5 (Data: Christidis <i>et al.</i> , 2020).....	26
Table 2.1 Key summer season maintenance responsibilities for each asset team across the LU network (Source: TfL, 2022b) .....	41
Table 2.2 Key winter season maintenance responsibilities for each asset team across the LU network (Source: TfL, 2022b) .....	42
Table 2.3 Train frequency statistics in peak morning time across the LU network (Data: TfL, 2021c).....	45
Table 2.4 Definition of key terminology used to describe operational status across the LU network (Source: TfL, 2022j) .....	46
Table 2.5 Key findings from studies that analyse weather and delay minutes across GB's railway network.....	48
Table 3.1 Details of data used for this study .....	62
Table 3.2 Travel direction of LU lines referred to in this study .....	67
Table 3.3 Asset management system used for each LU line at TfL within the study period ..	73

Table 3.4 Additional information added to Ellipse and Maximo equipment data to conduct the analysis of this study .....	75
Table 3.5 Descriptions of the available UKCP18 climate projection products for temperature variables (Source: Met Office, 2019d) .....	77
Table 3.6 Key climate thresholds for temperature used in this study.....	84
Table 4.1 Key values of the box plot distributions in Figure 4.5 .....	100
Table 4.2 Key values of the box plot distributions in Figure 4.7 .....	102
Table 4.3 Key values of the box plot distributions in Figure 4.9. LU line the station platform belongs to is provided as an initial in parentheses.....	105
Table 4.4 Number of annual days <i>per</i> climate threshold for the study period. The orange cells indicate years higher than the average (mean) number of annual days exceeding each threshold, and the blue cells indicate years lower than the average (mean) number of days. Those in the darker shading are the years with the highest and lowest number of days <i>per</i> climate threshold. ....	106
Table 4.5 Regression results from comparing $t_{mean}$ from the tunnel temperature estimation model outputs with observed $t_{mean}$ for the study period.....	111
Table 4.6 Regression results from comparing $t_{max}$ from the tunnel temperature estimation model outputs with observed $t_{max}$ for the study period.....	117
Table 4.7 Regression results from comparing $t_{min}$ from the tunnel temperature estimation model outputs with observed $t_{max}$ for the study period.....	120
Table 4.8 Regression results from comparing $\Delta t$ from the tunnel temperature estimation model outputs with observed $\Delta t$ for the study period .....	121
Table 5.1 WOs raised on the Central line corresponding with the highest fault exposure rate on 28/02/2018.....	129
Table 5.2 WOs raised on the Central line corresponding with the $t_{mean}$ exposure rate of 26-27°C .....	132
Table 5.3 WOs raised near Edgware Road station on the H&C lines corresponding with a $t_{mean}$ fault exposure rate of 27-28°C .....	147
Table 5.4. Reactive WOs raised on the Victoria line corresponding with the highest fault exposure rates, exceeding one standard deviation.....	164

Table 6.1 1981-2010 baseline monthly descriptive statistics for the Greater London administrative region (Source: Met Office, 2018) .....	175
Table 6.2. Absolute and anomaly projected monthly $t_{max}$ for the Greater London administrative region under each RCP scenario, 90 <sup>th</sup> percentile. Values were calculated from the monthly 1981-2010 baseline values from Table 6.1 .....	177
Table 6.3 Average annual share of each climate scenario reporting temperatures outside of the observed $t_{max}$ exposure frequency range .....	185
Table 6.4 Average annual share of each climate scenario reporting lower bound temperature intervals $\geq 0.001$ .....	186
Table 7.1 Upper and lower fault thresholds of $t_{min}$ and $t_{max}$ per LU line and network type for point-related assets, derived from the fault rate analysis chapter. Fault thresholds are based on the first instance the temperature variable exceeded one standard deviation of the mean fault exposure rate at the higher and lower temperature ranges. A dash (-) indicates that no fault threshold was exceeded across the results, while N/A indicates that the respective LU line does not run through the network type, so there are no results to show. ....	203
Table 7.2. Estimated frequency of days exceeding key $t_{max}$ asset failure thresholds for Network Rail in London, compared with a 1961-1990 baseline (Source: Network Rail, 2020).....	216

## List of definitions

Term	Definition
°C	degrees Celsius
$\Delta t$	diurnal temperature range
$a$	temperature uplift
AMIS	Asset Management Information System
AR5	IPCC's Fifth Assessment Reports
AR6	IPCC's Sixth Assessment Reports
ARP3	Adaptation Reporting Power, third round
ARP	Adaptation Reporting Power
$b_0$	slope coefficient
$b_1$	intercept coefficient
$b$	scaling coefficient
CCC	Climate Change Committee
CCRA	Climate Change Risk Assessment
CEDA	Centre for Environmental Data Analysis
CET	Central England Temperature
CH <sub>4</sub>	methane
CMIP5	Coupled Model Inter-comparison Project Phase 5
CO <sub>2</sub>	carbon dioxide
DC	direct current
$df$	degrees of freedom
EB	eastbound
FTR	failed to reverse
GB	Great Britain
GHG	greenhouse gas
GLA	Greater London Authority
H&C	Hammersmith & City
HadGEM3-GC3.05	Met Office Hadley Centre global climate model
ICT	information communication technology
IPCC	Intergovernmental Panel on Climate Change
IR	inner ring; anticlockwise
KLM	type of safety fastener/retaining clip used on point assets
km	kilometres
LCH	lost customer hours
LCS	location coding system

Term	Definition
LU	London Underground
m	metre
MIDAS	Met Office Integrated Data Archive System
NB	northbound
OR	outer ring; clockwise
ppm	parts <i>per</i> million
$R^2$	coefficient of determination
RCP	Representative Concentration Pathway
<i>RSD</i>	relative standard deviation
<i>RSE</i>	residual standard error
RSSB	Rail Safety and Standards Board
SB	southbound
<i>SD</i>	standard deviation
<i>SE</i>	standard error
SES	subway environment simulation
SFT	stress-free temperature
SoGR	State of Good Repair
SRC ID	source identification code (for UK Met Office weather stations)
$t_d$	time lag delay
TfL	Transport for London
$t_{max}$	daily maximum temperature
$t_{mean}$	daily mean temperature
$t_{min}$	daily minimum temperature
TRaCCA	Tomorrow's Railway and Climate Change Adaptation
UHI	urban heat island
UITP	International Association of Public Transport
UK	United Kingdom
UKCP18	UK's climate projections, released in 2018
UNFCCC	United Nations Framework Convention on Climate Change
W&C	Waterloo & City
WB	westbound
$Wm^{-2}$	watts <i>per</i> square metre
WMO	World Meteorological Organisation
WO	work order
WRCCA	Weather Resilience and Climate Change Adaptation
WSDI	Warm spell duration index

# Chapter One | Introduction

## 1.1. Background

Access to and the operation of transport infrastructure, such as the London Underground (LU) network, is a necessity of modern life. The movement of people and goods is intrinsically connected with economic prosperity, and transport networks are a lifeline for many individuals and communities. Provision of equitable access for all to quality, reliable, sustainable, and resilient infrastructure is within target 9.1 of the United Nations' 17 Sustainable Development Goals (UN-DESA, 2021).

Climate change threatens to disrupt the operation of transport networks, and when they fail to operate, it can lead to severe consequences. Change is already happening; manifested through gradual changes in mean climate indicators such as temperature and precipitation, as well as through changes in frequency and/or intensity of extreme weather events such as heatwaves, pluvial floods, and drought (IPCC, 2021). Extreme weather events have the capacity to grind a transport network to a halt in different ways, and damage to a single asset within a transport node can cut off services to a large proportion of a population who depend on it.

An example of climate-driven disruption to a transport network was the coastal railway line damage at Dawlish, England in February 2014. The sea wall beneath the railway collapsed following a very strong winter storm season, with an empirical relationship to sea level rise (Dawson *et al.*, 2016). Train services were suspended for 52 days (Network Rail, 2014), affecting the whole region that relies on that railway line. Dawson *et al.*, (2016) highlighted that such events are likely to continue happening to varying extents in all future sea level scenarios

and any policy response may still necessitate cost increases. Therefore, transport operators must be aware of, and prepare accordingly for, the impact of future climate change on their network.

Temperature hazards on the LU network are a well-known and very specific challenge that TfL is responsible for managing, which is introduced in Section 1.1.1 and 1.1.2. This study therefore explicitly focuses on temperature, with the term “climate change” throughout referring to the ways in which temperature variables may change, either in terms of their gradual change or the change in the characteristics of extreme temperatures, as introduced in Section 1.2.

### **1.1.1. The London Underground: a brief history**

The LU network is the oldest underground railway (also known as a metro system) in the world and is currently owned and operated by Transport for London (TfL). The first underground railway opened between Paddington and Farringdon on 9 January 1863. Construction of other underground railway lines followed quickly through private developments. The earliest lines comprised a cut-and-cover construction method to build tunnels running directly beneath the roads above, which was more cost-effective than excavating tunnels as it avoided the cost and risk of property demolition (Green, 2019). Steam traction trains were the only locomotive technology available at the time, thus this method could incorporate ventilation in the form of blowholes so fumes and steam from the combustion process could escape the tunnels. This part of the network is known as the sub-surface and is approximately 8% of the total LU network track length.

Deep mined “tube” tunnel construction followed in the early 20<sup>th</sup> century as track electrification was developed. Excavating the earth to form the tunnels used an innovative tunnelling shield, designed by Marc and Isambard Kingdom Brunel (Falconer, 2008). This enabled trains to run

beneath the city of London without disrupting or being disrupted by other traffic on the surface. It also allowed passengers to cross London beneath the River Thames instead of over the limited bridges or across the water. Apart from the Victoria line (constructed in the 1960s) and the Jubilee line (constructed in the 1970s; extended in the 1990s), the deep tube tunnels are over 100 years old and in total comprise approximately 37% of the entire LU network track length. The remaining track across the LU network (approximately 55%) is on the surface – outside of the city centre, running through the suburbs.

As of September 2021 (when the Northern line extension to Battersea Power Station opened) the LU network is formed of 11 operating lines and approximately 400km of track, serving 272 stations. It is the sixth-longest metro system in the world and the longest network outside of the Asia-Pacific region (UITP, 2022). The capacity of TfL's rail network in London further increased in 2022 when the Elizabeth line opened, though it is not explicitly considered an LU line.

Table 1.1 shows the general characteristics of each LU line, including the type of tunnel the line operates on upon entering the centre of London. The number of stations and total track length total to higher amounts, as several stations are interchanges and some parts of the network share track. See the Appendices (Appendix A) for a reference map of the LU network, including the tunnel sections (though it excludes the Northern Line extension and the Elizabeth line).



Table 1.1 Key data on each LU line (Data: TfL, 2021a)












LU line	Line colour	Opening year	Total track length (km)	No. of stations	Tunnel type
Bakerloo		1906	23.2	25	Deep tube
Central		1900	74.0	49	Deep tube
Circle		1884	27.2	36	Sub-surface
District		1868	64.0	60	Sub-surface
Hammersmith & City		1864	25.5	29	Sub-surface
Jubilee		1979	36.2	27	Deep tube
Metropolitan		1863	66.7	34	Sub-surface
Northern		1890	58.0	52	Deep tube
Piccadilly		1906	71.0	53	Deep tube
Victoria		1968	21.0	16	Deep tube
Waterloo & City		1898	1.5	2	Deep tube

Figure 1.1 shows the layout of the LU network at that time relative to the administrative boundary of Greater London. The network is primarily north of the River Thames, which runs through the city centre and to the east. Most LU lines' termini are in the outer suburban zones of London. The Circle line loops around central London, connecting with most of the other LU lines, shown in Figure 1.2. All the LU lines include a segment of either sub-surface or deep tube tunnels near the city centre. The deep tube lines run beneath the Circle line loop, while the other sub-surface lines join the Circle line loop, with sections of their respective lines running parallel to it or sharing the same track.

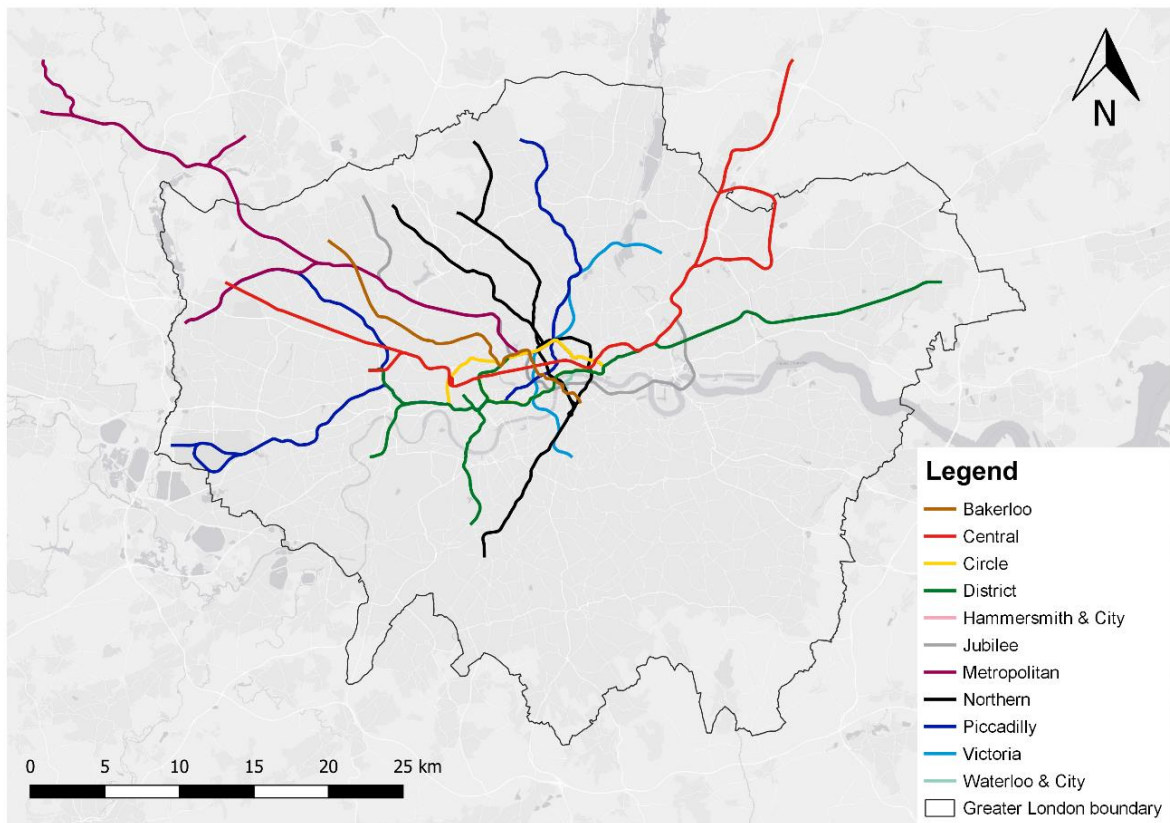


Figure 1.1 The LU network in the context of the Greater London administrative boundary

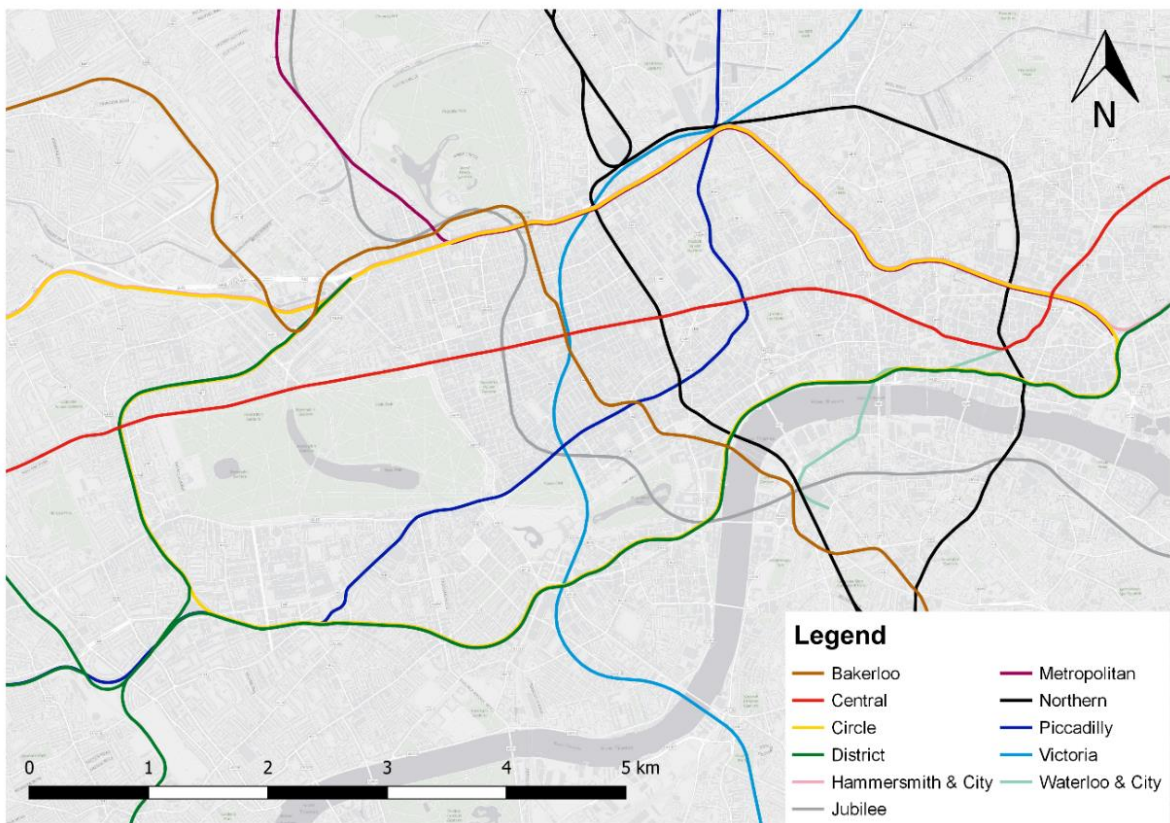


Figure 1.2 The central part of the LU network, showing examples of parallel/shared track sections across the LU lines

The LU network is also one of the busiest in the world in terms of passenger ridership. In 2019, the annual number of LU passenger journeys was 1.4 billion (TfL, 2022g), being one of 15 metro networks worldwide recording total annual passenger journeys greater than 1 billion (UITP, 2022). Since the start of their published data (April 2010), LU ridership gradually increased, reaching a steady annual rate from 2015 to 2019. Although passenger numbers were severely impacted by the coronavirus pandemic since early 2020, LU network ridership has progressively recovered, shown in Figure 1.3. As of June-September 2022, TfL reported quarterly passenger journeys at 81% of the 2018/19 pre-pandemic baseline (TfL, 2022n).

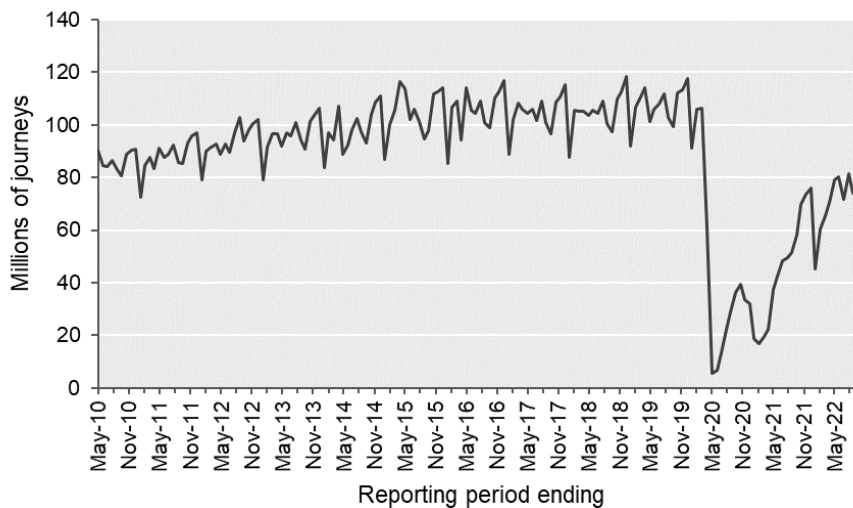


Figure 1.3 Passenger ridership on the LU network *per* 4-weekly reporting period from April 2010 to October 2022. The steep drop in ridership represents the impact of the coronavirus pandemic, which has since begun to recover (Data: TfL, 2022g)

### 1.1.2. Heat on the London Underground

TfL faces operational challenges in adverse weather conditions. One of these challenges is extreme heat in the deep tube tunnels (discussed in more detail in Section 2.2.2). Unlike the surface part of the LU network, which faces the direct effects of the weather at the time of occurrence, the tunnel environment is very different, as temperatures have gradually built up over more than a century (Botelle *et al.*, 2010). British media often report on the LU

temperatures in the deep tube tunnels, as certain sections of them can exceed 30°C on the hottest days of the year (The Evening Standard, 2017; The Independent, 2019).

Most of the deep tube tunnels were bored through a geological formation known as London Clay, shown in Figure 1.4. This formation is largely impermeable, with a mean thickness of 32m beneath central London (Paul, 2016). The clay can be easily excavated (Ellison *et al.*, 2004), and tunnelling provided a means to expand the railway system, with limited interference to near-surface infrastructure, such as sewer, gas and water pipes (Halliday, 2013). Unlike surface networks that are often directly influenced by daily weather, the deep tube tunnel temperatures remain relatively constant throughout the day and into the evening and temperature changes are driven by annual atmospheric and/or ground level temperature cycles (*e.g.*, Kimura *et al.*, 2018; Liu *et al.*, 2022b; Vasilyev *et al.*, 2022). Historically, the tunnel walls acted as a heat sink, absorbing excess heat and keeping temperatures stable. However, the long-term running of LU services and low ventilation capacity (Ampofo *et al.*, 2004; Mortada *et al.*, 2015), has reduced the effectiveness of the tunnel walls as a heat sink, which is associated with a rise in tunnel temperatures (Botelle *et al.*, 2010).

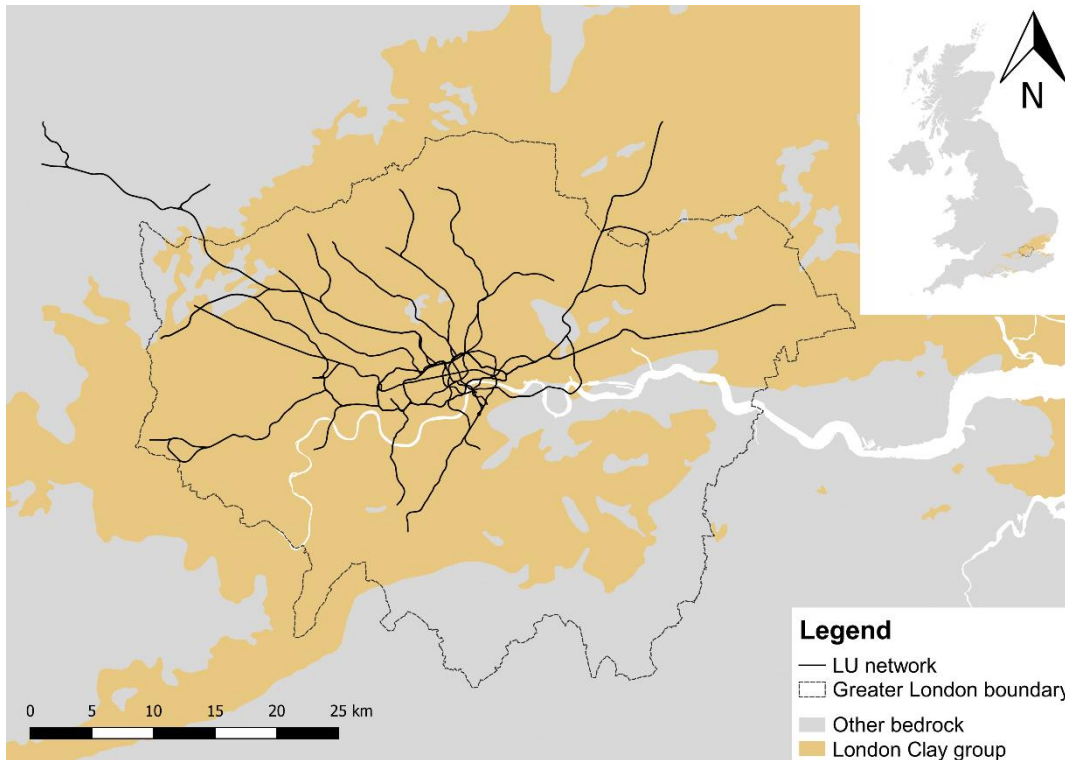


Figure 1.4 The location of London Clay bedrock across London and in the context of the LU network (Data: BGS, 2020)

LU tunnel temperatures were considered reasonable up to the 1950s (Gilbey, 2012); approximately 15°C year-round (Botelle *et al.*, 2010), due to the London Clay’s properties, which could absorb rejected heat from train operations. The Underground Electric Railway Company, which formerly owned and operated the LU network marketed its tunnels being cooler than the surface in the summer and warmer than the surface in the winter (see Figure 1.5). Continuous temperature recording across the LU network was set up in late 2005 as part of the LU Cooling the Tube Programme (Gilbey, 2012). These records show the extent to which the deep tube tunnel temperatures increased – which now experience fairly high constant temperatures throughout the year (Botelle *et al.*, 2010). Nevertheless, tunnel station platform temperature is linearly correlated to outside surface temperatures. An approximate relationship between these variables was estimated as:

$$t_{platform} = 0.36 \times t_{surface} + 19.50,$$

where  $t_{platform}$  is the mean station platform temperature and  $t_{surface}$  is the mean outside surface temperature (Gilbey *et al.*, 2011).

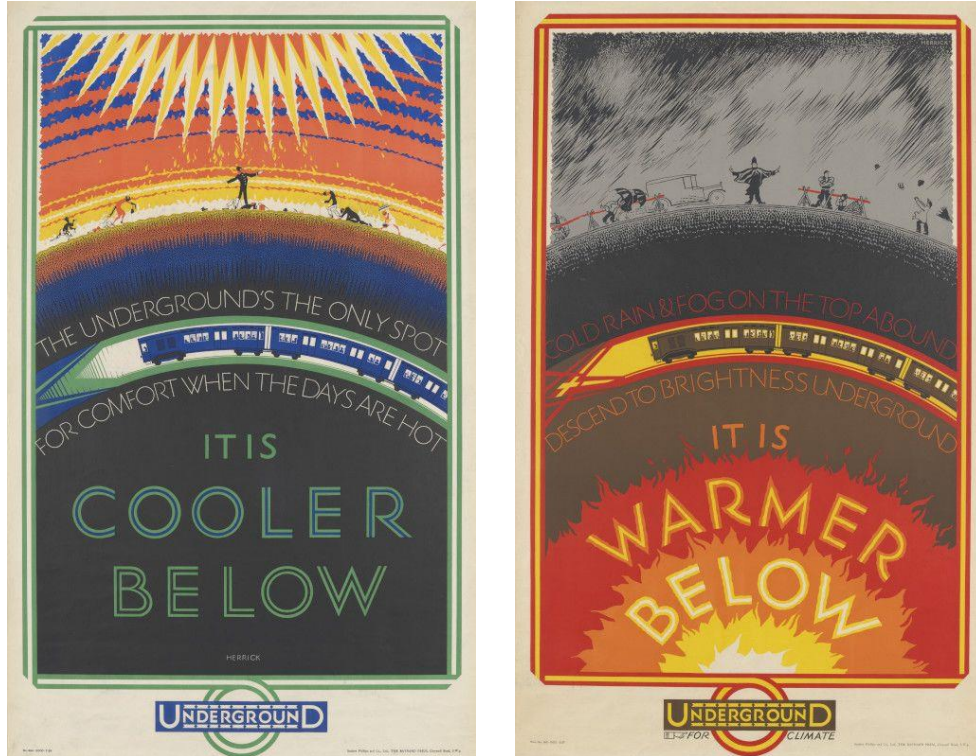


Figure 1.5 Advertisements for travelling on the LU network in the summer months (left) and the winter months (right), from almost a century ago. LU tunnel temperatures were lower than the present day and considered more comfortable for travel compared to surface temperatures, emphasised here as a key selling point (Source: Herrick, 1926, 1927)

Heat build-up is considered hazardous in metro network tunnels (Liu *et al.*, 2022a). High tunnel temperatures lead to passenger thermal discomfort, for heat affects almost every system in the human body (Wen *et al.*, 2020), and are also associated with an increased frequency of asset-related delays (Greenham *et al.*, 2020). Both issues have the potential to amplify the other and have safety and revenue implications for TfL. For example, if a passenger falls ill due to heat while on the LU network, train operations could be suspended while an emergency call is made. Similarly, if a heat-related fault suspended the LU network, passengers could fall ill if stuck on a suspended service – an incident that has happened before on the LU network (Hosken, 2014). This risk is carefully managed by TfL and the incident was a rare occurrence.

Literature evaluating the impact of climate change on railway networks focuses extensively on assets that are directly exposed to weather (discussed in Section 2.2.1). However, climate change could also affect tunnel temperatures further in the future (Sun *et al.*, 2021), and there are few examples of how such changes would affect tunnel assets. Assets under higher constant temperatures, with little daily or annual temperature fluctuation and a total absence of natural daylight or solar irradiance in a tunnel would assume different thermal tolerances; some may perform better while some may perform worse compared with the same asset on the surface. Understanding how climate change impacts temperature is therefore important to identify the extent of its effect on the different sections of the LU network.

## **1.2. Signals of climate change and its impact on observed temperature**

Since industrialisation, there have been unprecedented changes in the global climate system, which are primarily attributed to anthropogenic greenhouse gas (GHG) emissions such as carbon dioxide (CO<sub>2</sub>) and methane (CH<sub>4</sub>), which directly influence global mean surface temperature (IPCC, 2021). The scientific consensus is that to abate severe, widespread, and irreversible effects of climate change upon civilization, CO<sub>2</sub>, the primary anthropogenic GHG must refrain from reaching 450 parts *per* million (ppm), the equivalent of a 2°C increase in global mean surface temperature from pre-industrial levels. This is the basis upon which the Paris Agreement was designed, the legally binding international treaty on climate change (UNFCCC, 2015). As of December 2022, mean global monthly atmospheric CO<sub>2</sub> concentrations were approximately 419ppm, shown in Figure 1.6.

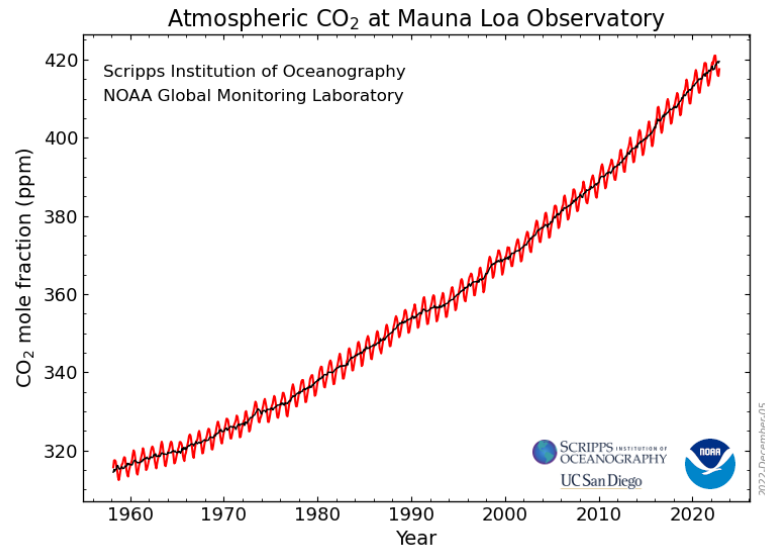


Figure 1.6 Trends in global atmospheric CO<sub>2</sub> since 1958, showing the continued increase in concentration. The red line shows the monthly global mean concentration, and the black line shows the monthly mean concentration after correction for the average seasonal cycle (Source: NOAA, 2022)

The Intergovernmental Panel on Climate Change (IPCC) shows that with every increment of global warming, changes in climate extremes become larger (IPCC, 2021). For extreme heat events, there is a high confidence in this increased level of change. Heat event attributions studies, compared with other extreme weather events have the longest history, particularly following the European summer heatwave of 2003 (NASEM, 2016). These studies demonstrate the importance of understanding temperature extreme changes as well as mean temperature change in the context of a changing climate for London and the LU network. The following sections describe the changes in each temperature parameter (mean temperature, temperature extremes, diurnal temperature range) from the global scale to the local scale (London).

### 1.2.1. Mean surface temperature change

Currently, the global mean surface temperature increase from pre-industrial times is approximately +1°C (IPCC, 2021). More specifically in the United Kingdom (UK), the early 21<sup>st</sup> century (2001-2021) was 1.6°C warmer than the earliest centennial average (17<sup>th</sup> Century)



from the Central England Temperature (CET) series, shown in Table 1.2. It signals that the UK climate is changing, and at a slightly accelerated rate than the global mean.

Table 1.2 Centennial averages for the CET series (°C), 1659-2021 (Data: Kendon *et al.*, 2022)

Season	17 <sup>th</sup> Century 1659-1700	18 <sup>th</sup> Century 1701-1800	19 <sup>th</sup> Century 1801-1900	20 <sup>th</sup> Century 1901-2000	21 <sup>st</sup> Century 2001-2021
Winter	3.0	3.5	3.7	4.2	4.9
Spring	7.5	8.1	8.1	8.4	9.2
Summer	14.9	15.5	15.2	15.3	16.1
Autumn	9.1	9.6	9.5	10.0	11.0
<b>Year</b>	<b>8.7</b>	<b>9.2</b>	<b>9.1</b>	<b>9.5</b>	<b>10.3</b>

### 1.2.2. Temperature extremes

Temperature extremes are either very high (hot extremes) or very low (cold extremes). Since the 1950s, hot extremes have increased and cold extremes have decreased globally (IPCC, 2021). The UK also experiences the same global trend (Kendon *et al.*, 2022), so research tends to focus on hot extremes. In the context of this study, this includes heatwave events. While heatwave definitions vary geographically, the UK defines them as a location where at least three consecutive days meet or exceed a specific temperature threshold, which varies across regions from 25°C to 28°C (Met Office, 2022e).

The UK Met Office publicly report on past severe weather events. Figure 1.7 shows the timeline of high temperature events throughout the summer season since these reports began in 1990. Over time, intervals between each event with the next decreased, with varying intensities and durations. The first reported event in August 1990 broke maximum temperature records that had not been observed in several decades, with a national maximum of 37°C (Met Office, 2012). Several UK weather stations upheld their 1990 records throughout other notable hot summers, such as in 2003, 2006 and 2019. In 2022, 40°C was recorded for the first time at three UK

weather stations, including London (Met Office, 2022d), exceeding most of the unbroken 1990 records. The scale of change in observed high temperatures in recent decades is considerable; only 60 years ago, a study of maximum daily temperatures recorded at Kew Gardens, London concluded that temperatures above 30°C were rare, with one such day expected in either June or July in four out of five years (Chandler, 1965).

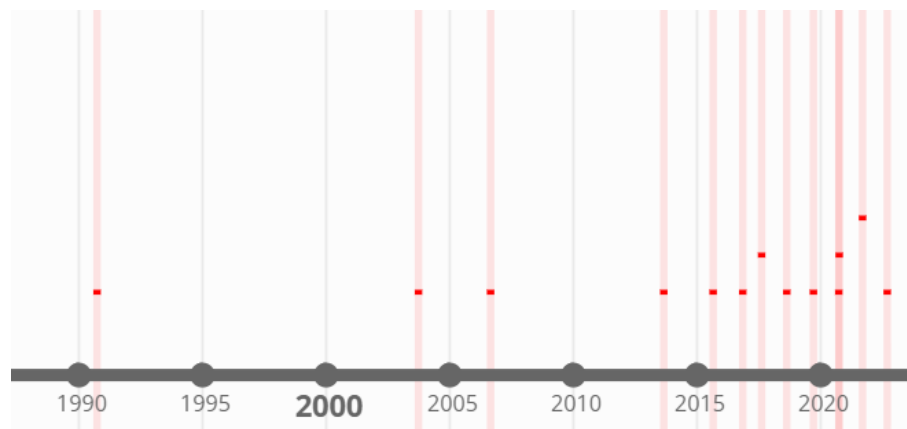


Figure 1.7 Timeline of high temperature events reported in the UK during the summer, 1990-2022. Each bar represents one high temperature event. The dark points differentiate high temperature events that occurred close together, as some of the bars overlap in the timeline. (Data: Met Office, 2022c)

Studies have placed various levels of climate change attribution to extreme events and as a result, quantified changes in extreme heat events. Stott *et al.* (2004) estimated that the risk of a heatwave of the European 2003 summer has at least doubled due to human activity, while Baker *et al.* (2021) estimated the conditions of the UK summer of 1976 (an exceptionally hot and dry period) are now significantly higher than before, by a factor of between 4 and 8. Using the CET series, Chapman *et al.* (2019) determined that summer heatwave activity has already increased by an overall twofold to threefold since the late 1800s. Early analysis of the July 2022 heat event showed that human activity made the event at least ten times more likely to occur (Zachariah *et al.*, 2022).

Although mean surface temperatures have increased, cold extremes still occur. Figure 1.8 shows past low temperature events across the UK. These are less frequent than high temperature events and are also more sporadic. The first low temperature event reported in this series since 1990 was in 2008. Both low and high temperature extremes were reported in a calendar year for 2013, 2018, 2021 and 2022. However, the temperatures during cold events in Figure 1.8 were not record-breaking. The lowest temperature recorded in the UK was  $-27.2^{\circ}\text{C}$ , first reported in 1895, (Met Office, 2022a). In the Southeast of England, the lowest reported temperature was  $-19.5^{\circ}\text{C}$  in January 1982. This is compared with the most recent low in London of  $-7.6^{\circ}\text{C}$  in 2022 (Met Office, 2023a).

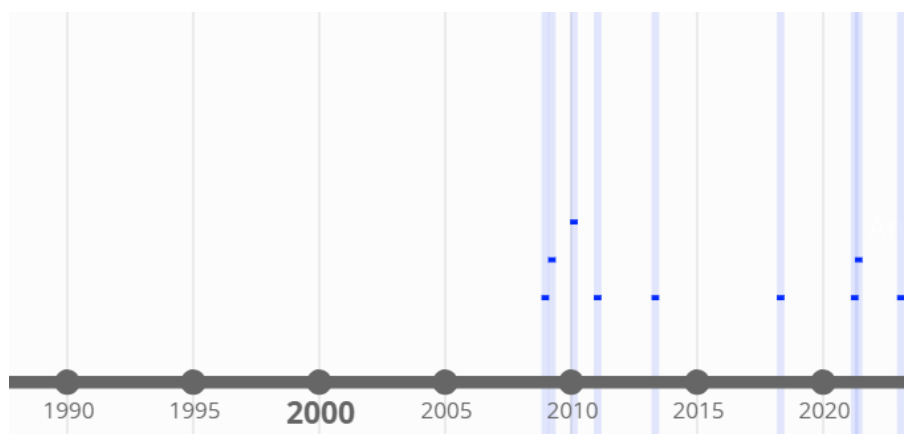


Figure 1.8 Timeline of low temperature events (including frost and snow) reported in the UK, 1990-2022. Each bar represents one low temperature event. The dark points differentiate low temperature events that occurred close together, as some of the bars overlap in the timeline. (Data: Met Office, 2022c)

### 1.2.3. Diurnal temperature range

Diurnal temperature range ( $\Delta t$ ) is the difference between minimum and maximum temperatures over a 24-hour period, and is a useful climate attribution indicator (Braganza *et al.*, 2004). Change in  $\Delta t$  impacts natural systems (Zhang *et al.*, 2022), agricultural yields (Hernandez-Barrera *et al.*, 2017), as well as human health and mortality (Lee *et al.*, 2018; Davis *et al.*, 2020). Globally, there is a knowledge gap in observed change in  $\Delta t$  due to data gaps and low

confidence, especially pre-1950 (IPCC, 2013, 2021). Data since the 1950s signals a global decrease in  $\Delta t$  (Sun *et al.*, 2019). In the UK, however,  $\Delta t$  increased slightly (Kendon *et al.*, 2022). Zhang *et al.* (2018) reported a 1993-2006 annual average  $\Delta t$  in England of 7.3°C, with a London average of 7.1°C. London's  $\Delta t$  varied between 1.0°C and 19.1°C.

### **1.3. Contributing factors to thermal environments across the LU network**

In addition to changes in climate, there are other anthropogenic factors that contribute to the thermal environment across the LU network. The following sections discuss the effect of the urban heat island (UHI) on surface temperatures, and the effect of train operations and the constraints of tunnel infrastructure on tunnel temperatures.

#### **1.3.1. On the surface: the urban heat island effect**

Mass rapid transit networks like metros are usually in dense, urban environments. Urban air temperatures are often warmer than their rural surroundings, a phenomenon known as the UHI effect (Oke, 1973). Urbanisation leads to changes in surface albedo and vegetation cover that modifies the near-surface climate (Taha, 1997). However, UHI intensity (the temperature difference between an urban area and their rural surroundings) across different urban environments is not necessarily homogenous (Oke, 1973). Differences in UHI intensity can be attributed to multiple complex factors regarding background climate (Zhao *et al.*, 2014; Manoli *et al.*, 2019) as well as city and population size (Oke, 1973; Manoli *et al.*, 2019). As temperatures increase, city temperatures will be elevated due to the UHI effect. However, UHI intensity may only increase slightly relative the overall temperature change (Lauwaet *et al.*, 2015), but is nevertheless a significant challenge for cities in the future.

London's UHI is widespread across Greater London, and the effects are greater at night. As shown in Figure 1.9, most of Greater London's UHI intensity is between +2°C and +3°C compared with its background rural temperatures (a value of 0 in Figure 1.9). London's UHI intensity also varies spatially and temporally. The Greater London Authority (GLA) report UHI intensities between +3°C and +4°C in the warmest parts of the city (GLA, 2011), and Kolokotroni and Giridharan (2008) found mean Central London nocturnal UHI intensities of between +1.6°C and +3.1°C. However, during a heatwave summer in London, there is little evidence of UHI intensification across the city compared to an average summer (Holderness *et al.*, 2013), though this does not imply that the risks associated with heatwaves are reduced.

A considerable proportion of the surface part of the LU network runs through parts of the city where London's mean UHI intensity would be at least +2°C. Conversely, where London's UHI is greatest (in the city centre), most of the network is underground. Instead, this part of the network is subjected to other factors in the tunnels, which are discussed in the following section.

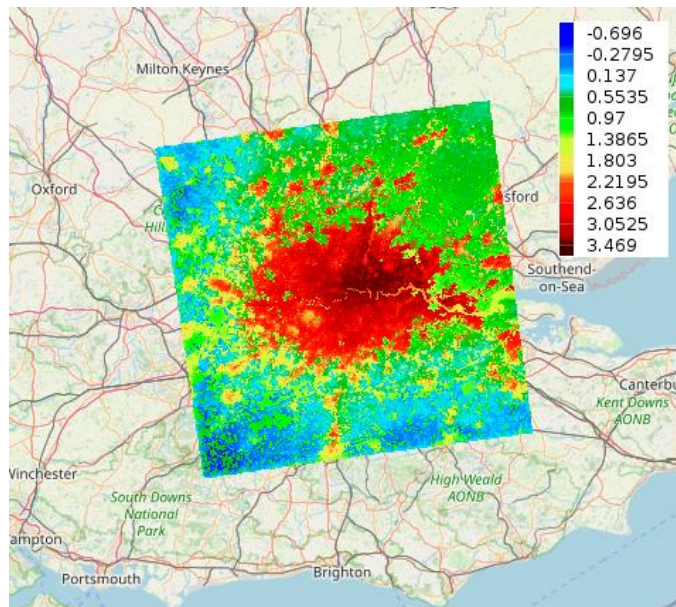


Figure 1.9 UHI intensity for the Greater London Area for an example summer, with altitude-corrected midnight temperatures according to the UrbClim model (Lauwaet *et al.*, 2015) (Source: VITO, n.d.)

### **1.3.2. In the tunnels: infrastructure and operations**

As mentioned in Section 1.1.2, the gradual build-up of temperature in deep tube tunnels on the LU network was primarily owed to train operations. Quantifying heat sources in the tunnels, particularly anthropogenic sources, is important to understand the extent of their effect beyond the influence of external climate conditions. Mortada *et al.* (2015) conducted a study modelling heat sources on the Central line, one of the LU lines with the hottest tunnels (see Figure 1.10). Mortada *et al.* demonstrated that train braking was the primary heat source (61%), followed by passengers (combined train and station passengers of approximately 34%). While the model developed by Mortada *et al.* is a good representation of the Central line tunnels, the climatic boundary conditions (1996-2005) it uses are not representative of recent changes in the climate, particularly the increased frequency of extreme heat events (see Section 1.2.2). Indeed, this was published prior to the most recent increase in extreme heat events (post-2015) and therefore may not have been a consideration. Moreover, the climatic parameters set for the model were not accounted for as a heat source, although specified ventilation capacity was built into model scenarios for the study. Often the complexity of these can lead to ventilation being removed from tunnel studies altogether *e.g.* Zhang and Li, (2019). Nevertheless, the contribution of train braking is considered the primary factor influencing heat conditions in the LU tunnels.

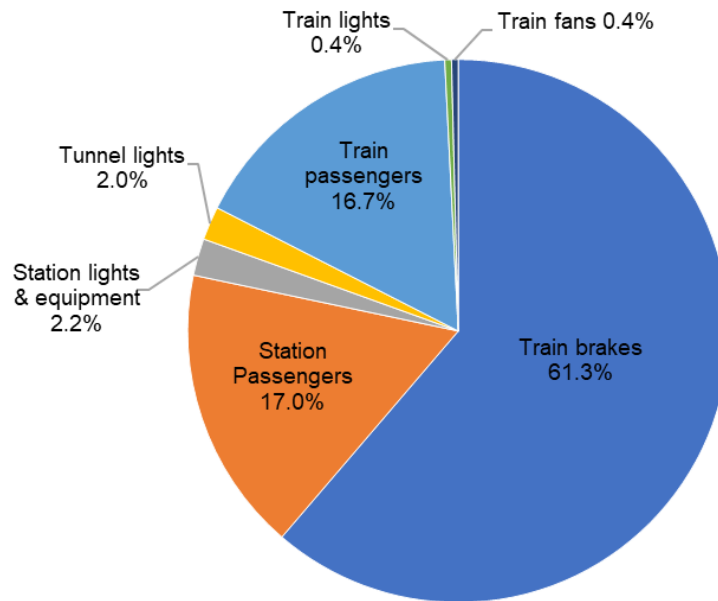


Figure 1.10 Modelled peak time heat source distribution in the LU tunnels for 2013 on the Central Line (Data: Mortada *et al.*, 2015)

Due to the thermal discomfort risk to LU staff and passengers, TfL have already taken action to try and limit excessive tunnel temperatures. This includes introducing regenerative braking systems to trains across the LU network, which redirect heat energy produced from train braking into electricity. Regenerative braking of trains is thought to have the greatest effect on reducing tunnel temperatures than other heat sinks (Mortada *et al.*, 2015; Zhang and Li, 2019). All but two of the LU lines' rolling stock (Bakerloo and Piccadilly lines) are capable of regenerative braking.

The level of impact of climate change, including extreme temperatures to the LU network is also dependent on asset vulnerability and exposure. The following section positions the discussed heat hazards on the LU network (*i.e.*, climate change, extreme temperature, contributing factors) in the broader context of risk of LU's infrastructure to heat.

## 1.4. The concept of climate risk

Railway assets are at risk to the impacts of climate change. Risk depends on the magnitude of the hazard, vulnerability, and exposure, illustrated in Figure 1.11. Here, risk is the potential of assets failing to operate across the LU network. Hazard is the occurrence of temperature events likely to cause asset damage, namely extreme heat; vulnerability would be an asset's sensitivity, susceptibility, or capacity to operate; and exposure being the presence of an asset being adversely affected. The specific heat-related risk to assets is discussed in detail in Section 2.2.1 and Section 2.2.2, while the ways these risks are quantified across Great Britain's (GB's) railways and the LU network are discussed in Section 2.3.



Figure 1.11 Risk Propeller conceptualising the interactions among the determinants of risk. It illustrates that risk comprises the magnitude of hazard, vulnerability, and exposure (Source: IPCC, 2022)

Since the publication of the fifth IPCC assessment reports (AR5) between 2013 and 2014, our understanding and evaluation of climate change and climate risk has advanced (IPCC, 2022). Risks do not occur in isolation, nor necessarily by single determinants of risk. As infrastructure becomes more interconnected, particularly between infrastructure sectors (*e.g.*, energy, telecommunications, transport), climate risk becomes more complex due to the responses of risk determinants as well as the risks themselves upon others (Simpson *et al.*, 2021). Pescaroli and Alexander (2018) presented three pertinent examples of cross-risk connections in Table 1.3.



They show how different systems and drivers lead to further risks. The primary types of connections among these examples are interacting (combined), interconnected (closely linked), cascading (triggering another), or compounding (exacerbating).

Table 1.3 Examples of cross-risk connections, emphasising the complexity of risk and how one risk or determinant of risk can be linked to another (Adapted from: Pescaroli and Alexander, 2018)

Disaster	Description of risk
Volcanic eruption of Eyjafjallajökull, Iceland, April 2010	Volcanic ash travelled an unusual prevailing north to north-westerly flow between Iceland and Northwest Europe ( <b>compound risk</b> ), affecting global networks dependent on aviation ( <b>interconnected risk</b> ), disrupting infrastructure thus affecting society ( <b>cascading risk</b> ).
Earthquake, tsunami and nuclear meltdown of Daiichi power plant, Japan, March 2011	An earthquake triggered a tsunami ( <b>interacting hazard</b> ) affecting highly coupled infrastructure ( <b>interconnected risk</b> ), leading to secondary emergencies such as loss of vital services ( <b>cascading risk</b> ). The earthquake triggered a small, localised landslide ( <b>interacting risk</b> ) cutting off the power plant from the electricity grid ( <b>interconnected risk</b> ), leading to a nuclear meltdown ( <b>cascading risk</b> ).
Hurricane Sandy, United States, October 2012	Storm winds from landfall caused direct damage and generated a storm surge, causing flooding ( <b>interacting risk</b> ), as cold Arctic air intensified cold weather and snowstorms inland ( <b>compounding risk</b> ). The area affected by Sandy was of strategic economic importance ( <b>interconnected risk</b> ). The President made a new declaration of emergency regarding the impacts to energy ( <b>cascading risk</b> ), and 50 deaths were attributed to the extended power outages and cold weather ( <b>compounding and cascading risk</b> ).

Complex risks with cross-connections are however not static over time; they require constant reviewing and updating, as new knowledge emerges to improve decision support (Pescaroli and Alexander, 2018; Simpson *et al.*, 2021). Therefore, a recurrence of these examples in future may not be the same. The characteristics of the risk determinants and the connections between them may change, such as exacerbating due to climate change, or a new risk determinant could manifest itself in future. Conversely, responses to reduce climate risk (*i.e.*, climate change

adaptation) may have intended (risk reduction) and unintended outcomes (maladaptation, lock-in) to previous cross-connections in future. It is therefore important to conduct iterative processes in managing complex climate risks.

## **1.5. Policy context**

Managing climate risk in the UK comprises part of The Climate Change Act (2008), which is mandated by the UK government. There is a five-yearly adaptation policy cycle, where a comprehensive risk assessment is conducted to inform actions for the devolved administrations' National Adaptation Plans. The Climate Change Committee (CCC) produce independent reports *e.g.*, CCC, (2021a) to advise the government on the climate risks across the UK, then the government formally publishes its Climate Change Risk Assessment (CCRA) based on the CCC's advice and recommendations. The Climate Change Act also established the Adaptation Reporting Power (ARP), which invites bodies such as infrastructure owners and operators (including TfL) across several sectors (*e.g.*, power, water, transport) to report on their climate preparedness as part of the five-yearly cycle. The CCC review the ARP submissions to the government (*e.g.*, CCC, 2022), providing a snapshot in time of the national progress towards more climate-resilient infrastructure. Currently, the UK is in the third policy cycle (ARP3).

The eight priority risk areas for the UK are cross-cutting issues rather than sector-specific, based on 61 risks and opportunities identified by the (CCC, 2021a), as summarised in Table 1.4. Several of these priority risks may consider railway infrastructure a component, either as a risk or a determinant of risk. For example, Priority 5 highlights a cascading risk of the loss of transport network disrupting the food chain. Similarly, the failure of a power system in Priority 6 can disrupt train operations such as through station closures (*e.g.*, Greenham *et al.*, 2020);

another cascading risk. The CCC also frame these UK climate risks to transport in a sector-specific briefing document (CCC, 2021b), of which there are seven risks. These include cascading failures, river/surface/groundwater flooding, coastal flooding/erosion, slope/embankment failure, subsidence, and high/low temperatures, high winds, and lightning. Temperature risk is ranked high by urgency, with “more action needed” to address the risk and respond appropriately to it.

Table 1.4 Current priority climate risk areas for the UK according to the 2022 CCRA (Source: HM Government, 2022; CCC, 2021a)

<b>Priority</b>	<b>Risk area</b>
Priority 1	Risks to viability and diversity of terrestrial and freshwater habitats and species from multiple hazards
Priority 2	Risks to soil health from increased flooding and drought
Priority 3	Risks to natural carbon stores and sequestration from multiple hazards leading to increased emissions
Priority 4	Risks to crops, livestock, and commercial trees from multiple hazards
Priority 5	Risks to supply of food, goods, and vital services due to climate-related collapse of supply chains and distribution networks
Priority 6	Risks to people and the economy from climate-related failure of the power system
Priority 7	Risks to human health, well-being, and productivity from increased exposure to heat in homes and other buildings
Priority 8	Multiple risks to the UK from climate change impacts overseas

Further research into the climate risks to railway infrastructure specifically in Great Britain (GB) are available from the Rail Safety and Standards Board (RSSB), who commissioned a research report: “Tomorrow’s Railway and Climate Change Adaptation” (TRaCCA) (RSSB, 2016a). Although progress on railway research has continued, the TRaCCA report gave a holistic view of the climate risks to British railway infrastructure at the time and in future. It found that response to extreme weather is inconsistent, due to siloed ways of working across the railway organisations and a lack of collaboration between the industry and other sectors.

Vulnerabilities are consequently varied across Britain's railways due to different levels of response and preparedness, resulting in spatially varied levels of climate risk.

In March 2023, the CCC reported to Parliament on the UK's progress in adapting to climate change (CCC, 2023). As part of the transport chapter, the rail industry was evaluated as having credible planning for adaptation, though mixed progress in terms of delivery and implementation of them. Additionally, the review identified that weather impacts on the rail sector, particularly heat, have increased, and the enabling factors to address this include data and monitoring, funding and investment, and governance. This emphasises the importance of understanding heat risk to infrastructure in the context of climate change as the challenge extends beyond the LU network.

## **1.6. Future climate change**

Climate risks are expected to be affected by future climate change. There is a time lag between increases in GHG concentrations and the maximum effect it has on increasing global mean surface temperature, possibly around decade on average (Ricke and Caldeira, 2014). Therefore, the GHG emissions from past decades are likely associated with the present-day shifts in global climate, and the current rate of GHG emissions locks in a rate of near-term future warming and preparing a response to these future changes is beneficial.

To articulate the potential future pathways of changing climate risk, The IPCC AR5 reports developed four future climate scenarios, which are expanded upon in the latest Sixth assessment reports (AR6) to five scenarios (IPCC, 2021). The AR5 scenarios (IPCC, 2013), known as Representative Concentration Pathways (RCPs) specify atmospheric GHG concentrations and corresponding emissions based on a peak or stabilisation of radiative forcing by 2100, measured

as watts *per* square metre ( $\text{Wm}^{-2}$ ). Estimated future change in global mean temperatures can then be estimated via models based on the assumptions of atmospheric GHG concentrations for the RCPs. The AR5 RCPs are described in Table 1.5. Based on this table, achieving the Paris Agreement goal of limiting mean global surface temperature warming to well below  $+2^\circ\text{C}$  pre-industrial levels, (although ideally below  $+1.5^\circ\text{C}$ ) would require a global effort to follow a pathway as close to RCP 2.6 as possible, or more likely the AR6 Shared Socioeconomic pathway of  $1\text{-}1.9 \text{ Wm}^{-2}$  (IPCC, 2021). Current global policies and action to limit increasing GHG emissions, however, are estimated to result in warming of approximately  $+2.7^\circ\text{C}$  by 2100 (Climate Action Tracker, 2022), arguably tracking around the RCP 6.0 scenario trajectory, which is approximately  $+2.8^\circ\text{C}$ ,  $\pm 0.5^\circ\text{C}$  (see Table 1.5).

Table 1.5 Summary of each AR5 future emissions scenario, with each scenarios' likely range of estimated mean global surface temperature increase for 2081-2100 relative to 1850-1900 (Data: IPCC, 2013)

<b>RCP</b>	<b>Scenario description</b>	<b>Temperature increase</b>
2.6	GHG emissions peak in the near-term, decreasing substantially into the coming decades and below present-day levels by 2100	$1.6^\circ\text{C} \pm 0.4^\circ\text{C}$
4.5	GHG emissions are medium-low. Emissions gradually increase up to around mid-21 <sup>st</sup> century, then gradually decrease, stabilising slightly above present-day levels by 2100	$2.4^\circ\text{C} \pm 0.5^\circ\text{C}$
6.0	GHG emissions are medium-high. Emissions continue to increase beyond the RCP 4.5 scenario and accelerate beyond mid-21 <sup>st</sup> century, then decrease, stabilising higher than present-day levels by 2100	$2.8^\circ\text{C} \pm 0.5^\circ\text{C}$
8.5	GHG emissions are highest, continuing to rise throughout the 21 <sup>st</sup> century. The increase begins to decelerate after the mid-21 <sup>st</sup> century but are not yet stabilised	$4.3^\circ\text{C} \pm 0.7^\circ\text{C}$

### 1.6.1. UK climate projection scenarios

The UK Met Office produce climate projections for the UK derived from a range of data from climate models around the world. The latest release of climate projections was in 2018, known

as UKCP18. These projections consist of several spatial resolutions for the UK and scenarios, which align with the IPCC AR5. The climate projection parameters in UKCP18 include temperature, precipitation, sea level rise, humidity, wind speed, sea level pressure, cloud cover, and long- and short-wave radiation.

Summarised in the UKCP18 Science Overview Report (Lowe *et al.*, 2019), the future UK climate compared to recent observations estimates hotter, drier summers and milder, wetter winters. The extent of the change is dependent on which climate projection scenario is most likely to occur. Furthermore, each scenario comprises a range of percentile values, such as the examples shown in Figure 1.12. Percentile information is useful for projections, especially for periods of time further in the future, due to the increased uncertainty over time as well as to address the natural variation in seasons which may still occur, such as some cool summers and some wet summers (Lowe *et al.*, 2019).

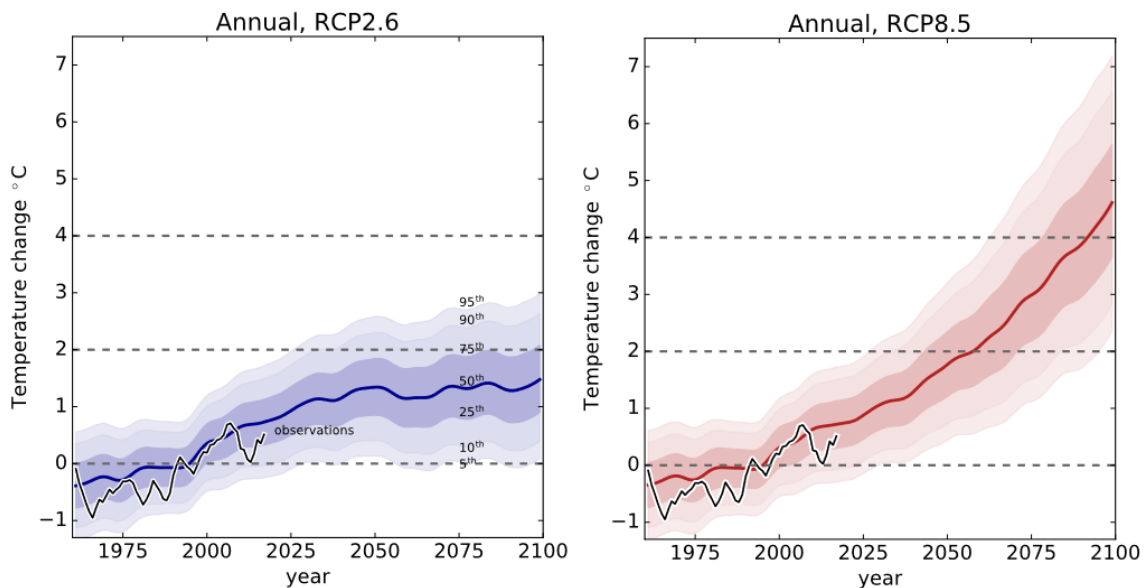


Figure 1.12 UKCP18 mean temperature change trajectories for the lowest (RCP 2.6, blue) and highest (RCP 8.5, red) future emissions scenarios, up to 2100. The shaded areas outside the lines represent different percentile values of the scenario, with the solid line representing the median (50<sup>th</sup> percentile). Past temperature observations are shown in the solid black line (Source: Lowe *et al.*, 2019)

Several studies have used UKCP18 data to estimate extreme temperatures in a future UK climate, particularly for the summer months (June, July, August). The summer heat of 1990 prompted a review of extreme high temperatures on track buckling risk for Britain’s railway industry (*i.e.*, Hunt, 1994). Having used 1952 climate data for this review, the estimated return period of a maximum daily temperature of 33°C for the whole of the UK was 5.5 years, and for 36°C was 15.5 years. Compared with the most recent comprehensive analysis by Christidis *et al.* (2020), these return periods have already reduced. In Table 1.6, a maximum daily temperature of 35°C in the present day is almost equivalent, if not more frequent than a past maximum daily temperature of 33°C.

Table 1.6 Estimated present and future return periods of high maximum daily temperatures in the UK, showing how future return periods are expected to reduce substantially, especially the occurrence of a maximum daily temperature of 40°C even in the medium-low scenario of RCP 4.5 (Data: Christidis *et al.*, 2020)

<b>Maximum daily temperature</b>	<b>Scenario</b>	<b>Estimated return period</b>
30°C	Present day (2020)	1.1 – 1.2 years
	RCP 4.5 (2100)	1.0 – 1.1 years
	RCP 8.5 (2100)	1 year
35°C	Present day (2020)	4 – 5 years
	RCP 4.5 (2100)	2 – 3 years
	RCP 8.5 (2100)	1 – 2 years
40°C	Present day (2020)	100 – 300 years
	RCP 4.5 (2100)	15 years
	RCP 8.5 (2100)	3.5 years

Climate change predicts return periods of extreme high temperatures to reduce further, accelerating particularly for temperatures of 40°C by 2100. Other studies have estimated similar outcomes with temperature high extremes for the UK using UKCP18. For instance, Hanlon *et al.* (2021) estimate hot days to increase an average of between 5 and 39 days *per year*, scenario dependent. Additionally, UKCP18 data suggests that extreme high temperatures in the UK may

increase faster in future than the change in global mean surface temperature (Kennedy-Asser *et al.*, 2021). Such results emphasise the urgency for action to limit the effects of these rates of change in climate and extreme temperatures on transport infrastructure, such as the LU network.

### **1.6.2. Adapting to future climate change**

TfL, like other railway network owners and operators, need to respond to changing climate risk on their assets and consider the climate projection scenarios. Many of these organisations are already reporting their progress in how they are taking steps to address climate change in their business practices via the ARP process. The response to reduce climate risk relating to temperature for LU would be in addressing change in risk such as:

- the hazards of increasing mean temperatures, and change in extreme temperature characteristics (frequency, intensity, duration).
- any change in asset vulnerability from the current state, although asset ageing is presumably the most reasonable known information.
- exposure change, such an increase or decrease in areas affecting an asset that are shaded or sheltered from sunlight.

Adapting transport networks such as the LU to climate change has historically focused on technical engineering solutions for physical infrastructure to prevent them from failing in conditions that exceed the original design thresholds (Koetse and Rietveld, 2012). This is mainly because the approach for transport adaptation often comes from an infrastructure, and by proxy, a financial perspective, due to business costs associated with assets that have a long lifespan. Investments in infrastructure (*i.e.*, interventions, upgrades, replacements) are quasi-irreversible, so when appropriately timed to the correct design parameters, such as a wider range



of conditions than the present day, they should withstand the effects of climate change (Fankhauser *et al.*, 1999). For heat, Network Rail is doing this by painting vulnerable assets white to reflect solar radiation, installing track on reinforced concrete at vulnerable locations, and re-tensioning overhead lines (Network Rail, 2021b). TfL is also focusing on near-term actions in their latest business plan to renew several assets, which includes replacing 35km of LU track and 700 LU rolling stock vehicles (TfL, 2022a).

### **1.7. Research context: A climate-resilient London Underground network**

In December 2018, the Mayor of London declared a climate emergency, setting a target for London to become net zero-carbon emitting city by 2030 (London Assembly, 2020). This is more ambitious than the national policy target of net zero by 2050 (The Climate Change Act 2008, c.27). London's climate emergency declaration also encompasses the need to answer how the city can build their climate resilience. While there is not necessarily a universal definition, resilience in terms of climate is understood as the necessary responses to cope with a hazardous event to maintain a system's essential function (IPCC, 2022) – in this case, the LU network. London's resilience to heat is important because the risk is interpreted as undervalued by some organisations, investors, and the public (London Assembly, 2020).

*This study aims to use a systematic, data-driven approach to quantify the impact of present and future temperature-related hazards on railway assets across the LU network.*

By achieving this aim, TfL gain new insight into risk of their assets to climate change, so it can respond appropriately to increase the climate resilience of LU network's now and in future. It will also contribute to knowledge on climate risk on railways on the relationship between

temperature and its assets, particularly as the focus is at the city scale on a metro system and its spatial complexities, which is often overlooked at the national scale of railway research.

To achieve the research study aim, the following objectives are:

1. Critically review the literature on delay and fault metrics that quantify the impact of weather and climate on railway infrastructure.
2. Distinguish the changes and differences in the thermal environment across the LU network.
3. Investigate and interrogate the relationships between LU asset faults recorded by TfL and the thermal environment.
4. Utilise the relationships to estimate potential change in asset failure trends on the LU network in accordance with future climate change scenarios.
5. Critically evaluate the method used to produce the results, suggesting areas for future development of the approach and research direction.
6. Suggest ways that the findings can support decision-making processes for the adaptation of railway and metro networks to climate change, with recommendations for the key stakeholders involved.

## **1.8. Thesis structure**

This thesis presents the work undertaken to meet the objectives of the study and achieve the aim of quantifying the impact of present and future temperature-related hazards on the LU network. Here, **Chapter One** introduced the LU network, its history leading up to the heat challenges it presently faces, and framing climate change as part of the challenge. **Chapter Two** reviews the literature associated with impact analysis of assets to weather and climate

change across the transport sector. It also highlights the knowledge gaps pertaining to methodological approaches and data quality. The literature review in this chapter postulates the research direction. **Chapter Three** describes the methodological approach to the study, including the data obtained and the processes used to conduct the analysis. There are three subsequent chapters that present the results from the methodological approach. Firstly, **Chapter Four** presents results that differentiate the thermal environment across the LU network, as well as presenting the state of the current climate. Secondly, **Chapter Five** applies findings from the previous chapter to conduct the main part of the study, presenting the relationships between the thermal environment and asset faults. This includes a deeper analysis of interesting results. Thirdly, **Chapter Six** presents results on the potential direction of the thermal environment across the LU network under future climate change, including an estimation of change in asset faults as a result. Next, **Chapter Seven** discusses the findings in the wider context of climate change adaptation and achieving more climate-resilient transport, recommending ways to support future decision-making of key stakeholders within TfL, as well as the wider railway and transport sectors. It also critiques the methodological approach for this study and discusses the future research direction. This thesis is concluded in **Chapter Eight**, summarising how this research addressed the aim and objectives, including some overarching recommendations for TfL and its stakeholders. References and Appendices can be found after this final chapter.

# Chapter Two | Literature review

## 2.1. Overview of literature review

Chapter One introduced the challenges associated with heat and climate change on the LU network. While the challenges differ between the surface and tunnels, climate change is a significant factor exacerbating operational challenges now and in future across the entire network. This chapter begins by reviewing the impacts of heat and climate change on railway infrastructure, and how this is assessed to date in the national context and by TfL. It then introduces the current approaches TfL take to prepare and respond to temperature, particularly during extreme heat events. Then, it critically reviews research on methods and metrics that measure disruption on transport networks with respect to TfL's current approaches. It follows by identifying resulting key operational temperature thresholds for railway assets where available in the literature and compared with those across the LU network. Finally, with the latest information on future climate change, inferred change in operational thresholds are discussed. Through evaluating the literature, this chapter ends by outlining the necessary actions of TfL to deepen their understanding of operational performance under changing climate conditions for maintenance and asset protection purposes.

## 2.2. Impact of heat and climate change on railway infrastructure

The complexities around heat risk on the LU network discussed throughout Chapter One highlights the importance of understanding the differences in climate exposure and vulnerabilities among network types. Heat hazards are well understood, but there is less known about other heat risk determinants (*i.e.*, exposure and vulnerability). Therefore, the following

sections discuss similarities and differences of these heat-related determinants of risk, divided between the surface and the tunnels (both sub-surface and deep tube).

### **2.2.1. Surface assets**

Surface assets, in the context of this study, are those located above the ground. They may be fixed directly on or into to the ground, fitted on to an asset fixed on or in the ground, or contained within infrastructure built on the ground. Most research to date on railway asset risk to weather and climate both in and outside of the UK are focused on surface assets, as they comprise most of a railway's network. As a result, there is a relatively mature level of knowledge pertaining to the impacts of temperature-related weather and climate change on railway networks. Most of the LU's assets reside on the surface, given that it is the biggest proportion of the network.

Temperature-related hazards have the capability of adversely disrupting the usual performance of an asset, which is described as an impact. Impacts result in direct and indirect consequences to usual network operation. An asset's vulnerability in this context would be the characteristics that make it sensitive to a potential impact, and its exposure being the factors determining that sensitivity (Palin *et al.*, 2021). Figure 2.1 shows how temperature hazards lead to the indirect consequences that rail network operators are accountable for. While the two temperature hazards lead to different impacts, there are several overlapping direct consequences, which ultimately all feed into the same indirect consequences. This section continues by discussing the literature to date on temperature-related impacts and consequences for network operators for surface assets, focusing on high temperatures UK where applicable.

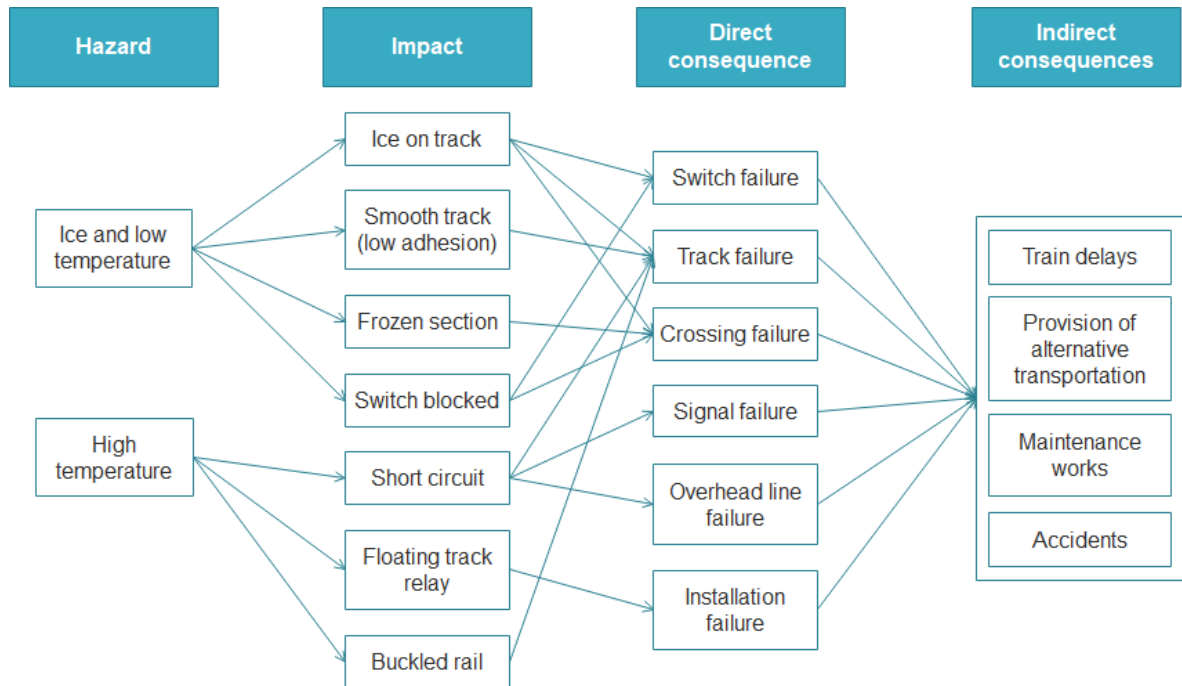


Figure 2.1 Examples of the relationships between temperature hazards, the impacts on railway assets, and direct/indirect consequences for the railway network. It shows how the environmental condition can impact an asset, that can lead to operational consequences for the railway network owner or operator (Adapted from: Palin *et al.*, 2021)

Heat-related failures on track assets are possibly the most well-covered topic in the research area of impact analysis of weather events on railway infrastructure. The primary reason for this is likely because the consequences of a track failure *e.g.*, train derailment, cascading delays to service, and scale of remedial work is extremely high. These consequences are intrinsically linked with financial costs to network owners and operators, which are also very high. Track buckling, shown in Figure 2.2, occurs when rail temperatures increase beyond a threshold they can withstand, and the metal is subjected to thermal expansion, creating deformities in the track that trains can no longer safely pass over. There are several parameters linked to rail vulnerability to temperature, including the type of rail, sleepers and ballast, track alignment quality, and stress-free rail temperature (SFT) – known as the temperature when rail is in a neutral state and there are no stressors acting upon it (Hunt, 1994). Additionally, exposure to high temperatures can vary spatially, as the combined effect of heat and sunlight influences rail

temperatures, and localised shading decreases exposure levels, reducing track buckling risk (Chapman *et al.*, 2006).



Figure 2.2 A buckled rail due to thermal expansion (Source: Skarova *et al.*, 2022)

Point assets on the railway network are also affected by heat, as they can lead to a switch or crossing failure. Points comprise part of a junction on a railway where tracks diverge or converge. Britain’s railway industry does not have a specific definition for a “point”, as it comprises several different assets that form a switch, being defined as “an assembly of two moveable switch rails, two fixed stock rails and other components to divert vehicles from one track to another” (Ellis, 2019). Switches are vulnerable to heat and are an interconnected risk to track assets. The moveable sections of track *i.e.*, the orange set of point/switch rails in Figure 2.3 have a limited lifespan due to wear and deformation from train travel over them (Network Rail, 2023a). Furthermore, past track buckle incidents were often associated with their proximity to a switch or crossing, as SFT reduces because of operational difficulties maintaining them (Hunt, 1994; Ryan and Hunt, 2005). Point assets are also vulnerable being formed of several smaller interacting components. Their exposure risk would also be comparable to track from a spatial perspective in terms of the effects of localised shading.

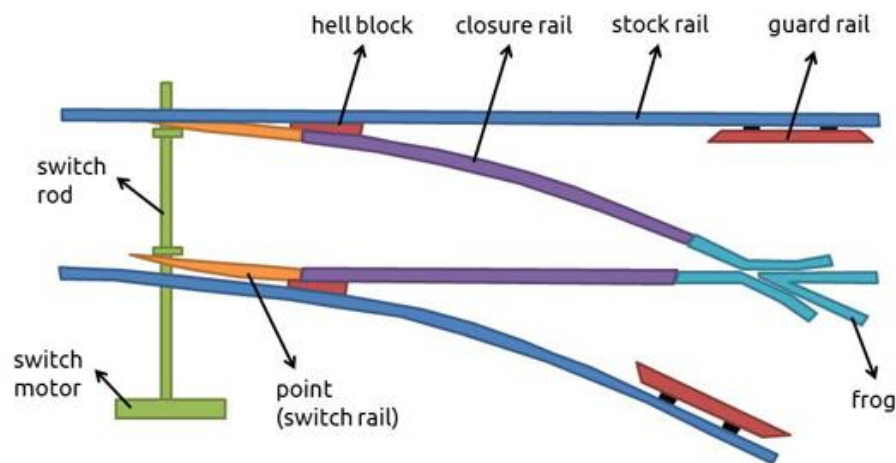


Figure 2.3 Schematic of a switch, where track in one direction converges with another. A set of points is shown in orange, showing how the asset is connected to track (Source: RailSystem, n.d.)

Switches and point asset failures can lead to signal failures, which are when trains are held at a red signal due to an issue ahead. Though less studied, signalling assets are often the greatest share of heat-related incidents by asset type across Britain’s railway infrastructure (Ferranti *et al.*, 2016, 2018). Signal failures and signalling incidents however can encompass a wide range of assets linked to track, switches, and telecommunications so the higher proportion of heat-related issues may be relative to the higher proportion of overall assets. Furthermore, signal failures are set up as a “fail-safe” system, so they are initiated before a train reaches a hazard. Signalling incident frequency is consequently not considered a high risk to railway operations (Ferranti *et al.*, 2016).

Finally, assets that supply power to electrified railways such as overhead lines and third rails can be affected by heat. While the LU network does not use overhead lines (it uses a four-rail system), heat can lead to sag due to thermal expansion, which affects the contact of the pantograph on the top of a train with the power supply from the overhead line (Palin *et al.*, 2013). On the other hand, third rail is thought to be more vulnerable to lower temperatures due to factors such as icing (RSSB, 2016a). This is exacerbated by increased exposure as third rail powered track is primarily in London and the Southeast of England. Additionally, these assets



depend on the supply of power, so should the source of power *i.e.*, a National Grid substation, be impacted by extreme weather, there is a cascading risk to train operations.

### **2.2.2. Tunnel assets**

The impact of temperatures on tunnel assets is far less studied as the impacts are assumedly far fewer – particularly on the basis that spatial variation in impact on surface assets is linked to shading or lack thereof. Given that tunnel assets are not directly exposed to outside conditions, even when tunnel temperatures are high, the risks and impacts are not comparable to the surface. An exception to this assumption would be the study of fire hazards in tunnels, as like track buckles on the surface, fire is perhaps the biggest safety risk in tunnels. Such studies review the impacts of ceiling temperatures of several hundred degrees Celsius on infrastructure that lead to structural damage (*e.g.* Mozer *et al.*, 2013). Current contributing factors affecting tunnel heat as discussed in Section 1.3.2 are unlikely to lead to fire risk.

Assets in tunnels on the LU network are otherwise the same as those on the surface. Assuming maintenance levels are the same, it is possible that asset vulnerabilities of assets such as track, switches and third and fourth rails are also similar. Greenham *et al.* (2020) identified a quadratic relationship between the frequency of tunnel asset-related delays, with increases at the lowest and highest daily maximum temperatures, but the relationship was not as profound as that of surface assets. This is indicative of some level of asset risk in tunnels to temperature. As the hazard characteristics differ to the surface, exposure may be reduced, but the extent of asset vulnerability is largely unknown.

### **2.3. Quantifying the extent of climate risk on railway assets**

As part of the national policy framework (see Section 1.5), Network Rail and TfL submitted ARP3 reports and were the only two operational railway networks to do so. These reports included risk assessments of their infrastructure to the impacts of weather and climate change. This section reviews and compares their findings in terms of climate risk quantification, with a focus on heat and temperature-related risk.

The risk assessment in Network Rail's ARP3 took a cross-cutting approach, influenced by the CCC's advice to government for the CCRA. It covers extreme temperatures, both hot and cold. The recent hot summers highlighted the vulnerabilities of GB's railway assets to high temperatures in particular (Network Rail, 2021b). Temperature risks to Network Rail assets are categorised into four types of hazards: heatwaves and extreme heat, extreme cold temperatures, higher average temperature, and sun glare. More asset types are at risk to heatwaves and extreme heat than the other three hazards, including geotechnical assets, rolling stock, vegetation, rail operations, track, signalling and overhead line equipment. Network Rail's risk scores for all temperature-related risks are moderate to major, with some expected to be severe under future climate conditions.

Network Rail quantify delays and their attribution to weather events via Schedule 8 delay compensation costs to train operating companies (TOCs) where the disruption is not the TOC's fault (Network Rail, 2023b). As such, the Schedule 8 mechanism enables the financial quantification of weather-related delays on Network Rail infrastructure. Figure 2.4 shows annual weather-related Schedule 8 costs. Damage from wind and flooding were the costliest weather events overall, and snow had a big impact in four years (coinciding with cold extremes

shown in Figure 1.8). 2013-2014 was the costliest year for weather-related delays overall, which was a year of particularly bad winter storms (see Dawson *et al.*, 2016). Total annual Schedule 8 costs also increased from around 2015, remaining higher than earlier years in Figure 2.4. As for heat, delay costs increased in recent years, but also showed some increase in relative contribution of overall costs. 2018-2019 and 2019-2020 had the greatest share of heat-related costs. Most heat-related delays also occurred in England as opposed to Scotland and Wales (Network Rail, 2021b). Network Rail’s Schedule 8 costs show how asset risk to climate is changing, owed to a potential combination of change in hazards (the climate and extreme weather), vulnerabilities (asset condition and levels of maintenance), exposure but also response.

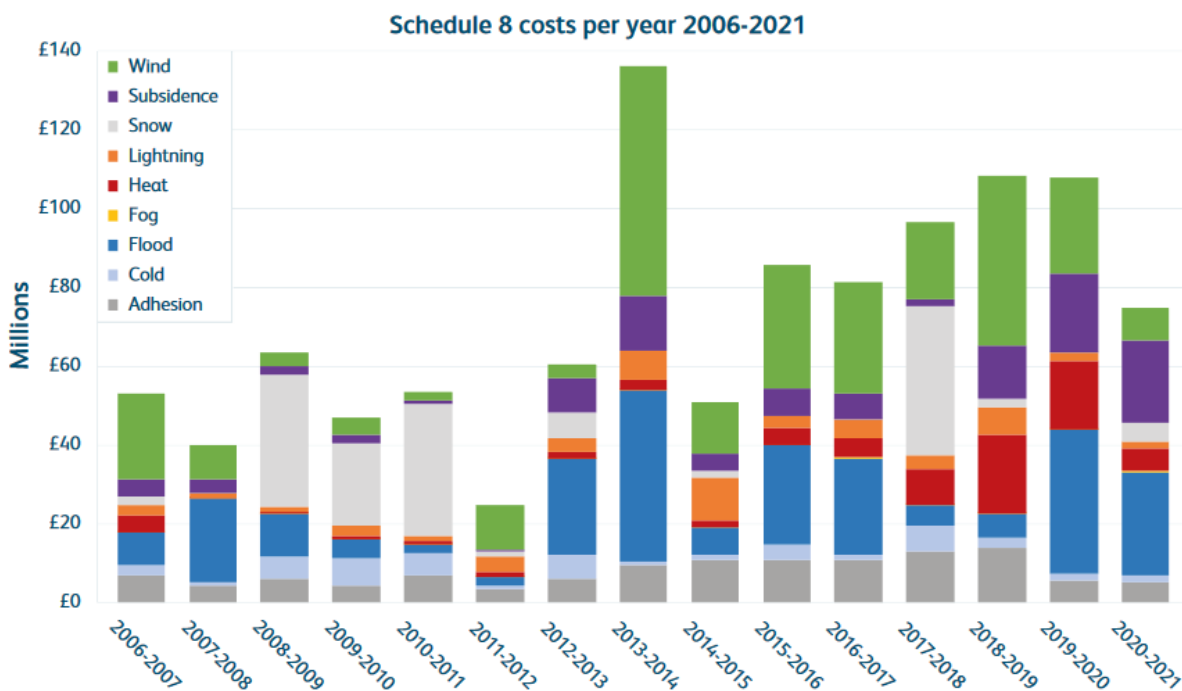


Figure 2.4 Total annual Schedule 8 compensation payments attributed to weather across Network Rail’s infrastructure. Note that these costs are not inflation adjusted but include an increase in the cost of a delay minute from around 2015 (Network Rail, 2021b)

As TfL owns and operates several transport systems across London, the risks of climate change to the LU network is only one, albeit a major component of its ARP3 (TfL, 2021b). Figure 2.5

shows the total number of risks *per* weather and climate hazard by each transport system. Although these data are not directly comparable with Figure 2.4, there are some comparisons and contrasts regarding climate risk characteristics between Network Rail and TfL.

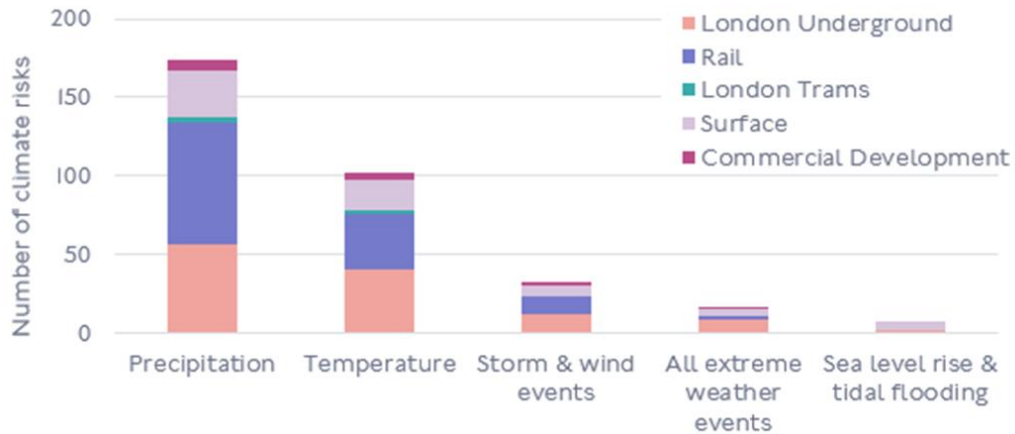


Figure 2.5 Total number of risks *per* climate hazard across TfL’s infrastructure, as identified by TfL based on best available professional judgement (Source: TfL, 2021b)

Firstly, the risk of storm and wind events in London are far lower than they are across GB. This could be explained by a lower hazard frequency, a lower vulnerability due to different assets used (*i.e.*, a fourth rail instead of overhead lines for power transmission), and a lower exposure in part due to the built-up environment protecting the city when high winds and storms do occur, as well as the proportion of the LU network running underground. However, the built environment has the potential to increase exposure at specific locations by creating wind tunnels between buildings.

Secondly, flooding is a high risk for both organisations. For the LU network, flood risk may vary because of the differing nature of the hazard (*i.e.*, more surface water flooding as opposed to fluvial flooding in some areas due to the urban environment) but could be either offset or worsened by asset vulnerabilities (*e.g.*, quality and condition of drainage assets and their capacities).

Finally, heat risk is a major risk to the LU network. The contributing factor of the UHI in Section 1.3.1 exacerbates the hazard, particularly on the surface. Similarly, the high constant tunnel temperature due to the contributing factors described in Section 1.3.2 characterises the heat hazard differently. This arguably makes this part of the LU network more vulnerable, despite a lack of sunlight exposure. However, tunnel asset vulnerabilities may be sufficiently offset if they have the capacity to withstand higher temperatures than the surface.

## **2.4. Weather and climate risk management on the LU network**

TfL are committed to ensuring the safety of its customers and staff as well as maintaining acceptable service levels in all weather conditions. The LU network utilises preventative seasonal maintenance to limit the likelihood of weather-related incidents on the LU network, and operational planning to mitigate the impact of weather-related incidents to customers. Additionally, TfL have plans to mitigate the impacts of extreme weather events (e.g., heavy rainfall, heatwaves) across the LU network. All these plans are considered by TfL as short- and medium-term in the context of weather and climate change management (TfL, 2021b). This section outlines the key actions currently in place on the LU network related to temperature, and reviews TfL's understanding of changes in temperature-related risk due to climate change.

### **2.4.1. Seasonal planning**

There is no pan-LU asset management regime for seasonal maintenance; it is driven at asset level. The overarching maintenance responsibilities primarily lie with asset managers, who set out the seasonal asset maintenance regimes, as documented in their Asset operations handbook (TfL, 2022b). Due to the variability of asset types and lifespans, the defined timescales to inspect and undertake maintenance on assets varies. For example, the schedule of inspections

for track assets ranges from maximum intervals of one to six months, or “as required”, depending on the equipment or asset (TfL, 2022i). On the other hand, the maintenance schedule for signalling assets is more stringent, with the majority of assets assigned explicit maintenance intervals between 12 and 16 weeks (TfL, 2022h). By 2050, climate change is thought to moderately affect maintenance activities across the LU, such as through increases in high temperatures and surface water flooding (TfL, 2021b).

Table 2.1 shows the key responsibilities *per* key asset team for the summer season across the LU network. Maintenance checks across the LU network in preparation for the summer are undertaken during the spring (TfL, 2022b). These maintenance activities are supported by the Hot Weather Plan (TfL, 2022f), which outlines maintenance plans conducted during the summer months. This plan also defines sections of the LU network with enhanced maintenance frequencies, suggesting that they may be sites more vulnerable to summer heat. Within these locations includes key interchange stations; sections of the Victoria and Jubilee lines following their respective upgrade and extension; and designated deep tube tunnel sections that are allocated heavy duty fans to improve air circulation in the summer.

Table 2.1 Key summer season maintenance responsibilities for each asset team across the LU network (Source: TfL, 2022b)

<b>Asset team</b>	<b>Key summer season maintenance responsibilities</b>
Stations	Provision and maintenance of air conditioning and ventilation systems before and through the season in all areas.
Signals	Removal of anti-icing compounds from air systems; adjustment of locks on pointwork.
Fleet	Maintenance of train cooling and ventilation systems prior to and through the season.
Track	Review rail stress levels, ensuring they are stress free to avoid excessive compression in heat; review point switch blades and protect vulnerable sites (for example, paint white)

Several winter maintenance activities are also specified in Table 2.2, most of which are related to the de-icing of assets. Winter checks begin during the summer (TfL, 2022b), and there is a Winter Contingency Plan which outlines further maintenance actions during the winter months (TfL, 2022e). However, there are no sections with enhanced winter maintenance frequencies; instead, there is a Core Route Strategy, that defines sections of the LU network (primarily on the surface) to be suspended should trains unable to run in extreme winter weather conditions, namely snow. TfL estimate minor levels of risk to power supply and green assets owed to low temperatures in future. However, when combined with frozen precipitation, there are additional minor and moderate risks across several other LU assets such as signalling, stations, embankments/cuttings and track (TfL, 2021b). As for the transitional seasons (spring and autumn), there are no temperature-related maintenance plans. Nevertheless, high diurnal temperature change often occurs in transitional seasons, so there are some future asset risks in these seasons. TfL identified that signalling assets were the LU asset most at risk to diurnal temperature change, classifying it as moderate (TfL, 2021b).

Table 2.2 Key winter season maintenance responsibilities for each asset team across the LU network (Source: TfL, 2022b)

<b>Asset team</b>	<b>Key winter season maintenance responsibilities</b>
Stations	Provision of de-icing materials; emergency provision of staff to assist with snow clearing; maintenance of station heating.
Signals	Provision of air system anti-icing ( <i>e.g.</i> , glycol) and maintenance of point heaters; keep track up to date on locations of failed point heaters
Fleet	Provision of de-icing equipment including de-icing fluid and sleet brushes; management of fleet ( <i>e.g.</i> , de-icing fluid levels); winterisation works including air system heating; direct current (DC) motor covers; maintenance of cab and saloon heating; de-icing depot sites including conductor rails and clearance of walkways.
Track	Provide manual de-icing techniques, tools and materials for walkways and roadways; provision of labour to clear snow and ice; manual de-icing of unheated points.

## **2.4.2. Response to extreme temperature events**

Second to surface water flooding, extreme heat events impact the most assets and receptors across the organisation (TfL, 2021b). While the overarching strategy to handle extreme hot and cold weather events are similar, this section focuses on the Hot Weather Plan due to these greater estimated risks. Furthermore, the Winter Weather Contingency plan identified 9 key risks to operations whereas the Hot Weather plan identified 13 key risks (TfL, 2022e, 2022f).

As *per* the Hot Weather Plan (TfL, 2022f), when hot weather is forecasted, TfL triggers a countdown process from three days before the anticipated heat is due to begin based on forecasts. There are four temperature thresholds (no risk, small risk, risk, and strong risk), and actions depend on which threshold is exceeded, discussed further in Section 2.6.1. Routine summer maintenance activities remain in place until three days prior to forecasted hot weather. From day three prior to the forecasted hot weather, there is a process of rapid preventative maintenance and monitoring. The extent of the actions depends on the anticipated temperature threshold for that day, so the higher the threshold, the more actions required. The plan integrates specific activities for stations, network-wide water supply, signalling assets, mechanical (ventilation) assets, track, and fleet. Should extreme hot weather exceed the strong risk threshold, senior operational staff are responsible for strategic decision-making about LU operations, including engagement with external stakeholders such as the Department for Transport, Network Rail, and the London Resilience Partnership. For example, TfL issued an advisory notification to discourage customer travel during the 40°C heat event due to the risks to the network and for customers (TfL, 2022k).

Understanding the statistical relationship between asset performance and weather events across the LU network can provide more data-driven insights into asset tolerances. This is particularly



important as the rail industry in GB had previously assumed assets were equally vulnerable to extreme weather events, which was not necessarily true (RSSB, 2016b). Therefore, the following section critically evaluates key metrics in the literature used and/or developed by railway networks and academia that correlate data between asset faults and weather observations. The intention is to assess the strengths and weaknesses of metrics' methodologies, and their relevance for the LU network in examining asset thresholds.

## **2.5. Measuring operational performance**

There are a wide range of methods to quantify and evaluate disruption to railway operations. Such disruption impacts the railway services, leading to delays for the users of the network. Delays can include instances where a train does not run to its planned schedule (is not punctual) or cancelled. Finding out the reason for a delay is known as attribution, and includes identifying the cause of the delay and the party responsible (Rail Delivery Group, 2020).

The origin, or root cause of a delay can vary. Preston *et al.* (2009) categorised delays into three sources: Operator causes (*e.g.*, train faults and shortage of crew), network infrastructure causes (*e.g.*, track and signalling faults), and external causes (*e.g.*, suicides, vandalism, or extreme weather). Across GB, inefficient and complicated delay attribution processes result in many commercial disputes and the reported “blame culture” throughout the GB railway industry, which can be time-consuming and costly (DfT, 2021). As critical infrastructure systems become increasingly connected and interdependent, attribution becomes more important to effectively monitor hazards and changing exposures and vulnerabilities, but also to help improve services.

The LU network is a high-frequency service, so it is not measured by punctuality to a scheduled timetable to the same extent as the national network. Table 2.3 provides an example of the way

trains are scheduled in terms of frequency. These frequencies change throughout the day in accordance with expected peak and off-peak travel periods. Because of the complexity across parts of the network, not all LU lines calculate a single train *per* hour metric. Nevertheless, a rate *per* km calculation is possible that normalises a metric across the LU lines. This shows that the train frequency varies across the network, highlighting the difference in demand for services in various parts of the city.

Table 2.3 Train frequency statistics in peak morning time across the LU network (Data: TfL, 2021c)

<b>LU line</b>	<b>Trains <i>per</i> hour at a.m. peak*</b>	<b>Trains in service at a.m. peak*</b>	<b>Total track length (km)</b>	<b>Train service <i>per</i> km**</b>
Bakerloo	22	31	23.2	1.34
Central	30	77	74.0	1.04
H&C	31	31	27.2	1.14
District	-	75	64.0	1.17
Jubilee	-	57	36.2	1.57
Metropolitan	16	48	66.7	0.72
Northern	-	97	58.0	1.67
Piccadilly	-	78	71.0	1.10
Victoria	36	41	21.0	1.95

\* a.m. peak time is approximately defined as 08:00 to 09:30, Mondays to Fridays, but timings may vary slightly within this timeframe by LU line. Only trains running through the Central London are shown, where data is provided. N.B. No information is available for the Waterloo & City line.

\*\* Not an official TfL metric. Derived from TfL data; calculated by dividing trains in service at a.m. peak by the total track length (km).

LU train punctuality to a schedule is arguably unimportant (Preston *et al.*, 2009), so the key terminology used by TfL to communicate when there is disruption are plausibly ambiguous. Table 2.4 shows the definitions as provided by TfL regarding service disruption. The ambiguity in definitions accounts for the difference in train frequency across the network. However, from an analytical perspective, this makes it difficult to measure operational performance quantitatively for the purposes of this study. Metrics are therefore a crucial component in

analysing operational performance and scrutinising infrastructure networks in efforts to improve their resilience to disruption. There are several different types of metrics that can be applied to quantify disruption to otherwise normal operation of a network. The following section outlines those used in the literature, including some directly involving the LU network.

Table 2.4 Definition of key terminology used to describe operational status across the LU network (Source: TfL, 2022j)

<b>Status</b>	<b>Definition</b>
Good service	Services running as expected
Minor delays	May take longer to reach destination, but do not recommend changing route
Severe delays	Service is significantly disrupted, may take a lot longer as usual to reach destination. Journey is likely to be busy and service may not travel all the way to advertised destination. Recommend changing route if possible
Suspended/ Part suspended	Line not running, either for whole or part of route, and will require using another service to finish journey
Planned closure/ Part closure	Closure as part of maintenance work or upgrades. Where possible, replacement bus services will run. Often quicker and easier to use an alternative route

### **2.5.1. Lost customer hours**

Lost customer hours (LCH) is a measure used by TfL exclusively for the LU network, calculating the reliability of the network. Any service disruption of two minutes or more in terms of time lost to customers is the threshold for logging delays. The value of LCH in each incident is weighted by factors such as day of the week, time of day, location, direction of travel, and duration of incident (TfL, 2020b). Therefore, a delay at an interchange station in central London during peak time on a weekday would generate a far higher LCH than a delay of the same length at a quieter, suburban station, late at night on the weekend. It is also important to note that public LCH reporting by TfL is not available beyond early 2020 due to the impacts of the coronavirus pandemic affecting the passenger demand data model (TfL, 2020b).

Greenham *et al.* (2020) tested the LCH metric among others to evaluate the correlation between customer delays on the LU network driven by LU assets and daily maximum temperatures. For LCH, the two variables analysed were the mean daily observed LCH and the mean delay LCH. Mean daily LCH had a strong, positive quadratic relationship with temperature, whereas mean delay LCH did not, nor was statistically significant. These contrasting LCH results challenge the metric's efficacy in quantifying heat-related delays. Furthermore, the LU delay data that LCH values derived from contained spatiotemporal inconsistencies due to subjectivity and errors in data entry by LU staff.

### **2.5.2. Delay minutes**

Delay minutes is a measure of passenger disruption based on the difference between scheduled and recorded times. Several studies, particularly on GB's national rail network analyse disruption via this metric as it can quantify the magnitude of a weather-related delay. Using delay minutes has produced extremely useful insights, some studies of which are summarised in Table 2.5. However, this metric has limitations in terms of applicability the LU network, due to the lack of timetabling (see Section 2.5). It would therefore not be possible to conduct a delay minute analysis to a similar level of precision as those undertaken in Table 2.5. This could explain, to the Author's knowledge, the fewer studies to date on weather-related delay analysis for the LU network relative to those using national railway data for GB via Network Rail.

Table 2.5 Key findings from studies that analyse weather and delay minutes across GB’s railway network

Study	Weather	Key finding
(Dobney <i>et al.</i> , 2009)	Heat	Simulated heat-related track buckling delays in the southeast increases from a £3.3m 30-year baseline, up to £24.7m in the 30-year time series for the 2080s under a medium-high emissions future climate scenario. Delay minutes are assumed to cost the network £50 <i>per</i> minute (the network mean at the time).
(Dobney <i>et al.</i> , 2010)	Heat	Using summer 2003 as weather analogue of a high emissions future summer in the 2080s, the cost of heat-related track buckling is estimated to double. Delay minutes were assumed to cost the network £73.47 <i>per</i> minute (the network mean at the time). Adjusted for inflation, a delay minute cost from 2010 in January 2023 would be approximately £103 <i>per</i> minute (BoE, 2023).
(Jaroszweski <i>et al.</i> , 2015)	Storms	Extensive delay propagation across the country identified because of flooding and landslips, causing 10,000 delay minutes from the single storm event with impacts lasting over two weeks.
(Fu and Easton, 2016)	Wind	Combining tree and wind data in a logistic regression to add value to wind-related delay data for prediction and decision-making purposes. Delay minutes helped in the exploratory analysis to identify “wind-sensitive” sections of the network (where delay minutes were highest).
(Ferranti <i>et al.</i> , 2016)	Heat	Comprehensive overview of heat-related failures in the southeast including spatial variance in delay minutes across regions (potentially due to differences in heat risk management practices); delay minutes and resulting costs are greater in signalling incidents and failures as opposed to track.
(Ferranti <i>et al.</i> , 2018)	Heat	Analysed heat-related failures on 30 <sup>th</sup> June - 1 <sup>st</sup> July 2015. All regions in GB experienced more than twice the average number of delay minutes on one or both days. Demonstrated a propagation of delay minutes across the country from critical node failures; identified delay minutes owed to preventative action such as emergency speed restrictions (>60% of delay minutes).

### 2.5.3. Average delay length

An average delay length is somewhat similar to delay minutes; calculated as the duration that a train is prevented from completing its scheduled journey, relative to the planned time it would otherwise take. TfL do not use this metric explicitly in their reporting of LU operations;

however, it is possible to calculate from delay data collected on the LU. Greenham *et al.* (2020) tested mean delay length in relation to temperature-related delays in the same way as LCH, finding a statistically significant, albeit weak, positive parabolic relationship. A similar study was conducted by Brazil *et al.* (2017) on the metro in Dublin, investigating differences between temporal trends (month of the year) and weather types (wind and/or rain) leading to delays. It found that journey times were on average 42 seconds faster under “good” weather conditions. However, this study did not investigate the underlying reasons behind the delays, so no further weather-related discussion can be interrogated. Furthermore, Börjesson and Eliasson (2011) highlight that “average delay” as an indicator of punctuality devalues the reduction of small delay risks. Applying this finding further would also imply that the gradual change in climate affecting risks to assets in operation a small degree could also be undermined by passengers or a network operator. This means that if the impact of changing weather on delays were minor, even if more frequent, they could be undervalued compared to a less frequent, considerably longer delay risk.

#### **2.5.4. Excess journey time**

Excess journey time is another passenger-focused metric, measured as the difference between actual journey time and scheduled journey time. It is akin to delay minutes but incorporates other factors beyond train-based elements that can delay a journey, to calculate total excess journey time. These include station based factors such as ticket purchase times and station closures, as well as planned engineering works (TfL, 2020a). TfL report on excess journey time for the LU network, but for the same reasons as LCH, have been unable to since early 2020.

Though not explicitly related to weather, Tsapakis *et al.* (2012) used a form of excess journey time to quantify the impact of industrial action by LU staff on its operations. However, their

analysis did not quantify excess journey times of LU network operations, rather the transport modal shift (*i.e.*, to car journeys) in response to the loss of LU services. As the study used automatic number plate recognition data to estimate excess journey time in vehicles between “strike days” and “non-strike days.” This method is replicable with other forms of monitorable data such as barrier entry and exit of passengers on the LU network, and thus can become a valuable metric to compare the potential causal effect of transport behaviours and modal shift. It is also useful in the context of weather impacts on choice of transport mode, although the response level in travel behaviour is usually greater with precipitation as opposed to temperature (Singhal *et al.*, 2014; Wu and Liao, 2020).

#### **2.5.5. Delay or fault frequency**

The number of times an asset fails or results in a delay can help identify patterns and trends leading to failure that help with attribution. Frequency-related data is less publicly reported, perhaps because it removes the customer-focused component. This is demonstrated by the presence of time-oriented metrics in research publications and data released by network operators such as delay minutes. However, frequency as a metric describes delay data in its simplest and most universal format, so it is highly valuable from the broader perspective of international benchmarking. Additionally, the relationship between frequency of delays and observed temperature on the LU network tested by Greenham *et al.* (2020) showed a strong, quadratic, and statistically significant correlation, so it justifies further investigation.

Nguyen *et al.* (2012) use fault frequency as a metric to develop a reliability assessment for heat-related failures of track, as a science-based predictor model had not previously existed. This is important in the context of track buckle risk as the network operators aim to limit occurrences to zero – a metric of frequency – due to the scale and magnitude of potential impacts. Similarly,

Ferranti *et al.* (2016) derived fault frequency data on Network Rail's assets from delay minute data, showing the proportion each asset's heat-related failure frequency as well as weekly incident rates.

Ferranti *et al.* (2016) also demonstrated "failure harvesting" across Network Rail assets in the southeast of England via fault frequency data. Failure harvesting is an occurrence whereby an infrastructure system's resilience to temperature increases over the course of the summer season, as failed assets and equipment are replaced (Chapman *et al.*, 2008). As a result, there are two additional factors to consider around heat-related failure. Firstly, it draws out early season heat as a key risk period to railways as opposed to exclusively peak summer temperature, which could impact summer maintenance scheduling. Secondly, it hypothesises that in the longer term, failure rates in future summers during peak maximum temperatures would begin to reduce. However, this study did not include future climate change data within the study parameters. In a future climate where maximum temperature records are broken further, it becomes less certain whether failure harvesting could in fact improve infrastructure resilience in future.

Oslakovic *et al.* (2012, 2013) conducted broader studies that combined fault frequency data attributed to temperature with climate projections for two railway tracks in The Netherlands. Fault frequency data was useful as it complemented the climate projection data used, compiled as estimated frequency distributions of days at temperature intervals *per* future climate change scenario. The baseline, which used total observed incidents as a function of temperature underpinned the estimated future fault frequencies for each scenario. However, this method only presents aggregated results for the study area, which, for these studies is reasonable as the study area is small, compared to that of a whole network. A network like the LU, with its



different network types and spatial temperature variances would require a level of disaggregated analysis to provide meaningful results for TfL.

Fisher (2020) addressed some of the limitations in earlier fault frequency studies through their methodological approach to quantify asset vulnerability to weather across Network Rail's infrastructure. The primary element added to the analysis was to integrate a normalisation factor; creating a fault exposure rate, which consequently eliminated spatial bias. Normalisation was necessary for the scale of the study due to spatial variances in weather, as it covered areas in Network Rail's most geographically northern and southern routes in England. The network was split into smaller grids, with the fault frequency of each grid divided by the respective frequency of weather parameters. The resulting fault exposure rates statistically improved results on the relationship between railway assets and weather conditions, but there are limitations considering extreme weather observations. Because extreme weather is so infrequent, a sample study period is not necessarily representative of these events, which is challenging for scaling fault exposure rates based on future climate change scenarios. There is a gap in research to date regarding how to represent extreme weather fault frequencies more accurately in the absence of sufficient data, especially as this tail data becomes more important to estimate the impact of future climate change.

#### **2.5.6. Fragility curves**

The term "fragility curve" is also applicable to coupled weather and asset analysis using frequency data. Fragility curves originated from seismic risk assessments at nuclear power stations (*e.g.*, Kennedy *et al.*, 1980) but more recent studies tested this method with other infrastructure sectors and hazards. As such, they are usually plotted with similar variables to other fault frequency-related studies, such as an integer bin for weather variables with fault

frequency, which also may be normalised to some extent. The fragility curve itself could comprise the line of best fit for the underlying data or a more complex mathematical approach to build the curve. Trends could be logistic or exponential, depending on the parameters used.

Studies conducted by Martinović *et al.* (2018), Martello *et al.* (2022), and Nieto *et al.* (2022) are examples of how fragility curve analysis worked within the transport sector. Martinović *et al.* (2018) developed fragility curves to predict the likelihood of slope embankment failures on a railway network caused by rainfall duration; Martello *et al.* (2022) estimated levels of damage on metro network assets based on saltwater flood depth; while Nieto *et al.* (2022) presented fragility curves for road embankments adjacent to different types of debris flow. Interestingly, none of these studies developed their fragility curves with industry fault data. Martinović *et al.*, (2018) and Nieto *et al.* (2022) focused on cascading and interconnected risks of a weather hazard causing another hazard before leading to a rail-related fault. As a result, industry fault data was not required. Their resulting fragility curves depended on technical knowledge of the landscape and existing literature to formulate a curve from a mathematical equation. On the other hand, Martello *et al.* (2022) conducted a survey that explored the tacit knowledge of key stakeholders such as professionals in infrastructure operations, and the results formed the fragility curves. There were some high levels of conformity among respondents at the asset scale of fragility curves, suggesting that utilising expert knowledge in conjunction with fault data to understand the relationship between weather events and infrastructure has significant value for a network like the LU.

Adding spatial data to fragility curve analysis can also refine them further (Dunn *et al.*, 2018). This is particularly important to consider for a network like the LU with different network types and spatial variance in temperatures. While Dunn *et al.* (2018) focused on the impacts of wind

on infrastructure in the energy sector, the methodology in principle is applicable to the transport sector. On the other hand, the reason for the high levels of accuracy was arguably because of the quality and quantity of data – covering 776 individual windstorms over a seven-year period. Compared to extreme heat events in a similar period for the UK, windstorms occur more frequently. Therefore, there were more wind frequency exposure data and hence greater inferred confidence in their findings and could prove more challenging to test with other, less frequent weather parameters.

A broader characteristic of fragility curves is that they form one of two parts of resilience, where the other half is the time to repair a failed asset (Dunn *et al.*, 2018). The fragility curve metric is therefore a valuable concept that improves fault frequency analysis, bridging the gap towards achieving a more holistic metric to measure network resilience.

### **2.5.7. Quantifying resilience**

The concept of measuring resilience as a metric by means of monitoring progress in climate change adaptation is rapidly gaining more attention internationally. However, universally defining resilience is difficult as it is multi-faceted and context specific. Consequently, a resilience-based metric cannot comprise a “one size fits all” approach. During COP26 in Glasgow, UK in November 2021, the UN-backed Race to Resilience global campaign was launched to catalyse a step-change in global ambition for climate resilience (UNFCCC, 2022). Race to Resilience (2021) define five different ways of working towards and tracking resilience; through a human-centric outcome, engaging at the company, country/region, individual/community, city, and natural system levels. Climate resilience of the LU network fits into this campaign. London belongs to the C40 cities organisation, who are part of the collaborative effort in the Race to Resilience 2030 target to expand affordable resilience public

transport (Race to Resilience, 2022). TfL are currently in the process of scoping and developing climate resilience metrics and have made particular progress with flood-related risk to date (TfL, 2021b).

D’Lima and Medda (2015) designed a resilience metric and applied it to the LU network, based on how fast the network recovers to its equilibrium state following a shock or disruption. Though not a climate-focused approach, the theory is useful from a risk perspective as the shock characteristics (*i.e.*, scale of risk) can be modelled to represent different extents of hazard, vulnerability, and exposure. Because the underlying data for this study is passenger-oriented, however, the method does not connect with the earlier stage of impact to infrastructure before it impacts train operations and consequently, the passengers. Applying this approach to infrastructure would require quantifying the resilience parameters to several assets or asset groups, which is more complex than the representation of resilience through passenger numbers.

Alternatively, Pant *et al.* (2016) took an asset-related approach to vulnerability with the potential to inform levels of resilience. It combines asset and passenger data to quantify impact magnitudes from multiple failure conditions (*i.e.*, interdependencies) for Network Rail’s key asset groups. Particularly useful findings from this study were that assets comprising signalling functions for the railway network were likely to cause the most passenger disruption, even where a small percentage of the assets were removed. Similarly, electricity as an infrastructure sector was most likely to cause the most passenger disruption. This was also followed by information communication technology (ICT), and both were the only infrastructure sectors likely to result in 100% passenger disruption across the railway network should their link to the national railway network be completely removed.

Both studies by D’Lima and Medda (2015) and Pant *et al.* (2016) demonstrate the complexity and idiosyncrasies in developing resilience metrics. While TfL are in the early stages of scoping resilience metrics for climate change, they lack a comprehensive baseline to build and develop them from (TfL, 2021b). It is arguably more prudent to establish baseline data with less complex metrics and build towards forming the appropriate resilience metric for climate change.

## **2.6. Temperature thresholds**

The outcome of metrics that measure operational performance with weather data is that they enable network operators to identify the thresholds of a weather parameter that could lead to asset failure and subsequently, delays across the network. A threshold would be the highest or lowest value of a weather parameter considered acceptable for safe network operations. Exceeding a threshold value would therefore be a risk to normal operations. Thresholds vary from place to place, due to variance in risk characteristics. For example, the railway track in Melbourne, Australia is considered stress neutral between air temperatures of 33°C and 44°C (Nguyen *et al.*, 2012), whereas for GB track owned and operated by Network Rail, it is usually around 27°C (Dobney *et al.*, 2010). The climate varies greatly between Australia and the UK, so the infrastructure design thresholds for heat are greater in Melbourne, and trains can consequently operate safely under higher temperatures. These thresholds do not, however, apply to all assets. Track is the primary focus of temperature thresholds, because as previously discussed, track failures carry an extremely high risk to railway operations. Consequently, there are knowledge gaps pertaining to the thresholds of non-track assets, and the impacts of climate change upon future risk and acceptable thresholds.

### 2.6.1. LU network thresholds

The LU network has pan-network thresholds, defined in the Hot Weather Plan and Winter Weather Contingency Plan (shown in Figure 2.6). Forecasts and weather observations tailored to the LU network underpin the current threshold parameters, data of which are collected from weather stations at several LU depots and sidings. However, thresholds are based on surface air temperature and are not reflective of tunnel temperature. Cold temperatures are also not explicitly defined quantitatively by risk, though rail snow may imply temperature by proxy to some extent. Rail ice risk is mentioned in the Winter Weather Contingency Plan, though not quantified; rather whether types of ice or frost are present or not. TfL’s ARP3 does mention these plans briefly as part of short- and mid- term resilience planning in its Appendices.

	No risk	Small Risk	Risk	Strong Risk
High temperatures	< 24°C	24°C - 26°C	27°C - 30°C	> 31°C
Rail snow	No settling snow	0 - 2cm	2 - 5cm	> 5cm

Figure 2.6 Key defined weather thresholds across the LU network according to the Hot Weather Plan and Winter Weather Contingency Plan (Adapted from: TfL, 2022f, 2022e)

### 2.6.2. Changing thresholds under future climate change

The LU network faces, like many other railway networks around the world, uncertainty in the extent that climate change may disrupt the relationship between current levels of network performance and extreme weather events, shifting thresholds. Future climate change may limit the efficacy of current maintenance practices and operational response to extreme weather events, so they will require periodic updates. Several risk factors are likely to play a role. While it is well understood in literature that hazards are worsening, vulnerabilities may also increase across assets owed to accelerated aging (Jelle, 2012; Tang *et al.*, 2018; Athanasopoulou *et al.*,

2020), or not meeting the required level of asset maintenance. There is an increasingly urgent need to understand potential change in risk, so that network operators like TfL can adequately prepare for future climate change.

## **2.7. Chapter summary and research justification**

This chapter reviewed TfL’s understanding of climate change and practices in managing operations during extreme temperatures across the LU network, while also critically reviewing methodologies of metrics used in recent research. Risk response by TfL is based on a threshold exceedance, like Network Rail (Fisher, 2020). Metrics applied in research also define thresholds, but most metrics used by TfL for the LU network described in this section are customer-focused for safety reporting reasons, but this has several implications for measuring weather and climate resilience of LU assets. Customer-focused metrics exclude a proportion of faults that may not affect operational services, leading to an oversight of important asset risks due to data bias. As customer-focused metrics require conversion processes derived from fault observations, resulting weather-asset relationships are limited due to the additional processing. Additionally, the impacts of the coronavirus pandemic showed first-hand how sudden change and/or loss in “normal” passenger levels severely affects the efficacy of customer-focused metrics for their intended purpose. Relying on such a metric to underpin weather thresholds for the LU network for decision-making would therefore have shortcomings now and in future.

Taking data-driven approaches is TfL’s aim in improving the resilience of LU infrastructure to weather and climate change (TfL, 2021b). Doing so would benefit TfL as it supports fact-based decision-making; organisational transparency; enhanced collaboration opportunities; and bias reduction (International Transport Forum, 2021). Currently, TfL largely rely on expert

professional judgement and tacit knowledge to understand their weather and future climate risks (TfL, 2021b), which is a similar situation to Network Rail and the wider railway infrastructure across GB (Fisher, 2020). This study sets out to test an objective, data-driven approach for temperature-related risk parameters across the LU network that are of substantial interest to TfL and its stakeholders. In doing so, the intent is to demonstrate where and how existing data can support current TfL practices for climate change adaptation purposes. The approaches and techniques are synthesised from several studies with the view to meet the needs of TfL and the LU network: improving near- and long-term future climate resilience.



# Chapter Three | Methodology

## 3.1. Chapter overview

Chapter Two reviewed the current approach by TfL in responding to climate change and extreme weather events with regards to temperature. It then critically evaluated the current literature on metrics that measure network performance, from the perspective of their use to identify performance thresholds against weather conditions and identify the most appropriate metric for this study. This chapter therefore presents the detailed methodological approach used to quantify the impact of heat and climate change to LU’s infrastructure. The structure of this chapter reflects the order of steps undertaken and the linkages between these steps, divisible into four key sub-sections (also reflective of the three results chapters), shown in Figure 3.1.

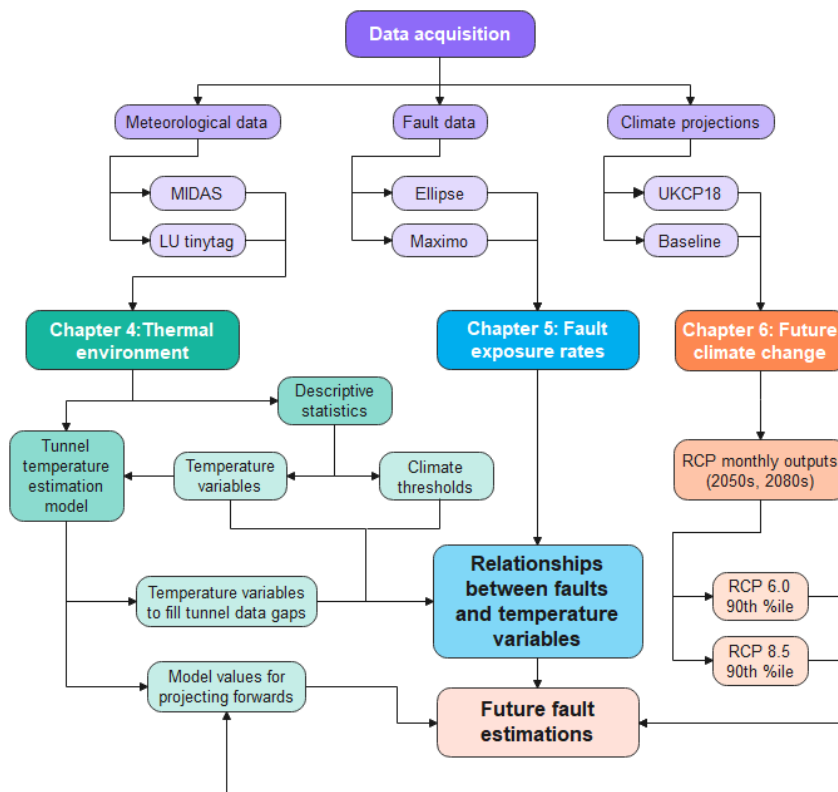


Figure 3.1 Linkages between stages of methodology for this study. Key results are emphasised in bold.

This chapter is formed of several sections that outline each process of this study in sequential stages. Firstly, Section 3.2 describes the data acquired for this study, and their spatial and temporal parameters. Section 3.3 then describes the methodological approach to analyse the thermal environment across the LU network. Section 3.4 describes the fault exposure rate process which investigates the relationship between LU fault data and different temperature variables calculated from Section 3.3. Finally, Section 3.5 outlines the approach to incorporating climate projections into the study parameters to define future temperature scenarios for the LU network and the impact that this may have on the frequency of faults.

## **3.2. Data acquisition and parameters**

This study used a range of secondary data derived from several sources. Table 3.1 describes these data, their parameters and the quality assurance processes conducted prior to analysis. Meteorological and climate projection data were compiled from online repositories via the UK Met Office, while TfL provided tunnel temperature and fault data explicitly for the purposes of this study. All observation data collected span a 13-year calendar period from 2006 to 2018 inclusive. This is because 2006 is the earliest point where TfL collected all relevant data relevant for this study.

Table 3.1 Details of data used for this study

<b>Data</b>	<b>Description and source</b>	<b>Timeframe</b>	<b>Data intervals</b>	<b>Spatial extent</b>	<b>Total no. of observations</b>	<b>Quality assurance process</b>
Surface temperature observations	Met Office Integrated Data Archive System (MIDAS), via the Centre for Environmental Data Analysis (CEDA) website (Met Office, 2019a)	2006-2018	Hourly	Single site (St. James's Park)	112582	1.2% of the total dataset had missing observations. Days without any observations for the 24-hour period were eliminated from analysis
UHI index	Simulations of the urban climate model UrbClim (De Ridder <i>et al.</i> , 2015) in raster format by the European Environment Agency and Copernicus Climate Change Service (2020)	2008-2017	N/A	100m resolution over London	1	Projected to UK coordinate reference system to validate spatial conformity to the Greater London administrative boundary and the LU network. Any stations outside of the UHI raster boundary applied the UHI index of the nearest station on its respective LU line within the raster boundary
Tunnel temperature observations	Provided directly by TfL	2006-2018	Hourly	Tunnel station platforms (sub-surface; deep tube tunnels)	6286808	14.5% of full days' data observations missing across all stations, to be combined with results from the tunnel temperature estimation model
LU fault data (known as work orders)	Provided directly by TfL	2006-2018	Variable	Whole LU network	45787	Discussed in Section 3.2.3
LU asset information	Provided directly by TfL	2006-2018	N/A	Whole LU network	12507	Discussed in Section 3.2.3
Baseline climate	Land observations by administrative region, via the UKCP18 Climate	1981-2010	Monthly	Greater London administrative boundary	3 x 240 (min, mean, max)	Observations pass through a range of quality assurance processes by the Met Office (Lowe <i>et al.</i> , 2019)

<b>Data</b>	<b>Description and source</b>	<b>Timeframe</b>	<b>Data intervals</b>	<b>Spatial extent</b>	<b>Total no. of observations</b>	<b>Quality assurance process</b>
	Projections User Interface (Met Office, 2018c)					
UKCP Probabilistic Projections	UKCP18 Climate Projections User Interface (Met Office, 2018c)	2050s, 2080s	Monthly	Greater London administrative boundary	3 x 999 sample (min, mean, max) <i>per</i> scenario	The Met Office conduct checks and continually add to and update the projections data (Met Office, 2023b)

### **3.2.1. Key study parameters and boundaries**

The core geographic study boundary are the termini stations of each LU line, inclusive of depots and sidings that follow termini stations. Most of the LU network falls within the Greater London administrative boundary that encompasses all 32 London boroughs. Due to the varied infrastructure across the LU network, this study grouped data and analyses based on several parameters, with the intent to investigate or explain trends, as well as potential anomalies. Data groupings are spatial, with the justifications for each grouping in the following sections.

#### **3.2.1.1. Network type**

The network is divisible into three core physical characteristics (hereinafter defined as LU “network type” or “part” of the LU network) based on the location of track in the context of geology, which are the primary breakdown of analyses: surface, sub-surface and the deep tube tunnels (also described as “tunnel” in the results), as shown in Figure 3.2. Grouping by network type is important because they differ in terms of environmental exposures, and the additional contributing factors upon temperature, *per* Section 1.3. The surface part is primarily the outer part of the LU network, which are typically the suburban zones of Greater London. The sub-surface part runs around inner London, closer to the city centre. The deep tube tunnels, while running through the city centre, also extend further out of the city centre than the sub-surface section. Most of the LU network resides north of the River Thames, with some exceptions. The Bakerloo, Northern and Victoria lines tunnels run beneath the River Thames to the south. The Jubilee line extension tunnel crosses beneath the River Thames three times, though both termini are north of the river. Two parts of the District line pass over the River Thames via the Fulham and Kew Railway Bridges in the southwest of Greater London.

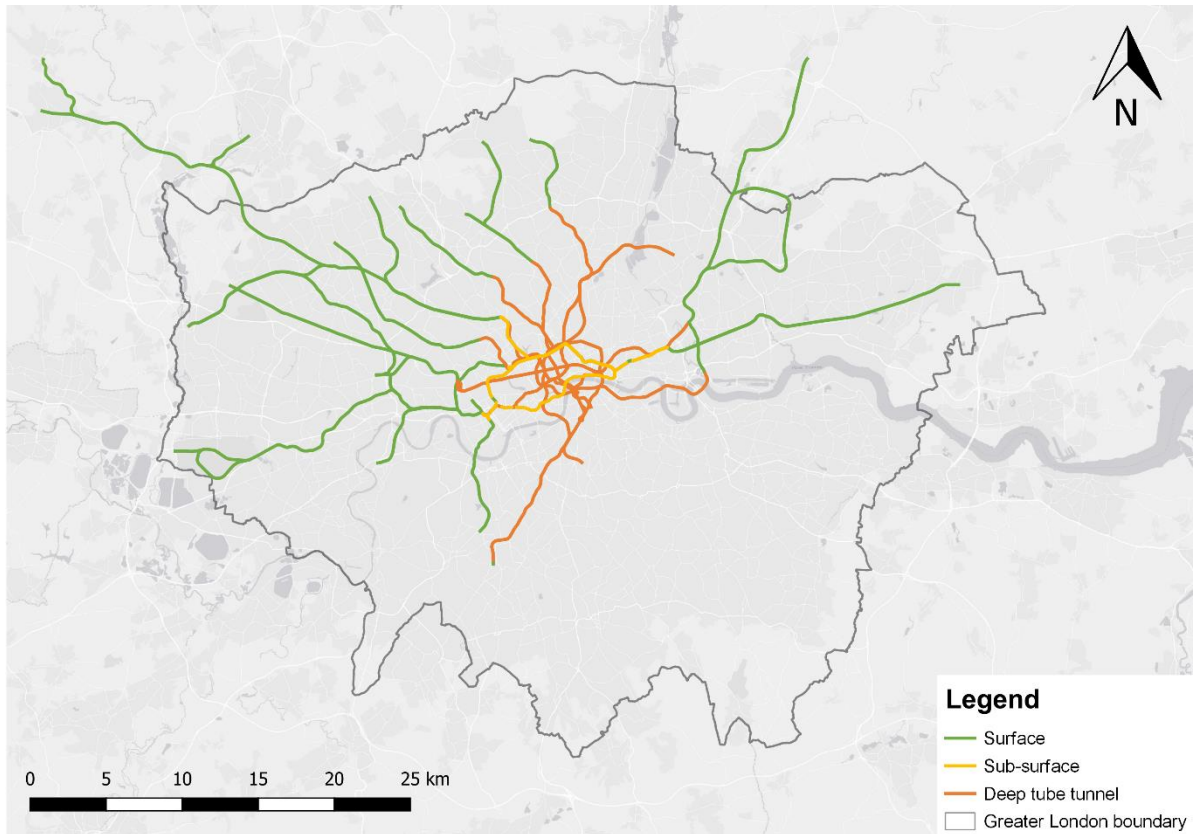


Figure 3.2 Division of LU network by network type

### 3.2.1.2. LU line

LU line is an important factor for data grouping. LU lines have different historical features as they were originally built by several private organisations (Halliday, 2013). Furthermore, LU network operations, asset renewals and engineering works are managed at line level, varying asset ages across the network. Examples include different rolling stock across each LU line and five different signalling systems (TfL, 2016b). Grouping by LU line ensures the outcomes of this study can support line-level decision-making.

At this stage, there was some further elimination of data in the study. The tunnel sections of the Hainault loop on the Central line and the Heathrow loop on the Piccadilly line, as these sections' platform temperature are not monitored and are cooler than the tunnels through the central part

of the LU network (Jenkins *et al.*, 2014). The Waterloo & City (W&C) line was also excluded, as it comprises a very short tunnel with two termini stations only, so is not comparable with the other LU lines.

### 3.2.1.3. Direction of travel

This study also grouped results by direction of travel of the trains across the LU network. This is because track is not shared by trains between direction of travel, and therefore there are separate assets for each direction. Additionally, the deep tube tunnels, and some of the sub-surface parts of the LU network operate through separate tunnels (see Figure 3.3). Therefore, there are differentiations in the piston effect between tunnels and stations (Pan *et al.*, 2013), particularly regarding distance from tunnel openings, resulting in an impact on tunnel temperatures. Table 3.2 shows the directions of travel allocated to each LU line, which are northbound (NB), southbound (SB), eastbound (EB), westbound (WB), clockwise via the outer ring (OR) track, or anticlockwise via the inner ring (IR) track.

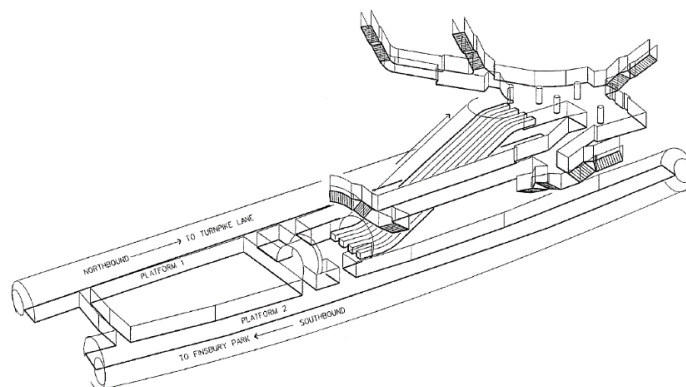


Figure 3.3 Axonometric drawing of Manor House station, Piccadilly line, showing the deep tube tunnels separated by direction of travel (Source: TfL, 2017a)

Table 3.2 Travel direction of LU lines referred to in this study

<b>LU line</b>	<b>Directions of travel</b>	
Bakerloo	NB	SB
Central	EB	WB
Circle	IR	OR
District	EB	WB
H&C	EB	WB
Jubilee	EB	WB
Metropolitan	EB	WB
Northern	NB	SB
Piccadilly	EB	WB
Victoria	NB	SB
W&C	NB	SB

### **3.2.2. Temperature observation data**

There were two secondary sources of temperature and meteorological data obtained for this study: from the UK Met Office; and that collected by TfL, described in Table 3.1. Multiple sources were necessary to gain a comprehensive understanding of the temperature ranges across the network types, LU lines and direction of travel.

#### **3.2.2.1. Surface temperature observations**

There are 21 Met Office weather stations within the Greater London boundary, with data over different time intervals recording a range of meteorological variables, including daily or hourly rain, daily or hourly surface temperature, mean wind, radiation, and soil temperature. Only four weather stations have continuous observations for the selected study period between 2006 and 2018. Their source identification (SRC ID) codes are St. James Park (SRC ID 697), Heathrow (SRC ID 708), Northolt (SRC ID) and Kew Gardens (SRC ID 723). Figure 3.4 shows the location of these weather stations in the context of Greater London and the LU network. The



St. James's Park weather station is most central geographically in Greater London of the four weather stations, while the others are located further to the west, which infers data bias to the west of London. There may also be data bias at the Heathrow weather station in particular as while the site is the most open, its observations may also be influenced by aircraft and vehicle activity (Grimmond, 2013).

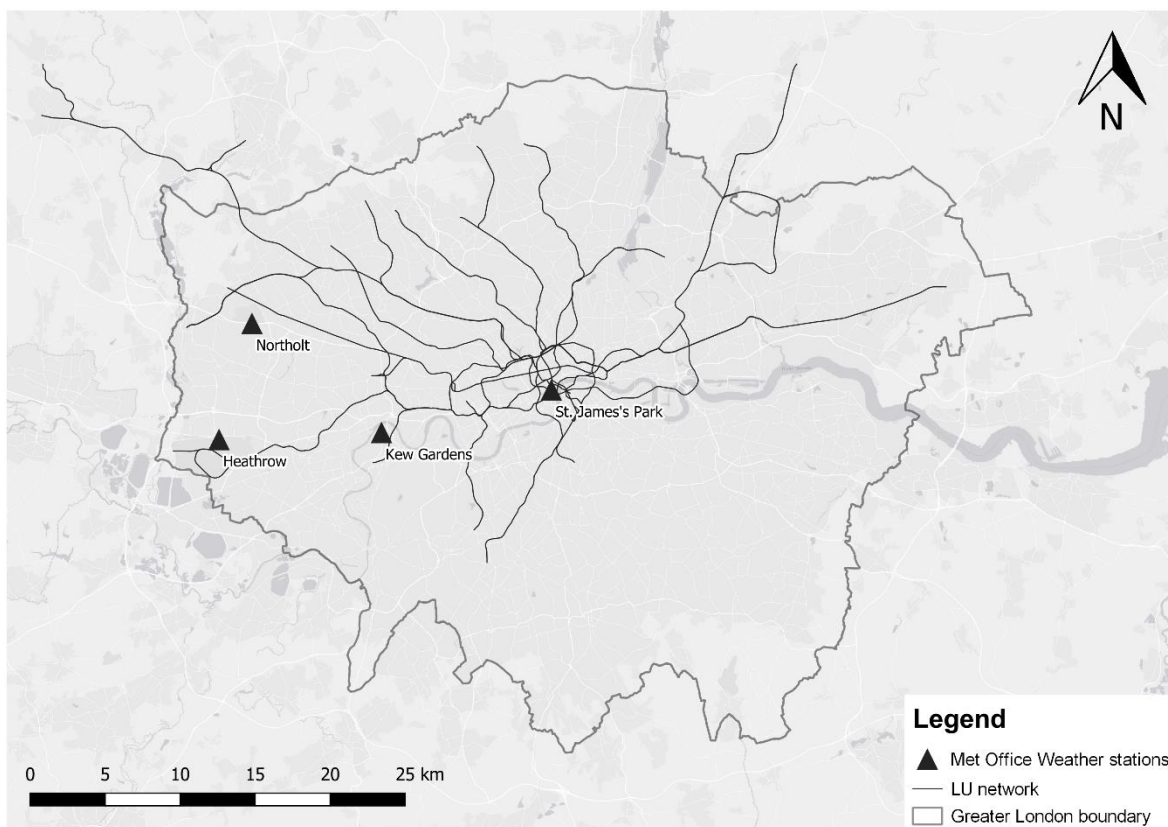


Figure 3.4 Met Office weather stations within the Greater London administrative boundary

The St. James's Park weather station's location is at coordinates 51.504 latitude, -0.129 longitude and is 5m above mean sea level (Met Office, 2021b). According to the Met Office, (2019a) MIDAS User Guide, the weather station's thermometer sits in a screen, out of direct sunlight, and 1.25m above the ground. Data collection at the weather station is automatic with a resolution of 0.1°C, and accuracy of  $\pm 0.2^\circ\text{C}$ . Thermometer calibration takes place every 8 years.

### 3.2.2.2. Spatial extrapolation of surface temperature using the urban heat island index

As described in Section 1.3.1, Greater London, like all major urban areas has an UHI. Its intensity varies across the city, decreasing towards the outer edges of the administrative boundary. Therefore, the St. James's Park observations, located in the city centre, are not representative of the temperature at other surface stations across the LU network, particularly in the suburban and less densely built-up parts of the city. To address this, a UHI index was applied to the St. James's Park observations to extrapolate temperatures across stations on the surface part of the LU network. Temperature variables were adjusted according to the UHI index *per* surface station to the nearest 100m, better reflecting the spatial distribution of temperature across the city. At the station level, the accuracy of fault exposure rate analysis (see Section 3.4) would thereby be improved.

Table 3.1 describes the UHI index used in this study, and Figure 3.5 shows the UHI index across London in the context of the Greater London administrative boundary and the LU network, at a 100m resolution. Extrapolating temperatures at other LU stations using the UHI index firstly required the value of the grid square that intersects St. James's Park weather station, which was +2.1°C. LU stations are the selected georeferenced points for spatial analyses across the LU network; this required the UHI index grid square values that intersect each LU station. For each LU station, correcting for UHI index required subtracting the difference between UHI index values at St. James's Park and the respective LU station from the temperature observation at St. James's Park weather station as follows:

$$t_{station} = t_{St.James} - (2.1 - UHI_{station}),$$

where  $t_{station}$  is the extrapolated temperature at the LU station,  $t_{St.James}$  is the observed temperature at St. James's Park weather station, and  $UHI_{station}$  is the UHI index of the grid square that the LU station is located.

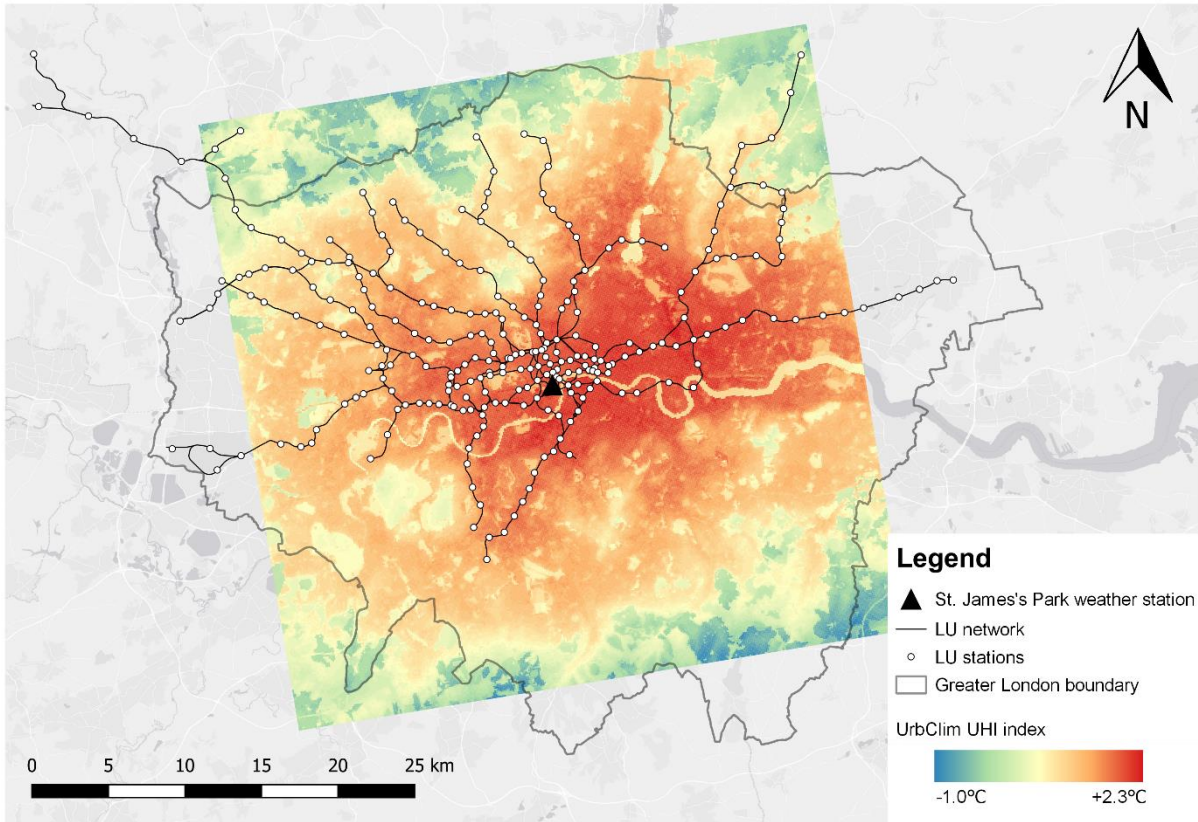


Figure 3.5 The UrbClim UHI index for London used in this study, in the context of the LU network and all stations

There are also 18 LU stations outside of the UHI index map. Referring to the interactive map of London available at the Urban Climate Service Centre (which extends beyond the boundaries of Figure 3.5 for a single summer), these 18 stations UHI intensity values do not deviate far from neighbouring stations within the boundaries. The inference for these stations is therefore to use the same UHI intensity of the nearest station on its respective operating line within the boundary of Figure 3.5.

To validate this approach, 20 sampled daily  $t_{mean}$  values from Kew Gardens and Northolt weather station observations within the study period were compared with derived daily

$t_{mean}$  calculated using the UHI extrapolation from the previous equation. In this case,  $t_{station}$  is the extrapolated temperature at the respective weather station,  $t_{St.James}$  remains the observed temperature at St. James's Park weather station, and  $UHI_{station}$  is the UHI index of the grid square that the weather station is located. As the UHI index at Kew Gardens is +1.1°C and for Northolt it is +0.1°C, using St. James's Park observations would overstate temperature variables, as the sampled weather station  $t_{mean}$  showed that both Kew Gardens and Northolt were on average 0.9°C lower than at St. James's Park. Using the UHI index calculation for the 20 randomly sampled days, the resulting daily  $t_{mean}$  values for Kew Gardens and Northolt were on average 0.6°C lower than daily  $t_{mean}$  derived from weather station observations, with a standard deviation of 0.8°C. The UHI calculation was more accurate at Kew Gardens where the difference was -0.1°C on average compared with -1.1°C at Northolt. Overall, the UHI calculation adjusted the  $t_{mean}$  at Kew Gardens and Northolt to align more closely (albeit slightly lower in some cases) to its respective weather station.

### **3.2.2.3. Tunnel platform temperature observations**

Since 2006, TfL have been recording temperature and relative humidity within the tunnel and sub-surface parts of the LU network using Tinytag TGP-4500 data loggers (Tinytag, 2019). The loggers are positioned across station areas such as platforms, concourses, and ticket halls. This study only used loggers positioned on the station platforms. These are mounted securely to the platform wall, one metre above platform floor, at the tail end of each platform. Data from the other loggers located on concourses and ticket halls, were not required for this study of tunnel temperatures, and were removed from the data prior to analysis, leaving one logger used *per* station platform. The loggers across the network collect the hourly mean, minimum and maximum temperature, and relative humidity *per* hour. The temperature observation resolution

is at 0.01°C and accuracy is around or slightly below  $\pm 0.5^\circ\text{C}$ , and most accurate between 20-30°C, shown in Figure 3.6.

The accuracy of temperature on the Tinytag loggers is important as LU tunnel temperature ranges are smaller than the surface. While the accuracy of observations at St. James's Park weather station are slightly better, more loggers across the LU network are necessary to capture the variance in temperature across the network. Therefore, the deployment of cost-effective sensors by TfL ensures conformity across the station platform observations, though at the expense of slightly less accurate measurements. Nevertheless, station platform observations across the LU network typically fall within the range where the loggers' accuracy is best, so the readings they capture are considered suitable for the purposes of this study.

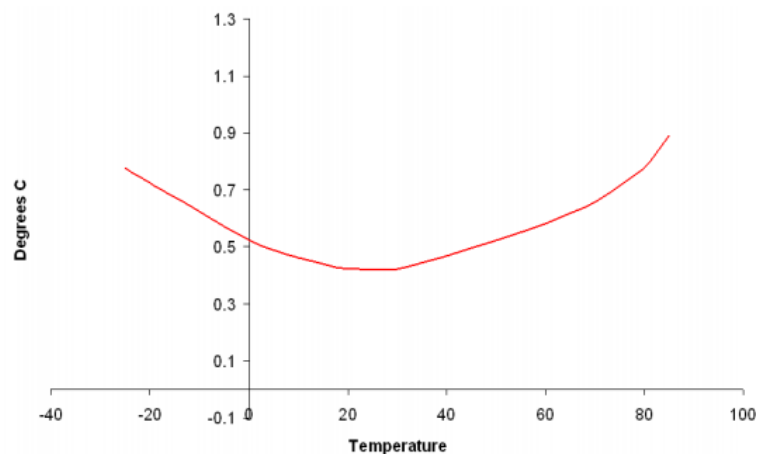


Figure 3.6 Temperature observation accuracy of the Tinytag loggers used across the LU tunnel station platforms (Source: Tinytag, 2019)

### 3.2.3. LU asset fault data

TfL provided internal data on assets and faults maintenance for this study. These data provided were a database of asset information, and a database comprising a log of any corrective or reactive maintenance or repair work to LU assets, known as work orders (WOs; also defined interchangeably as faults throughout this study). Corrective maintenance work is defined by

TfL as “faults that you find”, typically identified through other maintenance activity and then repaired outside of routine servicing, whereas reactive maintenance work is defined as “faults that find you”, in that they are service disruptions identified while equipment is in operation (TfL, 2022c). These data originate from two asset management systems, Ellipse and Metro Maximo, because of the public-private partnership contracts for maintenance on different LU lines in place prior to TfL taking responsibility of the LU network in 2003. Each system contains similar information, and Table 3.3 shows which system each LU line uses.

Table 3.3 Asset management system used for each LU line at TfL within the study period

<b>LU line</b>	<b>Asset management system</b>
Bakerloo	Ellipse
Central	Ellipse
Circle	Ellipse
District	Ellipse
Hammersmith & City	Ellipse
Jubilee	Metro Maximo
Metropolitan	Ellipse
Northern	Metro Maximo
Piccadilly	Metro Maximo
Victoria	Ellipse
Waterloo & City	Ellipse

### **3.2.3.1. Study asset group**

This study considers the asset subgroups of points and train stops, with the details shown in Table 3.1. Points are track junctions, (see Figure 2.3), and train stops, also known as trip stops or tripcocks are devices on tracks that automatically stop a train if necessary. These assets were selected because they are an intersection between signalling and track assets, which are both vulnerable to operational failure under high temperatures across the LU network (Greenham *et al.*, 2020) and the wider, national railway network (Ferranti *et al.*, 2016). It was also the asset

group suggested by TfL for this study following consultation with them. These asset subgroups are also suitable for spatial analysis for the asset location is fixed and identifiable. Figure 3.7 shows the asset hierarchies of Ellipse and Maximo. While there are differences in descriptions at asset level, the broader groupings are similar, implying both systems capture the same assets and therefore can be combined for aggregated analysis.

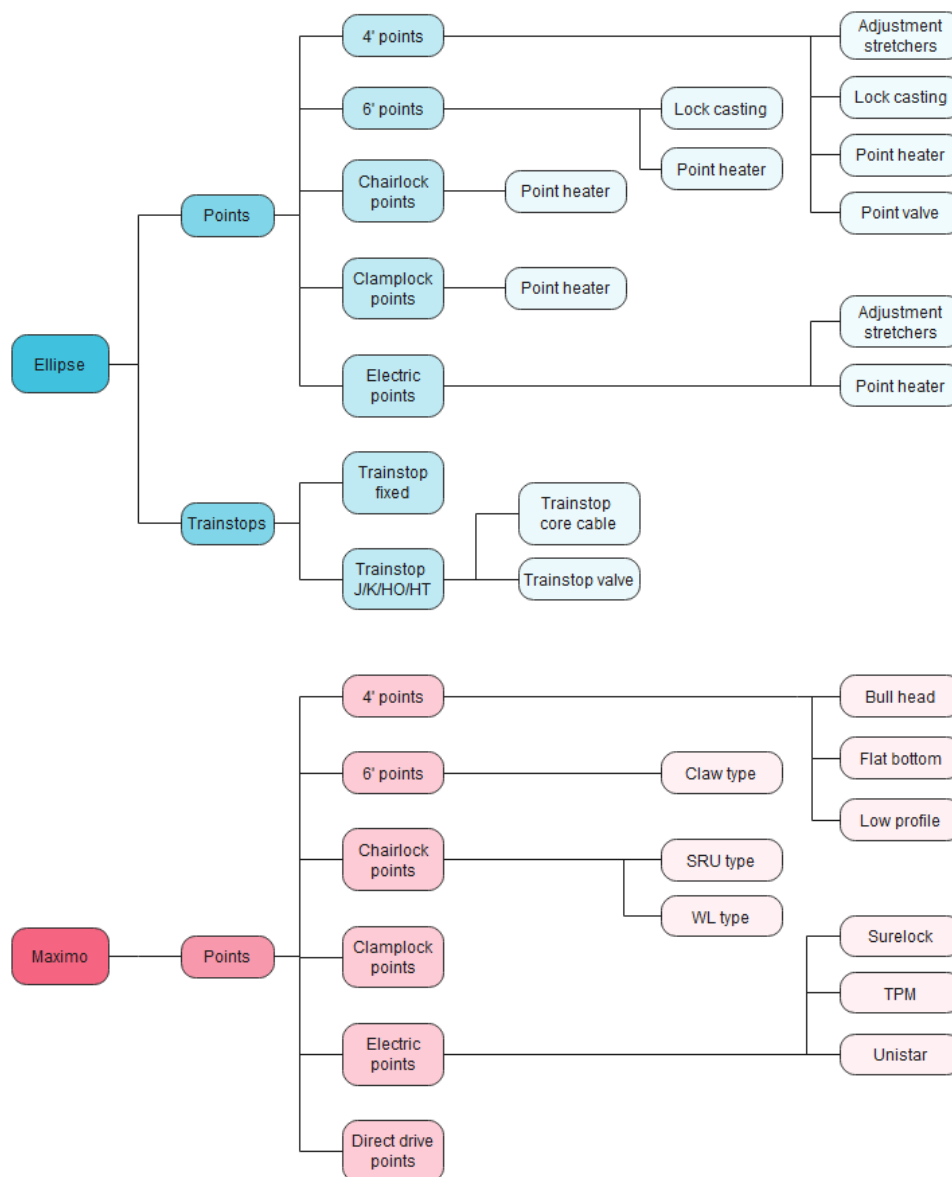


Figure 3.7 Hierarchy structure of point and train stop asset groups by asset management system analysed in this study

### 3.2.3.2. Pre-processing and quality assurance

Pre-processing was required before conducting any analysis with the fault and asset data. Additional information from the asset database were joined to the WO database to group data for analysis. The additional information is outlined in Table 3.4. These were combined by matching equipment codes in the WO database with corresponding parent or child codes in the asset database.

Table 3.4 Additional information added to Ellipse and Maximo equipment data to conduct the analysis of this study

<b>Information</b>	<b>Inclusion method</b>
Nearest LU station	Referencing the distance of the asset in meterage of its respective location coding system (LCS) identifier code in the equipment database to the full survey length of the LCS in metres in the LCS master file
Direction	Identifier within LCS code in the equipment database ( <i>e.g.</i> , D242/D <u>EB</u> LO = eastbound; D242/D <u>WB</u> LO = westbound)
Road type	Referencing the LCS code in the equipment database to the road type in the LCS master file
Network type	Inferred from nearest LU station and road type, sense-checked via map (Figure 3.2)

There were quality assurance checks conducted on the asset data before commencing analysis, especially as the Ellipse and Maximo systems have different structures. There were 12507 point and train stop assets in the asset database provided, each with an individual equipment code. 980 assets were not operational or in service from the database collation date. However, when reviewing the WO data, there were WOs raised against assets that were previously operational. Therefore, this study retained these assets in the database for fault exposure rate analysis (see Section 3.4). However, when classifying the asset's network type in accordance with road type,



567 assets were unclassifiable, this left a final count of 11940 assets used in this analysis: 8562 on the surface, 1188 across the sub-surface, and 2190 with in the deep tube tunnels.

Additional sense-checking of the combined database was also conducted. These were primarily manual spatial checks and adjustments to entries to ensure each WO correctly linked to its location. Checks included:

- Filtering by LU line to validate the LU stations and direction of travel.
- Filtering by each network type to validate the LU line.
- Filtering by key identifier text string sections of LCS to validate direction of travel and LU line.

#### **3.2.4. Climate projections**

The UK Met Office provides data on climate projections. The most recent UK climate projections launched in 2018 (UKCP18) and are available via free registration through the UK Climate Projections User Interface (Met Office, 2018c). A range of products is available for temperature projections up to the year 2100, described in Table 3.5. The following sections describe and justify the selected climate projection data parameters.

Table 3.5 Descriptions of the available UKCP18 climate projection products for temperature variables (Source: Met Office, 2019d)

<b>Product</b>	<b>Spatial resolution</b>	<b>RCP scenarios</b>	<b>Temporal resolution</b>
Probabilistic projections	25km	RCP 2.6, RCP 4.5, RCP 6.0, RCP 8.5	Monthly, seasonal, annual
Global projections	60km	RCP 2.6, RCP 8.5	Daily, monthly, seasonal, annual
Regional projections	12km	RCP 8.5	Daily, monthly, seasonal, annual
Local projections	2.2km	RCP 8.5	Hourly, monthly, seasonal, annual
Derived projections	60km	RCP 2.6	Daily, monthly

### 3.2.4.1. Climate variables and time slices

This study obtained monthly temperature anomalies (minimum, mean and maximum), at 1.5m for probabilistic projections at a 25km resolution for the administrative boundary of Greater London. The probabilistic projections were selected as they account for the range of emissions scenarios in accordance with the IPCC AR5 and address the scenarios relevant to TfL and their adaptation planning in Section 3.2.4.3. The monthly temperature anomalies are available in 30-decadal time slices, representative of the median decade within the time slice *e.g.*, the 2040-2069 time slice is representative of the 2050s. This study obtained data for all decadal time slides, but analysis focuses on the 2050s and the 2080s to provide a medium- and long-term outlook.

### 3.2.4.2. Baseline scenario

UKCP18 climate anomalies derive from three baselines (1961-1990, 1981-2000, and 1981-2010). Detailed in Table 3.1, this study used the 1981-2010 baseline in line with the State of

the UK Climate reports and the World Meteorological Organisation (WMO) use it as the standard (Met Office, 2018c), as the 1981-2010 baseline is representative of the present environment (WMO, 2017). Baseline data was obtained via the UKCP User Interface, which was added in April 2022 (Met Office, 2023b).

### **3.2.4.3. RCPs and probabilistic scenarios**

This study used the RCP 6.0 and RCP 8.5 scenarios to estimate change in future thermal environment and trends in fault-temperature relationships. Network Rail consider these two scenarios as essential for future planning, and TfL use the same scenarios (TfL, 2021b). RCP 6.0 is a compromise between likely emissions reductions as a result of the Paris Agreement (UNFCCC, 2015) and the current observed emissions and RCP 8.5 exemplifies extreme climate impacts should emissions reductions not be realised (Dale *et al.*, 2018). Therefore, these scenarios are utilised for impact assessments, asset/project design and activity planning (Network Rail, 2021a), whereby RCP 6.0 is the baseline scenario for decision-making and RCP 8.5 is used as a sensitivity test on assets with a lifespan beyond 2050, as reported in Network Rail's Route Weather Resilience and Climate Change Adaptation (WRCCA) plans (Network Rail, 2020).

UKCP18 provides outputs in data, maps, and graph format. As numerous model runs comprise the projections and uncertainties increase over time, derived percentile projections are obtainable, and these are used in the resulting products. For example, the probabilistic map products show a lower (10<sup>th</sup>) percentile, central estimate (50<sup>th</sup> percentile) and upper (90<sup>th</sup>) percentile. This study selected derived 90<sup>th</sup> percentile anomalies from both RCPs as its probability range aligns with Network Rail's priority on safety (Dale *et al.*, 2018), thus also relevant for TfL.

The pathway of future emissions will have implications on future policy and decision-making, particularly on that basis that adaptation and resilience strategies are oriented around ‘worst case’ scenarios, but it may lead to overestimating risks (Arnell *et al.*, 2021). Therefore, applying the 90<sup>th</sup> percentile to both RCP 6.0 and RCP 8.5 will differentiate the impacts in the two ‘worst case’ scenarios, particularly when their pathways diverge in the latter half of the 21<sup>st</sup> Century, illustrated in Figure 3.8. This deviation over time emphasises the importance of iterative reviews of adaptation planning to assess the climate trajectory in case changes in plans are necessary.

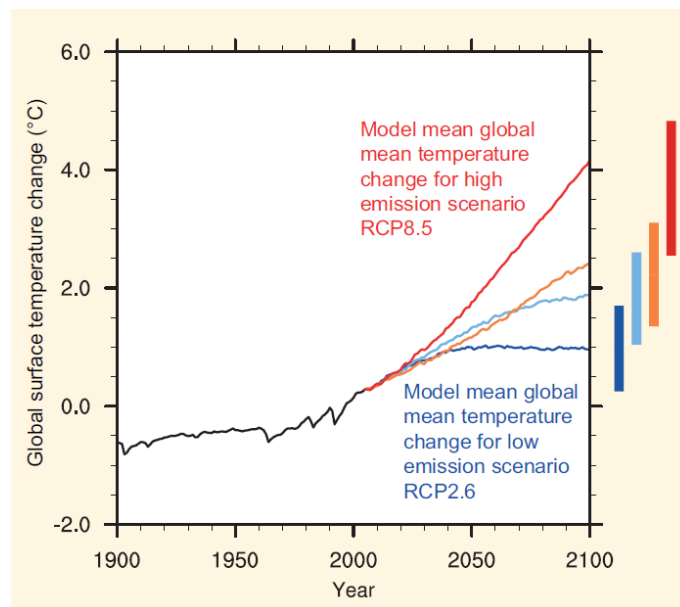


Figure 3.8 Estimated mean global surface temperature change according to each emissions scenario. RCP 8.5 is in red and RCP 6.0 is in orange, showing the divergence in temperature change between the scenarios during the 21<sup>st</sup> Century (Source: IPCC, 2013)

#### 3.2.4.4. Projection data sampling

The UKCP18 probabilistic projections comprise 3000 projections using over 100 simulations from two computer models; the Coupled Model Inter-comparison Project Phase 5 (CMIP5) and the Met Office Hadley Centre’s global climate model (HadGEM3-GC3.05) (Lowe *et al.*, 2019). These 3000 projections generate a distribution of projected climate variables for each RCP and

time slice. This study obtained a random sample of 999 of the 3000 projections. This sample size was taken on the basis that a 33% sample of data would be a reasonable representation of the projection data while also limiting the likelihood of capturing outliers generated from the ensemble. The UKCP18 User Interface generated the random samples, which vary for each combination of month, time slice and RCP.

#### **3.2.4.5. Selected projection data**

Figure 3.9 illustrates the selected monthly projection data for this study across every decadal time slice. The solid lines blue and orange lines show the mean values and shaded areas show two standard deviations of the sampled data. The grey dashed lines show the 90<sup>th</sup> percentile, which is where the 2050s and 2080s values came from for study's analysis.

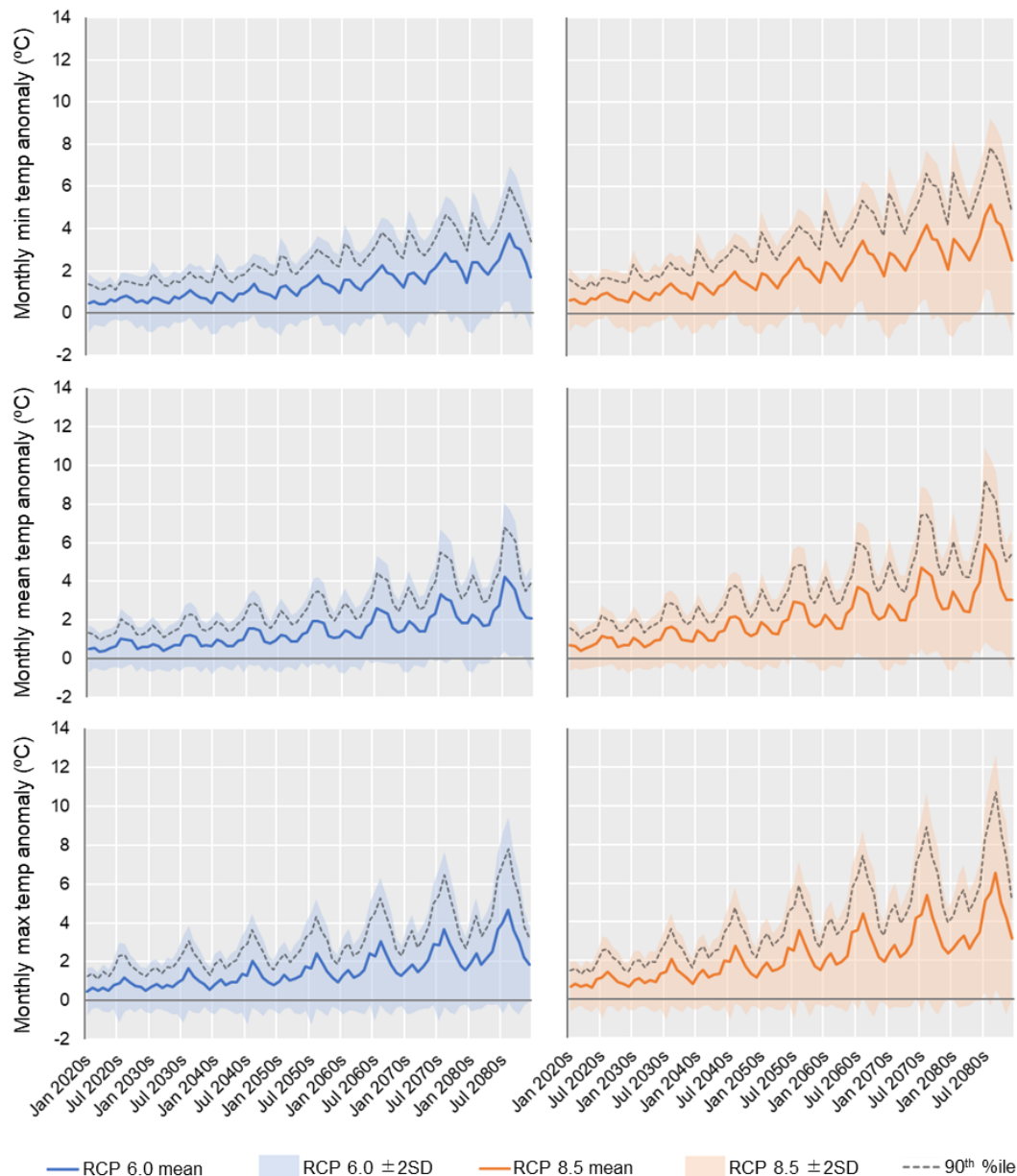


Figure 3.9 Distribution of climate projection data of temperature anomalies for minimum monthly temperature (top), mean monthly temperature (middle), and maximum monthly temperature (bottom) for RCPs 6.0 (left) and 8.5 (right) (Data: Met Office, 2018c)

Both emissions scenarios have similar trends across each temperature variable. Additionally, they show seasonal variability over time, with peak anomalies and standard deviations during the winter and summer months. The difference in projection values between the two scenarios widens over time, particularly after the 2050s. Figure 3.9 emphasises the importance of accounting for both scenarios because while the longer-term trends are similar, differences in

values between both RCPs and their temporal variability by month could affect the outcomes in the later stages of analysis.

### **3.3. Analysis of thermal environment**

Having collected all the data for this study, the first section of analysis was conducted, which was to analyse the thermal environment across the LU network. A variety of statistical methods was conducted in this analysis, which are summarised in this section, comprising two approaches. Firstly, this study considers key descriptive statistics that represent temporal and spatial characteristics across the LU network to ascertain general trends and anomalies. Secondly, this study undertakes a more detailed analysis of the thermal characteristics of tunnel temperatures. The relationship between surface temperature and tunnel temperature is complex and warrants the development of a tunnel temperature estimation model that quantitatively characterises on a more micro-scale (relative to the LU network) the spatial and temporal tunnel temperature characteristics. The model support later-stage analysis; estimating tunnel temperatures under future climate conditions in Section 3.5. The results of this analysis are presented in Chapter Four.

#### **3.3.1. Descriptive statistics**

To capture the thermal characteristics of the LU network, this study transformed hourly temperature observations compiled for this study into four daily temperature variables, mean temperature ( $t_{mean}$ ), maximum temperature ( $t_{max}$ ), minimum temperature ( $t_{min}$ ), and diurnal temperature range ( $\Delta t$ ). These are the principal descriptive statistics applied to weather station data, tunnel temperature data and future climate scenarios, discussed in more detail in Section 3.3.1.1.

### 3.3.1.1. Key temperature variables

Daily  $t_{mean}$  were calculated for each location (*i.e.*, St. James's Park weather station; each station platform Tinytag logger) as:

$$t_{mean} = \frac{\sum t}{n}, \text{ where:}$$

$\sum t$  = sum of all hourly temperature observations, from 00:00 to 23:00 inclusive

$n$  = number of observations.

Then, daily  $t_{min}$  and  $t_{max}$  were identified for each location, as the lowest and highest observations *per* day between 00:00 and 23:00 inclusive. Finally,  $\Delta t$  was calculated as daily  $t_{max} - t_{min}$ . Resulting daily variables were compiled for the full study period.

### 3.3.1.2. Climate thresholds

Climate thresholds are useful as there is no single definition of a weather or climate extreme (Met Office, 2018b). The Met Office refers to several indices related to surface temperature in the context of the UK climate (Met Office, 2018b, 2022e), shown in Table 3.6. These indices originate from the Expert Team on Climate Change Detection and Indices, who defined 27 metrics to objectively measure and characterise climate variability and change (ETCCDI, 2009). The exception is the hot day threshold, which was added by the Author to differentiate between heatwave days and days that also reach similar temperatures but not for an extended period. This study uses London-wide climatic thresholds for surface temperature, calculated using measurements from St. James's Park Met Office weather station to calculate the number of days that exceed each threshold for the study period.



Table 3.6 Key climate thresholds for temperature used in this study

Climate threshold	Definition
Warm nights	Days where daily surface $t_{min}$ is above the 90 <sup>th</sup> percentile centred on a five-day window for the baseline period (Met Office, 2018b)*
Warm days	Days where daily surface $t_{max}$ is above the 90 <sup>th</sup> percentile centred on a five-day window for the baseline period (Met Office, 2018b)*
Warm spell duration index (WSDI) days	Annual count of days with at least six consecutive days where daily surface $t_{max}$ is above the 90 <sup>th</sup> percentile as above (Met Office, 2018b)*
Summer days	No. of days daily surface $t_{max} > 25^{\circ}\text{C}$ (Met Office, 2018b)
Hot days	No. of days daily surface $t_{max} > 28^{\circ}\text{C}$
Heatwave days	Days where daily surface $t_{max} > 28^{\circ}\text{C}$ for at least three consecutive days (Met Office, 2022e)
Tropical nights	No. of days daily surface $t_{min} > 20^{\circ}\text{C}$ (Met Office, 2018b)

\* The Met Office baseline period is 1961-1990. However, for the purpose of this study, the baseline is from UKCP18 observed monthly data for the baseline period 1981-2010 for the administrative region of London.

In Table 3.6, the first three indices (warm nights, warm days, WSDI days) are calculated from baseline data, which for this study used 1981-2010 (see Table 3.1). However, the climate thresholds are a daily index whereas the baseline data is monthly. 90<sup>th</sup> percentiles were therefore calculated for each month, with a five-day rolling average to adjust the temperature for the days around the start and the end of each month.

### 3.3.2. Tunnel temperature estimation model

Tunnel temperatures on the LU network are often higher than the surface, as discussed in Section 1.1.2 and 1.3.2. It is important to understand how the tunnel temperatures respond to surface temperature change in the short- and long-term. Developing a tunnel temperature estimation model therefore served three purposes for this study. Firstly, it spatially and temporally quantified the relationship between daily temperature variables by tunnel station

platform. Secondly, it provided estimated temperature values to address tunnel station platform data observation gaps (see Table 3.1), maximising the WO data joined to temperature variables for the fault exposure rate analysis. Finally, under a changing climate, it will be important to understand how the thermal environment in tunnels may change long-term and the implications for LU operations, as well as health and safety of staff and customers. As UKCP18 projections only consider surface temperature, the model enabled a conversion into projected tunnel temperatures across the LU network.

### **3.3.2.1. The model**

This study adapts a model designed by Kimura *et al.* (2018) and applies it in a new context. The original purpose of the model was to explore historical differences between the outputs of subway environment simulation (SES) tools and temperature observations, which often led to equipment overdesign. Evaluating the methodology identified unrealised benefits of the model for the purpose of this study, as it also uses daily temperature variables.

A particular element of the model designed by Kimura *et al.* is that it does not factor geology. This is because past SES models resulted in the design of equipment with excessive capacities due to not capturing change in environmental conditions since their development. Geology can also be omitted as a factor for this adaptation of the model for London. The LU tunnel network is almost entirely cut through London clay (see Section 1.1.2), which is highly impermeable. Thus, elevated ground temperatures are localised around the tunnels, as groundwater cannot pass through to transfer heat (Bidarmaghz *et al.*, 2020). Inferring that geology as a heat sink is not a significant factor affecting present-day LU tunnel temperatures, which remain relatively constant, it is reasonable to apply this model for this study.

The model relies on using the following equation to predict tunnel temperatures by using surface temperature:

$$T_r(t) = (T_{oa} + a) + \{T_{ox}(t - t_d) - T_{oa}\} \times b, \text{ where:}$$

$T_r(t)$  = Predicted mean daily tunnel temperature ( $t_{mean}$ ), °C

$T_{oa}$  = Mean surface temperature of all  $t_{mean}$  observations for the time interval, °C

$a$  = Mean temperature uplift (difference in observed surface and tunnel  $T_{oa}$ ), °C

$t$  = Time, days

$t_d$  = Time lag delay, days

$T_{ox}$  = Observed mean daily surface temperature ( $t_{mean}$ ), °C

$b$  = Scaling coefficient (ratio of range in observed surface  $t_{mean}$  and tunnel  $t_{mean}$ )

Figure 3.10 illustrates the parameters of the equation. It requires past surface and tunnel temperature observations to extrapolate future tunnel temperatures. It also required data from at least one annual cycle to capture seasonal temperature fluctuation and yearlong means. Therefore, it used the surface and tunnel temperature observations as well as baseline and climate projection data described in Table 3.1 Details of data used for this study produced two sets of tunnel temperature estimations. Firstly, it produced daily  $t_{mean}$ ,  $t_{max}$  and  $t_{min}$  estimates *per* station tunnel platform using the surface temperature data for the study (described in this Section), producing the equation variables to estimate tunnel temperatures where there were observations gaps within the study period. Secondly, the model produced the baseline and estimated future tunnel temperatures across each climate projection scenario using these equation variables (see Section 3.5.1.2).

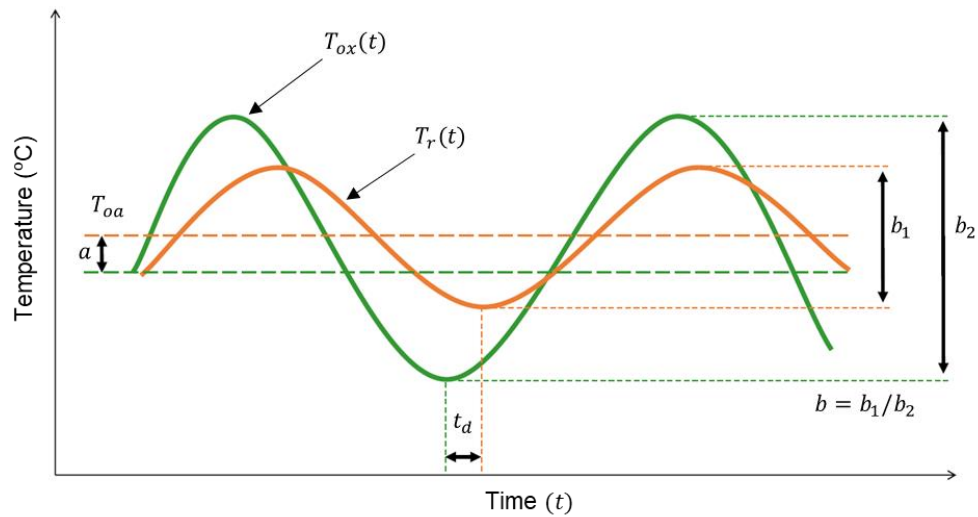


Figure 3.10 Parameters of the tunnel temperature estimation model equation (Adapted from: Kimura *et al.*, 2018)

### 3.3.2.2. Applying the model

Using the equation,  $a$ ,  $b$  and  $t_d$  values were obtained for each LU station platform. Firstly,  $t_d$  were identified by cross correlating the 7-day rolling surface  $t_{mean}$  with the 7-day rolling tunnel  $t_{mean}$ . Using a 7-day rolling average as *per* Kimura *et al.* (2018) means that outliers are less likely to affect the cross-correlation and thus overall correlations are clearer. The selected value for each location's respective  $t_d$  is that with the largest cross-correlation coefficient. Code was designed in RStudio to apply the model, with sample code available in the Appendices (Appendix B).

In some instances,  $t_d$  was anomalously high. Further investigation of these instances showed that when graphing the cross correlation, they were often characterised by a “wave” of cross correlation coefficient peaks over time. This is not typical, as most cross correlations in this study had one distinct peak coefficient. For the anomalous readings, the  $t_d$  selected was the first peak closest to  $t_d = 0$ , such as that shown in Figure 3.11. Nevertheless, this was not possible to determine at some station platforms so the original  $t_d$  was retained.

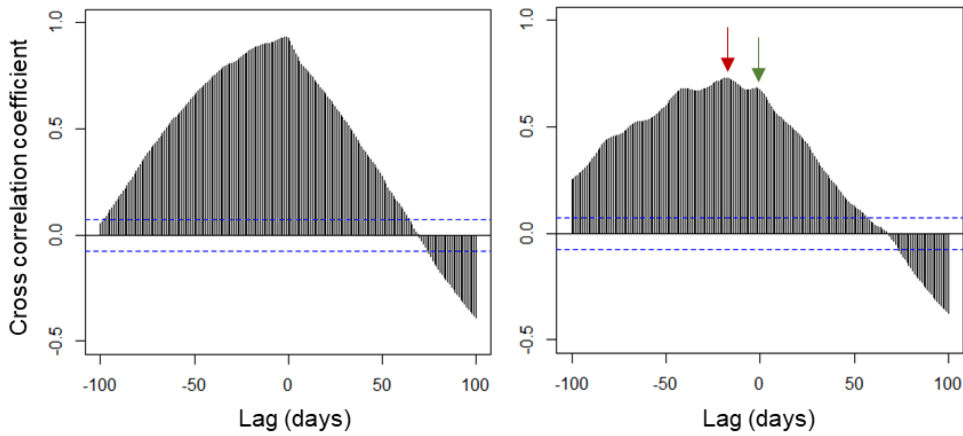


Figure 3.11 Examples of the differences in cross correlation trends by platform. A typical cross correlation for this study is on the left, whereas an anomalous cross correlation is on the right. The red arrow indicates the value of  $t_d$  with the highest cross correlation coefficient reported by the code script used for this analysis, whereas the green arrow indicates the peak closest to  $t_d = 0$ ; the value selected for this platform upon further investigation

Kimura *et al.* (2018) derived  $a$  and  $b$  variables from logarithmic approximation, using tunnel length as a parameter. This is because other parameters such as train frequency and type of tunnel (single or double track) showed little variance across their study areas. However, parameters such as train frequency may have a greater moderating effect on the LU network (see Section 1.3.2) compared with subways in Japan – who introduced cooling systems in both tunnels and trains, such as on the Tokyo Metro after 1971 (Golany and Ojima, 1996). Therefore, to ascertain the values of  $a$  and  $b$  for the LU network more accurately, the model equation was converted into a linear form, where  $T_r(t)$  = observed platform temperature, to solve for  $a$  and  $b$  as *per* the following equation:

$$T_r(t) - T_{oa} = \{T_{ox}(t - t_d) - T_{oa}\} \times b + a.$$

Figure 3.12 shows an example of balancing the converted equation using data at one station platform. The linear regression of  $T_r(t) - T_{oa}$  against  $T_{ox}(t - t_d) - T_{oa}$  for each location provided the values of  $a$  and  $b$  simultaneously in the trend line, where  $a$  is the  $y$ -intercept and

$b$  is the gradient. All equation variables *per* LU station platform for the study period are available in the Appendices (Appendix C).

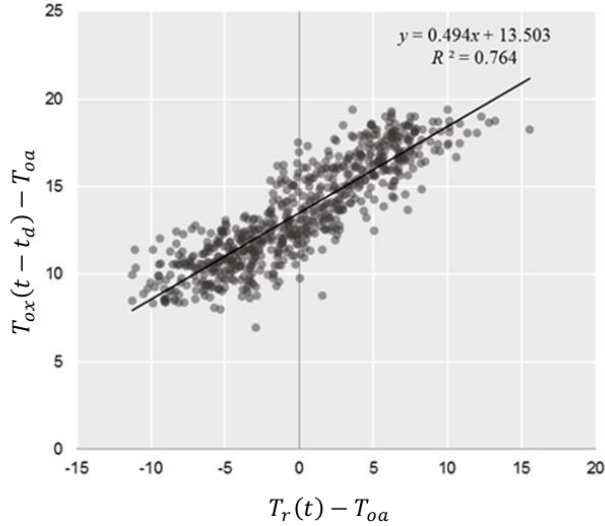


Figure 3.12 Scatterplot of sample data (Covent Garden station, Piccadilly line, westbound platform, 2015-2016) showing how to identify  $a$  and  $b$  values of the tunnel model.

The tunnel temperature estimation model process was repeated for daily  $t_{min}$  and  $t_{max}$ . Estimating  $t_{max}$  is particularly important as peak temperatures form part of the LU standard on managing tunnel heat and ventilation in public areas (TfL, 2016a). This would use the same equation as  $t_{mean}$ , but changing the variables to  $t_{min}$  and  $t_{max}$ . To determine estimated  $\Delta t$ , estimated  $t_{min}$  was subtracted from estimated  $t_{max}$ .

### 3.3.2.3. Model validation

Estimated and observed temperatures were compared through linear regression and evaluated via the regression coefficients, to determine the accuracy of the model compared to tunnel temperature observations. The results were reported collectively *per* LU tunnel (*e.g.*, Bakerloo NB) for each temperature variable.

### 3.4. Fault exposure rate analysis

The study analyses the relationship between faults and temperature variables using a similar approach to Fisher (2020) and Greenham *et al.* (2020). Key temperature variables were joined to fault data; matched by date. RStudio was utilised to join the data, and sample code is shown in the Appendices (Appendix D). Estimated temperature variables derived from the tunnel temperature estimation model were then joined where there were any gaps in observed temperatures across the WO data. The combined data were then aggregated in different ways to identify trends in faults *per* temperature bin as a fault exposure rate. The results of the analysis described within this section are presented in Chapter Five.

#### 3.4.1. Calculating the fault exposure rate

To gain an equitable understanding of the relationships between temperature and faults across the LU network, data required normalising to create fault exposure rates. This is primarily because of the temperature variance across the network at any given time and the differences in asset distribution. The fault exposure rate calculation used in this study can be expressed as:

$$\text{Fault exposure rate } t_n = \left( \frac{\sum \text{work orders } t_n}{\sum \text{temperature exposure frequency } t_n} \right) / \text{Assets}_n, \text{ where:}$$

$t_n$  = the temperature bin *per* respective part of the LU network by LU line and network type,

$\sum \text{work orders } t_n$  = the sum of work orders at temperature  $t_n$  *per* LU station,

$\sum \text{temperature exposure frequency } t_n$  = the sum of days at temperature  $t_n$  *per* LU station,

$\text{Assets}_n$  = the number of assets recorded *per* respective part of the LU network by LU line and network type.

Temperature exposure frequencies and WOs were tabulated for each temperature bin *per* LU station, LU line, direction of travel, and network type. These two variables were divided, the resulting values summed, and then divided by the total number of assets for the respective part of the LU network. For example, the frequency of WOs near a station when daily  $t_{max} = 22^{\circ}\text{C}$  is divided by the count of days in the study period that the station experienced a daily  $t_{max}$  of  $22^{\circ}\text{C}$ . The same calculation was then conducted for all LU stations across the LU line and network type, for all temperature bins. The rates for each station were summed *per* temperature bin, then divided by the asset count for the LU line and network type. The resulting values *per* temperature bin were then plotted as line graphs.

#### **3.4.2. Identifying trends in the fault exposure rates**

The fault exposure rate line graphs also included additional statistics to help identify trends. These line graphs also include the mean fault exposure rate of all data reported in the graph, and two standard deviations of that mean. Each graph also included a lower bound line, calculated as 1 divided by the total occurrences of the temperature observations across the reported data. The lower bound highlighted infrequent temperature occurrences, that may otherwise affect the reliability of the fault exposure rates at that temperature bin.

#### **3.4.3. Determining temperature thresholds**

Determining the statistical significance of the relationship between fault exposure rates and temperature involved a form of threshold analysis. This approach was selected as temperature thresholds are the key driver of TfL's extreme weather response planning (*i.e.*, Hot Weather Plan; Winter Weather Contingency Plan). Standard deviations of the mean fault exposure rate of all data in each line graph were used to determine thresholds, and to initiate further discussion



into the data behind the fault exposure rates exceeding these thresholds. Fault exposure rates exceeded the one standard deviation were determined statistically significant and those exceeding two standard deviations were very statistically significant (Fisher, 2020). Results discussion also took the lower bound into account if statistically significant peaks in the fault exposure rate were affected by it.

### **3.5. Analysis of climate projections**

This study projected future temperatures across the LU network by using UKCP18 climate projections, and then used these to estimate change in faults in the future. Two stages of analysis were undertaken. Firstly, the UKCP18 climate projections selected for this study (RCP 6.0 and RCP 8.5; 2050s and 2080s; 90<sup>th</sup> percentile) required transforming from their anomaly values into actual values from the 1981-2010 baseline, which could then also be applied into the tunnel temperature estimation model to compare the rate of change of present-day thermal environment with the future climate scenarios. Secondly, the climate projection data required transforming from monthly values into a form of estimated days *per* year for each future climate scenario, forming an annual estimated temperature exposure frequency. Then, estimated future faults were inferred from the fault exposure rates, using the resulting temperature exposure frequencies. Results from this section are presented in Chapter Six.

#### **3.5.1. Projected change in thermal environment**

Given the emphasis on conducting analyses by network type, was also important to differentiate the future thermal environments as such. This was conducted in two ways: future surface temperatures were derived directly from UKCP18 data, while future sub-surface and deep tube

tunnel temperature were estimated via the tunnel temperature estimation model, with inputs also from the UKCP18 data.

### **3.5.1.1. Future surface temperatures**

Baseline data were added to the anomaly data for each scenario obtained in Figure 3.9 to provide the estimated monthly temperature variables. To convert the monthly estimated values into estimated daily values, the monthly relative standard deviations *per* baseline month for the full baseline time interval were calculated. Relative standard deviations were applied to the projected 90<sup>th</sup> percentile monthly values to estimate future absolute standard deviations. By using a normal distribution function with the absolute standard deviations, it was possible to determine a temperature distribution in percentage terms *per* month for each scenario. These percentages could then be converted into estimated days *per* month, then summed to give an estimated annual temperature frequency exposure *per* 1°C temperature bin in each scenario.

UKCP18 climate projections provide only a single value for Greater London. This is analogous to the single daily temperature value used from St. James's Park in Section 3.2.2.1. To gauge an understanding of the spatial variance in climate projections of heat, the UHI index was utilised. The mean UHI for the Greater London administrative boundary was inferred as the UHI intensity of UKCP18 climate projection values for Greater London. The mean UHI index was compared with the total surface LU station UHI index distribution. This indicated the proportion of surface LU stations likely to estimate higher or lower temperatures than the single Greater London projection value, which could in turn affect future estimated faults. However, these findings remain as a reference for discussion and are not integrated into the analysis, as they would add further additional unknown and uncontrolled variables to the analysis.

### 3.5.1.2. Future sub-surface and deep tube tunnel temperatures

To project tunnel temperatures at station platforms across the LU network, the tunnel temperature estimation model converted projections from surface temperatures to estimated tunnel temperatures. The same model is used from Section 3.3.2.1, but omitted  $t_d$ . For projection estimates,  $t_d$  was omitted because the temporal scale of climate projection data (monthly) was larger than the typical scale of  $t_d$  in the results, which was days. Therefore, in the context of monthly scale projections, its effect was assumed negligible. RStudio was utilised to conduct the estimations, and sample code is shown in the Appendices (Appendix E).

### 3.5.2. Calculating change in work orders under future climate change scenarios

This study used the future climate projections to investigate how asset failures may change under different climate scenarios. A simple theoretical relationship used by Andersson and Chapman (2011) and Oslakovic *et al.* (2013) derived their failure rates which could then be extrapolated for future estimated faults as follows:

Total fault exposure rate for temperature variable  $x$   $\times$  Annual number of days *per* temperature variable  $x$ , where:

$x$  = one 1°C temperature bin.

This required calculating an estimated number of days *per* year for every temperature bin for the baseline and the four projected scenarios used in this study.

### **3.6. Chapter summary**

Having reviewed TfL's approach to managing temperature across the LU network and the literature on measuring asset performance with metrics in Chapter Two, this chapter outlined the methodological approach to acquiring, handling, and analysing an extensive array of data to evaluate the impacts of heat and climate change upon point and train stop assets across the LU network. The methodology accounts for the ways in which derived daily descriptive statistics ( $t_{min}$ ,  $t_{mean}$ ,  $t_{max}$ ,  $\Delta t$ ) from 13 years of hourly temperature data help characterise the thermal environment across the surface, sub-surface and tunnel sections of the LU network; determine tunnel temperature via an estimation model to coalesce data gaps in observations; and identify the extent of fault exposure rates to temperature. Then, the results from the tunnel temperature estimation model and fault temperature relationship analyses were integrated with climate projection data to estimate the resulting impacts of change in temperature owed to climate change upon point and train stop assets. The following three chapters each present a suite of results: Thermal environment (Chapter Four), Fault exposure rates (Chapter Five), and Future climate change (Chapter Six).

# Chapter Four | Thermal environment

## 4.1. Chapter overview

Chapter Three detailed the methodological approach to this study. This chapter provides results that spatially and temporally describe the present-day climate across the LU network. Firstly, Section 4.2 presents the key descriptive statistics of temperature across the LU network by network type, using the observational data obtained for this study. Then, the rate of climate change in the study period is presented. Next, Section 4.3 addresses the tunnel temperature estimation model, to enhance the observed temperature data with estimated values where there are data gaps, preparing values for the fault rate analysis and the application of equation variables to climate projections. To summarise, Chapter Four provides a comprehensive and robust analytical description of the thermal environment across the LU network that can be used for reference throughout the analysis.

## 4.2. Descriptive statistics

Descriptive statistics are useful to characterise the thermal environment of the LU network and were generated from temperature datasets from 2006 to 2018 from the Met Office weather station at St. James's Park, and station platform temperature loggers across the sub-surface and tunnel parts of the LU network. As mentioned in Section 3.2, the results in this section highlights intermittent data gaps mentioned previously in Table 3.1. These are primarily in 2007 (surface) and between late 2012 and early 2013 (sub-surface and tunnel). There are periodical data gaps at some station platforms across the sub-surface and tunnel parts of the network, affecting the weighting of the descriptive statistics calculated in the following section.

### 4.2.1. Temperature variables

The thermal environment across the LU network is spatially and temporally variable. When grouped by network type, temperature variables differed greatly. Figure 4.1 shows the daily  $t_{mean}$  over time by LU network type. The tunnels were warmest year-round whereas the sub-surface was similar to the surface, albeit slightly warmer. The difference in daily  $t_{mean}$  between the tunnel and surface/sub-surface was smaller in the summer and greater in the winter. The warmest  $t_{mean}$  was in the tunnels during 2006 and 2018, with peak summer daily tunnel  $t_{mean}$  exceeding 30 °C once in 2018. The coldest observations were on the surface, reaching 0°C in early 2010 and early 2018. Tunnel observations rarely fell below 20°C year-round.

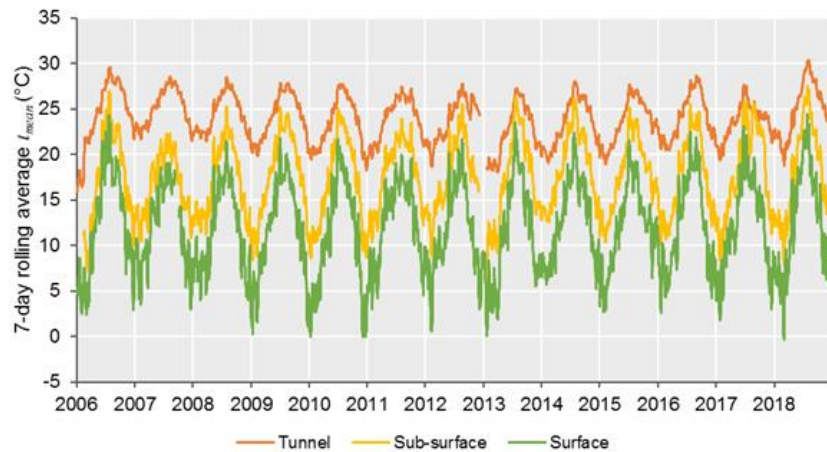


Figure 4.1 7-day rolling average of  $t_{mean}$  observations for each network type of the LU network

Figure 4.2 shows the difference in  $t_{min}$  by network type. Trends were comparable to  $t_{mean}$ ; however, the sub-surface observations, particularly the summer peaks were higher than the corresponding surface observations; oftentimes closer to the tunnel observations. The warmest  $t_{min}$  across the LU network were also in the tunnels during 2006 and 2018. Some outlier trends were apparent in the tunnels in late 2012. This is due to a break in Tinytag data collection until late January 2013 at all platforms except for two on the Northern line in the northbound

direction (Belsize Park and Tottenham Hale), skewing the results shown (upweighted from few observations).

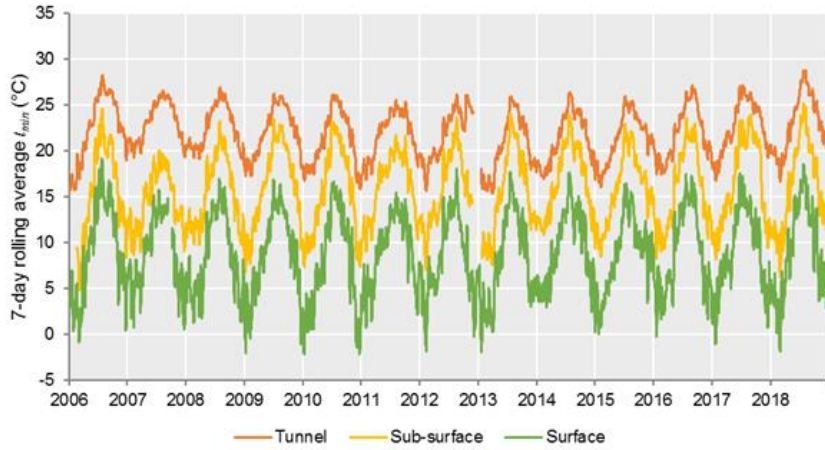


Figure 4.2 7-day rolling average of  $t_{min}$  observations for each network type of the LU network

Figure 4.3 shows the difference in  $t_{max}$  by network type. There is a clear contrast between network trends overtime. Most notably, (i) all parts of the network experienced similar peak summer temperatures; and (ii) sub-surface observation trends are similar to surface observations, albeit slightly warmer during winters. As with  $t_{mean}$  and  $t_{min}$ , the highest  $t_{max}$  observations were on the surface in 2006 and in the tunnels in 2018.

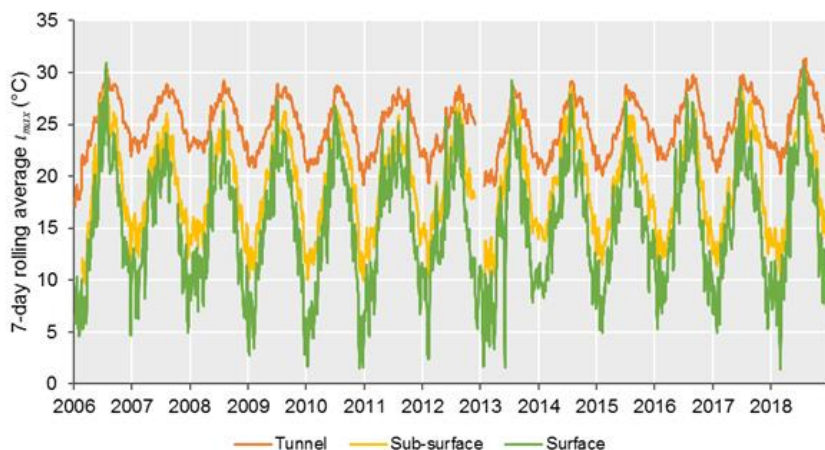


Figure 4.3 7-day rolling average of  $t_{max}$  observations for each network type of the LU network

Figure 4.4 shows diurnal temperature range, ( $\Delta t$ ) by network type over time. Tunnel  $\Delta t$  was very low throughout the year. The sub-surface also observed much lower  $\Delta t$  than the surface, primarily due to lower range in sub-surface  $t_{min}$ . There were also outliers in the tunnel in 2012 and 2017 as shown in the other variables' graphs.

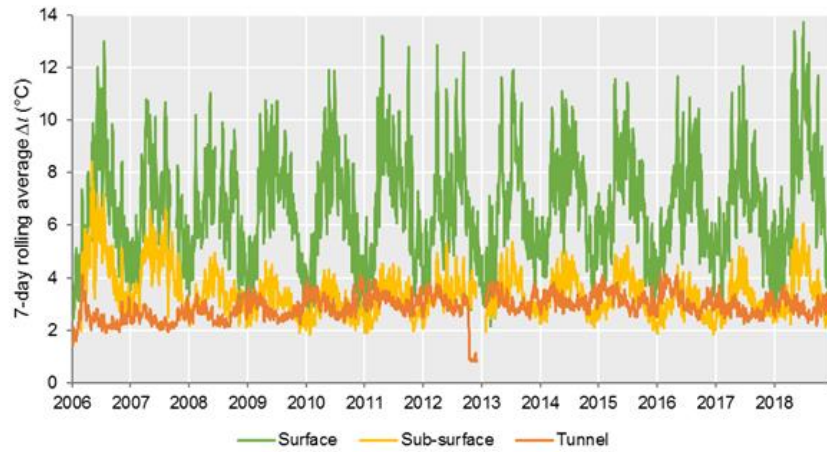


Figure 4.4 7-day rolling average of  $\Delta t$  observations for each network type of the LU network

#### 4.2.1.1. Distribution of surface temperature variables

To further describe the thermal environment, the following sections describe the distribution of temperature variables. The surface temperature only considers one location (St. James's Park Met Office weather station), so Figure 4.5 shows the distribution of the four surface temperature variables throughout the study period and Table 4.1 shows the key values within the distributions. The first three box plots from the left ( $t_{min}$ ,  $t_{mean}$ ,  $t_{max}$ ), show similar distributions, each with increasing values than the previous temperature variable. However, the temperature ranges extend across each of these three variables, and  $t_{max}$  has a higher interquartile and upper quartile range, and one outlier temperature. The  $\Delta t$  box plot highlights the difference in distribution between  $t_{min}$  and  $t_{max}$  – because the range of  $t_{max}$  is greater than  $t_{min}$  at higher temperatures, it drives some particularly high observed  $\Delta t$ .



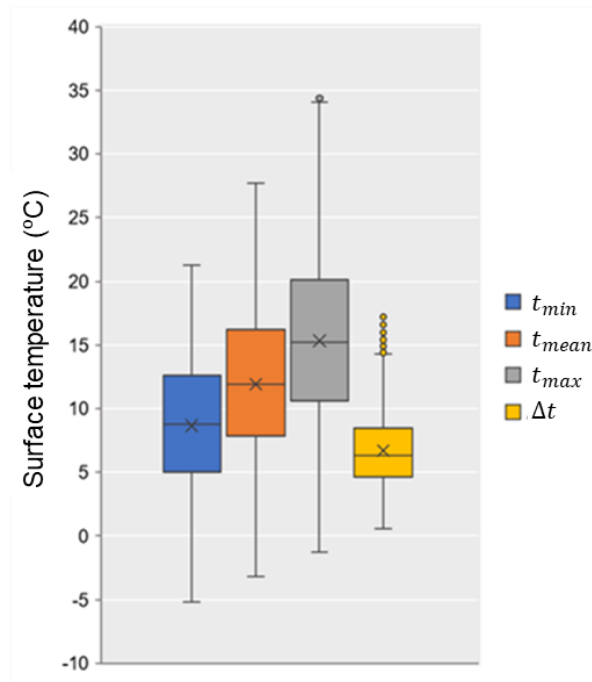


Figure 4.5 Distribution of surface temperature by daily temperature variable based on the observations at St. James’s Park weather station for the study period

Table 4.1 Key values of the box plot distributions in Figure 4.5

Variable	Temperature (°C)	Date
Average annual $t_{min}$	8.7	-
Lowest daily $t_{min}$	-5.2	21/12/2010
Highest daily $t_{min}$	21.3	26/07/2006
Average annual $t_{mean}$	11.9	-
Lowest daily $t_{mean}$	-3.2	28/02/2018
Highest daily $t_{mean}$	27.7	01/07/2015
Average annual $t_{max}$	15.4	-
Lowest daily $t_{max}$	-1.3	28/02/2018
Highest daily $t_{max}$	34.4	01/07/2015
Average annual $\Delta t$	6.7	-
Lowest daily $\Delta t$	0.6	11/02/2015
Highest daily $\Delta t$	17.2	08/09/2012

Figure 4.5 also shows several  $\Delta t$  outliers. There were 50 outliers of high  $\Delta t$  in the study period. These outliers are important to consider as they may indicate a signal of change in climate, where warm days are extending beyond their normal distribution in the year, which may have

implications for asset performance. Figure 4.6 shows when in the year the  $\Delta t$  outliers occurred. They were mainly during April, though interestingly far fewer during the months before and after. Overall, the season with the most anomalies is during the summer (June-August), quickly tailing off through the autumn.

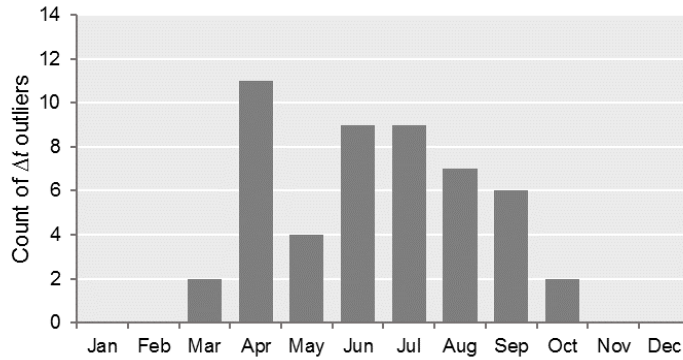


Figure 4.6 Distribution of  $\Delta t$  outliers throughout the year

#### 4.2.1.2. Distribution of sub-surface temperature variables

Sub-surface temperature observations comprise multiple station platforms. Therefore, the following results are an aggregation of all station platforms for each direction of travel. Figure 4.7 shows the distribution of temperature across the platforms for the EB, WB, IR and OR directions of the sub-surface part of the network. Table 4.2 shows the key values within the distributions. The spread of the  $t_{min}$ ,  $t_{mean}$  and  $t_{max}$  plots are very similar, with all outlier observations in colder temperatures, implying that some station platforms are likely more exposed to the surface temperature compared to the rest of the LU network. There are also greater ranges in all four temperature variables across the EB/WB box plots as opposed to the IR/OR ring box plots. This suggests that station platforms along the EB and WB tracks may be more exposed to surface temperatures than the IR/OR tracks.

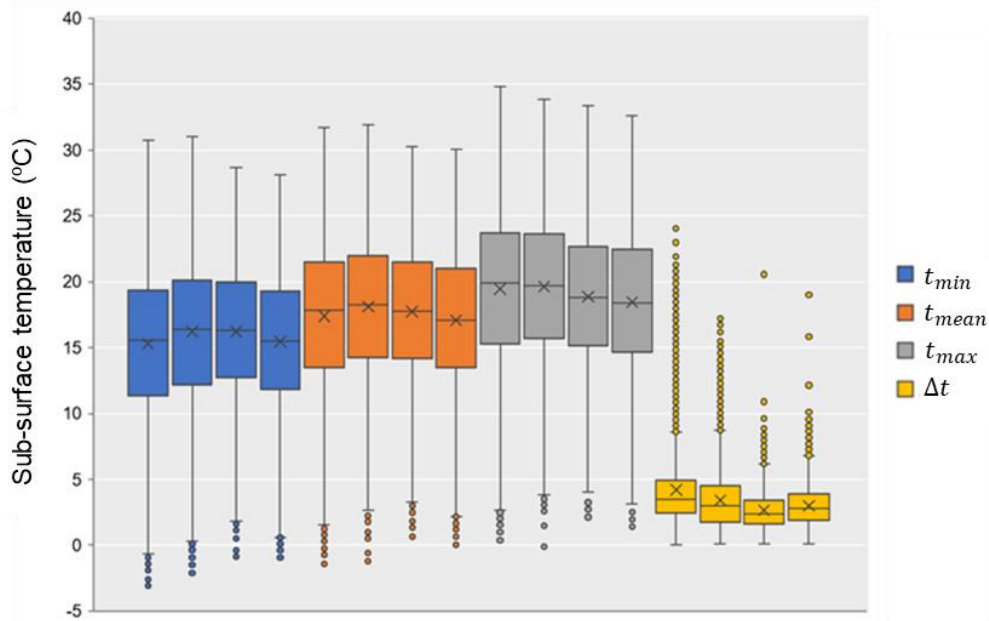


Figure 4.7 Distribution of sub-surface temperature by temperature variable based all sub-surface station platform observations for the study period. Plots from left to right for each variable: EB, WB, IR, OR

Table 4.2 Key values of the box plot distributions in Figure 4.7

Variable	Temperature (°C)	Date	Station platform
Average annual $t_{min}$ range	15.3 - 16.2	-	-
Lowest daily $t_{min}$	-3.1	07/01/2009	South Kensington EB
Highest daily $t_{min}$	31.0	27/07/2018	Bank WB
Average annual $t_{mean}$	17.1 - 18.1	-	-
Lowest daily $t_{mean}$	-1.4	10/01/2009	South Kensington EB
Highest daily $t_{mean}$	31.9	27/07/2018	Bank WB
Average annual $t_{max}$	18.4 - 19.6	-	-
Lowest daily $t_{max}$	-0.1	28/02/2018	Paddington WB
Highest daily $t_{max}$	34.8	22/07/2013	Paddington EB
Average annual $\Delta t$	2.7 - 4.2	-	-
Lowest daily $\Delta t$	0.1	06/07/2009	Bank EB
Highest daily $\Delta t$	24.0	21/04/2010	Paddington EB

There were also a large proportion of anomalously high observations of daily  $\Delta t$ . In the EB and WB directions, these were almost entirely owed to the observations recorded at Paddington station. Figure 4.8 shows the sub-surface platforms for Paddington station. The anomalies could

be explained by the built form, as sunlight can reach the platform from the roof windows. Additionally, the natural light on the tracks in the background implies some direct access to the surface environment.



Figure 4.8 Paddington sub-surface station platform for the District and Circle lines (Source: McKenna, 2005, CC BY-SA 4.0)

#### **4.2.1.3. Distribution of deep tube tunnel temperature variables**

The deep tube tunnel temperature observations are also across multiple station platforms, therefore the results in this section are aggregations of the station platform data for each LU line and direction of travel. Figure 4.9 shows the distribution of each temperature variable by LU tunnel and direction of travel while Table 4.3 shows the key values within the distributions. The box plots show that temperature ranges across the tunnel parts of the network are higher than the rest of the network. Temperatures also vary by LU line, and direction of travel. The Bakerloo and Central lines also show distinct differences in lower observed temperature variables by direction of travel. The Jubilee line also shows cooler temperatures than the rest of the tunnel network, which is perhaps due to its age (see Table 1.1), and the inclusion of platform temperature observations on the Jubilee line extension partway through the study period. These

particular observations may be responsible for lowering the observed temperature distribution as the extension was designed with a greater ventilation capacity (Jones, 1999). There were also several outliers across the box plots among all four temperature variables. These are mainly at lower temperatures, suggesting that some station platforms are likely to be more exposed to surface temperatures. When reviewing the data for each LU tunnel, the anomalies were primarily the station platform near one or both tunnel openings.

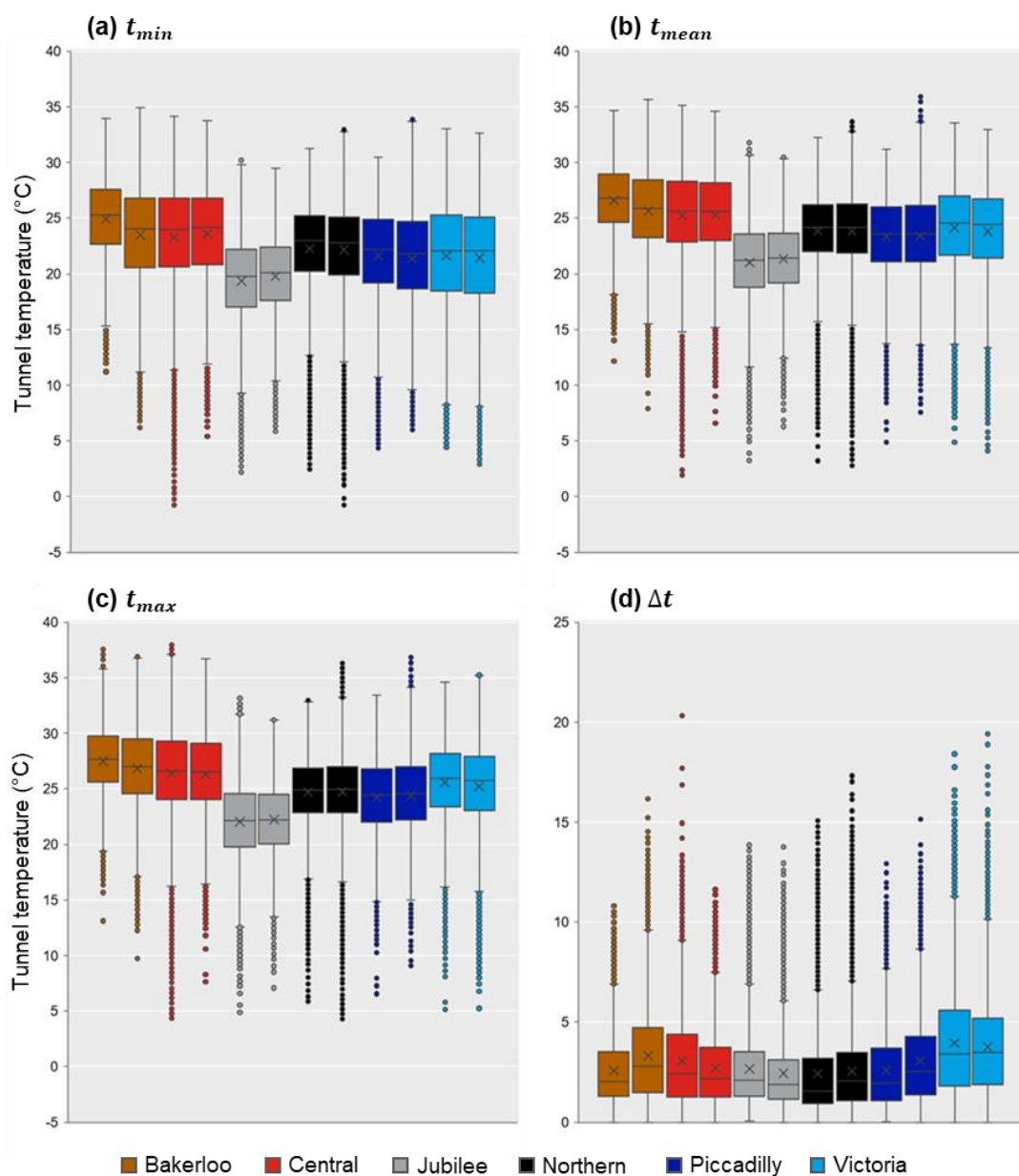


Figure 4.9 Distribution of tunnel temperature by  $t_{min}$  (a),  $t_{mean}$  (b),  $t_{max}$  (c) and  $\Delta t$  (d) based all tunnel station platform observations for the study period. The left plot of each LU line is the NB/EB tunnel, and the right plot is the SB/WB tunnel

Table 4.3 Key values of the box plot distributions in Figure 4.9. LU line the station platform belongs to is provided as an initial in parentheses

Variable	Temperature (°C)	Date	Station platform
Average annual $t_{min}$ range	19.4 - 24.9	-	-
Lowest daily $t_{min}$	-0.8	01/03/2018	Oval SB (N)
Highest daily $t_{min}$	34.9	06/08/2006	Edgware Road SB (B)
Average annual $t_{mean}$	21.0 - 26.6	-	-
Lowest daily $t_{mean}$	1.9	26/12/2010	Shepherd's Bush EB (C)
Highest daily $t_{mean}$	35.9	08/08/2008	Covent Garden WB (P)
Average annual $t_{max}$	22.0 - 27.5	-	-
Lowest daily $t_{max}$	4.3	28/02/2018	Oval SB (N)
Highest daily $t_{max}$	38.1	28/07/2006	Bethnal Green EB (C)
Average annual $\Delta t$	2.4 - 4.0	-	-
Lowest daily $\Delta t$	0.0	Various	Various
Highest daily $\Delta t$	20.3	06/06/2006	Liverpool Street EB (C)

#### 4.2.2. Climate thresholds

This study used climate thresholds identify time intervals that were warmer than the climatological norm. Table 4.4 shows the number of days *per* year that exceeded each climate threshold (defined in Section 3.3.1.2). Overall, 56% of days within the study period exceeded at least one climate threshold. There were substantially more warm nights and warm days *per* year, but there was a large annual variability throughout the study period. However, the WDSI index annual range was small, suggesting that extended periods of warm days are similar throughout a given year. There were fewer days of the remaining four thresholds, but this was expected as they represent the highest observed temperatures which only occur during one part of the year.

These statistics provide insights into key climatic observations during the study period. For instance, 2006 and 2018 were overall the warmest years of the study period, and 2018 ranked highest combined for all seven climate thresholds. The coolest summers of the study period

were in 2007, 2008, 2009 and 2015, as they experienced the least extreme heat events (lowest combined rank of summer days, hot days, heatwave days and tropical nights). Furthermore, 2014 and 2011 had some of the greatest overall warm days and nights, however this did not necessarily correlate with a greater exposure in hot days, heatwave events or tropical nights.

Table 4.4 Number of annual days *per* climate threshold for the study period. The orange cells indicate years higher than the average (mean) number of annual days exceeding each threshold, and the blue cells indicate years lower than the average (mean) number of days. Those in the darker shading are the years with the highest and lowest number of days *per* climate threshold.

Year	Warm nights	Warm days	WSDI days	Summer days	Hot days	Heatwave days	Tropical nights
2006	216	135	59	38	19	18	3
2007	182	123	59	5	1	0	0
2008	167	98	37	14	2	0	0
2009	191	114	57	18	5	4	0
2010	138	71	25	22	6	0	0
2011	189	137	63	20	6	0	0
2012	167	98	29	22	5	0	1
2013	148	90	27	28	9	6	0
2014	225	152	59	24	5	0	0
2015	181	126	60	16	3	0	1
2016	195	105	23	24	10	9	0
2017	200	125	61	22	8	8	0
2018	202	160	64	51	22	16	2
<b>Average</b>	<b>184.7</b> <b>(50.6%)</b>	<b>118.0</b> <b>(32.3%)</b>	<b>47.9</b> <b>(13.1%)</b>	<b>23.4</b> <b>(6.4%)</b>	<b>7.8</b> <b>(2.1%)</b>	<b>4.7</b> <b>(1.3%)</b>	<b>0.5</b> <b>(0.1%)</b>

### 4.3. Estimating tunnel temperatures

As mentioned in Section 3.3.2, the tunnel temperature estimation model used throughout this study serves two purposes. In this chapter, the descriptive statistics showed data gaps across sub-surface and deep tube tunnel temperatures, influencing the weighting of average

temperatures by LU network type. As Chapter Five presents results on the relationships between WOs and daily temperature variables, the tunnel temperature estimation model addresses the gaps following the joining of WOs and temperature observations. The tunnel temperature estimation model consequently reduces the number of WOs eliminated from analysis. Secondly, as Chapter Six presents results on the effect of future climate change upon the LU network, the tunnel temperature estimation model addresses the missing data in estimating future tunnel temperatures owed to climate change, by using the equation variables.

This section provides the results of the tunnel temperature estimation model, using past temperature observations from the Met Office St. James's Park weather station and the station platform observations across the LU network. This section presents the three tunnel model variables: time lag delay ( $t_d$ ), temperature uplift ( $a$ ), and scaling coefficient ( $b$ ) for  $t_{min}$ ,  $t_{mean}$  and  $t_{max}$ ; by LU line and direction. This includes a regression analysis between observed and estimated temperatures. The variables *per* station platform are reported in the Appendices (Appendix C).

#### **4.3.1.1. Mean daily temperature ( $t_{mean}$ )**

Figure 4.10 shows the mean and one standard deviation of  $t_d$  across all LU tunnels for  $t_{mean}$ . In most cases, mean  $t_d$  did not exceed four days, However, there were discrepancies in the range of  $t_d$  values across each LU tunnel. The distribution of  $t_d$  was greatest on the Bakerloo and Northern lines, particularly in the northbound direction. However, few station platforms had a high  $t_d$  (*e.g.*, greater than approximately 5 days) were small ( $n = 24$ ). Figure 4.11 shows these station platform locations. Many high  $t_d$  values were at interchange stations or near curved track, which may be influencing factors – in that a meandering or other nearby tunnel



could play a role in a greater delay in subsequent rate of tunnel heat gains or losses compared with surface temperature.

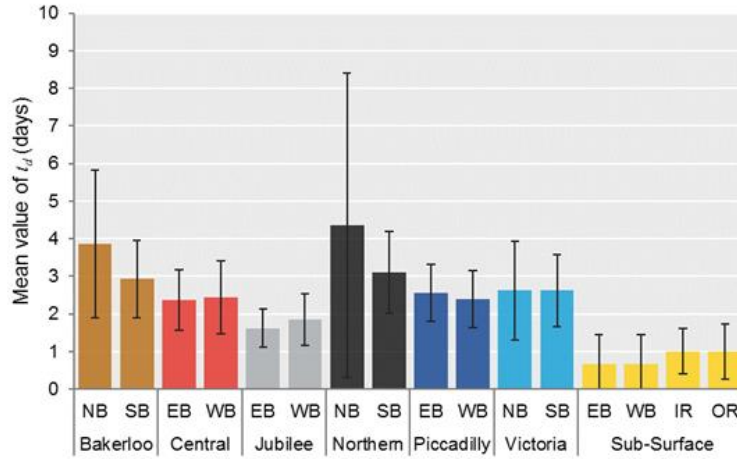


Figure 4.10 Mean value of  $t_{mean} t_d$  per LU station platform for the study period, grouped by LU line and direction of travel. Error bars indicate one standard deviation

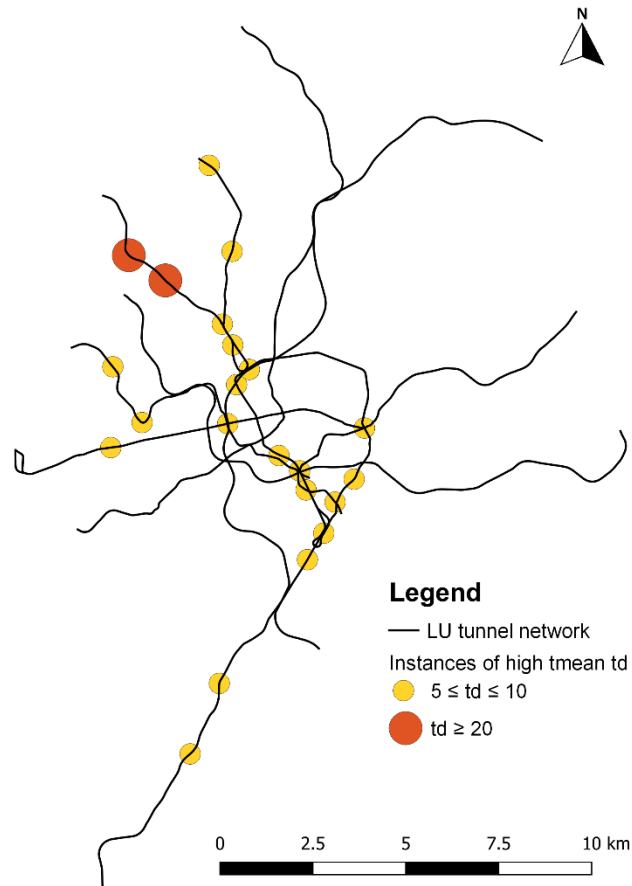


Figure 4.11 Locations of instances across the LU tunnel network where  $t_{mean} t_d \geq 5$  days in one or both directions of travel

The stations with the highest  $t_d$  were the northernmost stations on the Northern line, in the northbound direction: Belsize Park ( $t_d = 20$  days) and Hampstead station ( $t_d = 21$  days). These stations are two of the deepest below ground level (36.0m and 58.9m respectively). Furthermore, platform access to these stations is via lift or stairs as opposed to escalators, as shown in Figure 4.12. There are, however, no discernible trends or similarities among these stations across combined characteristics (*e.g.*, tunnel depth, distance in tunnel, track and/or station geometry, operational externalities to environment such as train frequency) to confidently explain why these locations are outliers.

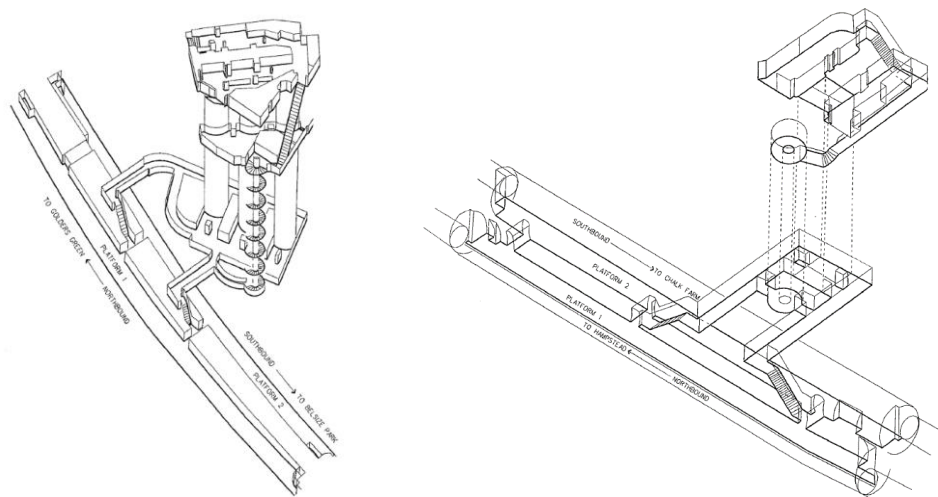


Figure 4.12 Axonometric drawings of Hampstead station (left) and Belsize Park station (right) (Source: TfL, 2017a)

Figure 4.13 shows the mean and one standard deviation of the temperature uplift ( $a$ ) *per* LU line and direction of travel for  $t_{mean}$ .  $a$  was approximately between 9°C and 14°C among the deep tube tunnels and 5°C across the sub-surface part of the LU network. The deep tube tunnel temperature uplift also did not exceed 16°C, shown across the Bakerloo and Central lines, implying a possible upper limit to tunnel temperature uplifts. There were no outliers, thus temperature uplifts are broadly constant and stable throughout each LU tunnel.

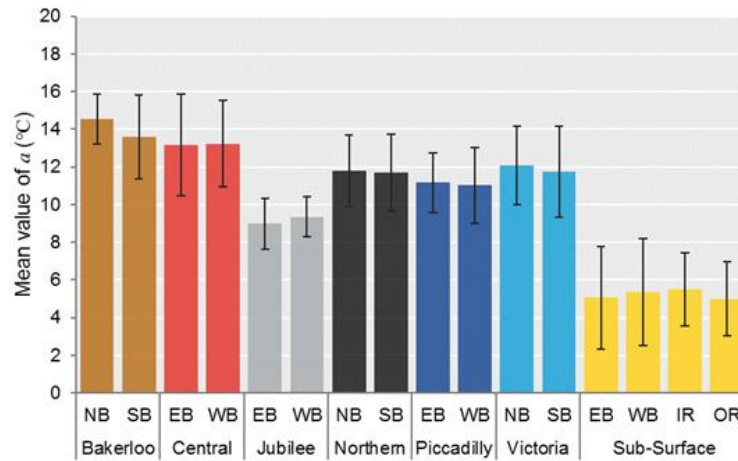


Figure 4.13 Mean value of  $t_{mean} a$  per LU station platform for the study period, grouped by LU line and direction of travel. Error bars indicate one standard deviation

Figure 4.14 shows the mean and one standard deviation of the scaling coefficient ( $b$ ) per LU tunnel for  $t_{mean}$ . Among the deep tube tunnels, the mean value of  $b$  was approximately between 0.4 and 0.5, indicating that temperature flux over time in the deep tube tunnels was approximately half the scale of that observed on the surface. Contrastingly, the mean value of  $b$  across the sub-surface part of the LU network was double that of the deep tube tunnels, at 0.8.  $a$  and  $b$  were negatively correlated as expected and describes the intuitive relationship between the tunnel environments (e.g., depth, ventilation capacity) and surface temperature.

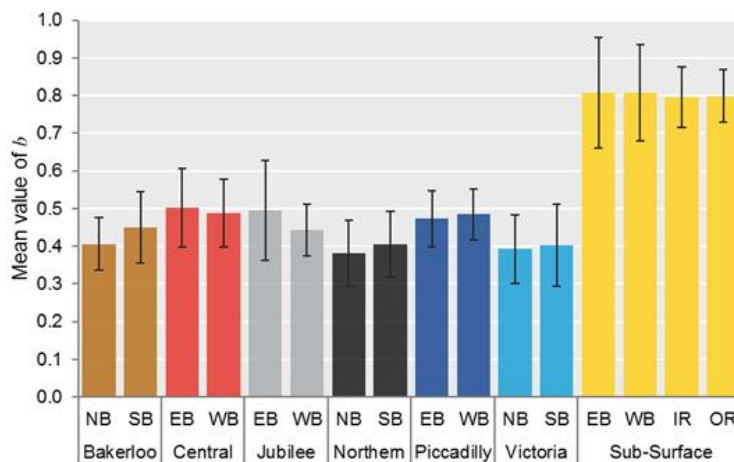


Figure 4.14 Mean value of  $t_{mean} b$  per LU station platform for the study period, grouped by LU tunnel. Error bars indicate one standard deviation

To validate the accuracy of the tunnel temperature model, linear regression was conducted (see Section 3.3.2.3), comparing the observations as dependent variables and estimated temperatures as independent variables. Table 4.5 shows the regression results and coefficients for  $t_{mean}$  per LU tunnel.

Table 4.5 Regression results from comparing  $t_{mean}$  from the tunnel temperature estimation model outputs with observed  $t_{mean}$  for the study period

LU tunnel	$R^2$	$b_1$	$SE(b_1)$	$b_0$	$p$	$RSE$	$df$
Bakerloo NB	0.709	2.528	(0.061)	0.905	<0.001	1.628	65165
Bakerloo SB	0.780	-0.215	(0.054)	1.008	<0.001	1.752	65090
Central EB	0.837	0.000	(0.043)	1.000	<0.001	1.670	67586
Central WB	0.825	0.000	(0.045)	1.000	<0.001	1.598	67962
Jubilee EB	0.754	0.001	(0.059)	1.000	<0.001	1.774	41877
Jubilee WB	0.710	-0.126	(0.068)	1.006	<0.001	1.718	41859
Northern NB	0.746	0.048	(0.035)	0.998	<0.001	1.608	115439
Northern SB	0.769	-0.019	(0.034)	1.001	<0.001	1.607	154434
Piccadilly EB	0.813	0.000	(0.041)	1.000	<0.001	1.453	76994
Piccadilly WB	0.798	0.001	(0.042)	1.000	<0.001	1.578	76628
Victoria NB	0.587	0.000	(0.077)	1.000	<0.001	2.482	69742
Victoria SB	0.634	0.000	(0.044)	1.000	<0.001	2.471	69729
Sub-Surface EB	0.935	-0.092	(0.028)	1.005	<0.001	1.417	29245
Sub-Surface WB	0.921	0.000	(0.038)	1.000	<0.001	1.501	21085
Sub-Surface IR	0.872	0.097	(0.036)	0.986	<0.001	1.654	28892
Sub-Surface OR	0.910	0.000	(0.031)	1.000	<0.001	1.501	33088

Standard errors are reported in parentheses  
 $SE$  = standard error,  $RSE$  = residual standard error,  $df$  = degrees of freedom

Firstly, the regression results were statistically very significant across all LU tunnels ( $p < 0.001$ ). The coefficients of determination ( $R^2$ ) were quite high across the LU network, ranging from 0.587 (Victoria line NB) and 0.935 (Sub-Surface EB), which indicates that a large proportion of the variance for observed  $t_{mean}$  tunnel temperatures, could be explained by the estimated  $t_{mean}$  tunnel temperatures.  $R^2$  also varied slightly between the LU lines' directions of travel.

For example, the Bakerloo SB  $R^2$  was greater than NB.  $R^2$  was lowest on the Victoria line, suggesting that other factors may influence the variance in the tunnel temperatures. For example, the Victoria line trains operate more frequently than other LU lines and may therefore generate relatively more operational heat, as previously discussed in Section 1.3.2.

The intercept, or  $b_1$  coefficients of all LU tunnels did not deviate greatly from 0, indicating that if the model were to estimate a tunnel platform  $t_{mean}$  of 0°C, the observed temperature was likely to also be 0°C. There was, however, one outlier: Bakerloo line NB, which was approximately +2.5°C; suggesting that the model may have underestimated  $t_{mean}$  across this tunnel. Nevertheless, the standard error of  $b_1$  coefficients were small ( $< 0.1$ ) for all LU tunnels, suggesting that there is confidence in the precision of estimates from this regression analysis.

Similarly, the slope of the model variables, or  $b_0$  of all LU tunnels did not deviate greatly from around 1, implying that the predicted change in the tunnel platform model variables for  $t_{mean}$  also equated to the same rate of change in the observed tunnel platform  $t_{mean}$ . The greatest outliers in these results were also across the Bakerloo NB tunnel, where the slope indicates that the predicted change in observed tunnel platform  $t_{mean}$  changes at a slightly slower rate than the model.

The residual standard error ( $RSE$ ) measures how well the regression model fits the dataset. In Table 4.2, the  $RSE$  values varied between 1.42 and 2.48.  $RSE$  were normally distributed, shown in Figure 4.15 and Figure 4.16. Most residual values did not deviate greatly from 0, in most cases this was 20-25% of days in the study period. The only LU tunnels with different trends were on the Victoria line. They were less normally distributed and less concentrated around 0, explaining the higher  $RSE$ .

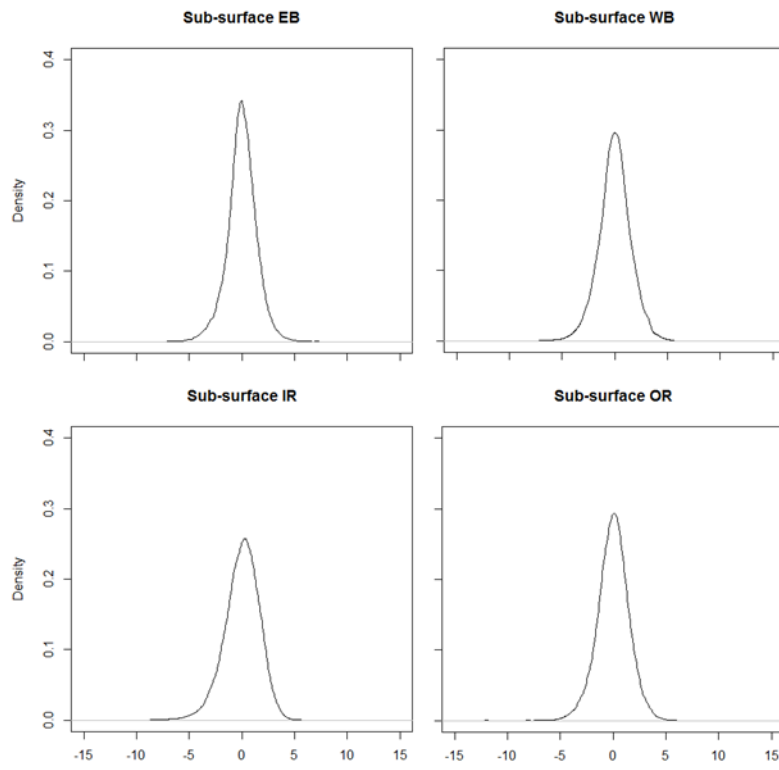


Figure 4.15 Regression residual density plots of  $t_{mean}$  per LU sub-surface direction of travel

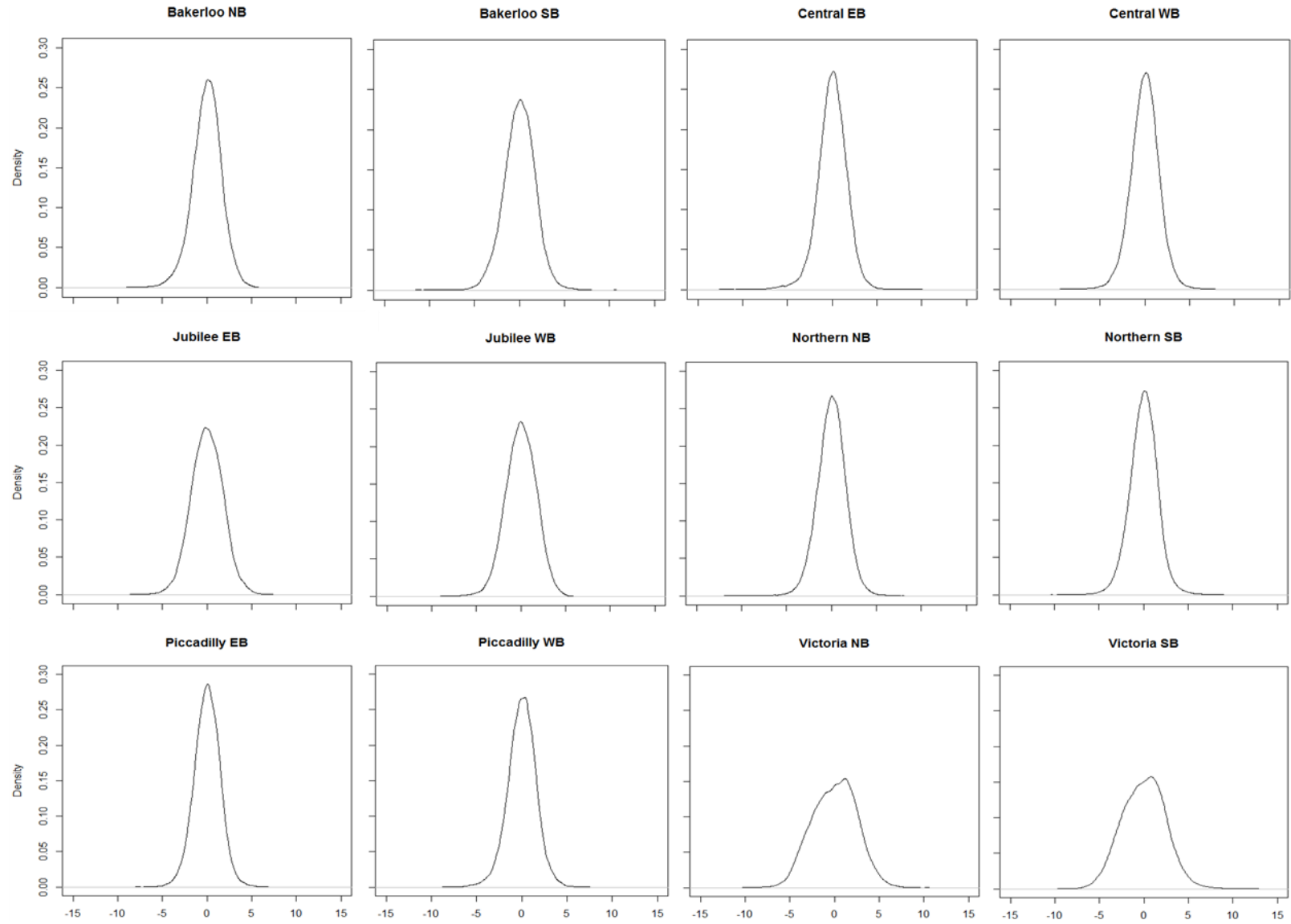


Figure 4.16 Regression residual density plots of  $t_{mean}$  per LU deep tube tunnel

### 4.3.1.2. Maximum daily temperature ( $t_{max}$ )

Figure 4.17 shows the mean and one standard deviation of  $t_d$  per LU tunnel for daily  $t_{max}$ . Compared with  $t_{mean}$ ,  $t_d$  values were similar. However, they were greatest on the Bakerloo, Northern and Victoria lines, particularly in their NB directions. Standard deviations were also greatest on these lines and more station platforms reported  $t_d > 20$  (seven compared with two), including those in Figure 4.12. A greater lag in  $t_{max}$  suggests that there is a slower build-up and release of higher temperatures and illustrates the potential maximum thermal capacity of tunnel walls across the LU network and heat retention within the tunnels.

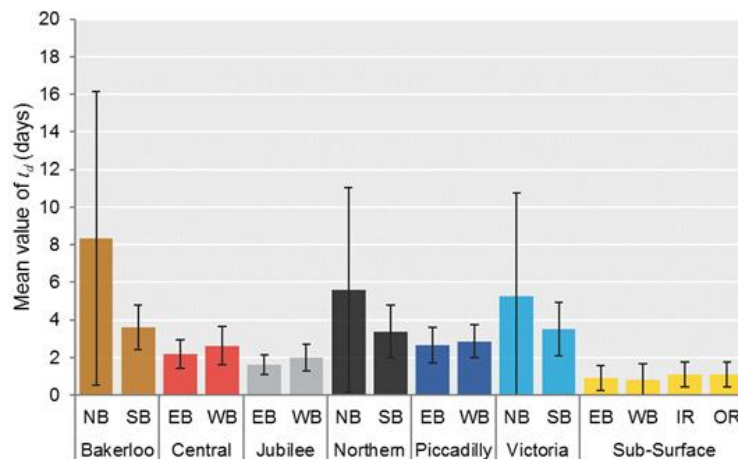


Figure 4.17 Mean value of  $t_{max}$   $t_d$  per LU station platform for the study period, grouped by LU tunnel. Error bars indicate one standard deviation

Figure 4.18 shows the mean and one standard deviation of  $a$  per LU tunnel for daily  $t_{max}$ . Compared with  $t_{mean}$ , the mean value of  $a$  and their distributions across the LU lines were very similar, though approximately  $2^{\circ}\text{C}$  lower. Figure 4.19 is similar, where the mean and one standard deviation of  $b$  per LU tunnel was slightly lower. This may also be indicative of an absolute upper thermal limit in tunnel temperatures.



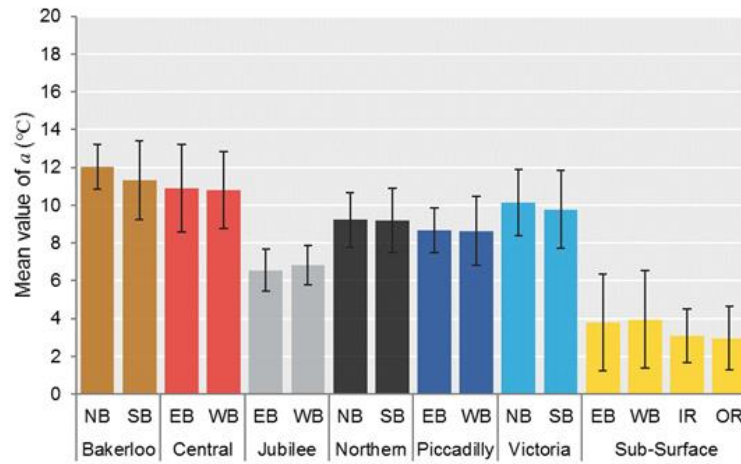


Figure 4.18 Mean value of  $t_{max} a$  per LU station platform for the study period, grouped by LU tunnel. Error bars indicate one standard deviation

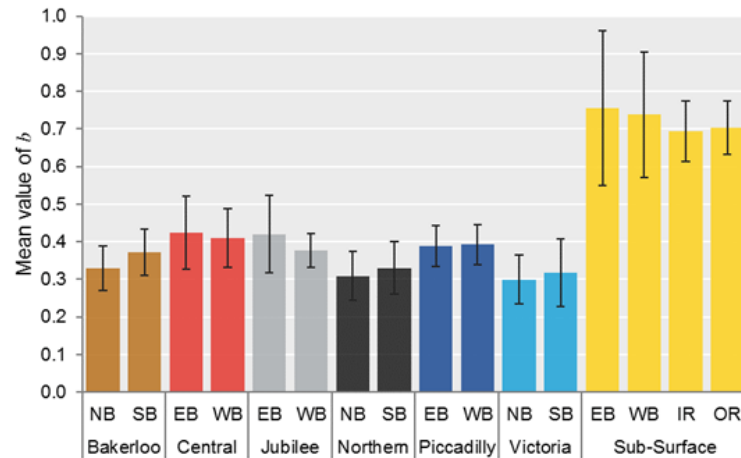


Figure 4.19 Mean value of  $t_{max} b$  per LU station platform for the study period, grouped by LU tunnel. Error bars indicate one standard deviation

Table 4.6 shows the linear regression results for observed and estimated daily  $t_{max}$ . While all results were very statistically significant ( $p < 0.001$ ), all LU lines reported slightly lower  $R^2$  values than  $t_{mean}$ . Therefore, a lower proportion of the variance for observed  $t_{max}$  tunnel temperatures were explained by the modelled  $t_{max}$  tunnel temperatures. This suggests that other factors beyond surface temperature influenced tunnel  $t_{max}$ , though perhaps only by a small degree. Furthermore, as these were variations in a daily value, other influencing factors may have had a sub-daily effect. The  $b_1$  coefficients did not deviate greatly from 0, although most LU tunnels were marginally negative. This means that the model may have very slightly

overestimated tunnel  $t_{max}$ . For example, if the observed  $t_{max}$  was 0°C, the estimated  $t_{max}$  was slightly greater than 0°C. Standard errors of  $b_1$  were slightly greater compared with  $t_{mean}$ , although still low, so there is still a sufficient level of confidence in the estimates. The slope coefficients ( $b_0$ ) of all LU tunnels also did not deviate greatly from 1, therefore the predicted change in observed tunnel platform  $t_{max}$  changed at a proportionate rate to the model.

Table 4.6 Regression results from comparing  $t_{max}$  from the tunnel temperature estimation model outputs with observed  $t_{max}$  for the study period

LU tunnel	$R^2$	$b_1$	$SE(b_1)$	$b_0$	$p$	$RSE$	$df$
Bakerloo NB	0.693	-0.055	(0.072)	1.002	<0.001	1.601	65167
Bakerloo SB	0.750	0.056	(0.061)	0.998	<0.001	1.791	65090
Central EB	0.812	-0.013	(0.049)	1.000	<0.001	1.697	67609
Central WB	0.807	-0.015	(0.050)	1.000	<0.001	1.599	67988
Jubilee EB	0.731	-0.006	(0.066)	1.000	<0.001	1.812	41876
Jubilee WB	0.693	0.026	(0.073)	1.000	<0.001	1.724	41860
Northern NB	0.699	-0.125	(0.041)	1.000	<0.001	1.589	155447
Northern SB	0.728	-0.010	(0.039)	1.000	<0.001	1.627	154440
Piccadilly EB	0.778	-0.105	(0.047)	1.004	<0.001	1.466	76997
Piccadilly WB	0.767	-0.017	(0.049)	1.001	<0.001	1.592	76634
Victoria NB	0.543	-0.040	(0.089)	1.001	<0.001	2.360	69742
Victoria SB	0.577	-0.018	(0.082)	1.001	<0.001	2.456	69729
Sub-Surface EB	0.860	0.752	(0.046)	0.944	<0.001	2.199	29249
Sub-Surface WB	0.886	-0.187	(0.050)	1.003	<0.001	1.804	21087
Sub-Surface IR	0.862	0.000	(0.046)	1.000	<0.001	1.758	28891
Sub-Surface OR	0.881	0.002	(0.039)	1.000	<0.001	1.755	33088

The  $t_{max}$   $RSE$  were also similar to  $t_{mean}$ . However, all but three tunnels (Bakerloo NB; Victoria NB and SB) reported slight increases in residual standard errors compared with  $t_{mean}$ . These tunnels exhibit slightly outlier trends throughout the tunnel temperature estimation model, so are perhaps affected more by other factors than the surface temperature.

#### 4.3.1.3. Minimum daily temperature ( $t_{min}$ )

Figure 4.20 shows the mean and one standard deviation of  $t_d$  per LU tunnel for  $t_{min}$ . They were also similar to  $t_{mean}$  and  $t_{max}$ , though lower. Four station platforms reported values of  $t_d$  greater than 5, including Hampstead ( $t_d = 20$ ) and Belsize Park ( $t_d = 19$ ) in Figure 4.12. Figure 4.21 and Figure 4.22 show the means and one standard deviation of  $a$  and  $b$  respectively per LU tunnel for  $t_{min}$ . The trends are inverse to  $t_{max}$  relative to  $t_{mean}$ , where  $a$  was higher and  $b$  was lower. This quantitatively illustrates the extent that tunnels retained heat even during low surface temperatures.

Table 4.7 shows the linear regression results for all  $t_{min}$ . All LU tunnels were also statistically very significant ( $p < 0.001$ ). However, some of the  $R^2$  values were greater than  $t_{mean}$  and  $t_{max}$ , such as Northern and Victoria lines in both directions. The values of  $b_1$  did not deviate greatly from 0, with the highest deviation from both Bakerloo tunnels and the sub-surface (EB and WB). Similarly, the values of  $b_0$  did not deviate greatly from 0. The  $RSE$  increased when compared with those reported for  $t_{mean}$  and  $t_{max}$ , varying between 1.80 and 3.06. This suggests that the model can estimate tunnel  $t_{min}$  but there is possibly a greater moderating effect outside of surface  $t_{min}$  impacting the tunnel  $t_{min}$ .

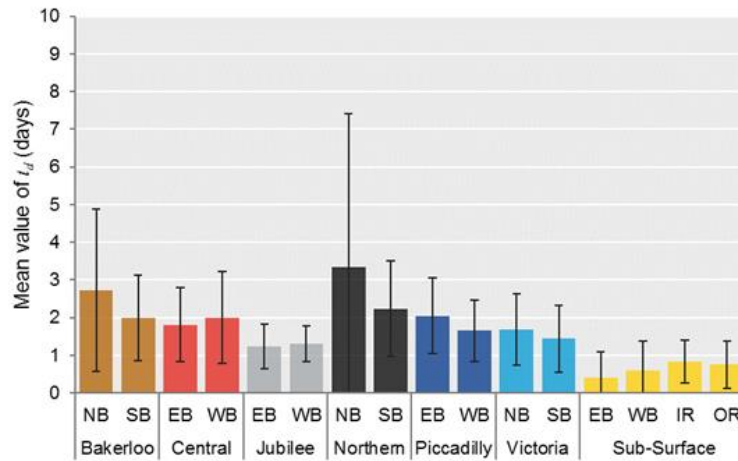


Figure 4.20 Mean value of  $t_{min} t_d$  per LU station platform for the study period, grouped by LU tunnel. Error bars indicate one standard deviation

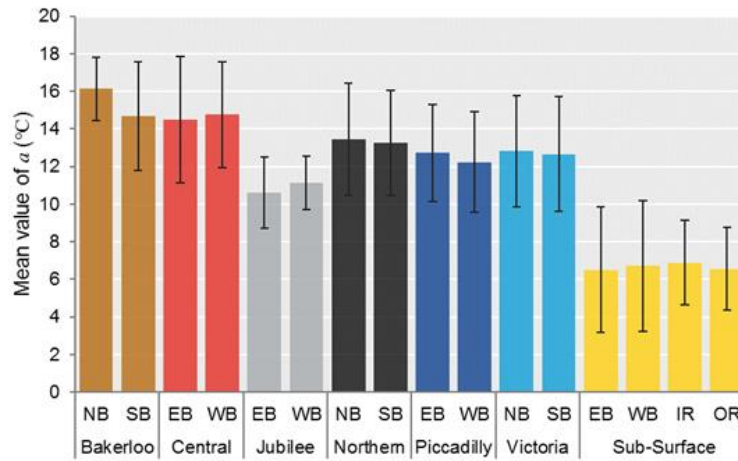


Figure 4.21 Mean value of  $t_{min} a$  per LU station platform for the study period, grouped by LU tunnel. Error bars indicate one standard deviation

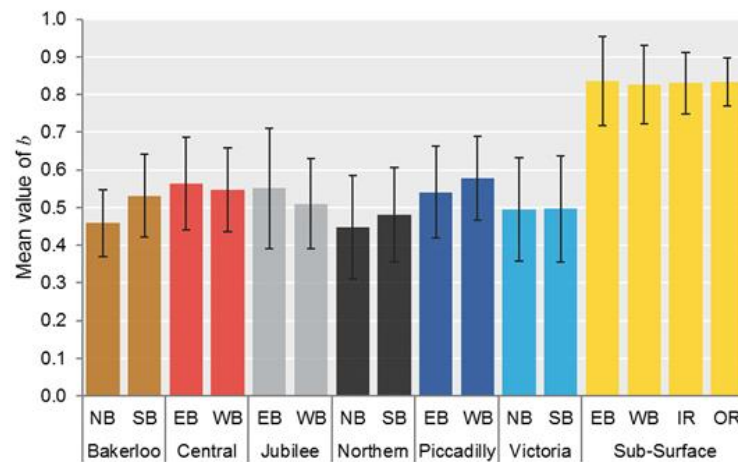


Figure 4.22 Mean value of  $t_{min} b$  per LU station platform for the study period, grouped by LU tunnel. Error bars indicate one standard deviation

Table 4.7 Regression results from comparing  $t_{min}$  from the tunnel temperature estimation model outputs with observed  $t_{min}$  for the study period

<b>LU tunnel</b>	<b><math>R^2</math></b>	<b><math>b_1</math></b>	<b><math>SE(b_1)</math></b>	<b><math>b_0</math></b>	<b><math>p</math></b>	<b><math>RSE</math></b>	<b><math>df</math></b>
Bakerloo NB	0.659	-0.693	(0.072)	1.027	<0.001	2.073	65167
Bakerloo SB	0.753	-0.409	(0.054)	1.017	<0.001	2.250	65090
Central EB	0.809	0.000	(0.044)	1.000	<0.001	2.092	67609
Central WB	0.771	-0.001	(0.050)	1.000	<0.001	2.102	67988
Jubilee EB	0.724	0.000	(0.059)	1.000	<0.001	2.118	41846
Jubilee WB	0.646	0.000	(0.072)	1.000	<0.001	2.224	41860
Northern NB	0.774	-0.026	(0.031)	1.001	<0.001	1.976	115447
Northern SB	0.774	0.001	(0.031)	1.000	<0.001	1.927	154440
Piccadilly EB	0.801	0.001	(0.039)	1.000	<0.001	1.871	76997
Piccadilly WB	0.765	-0.024	(0.043)	1.001	<0.001	2.116	76634
Victoria NB	0.609	-0.002	(0.066)	1.000	<0.001	3.062	69742
Victoria SB	0.655	0.000	(0.060)	1.000	<0.001	2.840	69730
Sub-Surface EB	0.880	0.109	(0.035)	0.972	<0.001	1.956	29249
Sub-Surface WB	0.892	-0.050	(0.041)	1.002	<0.001	1.847	21087
Sub-Surface IR	0.835	0.000	(0.044)	1.000	<0.001	1.923	28891
Sub-Surface OR	0.871	0.000	(0.034)	1.000	<0.001	1.800	33088

#### 4.3.1.4. Diurnal temperature range ( $\Delta t$ )

Estimated  $\Delta t$  was derived by subtracting estimated  $t_{min}$  from estimated  $t_{max}$ . Therefore, there are no tunnel model variables. The model does not perfectly predict tunnel temperatures, and there was often a small degree of error, shown in the residual density plots, for example, in Figure 4.15 and Figure 4.16. The impact of this, considering the annual temperature range in some of the LU tunnels is small, is that the resulting estimated  $\Delta t$  would produce some negative values. These were corrected to 0°C prior to the regression analysis, shown in Table 4.8. Consequently, the regression coefficients indicate that the model is less effective at estimating  $\Delta t$ .

Table 4.8 Regression results from comparing  $\Delta t$  from the tunnel temperature estimation model outputs with observed  $\Delta t$  for the study period

<b>LU tunnel</b>	<b><math>R^2</math></b>	<b><math>b_1</math></b>	<b><math>SE(b_1)</math></b>	<b><math>b_0</math></b>	<b><math>p</math></b>	<b><math>RSE</math></b>	<b><math>df</math></b>
Bakerloo NB	0.230	1.370	(0.010)	0.469	<0.001	1.449	65123
Bakerloo SB	0.430	1.126	(0.017)	0.664	<0.001	1.644	65066
Central EB	0.495	0.977	(0.010)	0.681	<0.001	1.568	67595
Central WB	0.337	1.185	(0.010)	0.560	<0.001	1.504	67976
Jubilee EB	0.347	1.127	(0.013)	0.579	<0.001	1.510	41873
Jubilee WB	0.230	1.152	(0.014)	0.530	<0.001	1.575	41854
Northern NB	0.560	0.619	(0.005)	0.745	<0.001	1.427	155372
Northern SB	0.472	0.824	(0.006)	0.678	<0.001	1.374	154395
Piccadilly EB	0.513	0.848	(0.008)	0.674	<0.001	1.344	76987
Piccadilly WB	0.426	1.126	(0.010)	0.633	<0.001	1.546	76612
Victoria NB	0.459	0.938	(0.014)	0.763	<0.001	1.929	69707
Victoria SB	0.361	1.271	(0.014)	0.663	<0.001	1.763	69696
Sub-Surface EB	0.395	1.807	(0.021)	0.561	<0.001	2.167	29244
Sub-Surface WB	0.521	1.370	(0.017)	0.579	<0.001	1.499	21084
Sub-Surface IR	0.205	1.877	(0.012)	0.291	<0.001	1.244	28888
Sub-Surface OR	0.260	2.003	(0.011)	0.333	<0.001	1.232	33084

#### 4.4. Chapter summary

This chapter presented results describing the thermal environment across the LU network. It showed how there are very notable differences in temperature observations across network types, LU lines, and station platforms. It demonstrated that there were gaps in observed station platform data across the sub-surface and deep tube tunnel parts of the LU network, and without addressing these, would lead to further data elimination and a potential impact to the fault exposure rate analysis in the next chapter. This justified the first reason to utilise a model in this study to estimate tunnel temperatures using surface temperatures as a proxy, providing a more complete dataset for the study period, but also quantify the extent of the moderating effect

surface temperatures had upon tunnel temperatures. Additionally, the model provides the capability to estimate future tunnel temperatures under differing climate scenarios.

The climate thresholds quantitatively showed how temperatures have changed in the study period, even relative to the recent baseline period. It is unambiguously warmer, with 56% of days in the study period exceeding at least one climate threshold. The latter years of the study period, mainly 2016-2018 experienced particularly notable periods of warmth, with nuanced increases in temperatures throughout the year and more extreme heat events occurring – which also amplified temperature increases in the tunnels. Since more prolonged record-breaking temperatures occurred since this study period, such as the first instance of 40°C in the UK in July 2022, it emphasises the importance of the results from this chapter and the implications for LU network.

The tunnel temperature estimation was statistically validated using linear regression and was a successful development on the study by Kimura *et al.* (2018). Additionally, the results helped to quantify the extent of other factors acting upon the thermal environment, based on the regression coefficients. However, the results showed differing degrees of error in the model at the scale of daily observations across the LU tunnels and among each temperature variable ( $t_{mean}$ ,  $t_{max}$ ,  $t_{min}$ ,  $\Delta t$ ). This stresses the importance of considering other factors that are likely impacting the thermal environment of the tunnel and sub-surface sections of the LU network beyond the surface temperature, as the model quantitatively highlights these via the small degrees of error in the regression results.

The next chapter provides the results for the fault exposure rate analysis for point and train stop assets over the study period. Results and variables from this chapter are utilised throughout the

fault exposure rate analysis, such as grouping by climate thresholds and using the tunnel temperature estimation model results to join temperature values to WOs prior to analysis.



# Chapter Five | Fault exposure rates

## 5.1. Chapter overview

Chapter Four presented results that characterised the current thermal environment of the LU network. Results included the distribution of daily temperature variables across the network ( $t_{mean}$ ,  $t_{max}$ ,  $t_{min}$ ,  $\Delta t$ ), the frequency of days in the study period that reached certain climate thresholds, and the utilisation and validation of a tunnel temperature estimation model. Results from Chapter Four contribute to this chapter, which examines fault exposure rates *per* temperature variable as defined by Fisher (2020). Data gaps in daily tunnel temperature variables are rectified using the tunnel temperature estimation model and merged with observations prior to analysis. Trends in fault exposure rates are presented for each LU line, distinguished by network type (surface, sub-surface, and tunnel) at incremental 1°C bins *per* temperature variable. They are then examined further; grouping fault exposure rates by whether WOs are reported as corrective or reactive, and whether faults exceed the defined climate thresholds.

## 5.2. Work orders

To develop fault exposure rates, data collected by TfL on WOs were required. As described in Chapter Three, TfL provided WO data from the two data management systems used across the LU network (Ellipse and Metro Maximo). Additional attributes (*e.g.*, nearest station, network type, daily temperature variables) were joined to each WO record to for aggregation (see Section 3.2.3.2).

### 5.2.1. Work order data overview

The combined point and train stop WO database from the asset management systems for this study comprised 45787 WOs from 2006 to 2018. 39629 were corrective (“faults that you find”) and 6158 were reactive (“faults that find you”). Figure 5.1 shows the distribution of corrective and reactive WOs over time. Mean WOs *per year* was 3522 with a standard deviation of 1237. The fewest annual WOs was in 2006 (951) and the most was in 2018 (5782).

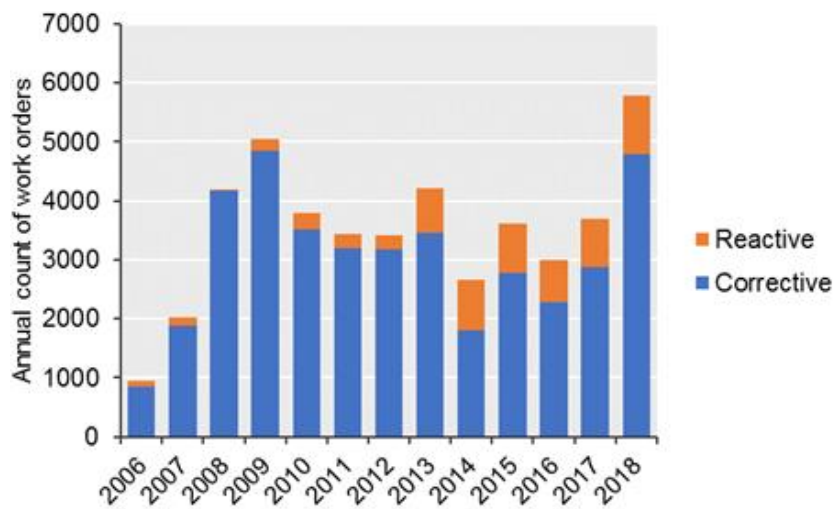


Figure 5.1 Type of WOs raised in the study period

Most WOs were corrective. The proportionate share between WO type varied from 99% corrective and 1% reactive in 2007 to 68% corrective and 32% reactive in 2014. In absolute terms, reactive WOs increased from 2013 and remained over 700 *per year*. Prior to 2013, reactive WOs were fewer than 300 *per year*. The most reactive WOs in a single year occurred in 2018 (997).

WOs also varied by their closed status. Figure 5.2 shows the annual distribution of WO closure status over time. Most WOs were “completed” when closed, so an action was undertaken to address the reason the WO was opened. 52% of WOs *per year* on average were classified as

“complete” when closed, ranging between 35% and 68% in any given year. However, each year there were several WOs with no closure status defined. This was an average of 29% *per* year, ranging between 10% and 55%. Up to 33% of WOs *per* year were also classified as not required/no fault found. The share of these was often greater where total annual WOs were highest – particularly in 2008, 2009 and 2018. Cancelled WOs were a small share; no more than 6% of WOs in any given year.

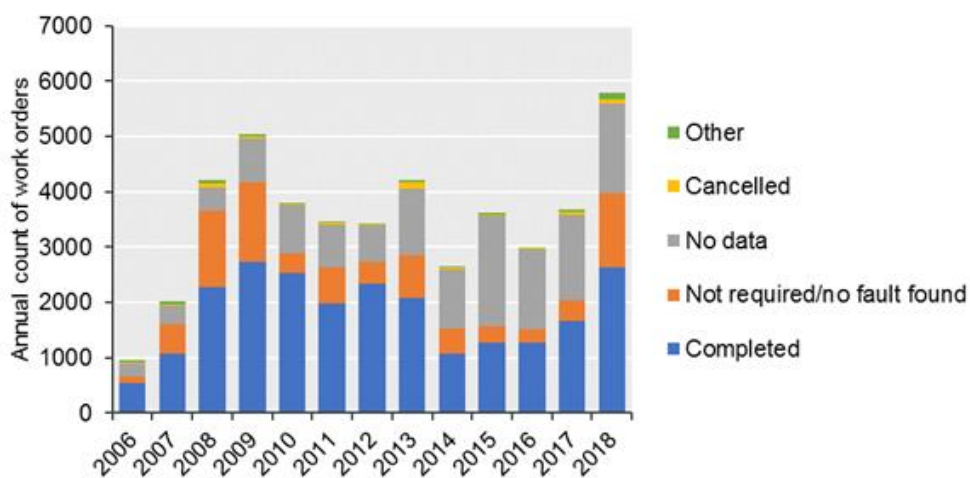


Figure 5.2 Status of WOs raised upon closure

Of all the WO data analysed, 21631 were raised on days exceeding at least one climate threshold (see Section 3.3.1.2 for definitions); slightly under half of all WOs (47%). Figure 5.3 compares the share of days and WOs within each climate threshold. It gives an indication as to whether more or fewer WOs occurred under each climate threshold relative to the proportion of days under the same climate threshold.

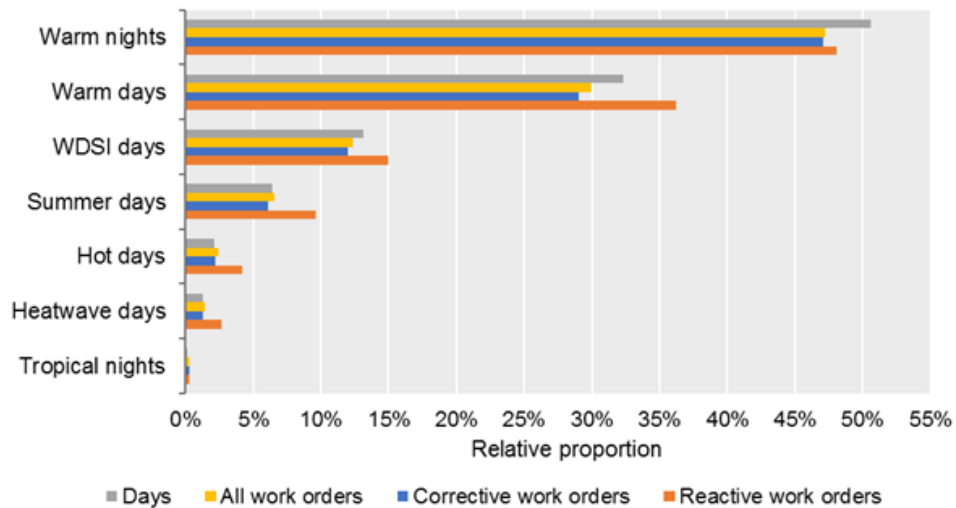


Figure 5.3 Relative proportion of days and WOs occurring during days that exceeded each climate threshold

Figure 5.3 shows different trends depending on WO type during days that exceeded at least one climate threshold. For year-round climate thresholds (warm nights, warm days, and warm spell duration index [WSDI] days), there was a lower share of WOs relative to the number of days. However, reactive WOs were proportionately greater for all days exceeding any climate threshold except for warm nights, and the difference between the proportionate corrective and reactive WOs increases with each climate threshold. On warm days and WSDI days, proportionate reactive WOs were greater than corrective by a factor of 1.2. For summer days, it was a factor of 1.6, for hot days, a factor of 1.9, and during heatwave days, a factor of 2.1. Tropical nights were the exception, where the trend decreased, with proportionate reactive WOs greater than corrective by a factor of 1.2.

### 5.2.2. Temperature variables

Daily temperature variables were joined to the WO dataset by date, nearest station, and network type. Therefore, there were 12 unique groups of WO data used for analysis. A small number of instances did not meet the joining criteria due to missing data in the WO. These WOs were

therefore eliminated from any further analysis, which was approximately 3% of the dataset. Then, the count of faults *per* station platform were normalised, as described in Section 3.4.1.

### **5.3. Fault exposure rates: surface**

The following sections of this chapter present the fault exposure rates from WOs starting with the surface part of the network, then the sub-surface part, and finally the deep tube tunnels. The surface part of the LU network spans the greatest length of track (see Section 1.1.1), the most point and train stop assets, and the most WOs. Every LU line selected for this study is therefore represented in some capacity across surface fault exposure rates.

#### **5.3.1. Daily mean temperature ( $t_{mean}$ )**

Figure 5.4 shows the surface  $t_{mean}$  fault exposure rates for the study period. Several LU lines' surface fault exposure rates showed increases at the highest and lowest temperature observations. In most cases, the fault exposure rate of each LU line was within the whole surface network mean. Fault exposure rates increased on some LU lines at higher and lower  $t_{mean}$ . Eight reactive WOs were raised on 28/02/2018, in four locations, when  $t_{mean}$  was below  $-4^{\circ}\text{C}$ , shown in Table 5.1. This date was the lowest observed  $t_{mean}$  within the study period. It also coincided with a strong easterly airflow that followed with snow showers and freezing rain (Met Office, 2018a). The faults that occurred on the point assets in the coldest conditions were primarily related to two issues. Firstly, points failed to reverse, which is when they cannot move to their intended position. Secondly, point heaters failed. Point heaters are specifically used to prevent the formation of ice and snow that would otherwise prevent the point's operation, and

while they are typically set up in the GB railway industry to withstand an ambient air temperature of up to -25°C, but not drifting snow (Ellis, 2019).

Table 5.1 WOs raised on the Central line corresponding with the highest fault exposure rate on 28/02/2018

<b>Time raised</b>	<b>Nearest station</b>	<b>Equipment type</b>	<b>Fault</b>
06:33	Hainault	4Ft Eh Points	Failing to reverse
08:30	South Ruislip	Surelock 4' Electric Points	Point heater not working
19:06	Loughton	Surelock 6' Electric Points	Point heater not working
19:07	Loughton	Surelock 6' Electric Points	Point heater not working
19:19	Loughton	Surelock 6' Electric Points	Point heater not working
20:11	Loughton	M63 Electric Points	Failing to reverse
20:11	Hainault	4Ft Eh Points	Signals unable to clear
22:04	Northolt	4Ft Eh Points	Failing to reverse

This fault exposure rate coincided with an exceptionally high lower bound and is consequently an anomalous occurrence. Similarly, fault exposure rates on the Bakerloo, District, and Metropolitan between -3°C and -2°C. A large proportion of these WOs were corrective, primarily on the Metropolitan line in some of the most north-westerly stations (*i.e.*, outside of the Greater London boundary). The WO database shows that these related to work that was undertaken to prevent the minimum gauge from being reached. However, all the reactive WOs within this temperature bin, of which there are ten, occurred around the same time as those reported in Table 5.1 (between 27/02/2018 and 02/03/2018). The fault exposure rate on the Victoria line was also high between -1°C and 0°C. There were 13 corrective WOs responsible for this at one station, which took place on 02/02/2009. Ten were however raised in error, overstating the fault exposure rate.

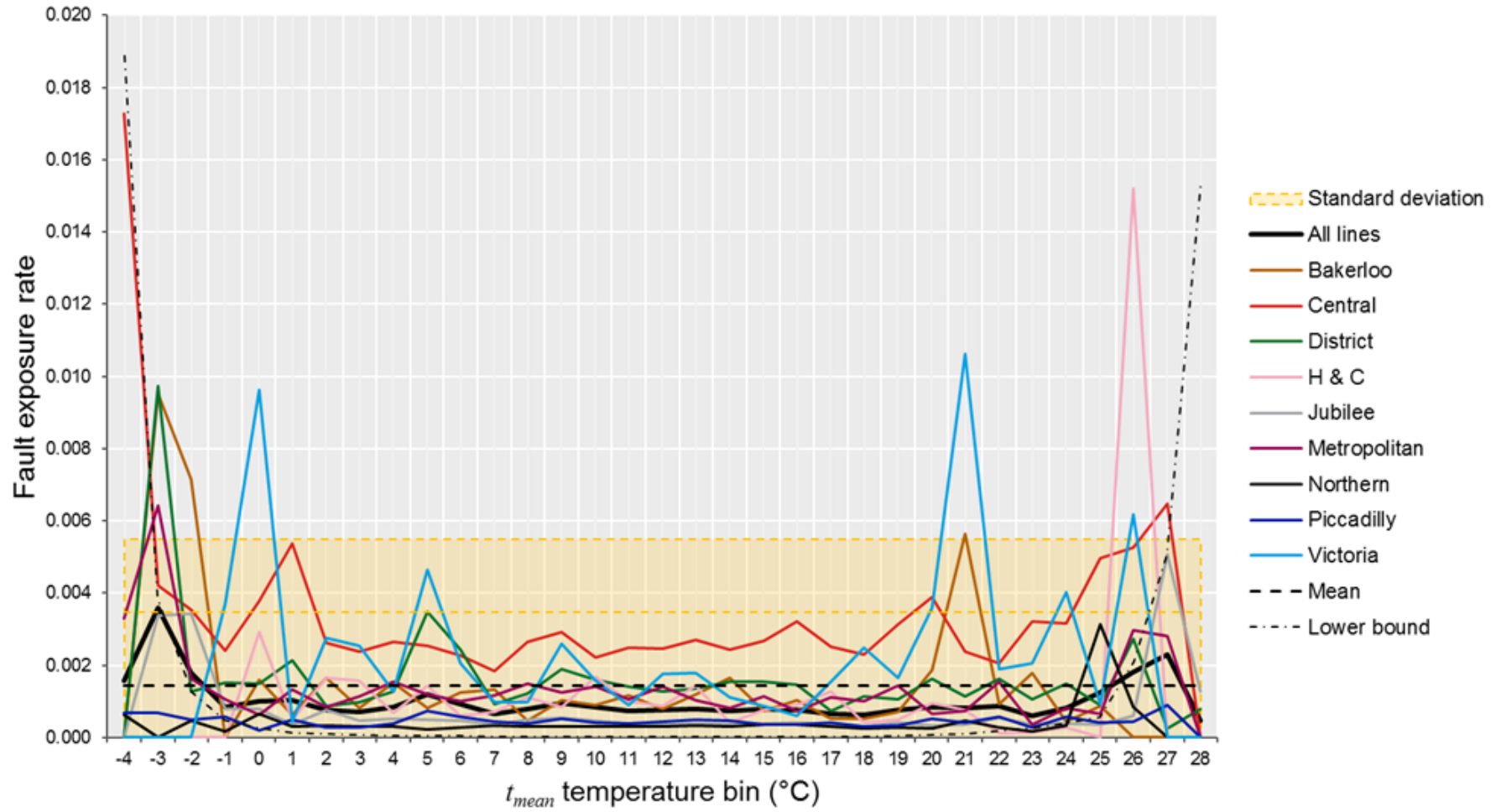


Figure 5.4 Fault exposure rates of  $t_{mean}$  per LU line for the surface part of the LU network

Figure 5.5 compares the fault exposure rate trends of  $t_{mean}$  between corrective and reactive WOs. The cold temperature peak fault exposure rate occurs at the same point (between -3°C and -2°C) but the trends leading up to those peaks differ. Reading the graph from right to left, the corrective fault exposure rate fluctuated as temperatures decreased, while the reactive fault exposure rate gradually increased. More corrective WOs may have kept reactive WOs low up to a point, as after -1°C, even with a greater corrective fault exposure rate, the reactive rate also increased.

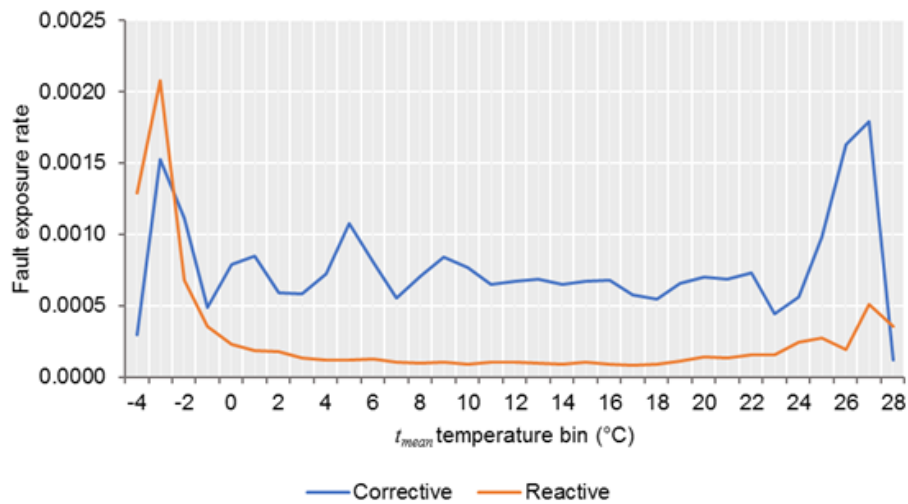


Figure 5.5 Difference in fault exposure rate trends of surface  $t_{mean}$  for all lines by WO type

As for higher  $t_{mean}$ , fault exposure rates begin to increase at approximately 20°C. The first LU lines that exceeded two standard deviations were the Victoria and Bakerloo lines, between 20°C and 21°C. Both lines' fault exposure rates were primarily driven by a mass raising of corrective WOs to replace fibre washers on 20/07/2018 across point assets. Following this, the Central, Hammersmith & City and Victoria lines' fault exposure rates exceeded two standard deviations between 25°C and 27°C, with the highest peak on the Hammersmith/Circle lines at 26°C. 13 Hammersmith & City line corrective WOs were raised at Hammersmith station. They were also regarding minimum gauge, like those raised in the colder temperatures on the Metropolitan line.



On the Victoria line, there were two WOs driving the fault exposure rate at 26°C, one corrective and one reactive. On the Central line, the fault exposure rate is the only one that gradually increases *per* temperature bin from around 21°C, until it exceeds two standard deviations at the 26-27°C temperature bin.

Table 5.2 shows the WOs raised that drove the Central line’s surface  $t_{mean}$  fault exposure rate between 26°C and 27°C. They were all corrective. The 2006 WO was the same type of fault raised in under cold temperatures (shown in Table 5.1), implying that the issue happens at both temperature extremes. Fitting or converting KLM clips comprised three of the six WOs in Table 5.2; these are a brand of safety fasteners used across many LU point motor assets. 330 WOs related to KLM clips were raised from mid-July 2018 until 1<sup>st</sup> October 2018. Of these WOs, 202 were completed across several stations on the LU network. The three WOs were part of 35 whose closed dates were an earlier than the date raised, suggesting that they were raised retrospectively.

Table 5.2 WOs raised on the Central line corresponding with the  $t_{mean}$  fault exposure rate of 26-27°C

Date raised	Nearest station	Equipment type	Fault
19/07/2006	Leyton	M63 Electric Points	Failing to reverse (FTR)
01/07/2015	Hainault	4Ft Eh Points	Drill out barring point
01/07/2015	Hainault	4Ft Eh Points	Walk boards required
26/07/2018	Leytonstone	4Ft Eh Points	Point motor safety fastener (KLM) clip conversion
26/07/2018	Leytonstone	4Ft Eh Points	Fit KLM clips
26/07/2018	Ealing Broadway	4Ft Eh Points	Point motor KLM clip conversion

Fault exposure rates by LU line in Figure 5.5 were very low at the highest recorded  $t_{mean}$ , between 27°C and 28°C. However, as the lower bound increased at these temperatures, this may be linked to a lack of data as these temperatures were rarely observed throughout the study

period. In Figure 5.5, comparing corrective and reactive fault exposure rates of  $t_{mean}$ , there were clear increases in both rates from 23°C to 27°C, demonstrating that the trends otherwise show that there were more WOs at higher temperatures.

There were two days primarily responsible for both peaks in the fault exposure rates. These were 01/07/2015 and 26/07/2018. They were the two hottest  $t_{mean}$  observations in the study period. Figure 5.6 shows how the daily number of corrective and reactive WOs change in the days leading up to and after these days, in the context of the hot day climate threshold. Although the scales differ between the two graphs, they show very different trends. 30/06/2015 was the day after the first hot day of the year and saw reactive WOs increase very quickly. This extreme heat event was very short (therefore neither were a heatwave day), with high overnight temperatures between the two hot days and then broken by thunderstorms across the country as temperatures dropped (Met Office, 2015).

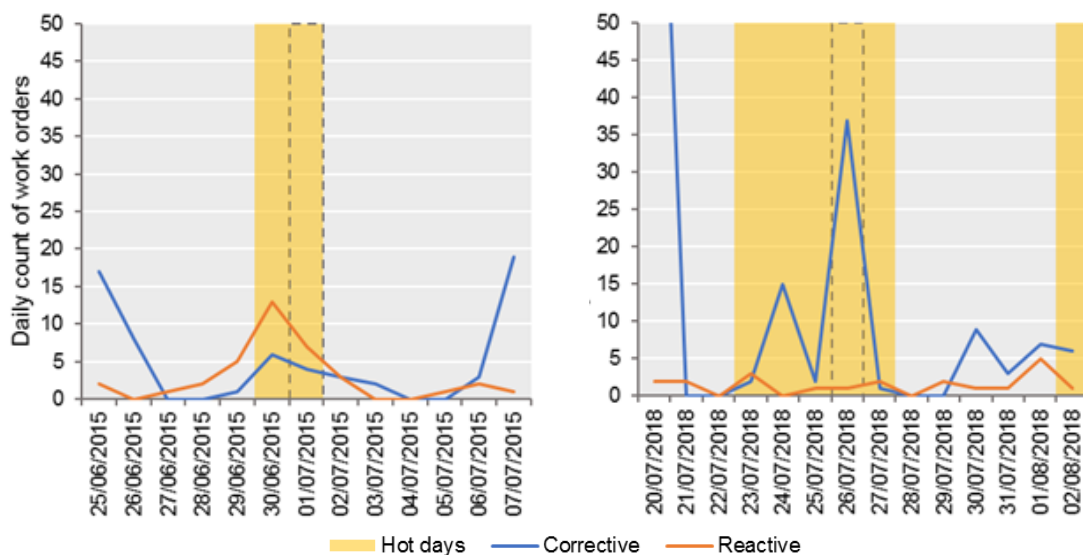


Figure 5.6 Daily count of surface corrective and reactive WOs in the days before and after the hottest two days of the study period. Days that fall into the hot day climate threshold are highlighted in yellow. The dotted line denotes the hottest day of that time interval, 01/07/2015 (left) and 26/07/2018 (right)

On the other hand, 26/07/2018 was a heatwave day; day four of a five-day spell. Eleven hot days preceded this heatwave event, which was the second heatwave event of the year (the first was 05-09/07/2018) and included one hot day early in the year (09/04/2018). There were 19 reactive WOs in the first heatwave of 2018, compared with six in the second heatwave. Seven reactive WOs were raised on the first hot day of the summer, which was 25/06/2018.

The reactive WO trends in Figure 5.6 demonstrated the potential presence of failure harvesting. This is where asset failures increase early in the spring or summer, when the first instances of high temperatures are observed (Chapman *et al.*, 2008; Ferranti *et al.*, 2016; Jaroszweski *et al.*, 2019). Then, as the faults in these locations are addressed and the assets fixed, the resilience of the network is improved, and the likelihood of future heat-related faults decreases, even as temperatures increase through the summer season. This is the likely case in the summer of 2018. However, as there were few hot days in 2015, no earlier failure harvesting occurred. The extremely high  $t_{mean}$  on 30/06-01/07/2015 consequently exacerbated the number of reactive WOs.

### **5.3.2. Daily maximum temperature ( $t_{max}$ )**

Figure 5.7 shows the surface  $t_{max}$  fault exposure rates for the study period. The extreme low and high temperature fault exposure rate peaks were greater than  $t_{mean}$  in Figure 5.4. The fault exposure rates at the absolute lowest and highest  $t_{max}$  were near zero for all LU lines. However, temperatures close to the lower bound line had the highest fault exposure rates that also exceeded two standard deviations, particularly at lower temperatures ( $t_{max} < 1^{\circ}\text{C}$ ).

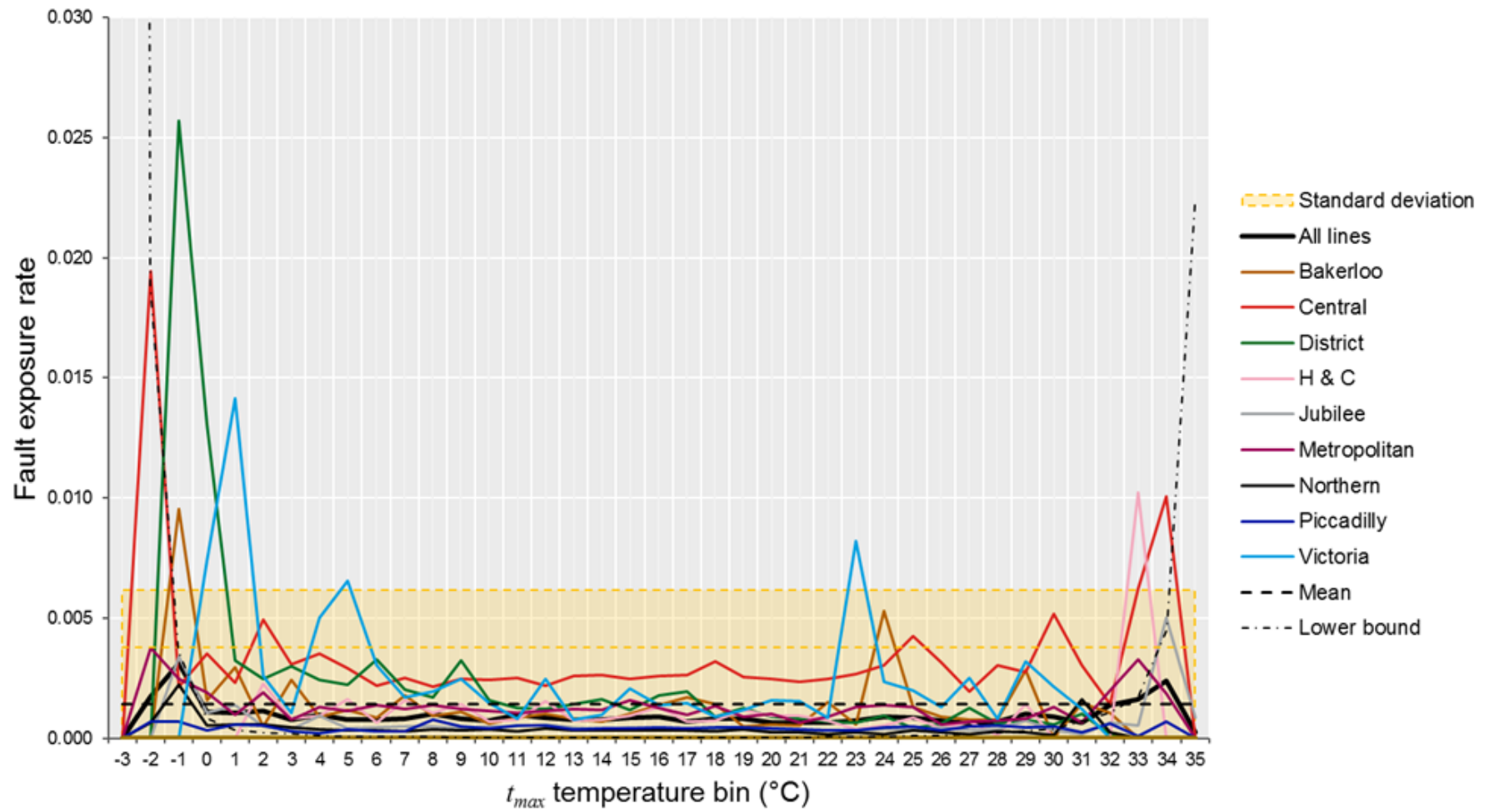


Figure 5.7 Fault exposure rates of  $t_{max}$  per LU line for the surface part of the LU network

The lowest  $t_{max}$  fault exposure rate peak was on the Central line, between  $-3^{\circ}\text{C}$  and  $-2^{\circ}\text{C}$ , which was due to one single day in the study period (28/02/2018). The Central line WOs on this day were the same as those in Table 5.1 plus an additional reactive one, near Woodford station in the northeast, where another point failed to reverse. The largest peak of the surface  $t_{max}$  fault exposure rate was on the District line between  $-2^{\circ}\text{C}$  and  $-1^{\circ}\text{C}$ . These comprised seven corrective and six reactive WOs, all also having occurred on 28/02/2018. The Bakerloo fault exposure rate at this temperature also exceeded two standard deviations, due to one reactive WO.

As one of the coldest days in the study period, Figure 5.8 shows where all the WOs were recorded across the surface part of the LU network on 28/02/2018. There were 39 WOs, the second-highest count of reactive WOs on a day of the study period (29; highest was 30). Most of the WOs raised were in the west. Some of the WOs were clustered in certain locations, such as the southwest on the District line. There were, however, no discerning geographic trends in these locations that could be a driving factor behind these WOs.

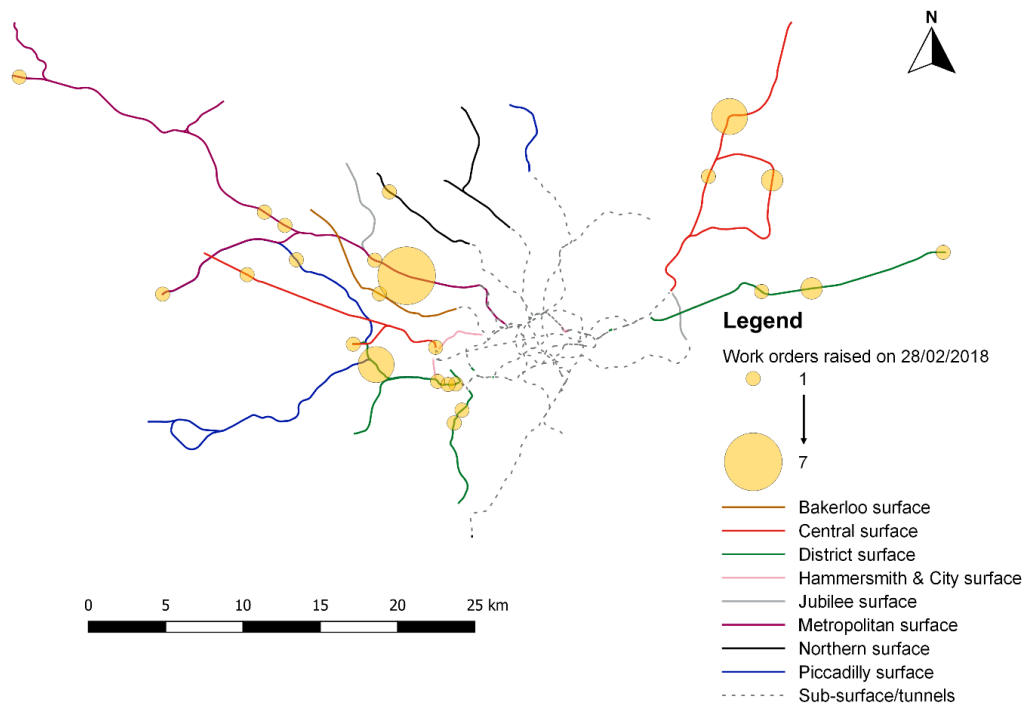


Figure 5.8 WOs raised on 28/02/2018 across the surface part of the LU network

The Victoria line fault exposure rate was also highest when  $t_{max}$  was low. The WOs raised when  $t_{max}$  was between 1°C and 2°C were the same WOs from 02/02/2009 that artificially inflated the trend in the  $t_{mean}$  fault exposure rate between 0°C and 1°C (see Figure 5.4). There was also a Victoria line fault exposure rate peak exceeding two standard deviations between 5°C and 6°C. This was due to 28 WOs, primarily corrective, with 18 raised on 20/11/2018 to replace a range of assets such as air hoses and motors across points at the Victoria line depot and Northumberland Park. Five reactive WOs also occurred on 05/01/2017 and 12/12/2017. Those from 05/01/2017 were the only reactive WOs raised across the network on that day, however those on 12/12/2017 were three of 13 reactive WOs, mainly raised in the morning and potentially indicative of  $t_{min}$  trends than  $t_{max}$ .

The first fault exposure rate to exceed two standard deviations under higher temperatures was on the Victoria line, between 22°C and 23°C. There were 10 WOs raised: seven corrective and three reactive. The corrective WOs were raised between early August and late September across several years for various reasons. The reactive WOs also happened on three different dates and report issues of air leaks in valves, points bobbing as a train passes over, and an observed gap in a switch tip.

There were three instances following the Victoria line fault exposure rate peak where one standard deviation was exceeded on other LU lines. One was on the Bakerloo line (between 23°C and 24°C), and two on the Central line (between 24°C and 25°C, and between 29°C and 30°C). The Bakerloo peak was linked to the mass raising of corrective WOs to replace fibre washers on 20/07/2018, as previously discussed. The first Central line peak comprised 158 corrective and 18 reactive WOs. 53 of the corrective WOs were related to the KLM clip conversions, also previously discussed. Excluding these WOs, the Central fault exposure rate

did not exceed one standard deviation at this temperature bin. The second Central line peak included fewer WOs: 44 corrective and four reactive. 43 of the WOs were raised during 16 different heatwave days across the study period, and 19 of these (both corrective and reactive) reported a point failure, either to reverse or normalise. Of all 48 WOs, 20 occurred in the west and 28 in the east, across multiple stations. This fault exposure rate was an indication that point-related failures under high temperature may be more likely to occur on the Central line compared to other LU lines, implying that its assets may have a lower operational temperature threshold.

At the very highest observed surface daily  $t_{max}$ , there was one fault exposure rate that exceeded one standard deviation (Jubilee line, between 33°C and 34°C) and two that exceeded two standard deviations (H&C lines, between 32°C and 33°C, and the Central line, between 33°C and 34°C). Firstly, the Jubilee line peak comprised 24 WOs, of which 22 raised were to undertake a “fault find” (an investigation of failure cause) on point heaters at Neasden Depot. Only one of these WOs was closed as complete; the remainder were cancelled; either “raised in error” or as “missed maintenance”, assuming that no faults were identified. The process of undertaking “fault finds” across the surface part of the LU network is relatively recent in the context of the study period, with a text search of the WO database returning 62 instances, with the first one raised on 12/12/2017. The Jubilee WOs were the first undertaken in the summer period, implying a newly implemented maintenance process. The H&C lines’ fault exposure rate peak between 32°C and 33°C comprised corrective WOs regarding minimum gauge at Hammersmith station, as previously discussed. Similarly, the Central line fault exposure rate peak between 33°C and 34°C included the same WOs reported in Table 5.2, including two additional WOs each on 19/07/2006 and 26/07/2018.

The surface  $t_{max}$  fault exposure rates largely mirrored surface  $t_{mean}$  fault exposure rates. Some LU lines had standout trends, such as on the District line during extreme low temperatures on the District line, and both extreme low and high temperatures on the Central line. Interestingly, fault exposure rates at the highest observed  $t_{max}$  temperature bins were low, when not accounting for corrective WOs that likely artificially inflated them.

To investigate the fault exposure rates further, climate variables and surface fault exposure rates were grouped by days *per* year before and after the annual peak  $t_{max}$  was reported. Figure 5.9 shows that slightly over half of warm nights (56%), warm days (56%) and WSDI days (55%) occurred on average before the observed peak  $t_{max}$  of its respective year. Slightly under half (49%) of all summer days on average occurred before the  $t_{max}$  peak. Only in some years, hot days (10 of 13 years) and heatwave days (5 of 13 years) occurred before the  $t_{max}$  peak. Where these occurred, it was usually less than half. Tropical nights only occurred before the annual  $t_{max}$  peak in 2006.

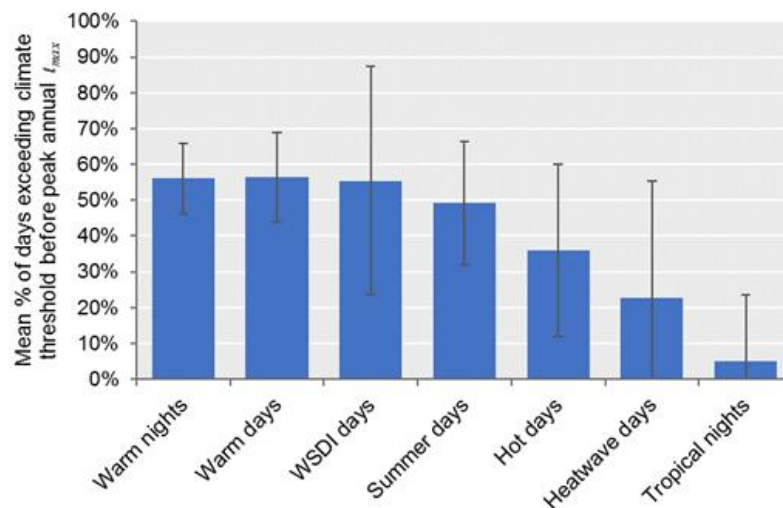


Figure 5.9 Mean percentage of climate threshold days *per* year that occurred before the annual peak surface  $t_{max}$  was reported for the whole study period. Error bars denote one standard deviation



There were striking differences in corrective and reactive fault exposure rates for the whole surface part of the LU network, depending on whether WOs were raised before or after the annual peak  $t_{max}$ , shown in Figure 5.10. Corrective fault exposure rates were similar across most temperature bins. However, the pre-peak fault exposure rate declined from between 25°C and 26°C, whereas the post-peak fault exposure rate increased quickly from between 31°C and 32°C. As for the reactive fault exposure rates, the pre-peak rates were much higher than the post-peak rates at both the hottest and coldest temperature bins. At between 25°C and 26°C, the pre-peak reactive rate increased, which was earlier than the post-peak rate. Therefore, reactive WOs raised around the first occurrences of somewhat higher temperatures in a year reduce the reactive WOs later in the year, after the peak  $t_{max}$  temperature for the year passed. This is another indication of failure harvesting. On the other hand, the post-peak corrective fault exposure rate peaked at higher temperatures. This was because it included the annual peak  $t_{max}$  days and were the likely temperature bins that the WOs on these specific days fell into.

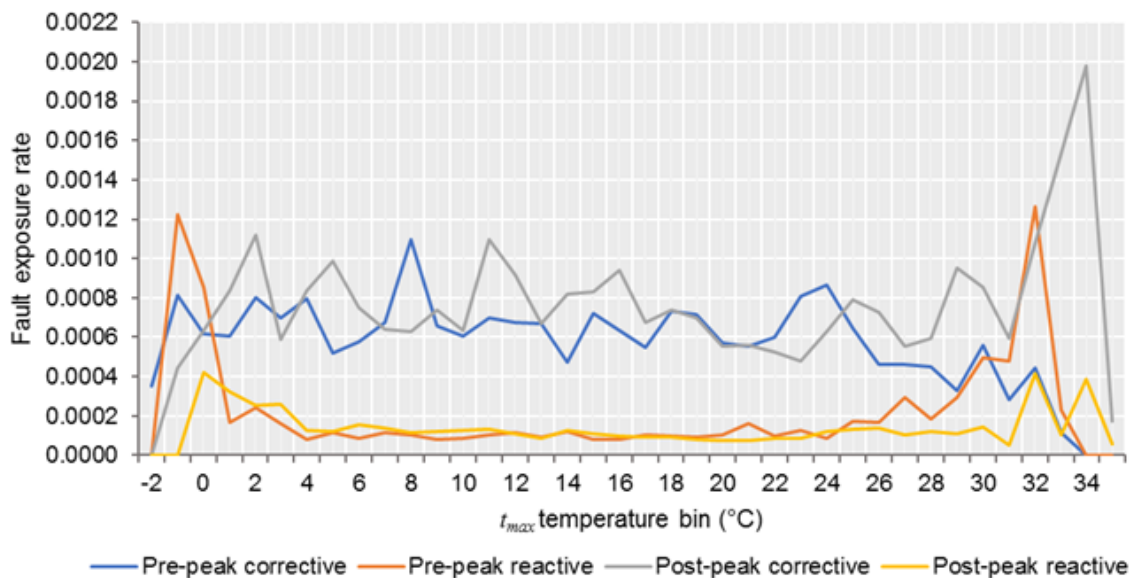


Figure 5.10 Fault exposure rates for all surface  $t_{max}$ , grouped by WO type; pre- and post- annual peak surface  $t_{max}$

### 5.3.3. Daily minimum temperature ( $t_{min}$ )

Figure 5.11 shows the surface  $t_{min}$  fault exposure rates for the study period. The rates by LU line were mostly low and around the network mean. The one standard deviation threshold was exceeded four times, twice on the District line when  $t_{min}$  was low and twice on the Central line, one each at high and low  $t_{min}$ . Two standard deviations were exceeded three times. The highest peak was on the District line, when  $t_{min}$  was between  $-6^{\circ}\text{C}$  and  $-5^{\circ}\text{C}$  and the other two were during higher temperatures, on the Victoria line between  $17^{\circ}\text{C}$  and  $18^{\circ}\text{C}$  and on the Bakerloo line between  $18^{\circ}\text{C}$  and  $19^{\circ}\text{C}$ .

The biggest peak on the District line's fault exposure rate was due to six WOs on 28/02/2018. The other two District line peaks exceeding one standard deviation of the mean were primarily associated with the mass raising of corrective WOs, including the mass replacement of fibre washers. The same WOs underpin the Victoria line peak between  $17^{\circ}\text{C}$  and  $18^{\circ}\text{C}$ . However, the WOs driving the Bakerloo line fault exposure rate peak between  $19^{\circ}\text{C}$  and  $20^{\circ}\text{C}$  were two corrective WOs at a depot. There are no other WOs raised on the Bakerloo line at a higher  $t_{min}$ .

Overall, there is little evidence in Figure 5.12 to suggest that daily  $t_{min}$  is a major contributing factor behind surface fault exposure rates peaks compared with  $t_{mean}$  or  $t_{max}$ . In part, this could be due to a smaller range in  $t_{min}$ , so each temperature bin has a higher temperature exposure frequency value acting upon the fault exposure rates, which the lower bound also indicates.

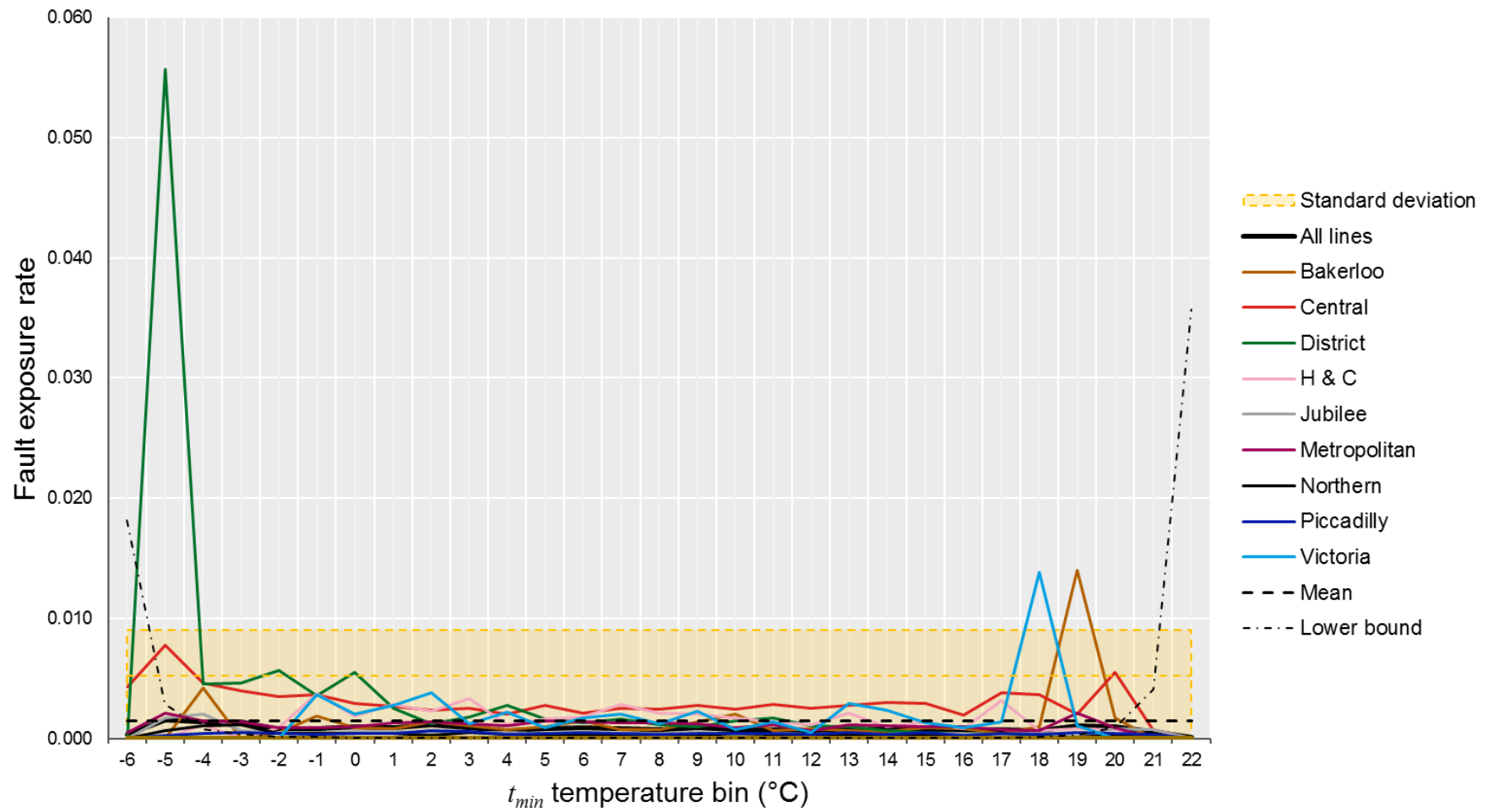


Figure 5.11 Fault exposure rates of  $t_{min}$  per LU line for the surface part of the LU network

#### 5.3.4. Diurnal temperature range ( $\Delta t$ )

Figure 5.12 shows the surface  $\Delta t$  fault exposure rates for the study period. All fault exposure rates were close to the network mean rate except for two instances, on the Bakerloo line and District line. These exceed two standard deviations, where daily  $\Delta t$  was below 2°C.

The lowest  $\Delta t$  fault exposure rate on the Bakerloo line was driven by nine WOs: eight corrective and one reactive. They all took place on 12/02/2013, which is one of six days in the whole study period where  $\Delta t < 1^\circ\text{C}$  and were all between mid-January and mid-February of various years. The largest  $\Delta t$  fault exposure rate on the District line was driven by 291 WOs. 269 of these were corrective, with 129 were marked as completed. Therefore, this rate, while still likely to be high, was artificially inflated.

Nevertheless, a high fault exposure rate when  $\Delta t$  was low, at least for corrective maintenance may not necessarily be problematic in the context of asset risk to temperature. The average  $t_{mean}$  of all the District line corrective WOs between 1°C and 2°C in  $\Delta t$  terms was 7.4°C. Therefore, few of these WOs associated with any of the fault exposure rates of the other surface temperature variables.

There was one small peak on the H&C lines where  $\Delta t$  was high (between 15°C and 16°C), although it did not exceed any standard deviation thresholds. There were 19 corrective WOs, 13 of which were on 01/08/2013 but nine were not required. Therefore, this rate was also likely artificially inflated.

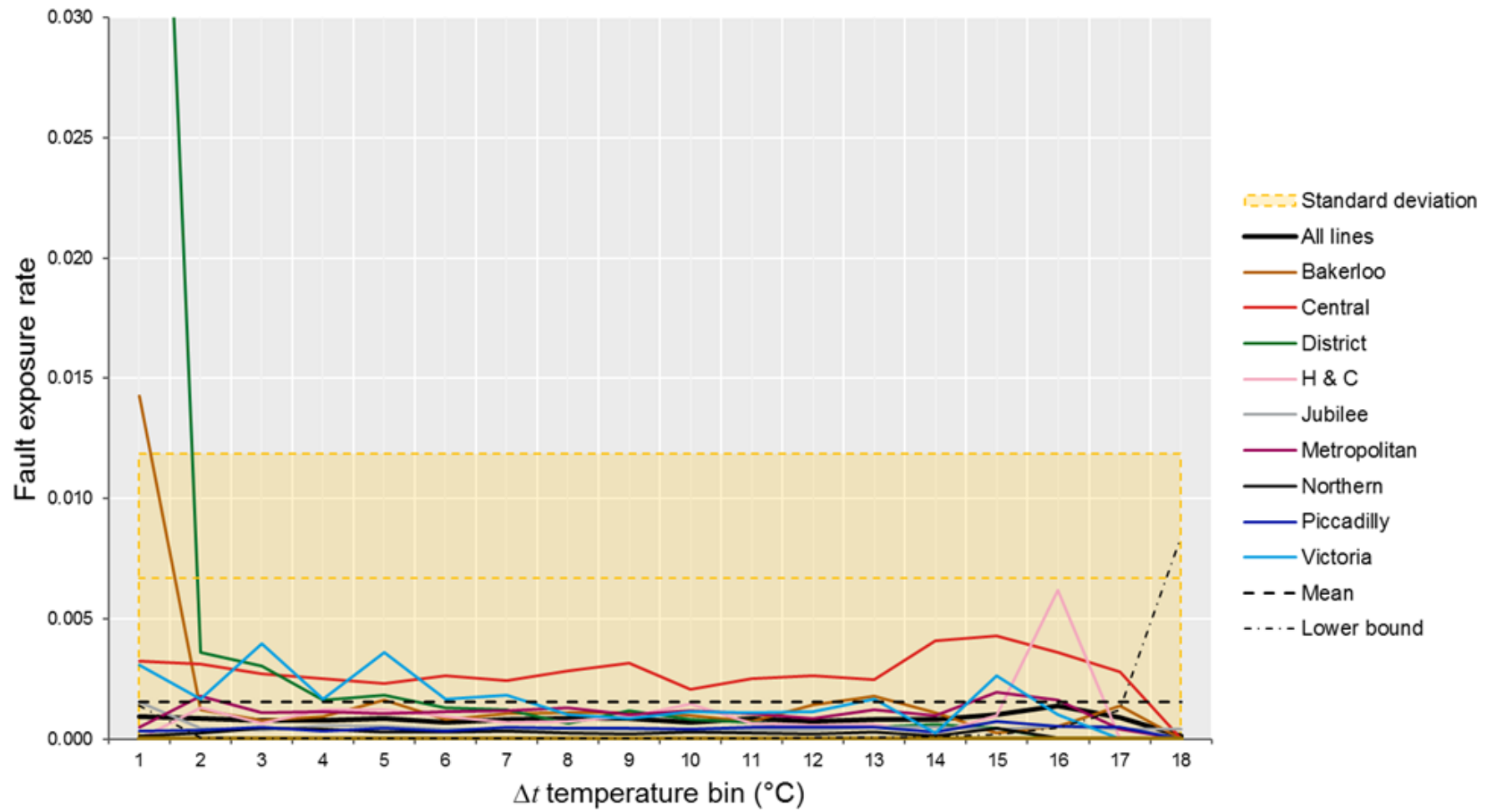


Figure 5.12 Fault exposure rates of  $\Delta t$  per LU line for the surface part of the LU network

## 5.4. Fault exposure rates: sub-surface

The sub-surface WOs that comprised the fault exposure rates were far fewer than the surface part of the LU network, thus their fault exposure rates were smaller than the surface. The total length of the sub-surface part of the LU network is also small (approximately 8%; see Section 1.1.1). Only the District, H&C and Metropolitan lines are included in this part of the LU network. A unique characteristic of this part of the LU network is that these lines share a large proportion of track and by proxy, associated assets. However, TfL group the sub-surface stations by LU line via the LCS structure and asset management systems. They allocate a specific LU line to each station – thus providing a single “owning line” for each LU station. These inform the subsequent groupings of sub-surface results.

### 5.4.1. Daily mean temperature ( $t_{mean}$ )

Figure 5.13 shows the sub-surface  $t_{mean}$  fault exposure rates for the study period. Parts of each LU lines’ fault exposure rate exceeded one standard deviation of the mean within the lower bound range. Furthermore, the total sub-surface network fault exposure rate exceeded two standard deviations once, when  $t_{mean}$  was between 6°C and 7°C: primarily driven by a high fault exposure rate on the District line. There were 111 WOs, all but two were corrective. Of these, 43 were closed as work completed therefore the fault exposure rate may be artificially inflated.

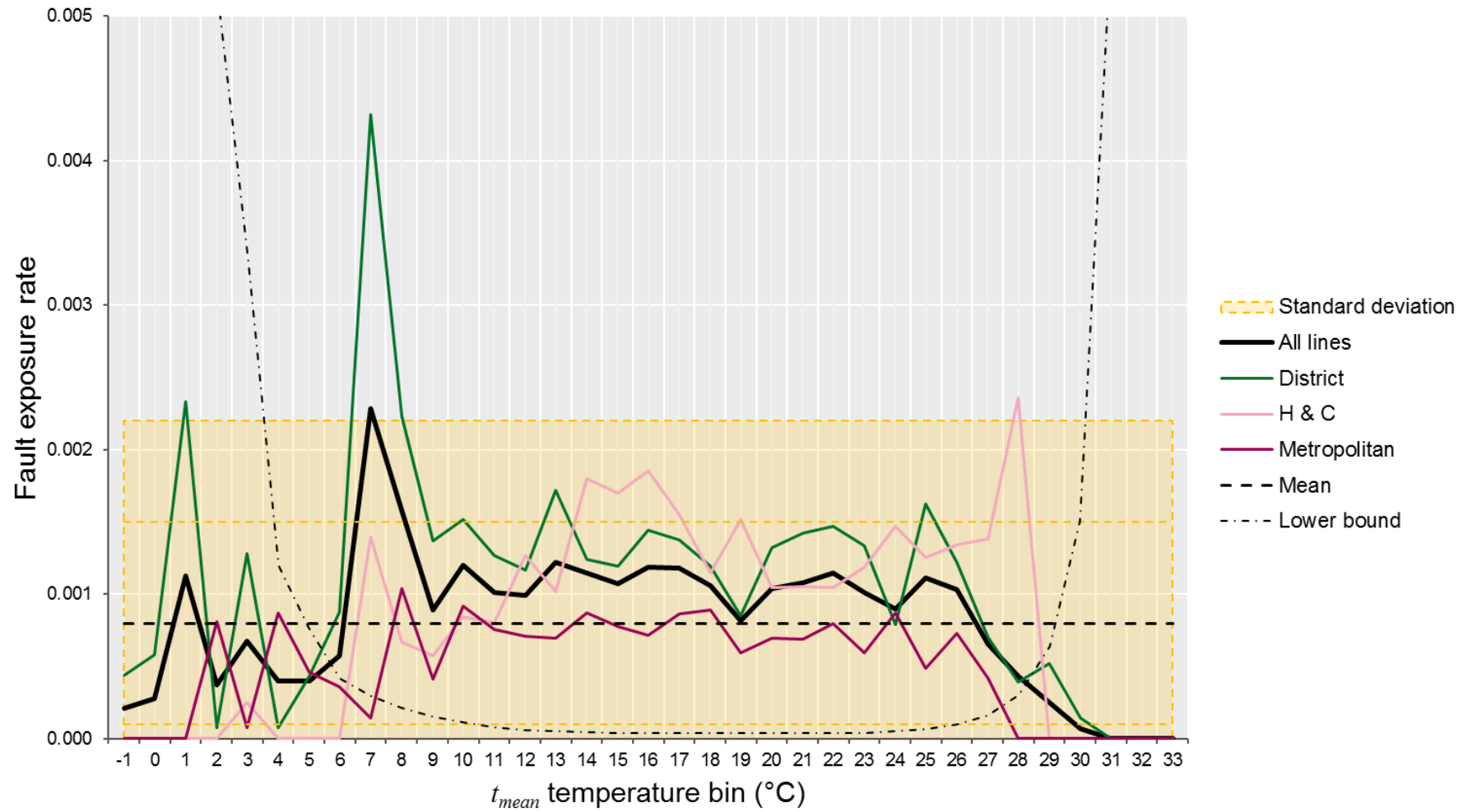


Figure 5.13 Fault exposure rates of  $t_{mean}$  per LU line for the sub-surface part of the LU network

There was also a peak in the fault exposure rate greater than two standard deviations on the District line between 1°C and 2°C. The lower bound was high, so this temperature exposure was an outlier. There was one corrective WO responsible for this peak that occurred on 02/03/2018, immediately following the coldest period in the study period (discussed in earlier sections). This WO was near High Street Kensington station, which is partially covered and therefore more likely more exposed to surface temperature than other sub-surface stations.

Under higher temperatures on the H&C line fault exposure rate exceeded two standard deviations between 27°C and 28°C. They were driven by seven WOs, all near Edgware Road station, shown in Table 5.3. All these WOs occurred on heatwave days. The corrective WOs were four of nine concerning minimum gauges. Interestingly, no reactive WOs required intervention, but the WO database did not explain why.

Table 5.3 WOs raised near Edgware Road station on the H&C lines corresponding with a  $t_{mean}$  fault exposure rate of 27-28°C

<b>Date raised</b>	<b>Maintenance type</b>	<b>Equipment type</b>	<b>Fault</b>	<b>Completed description</b>
18/07/2013	Corrective	Trainstop valve	Minimum gauge	Work completed
18/07/2013	Corrective	Trainstop valve	Minimum gauge	Work completed
18/07/2013	Corrective	Trainstop 10 core cable	Minimum gauge	Work completed
18/07/2013	Corrective	Trainstop 10 core cable	Minimum gauge	Work completed
09/07/2018	Reactive	Surelock 6' Electric Points	Signal passed at danger	Not required
09/07/2018	Reactive	Surelock 6' Electric Points	Signal failed to clear	Not required
24/07/2018	Reactive	Surelock 6' Electric Points	Points loss of indication when in reverse	No fault found

Like with surface temperature variables, there were differences in the sub-surface fault exposure rates between corrective and reactive WOs. There were also fewer reactive WOs than



corrective (659 compared with 5459). Figure 5.14 shows the difference in both sub-surface fault exposure rate trends for all corrective and reactive WOs. There was a cold temperature peak on the reactive fault exposure rate, linked to a WO raised on 28/02/2018 at Gloucester Road station. Both fault exposure rates peaked between 6°C and 7°C. The corrective peak correlates with the District line peak in Figure 5.13 and may be artificially inflated as discussed earlier in this section. However, the reactive peak was due to five different WOs at five different locations across the sub-surface network – two which also occurred on 28/02/2018.

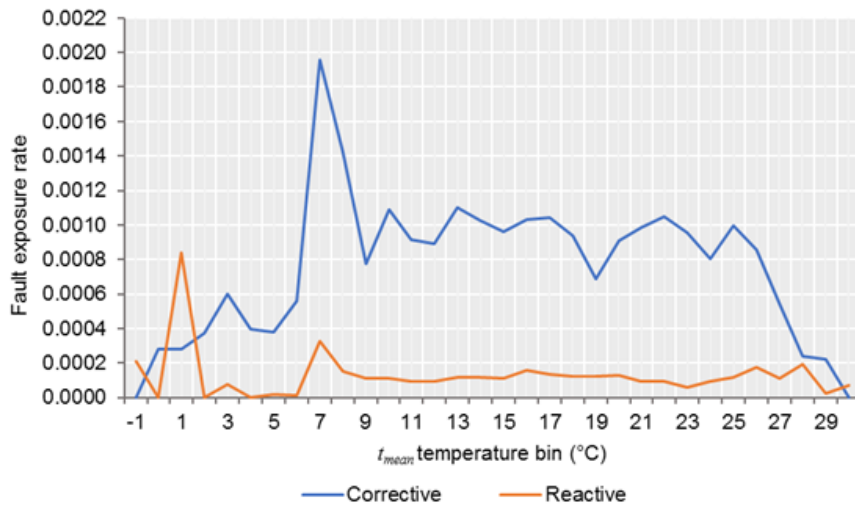


Figure 5.14 Difference in fault exposure rate trends of sub-surface  $t_{mean}$  for all lines by WO type

The sub-surface  $t_{mean}$  fault exposure rate peak between 6°C and 7°C was analogous to the surface  $t_{mean}$  fault exposure rate peak between -3°C and -2°C. Across the sub-surface stations, this is the first peak in fault exposure rates within the lower bound range at colder temperatures (see Figure 5.13). This demonstrates that the sub-surface infrastructure is, for the most part, sufficiently protected from outside weather, even on the coldest days. Nevertheless, these temperatures were still associated with higher corrective and reactive fault exposure rates. So, low sub-surface  $t_{mean}$  temperatures, while still above 0°C remained a greater risk to sub-surface point and train stop assets.

At higher temperatures, the corrective fault exposure rate decreased, while there were some fault exposure rate increases, particularly between 27°C and 28°C. Three of the six reactive WOs influencing this peak included those near Edgware Road station in Table 5.3, which were not required. The other three WOs were closed with work completed. This reactive peak was lower than the surface fault exposure rate peak, implying that under similar temperatures, sub-surface asset risk was lower than on the surface.

#### **5.4.2. Daily maximum temperature ( $t_{max}$ )**

Figure 5.15 shows the sub-surface  $t_{max}$  fault exposure rates for the study period. The rates were similar to  $t_{mean}$  in Figure 5.13. However, there were some slight differences in the  $t_{max}$  fault exposure rates peaks that exceeded two standard deviations compared with  $t_{mean}$ . On the Metropolitan line, there was a greater peak fault exposure rate peak at lower temperatures. On the District line, the second peak (within the lower bound range) was lower. As for the H&C lines, the highest  $t_{max}$  fault exposure rate was far greater. However, the underpinning WOs comprised largely of the same WOs as the sub-surface  $t_{mean}$  peaks.

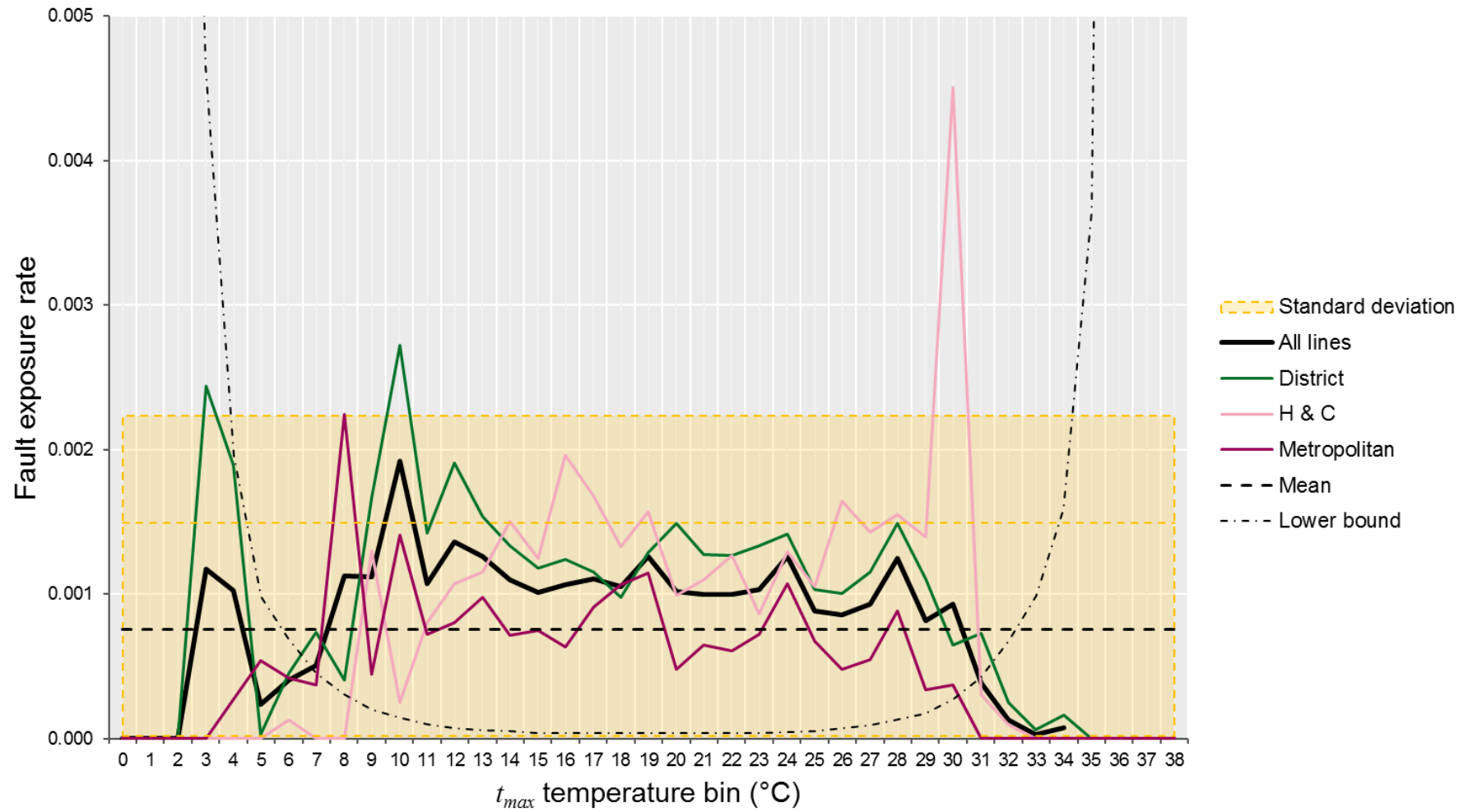


Figure 5.15 Fault exposure rates of  $t_{max}$  per LU line for the sub-surface part of the LU network

Figure 5.16 shows sub-surface corrective and reactive fault exposure rates before and after the annual peak surface  $t_{max}$ . Corrective fault exposure rates were similar, like the surface trends. The main difference was that there was a high pre-peak corrective fault exposure rate at low temperatures (between 4°C and 5°C). This was also despite there being 2.5 times more sub-surface  $t_{max}$  observations below 10°C before annual peak  $t_{max}$  than after. Additionally, there was a decrease in both corrective fault exposure rates at the highest temperatures.

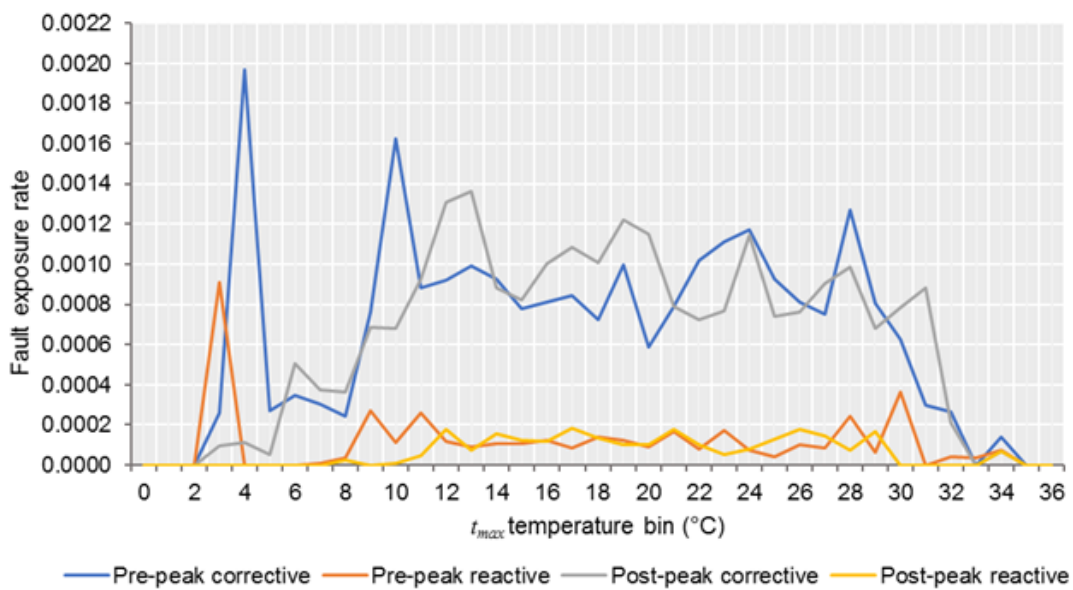


Figure 5.16 Fault exposure rates for all sub-surface  $t_{max}$ , grouped by WO type; pre- and post- annual peak surface  $t_{max}$

Regarding reactive fault exposure rates, the pre-peak rate extended across a greater temperature range than the post-peak rate. Pre-peak rates were also higher at these more extreme temperature intervals, such as between 29°C and 30°C, but the three WOs influencing this were not required as discussed in Section 5.4.1. There is consequently limited evidence of failure harvesting at high temperatures across the sub-surface part of the LU network compared with the surface part. However, there may be an indication of low temperature failure harvesting in the early parts of the year, as pre-peak rates are higher at low temperature compared with post-peak rates.

Additionally, the sub-surface fault exposure rates showed spatial variance, indicating that parts of the LU network experienced a greater exposure to heat-related faults. Certain stations were recurring in the analysis, so Figure 5.17 shows the total fault exposure rate for sub-surface  $t_{max}$  per station, combining each platforms' directions of travel. As fault exposure rates typically peak at the hottest and coldest temperature bins, there is confidence in deducing that a large total fault exposure rate is indicative of asset vulnerabilities near that station linked to high or low observed platform temperatures.

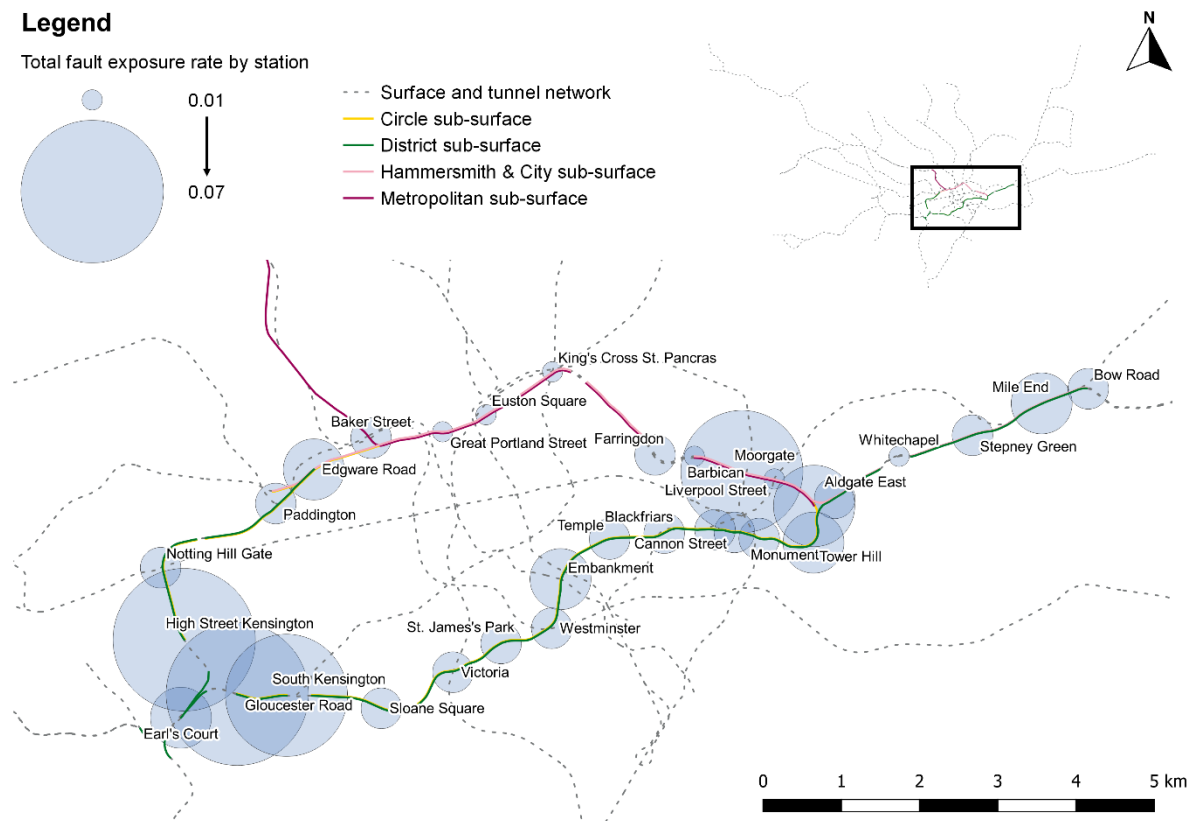


Figure 5.17 Total fault exposure rates for sub-surface  $t_{max}$  by station, which is the sum of all fault exposure rates per  $t_{max}$  temperature bin and therefore combines rates for high and low temperature observations but does not differentiate between them

There were two clusters of higher fault exposure rates across the sub-surface part of the LU network. One was in the southwest of the loop, which recorded the highest fault exposure rate of 0.07 at High Street Kensington, Gloucester Road, and South Kensington. The other cluster

was where the tracks join towards the east, with the largest fault exposure rate of 0.06 at Moorgate. Both clusters are near to track geometry curvature, joining track from other directions, as well as near tunnel openings that intermittently expose the track to the surface.

#### **5.4.3. Daily minimum temperature ( $t_{min}$ )**

Figure 5.18 shows the sub-surface  $t_{min}$  fault exposure rates for the study period. Most rates were close to the mean and did not deviate, implying that  $t_{min}$  had a lesser effect on sub-surface assets compared with other temperature variables, similar to the surface. One standard deviation was exceeded once on the Metropolitan line, and two standard deviations was exceeded twice on the H&C lines, all at high  $t_{min}$  and within the lower bound range.

The Metropolitan line fault exposure rate exceeded one standard deviation between 24°C and 25°C, comprising three corrective WOs at Euston Square and Farringdon. They were concerning minimum gauge (previously discussed at other stations in Section 5.4.1) and point motor clip conversions. These WOs were raised at the highest recorded  $t_{min}$  for both stations, which were some of the highest recorded across the IR and OR track. Interestingly, the days these WOs were raised were not on or following particularly hot days in the context of climate thresholds.

The H&C lines exceeded two standard deviations between 23°C and 24°C, and between 25°C and 26°C and were similar peaks in sub-surface  $t_{mean}$  and  $t_{max}$  fault exposure rates. Between 23°C and 24°C, there were 28 WOs raised, almost all nearest to Edgware Road station, and included the same WOs driving the  $t_{mean}$  fault exposure rate peak in Table 5.3. Three of the corrective WOs from Table 5.4 were also responsible for the peak between 25°C and 26°C.

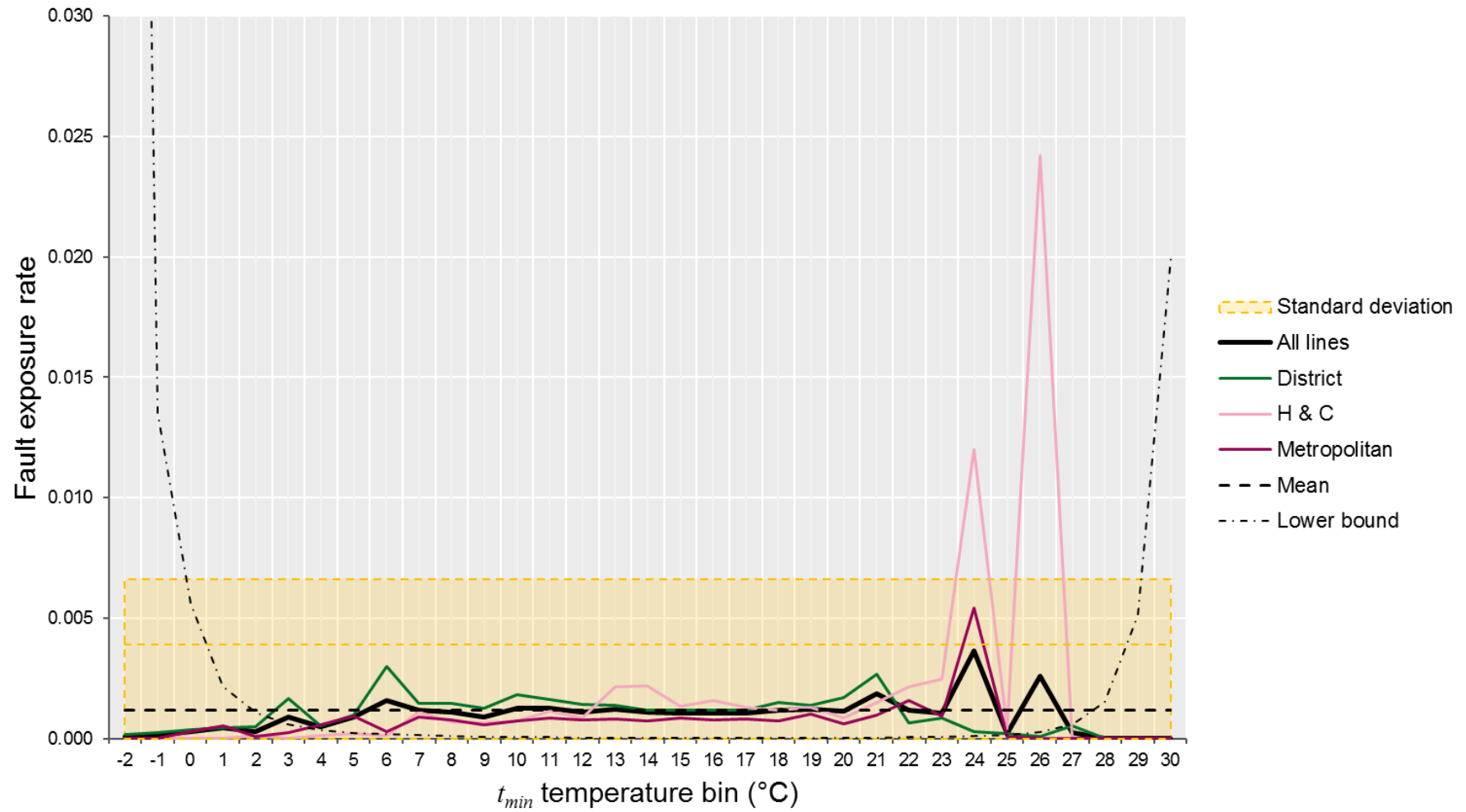


Figure 5.18 Fault exposure rates of  $t_{min}$  per LU line for the sub-surface part of the LU network

Few stations observed sub-zero platform  $t_{min}$  and only 10 WOs were raised in these conditions. Those that did were primarily to the west, such as at Gloucester Road, Paddington, and South Kensington. The only reactive WOs raised when  $t_{min} < 0^{\circ}\text{C}$  were on 28/02/2018 and 01/03/2018 at Gloucester Road and South Kensington respectively, where signals failed to clear.

Overall, while sub-surface fault exposure rates for  $t_{min}$  were limited, there were spatial variances, though not necessarily among the same stations as the sub-surface  $t_{mean}$  and  $t_{max}$  fault exposure rates. Figure 5.19 shows these three total fault exposure rates by station for the sub-surface part of the LU network. Most stations had a highest total  $t_{max}$  fault exposure rate. While some stations had similar rates across all three temperature variables,  $t_{min}$  fault exposure rates were much at some stations (e.g., Edgware Road, Farringdon, King’s Cross St. Pancras). These stations are also near tunnel openings and consequently closer to the surface. Therefore, Figure 5.19 further emphasises the station-specific effects on platform temperatures across the sub-surface part of the LU network, and the subsequent impact on fault exposure rates.

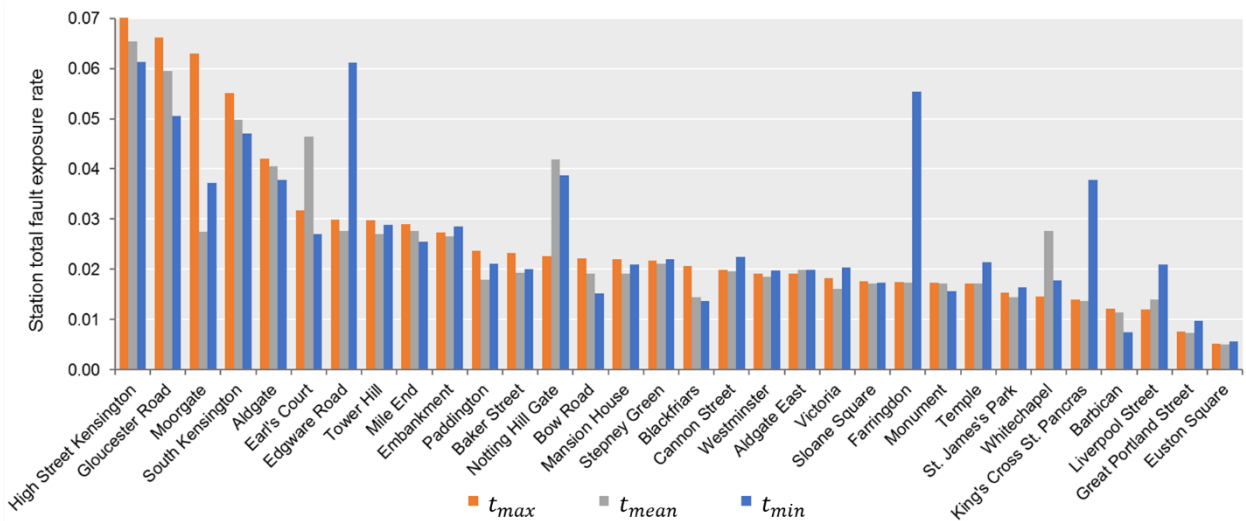


Figure 5.19 Differences in sub-surface fault exposure rates by station for  $t_{min}$ ,  $t_{mean}$  and  $t_{max}$



#### 5.4.4. Diurnal temperature range ( $\Delta t$ )

Figure 5.20 shows the sub-surface  $\Delta t$  fault exposure rates for the study period. The rates were different to the other sub-surface fault exposure rates and the surface  $\Delta t$  fault exposure rate. Here, the mean rate of all lines gradually increased from a  $\Delta t$  of 1°C, peaking at 10°C, when it exceeded two standard deviations of the mean. It decreased again as the lower bound increased. The District and Metropolitan line fault exposure rates followed similar patterns, with staggered peaks. However, the H&C lines' peaked at a lower and earlier  $\Delta t$ .

The peak fault exposure rate on the District line occurred between 8°C and 9°C. There were 124 WOs and three were reactive. Only 43 corrective WOs recorded work completed, as were two of the three reactive WOs. 89 of the corrective WOs raised at Gloucester Road, High Street Kensington, Sloane Square and South Kensington. Most of the WOs did not occur on a day exceeding a climate threshold, implying that a higher-than-average sub-surface  $\Delta t$  may not necessarily be linked to high surface temperatures. Furthermore, WO raised dates were spread across the year. The only months that did not record a WO at this peak were February, August, and December.

A similar peak on the Metropolitan line between 9°C and 10°C comprised 27 WOs. All were corrective, and 25 of them recorded work completed. 22 of the WOs were near Aldgate or Aldgate East, with 16 concerning minimum track gauge. Like the District line, few days the Metropolitan line WOs were raised on exceeded a hot day climate threshold, though 25 of the 27 exceeded the warm day climate threshold. WOs were also raised across fewer months of the year – in March, April, June, July, August, and October.

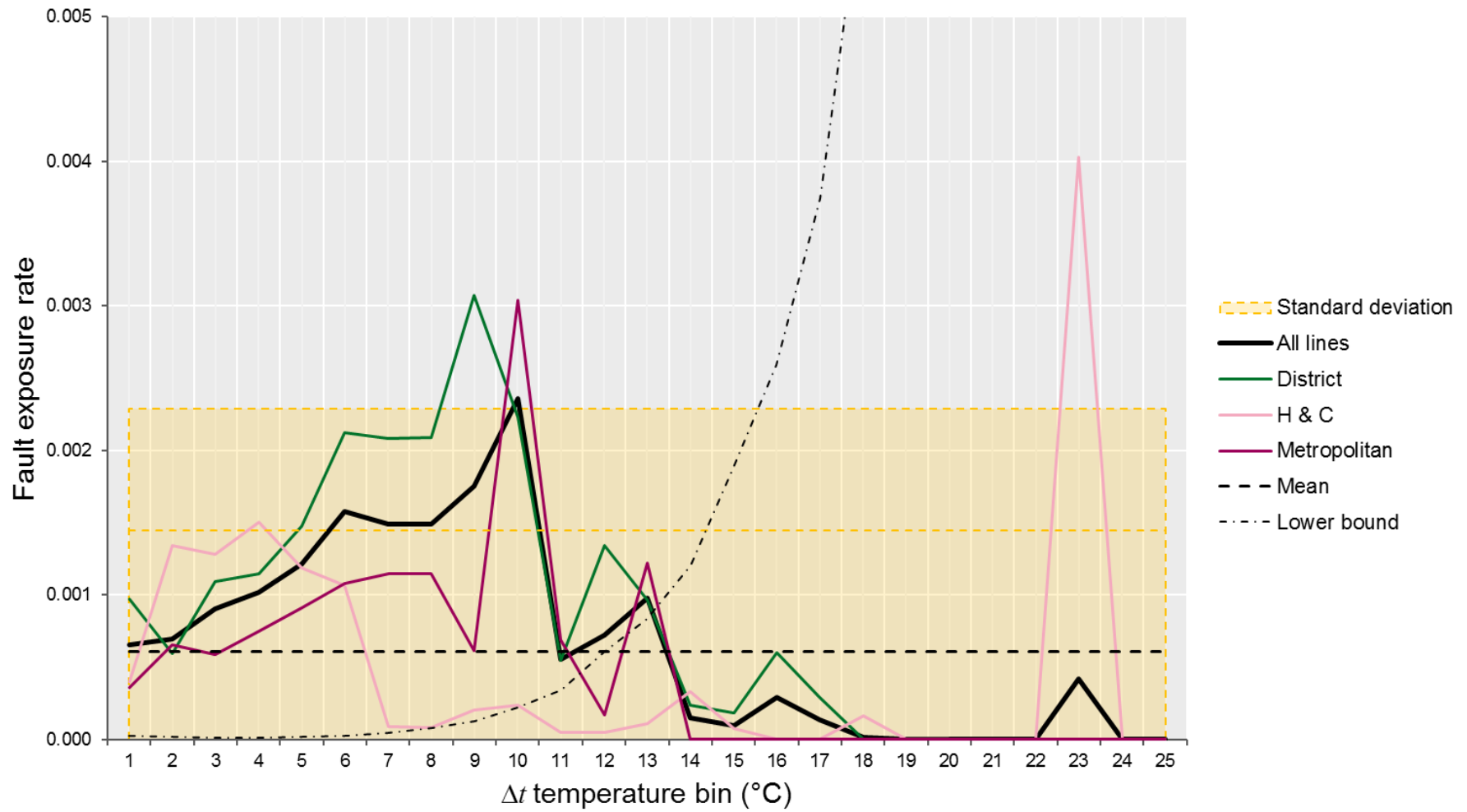


Figure 5.20 Fault exposure rates of  $\Delta t$  per LU line for the sub-surface part of the LU network

The fault exposure rates across all sub-surface LU lines gradually decreased after both peaks, followed by a large peak exceeding two standard deviations on the H&C lines between 22°C and 23°C. This instance is outside of the lower bound, so it is an outlier occurrence. The peak was due to two corrective WOs at Paddington station, raised on 22/04/2010. This was the only instance across the sub-surface network where  $\Delta t > 20^\circ\text{C}$ . Upon reviewing the temperature exposure data by station, Paddington station recorded both the highest  $\Delta t$  the highest frequency of  $\Delta t > 20^\circ\text{C}$ . They also occurred before the annual peak surface  $t_{max}$ ; occurring in the spring.

## **5.5. Fault exposure rates: deep tube tunnels**

As demonstrated in Chapter Four, the deep tube tunnel environments (herein described as “tunnels”) are notably different to the surface and the sub-surface. Tunnel assets are exposed to higher temperatures throughout the year, though still largely protected from the influences of the surface environment. There are more tunnel point and train stop assets than the sub-surface, but fewer than the surface. Tunnel stations are also some of the busiest in terms of passenger counts, therefore fault exposure rates are important in terms of quantifying the potential impact they may have to passengers, should they trigger delays.

For context, Figure 5.21 shows mean corrective and reactive tunnel WO trends *per* month. In the first six months of the year, corrective WOs were relatively similar month-on-month, with low variability. The reactive WO trends, while lower, gradually increased month-on-month. The most corrective and reactive WOs raised in a month occurred in July. The standard deviation is also high, and this is due to a very large number of WOs raised in July 2018 (301), compared with a monthly mean of 38 in July between 2006 and 2017. The high July 2018 corrective WO count was due to the mass raising of point motor clip conversions and fibre

washer replacements across the network. Reactive WOs were also highest in July, as was the standard deviation. This was due to WOs in July 2016, where 30 were raised, primarily near Elephant & Castle and Oxford Circus stations. Both corrective and reactive WOs drop in August, before increasing again to similar pre-July levels for the rest of the year. The corrective WO drop in August is possibly indicative of the effect of summer holidays and limiting WOs in the high tunnel temperatures.

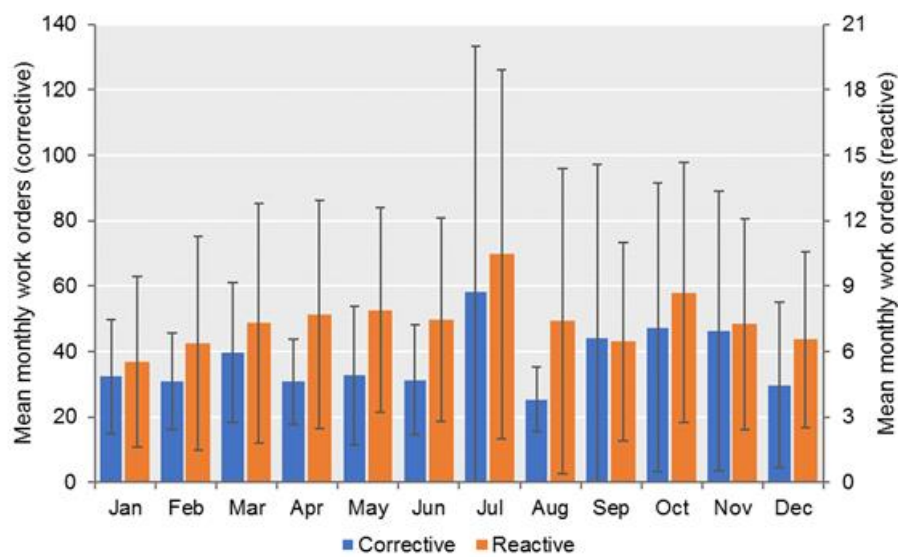


Figure 5.21 Mean monthly corrective and reactive WOs raised in the tunnel section for the entire study period. Error bars indicate one standard deviation of the mean. Note differing y-axis scales

Throughout this section, the fault exposure rates for each temperature variable show distinct, similar divisions by LU line. Fault exposure rates for the Bakerloo, Central and Victoria lines peaked substantially, while rates for the Jubilee, Northern and Piccadilly lines did not. These differences may be affected by the asset count normalisation procedure: the Bakerloo, Central and Victoria lines comprised 275, 43 and 51 assets respectively whereas the Jubilee, Northern and Piccadilly lines comprised 354, 773 and 694 respectively.

### 5.5.1. Daily mean temperature ( $t_{mean}$ )

Figure 5.22 shows the tunnel  $t_{mean}$  fault exposure rates for the study period. The Bakerloo, Central and Victoria lines have staggered peak fault exposure rates that exceeded two standard deviations at higher temperatures. There was also a very high peak on the Central line between 17°C and 18°C, due to a single corrective WO raised at Holborn station on 02/02/2009, where points failed to reverse or normalise. It was the only day the platform observed this temperature, and there was only one lower  $t_{mean}$  observation at that platform. There was an increase in the fault exposure rates preceding the Central line peak, exceeding one standard deviation, between 15°C and 16°C. This comprised 10 corrective WOs: eight at Bethnal Green and two at Marble Arch, occurring between January and April of varying years to undertake asset replacements.

Between approximately 20°C and 26°C, the tunnel fault exposure rates remained relatively consistent. The fault exposure rate on the Bakerloo line remained around the network-wide mean, whereas the Central and Victoria lines remained around one standard deviation of the mean. The tunnel fault exposure rates then peaked at high temperatures; exceeding two standard deviations began with the Victoria line (between 28°C and 29°C), then the Central line (between 29°C and 30°C), and finally on the Bakerloo line (between 32°C and 33°C). The Victoria line peak comprised 49 WOs. 45 were corrective and four were reactive. Most of the corrective WOs were raised during the first two and last two years of the study period, primarily in July. They were also raised across several stations. As for the reactive WOs, they were related to points failing to normalise or reverse, or a broken signal bond; a signal bond being the generic term for electrical connections and cabling related to electrical track circuits that detect passing trains (Ellis, 2019). Three of the four reactive WOs occurred within 17 days, during August 2018: two at Seven Sisters and one at Victoria.

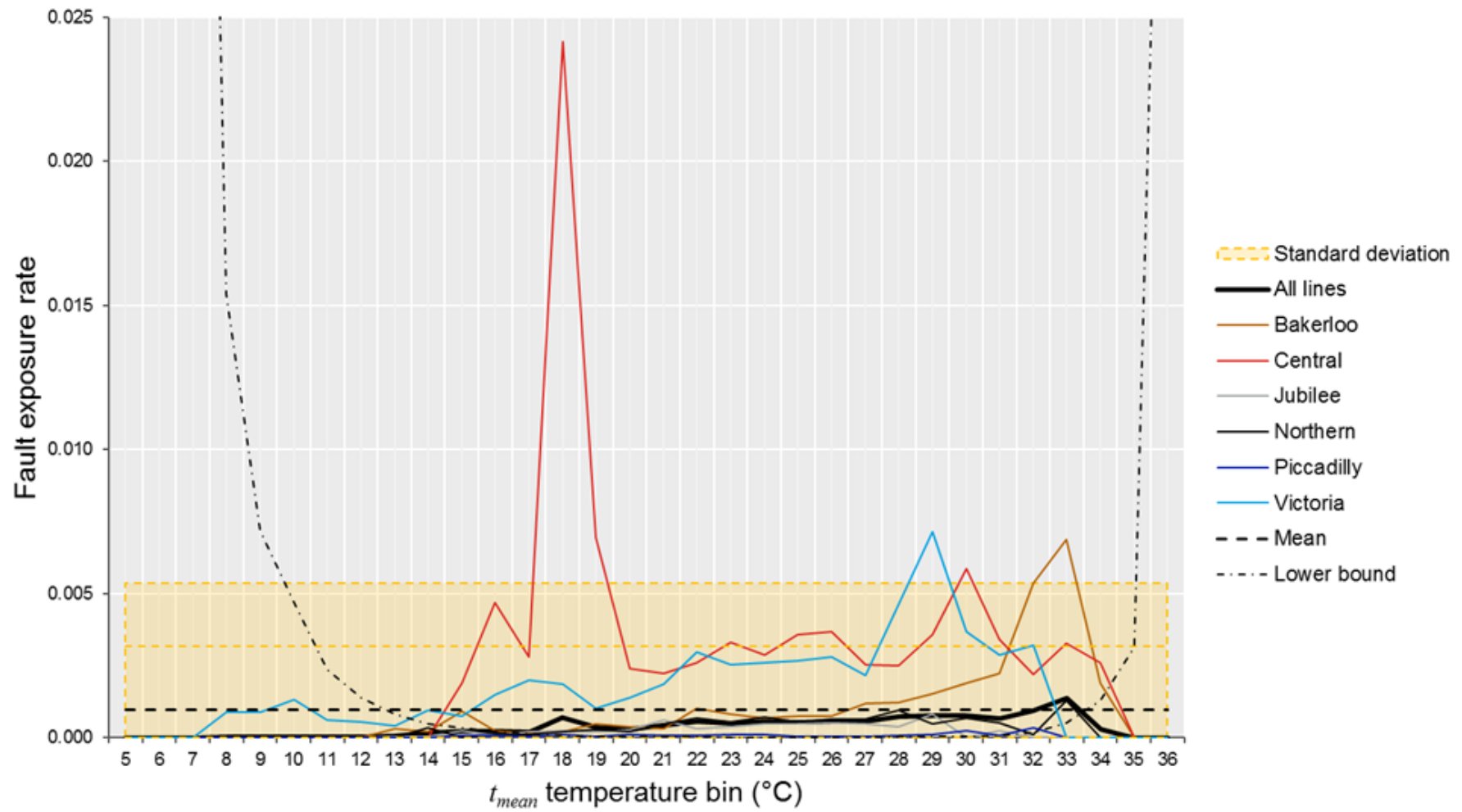


Figure 5.22 Fault exposure rates of  $t_{mean}$  per LU line for the tunnel part of the LU network

The second high temperature peak, on the Central line, comprised 55 WOs. 53 were corrective and 2 were reactive. They also occurred across several days throughout the study period. Many of these WOs were raised later in the year, particularly in September and October. There was also a distribution of WOs across several station platforms, so no station disproportionately skewed the peak. Regarding the reactive WOs, these were both at Marble Arch station, on 20/10/2017 and 25/09/2018. The first WO was due to a broken pin and the second was because the points failed to reverse.

The peak at the highest temperature bin on the Bakerloo line comprised 85 WOs. All but one was corrective. 61 of the WOs were part of a mass raising of fibre washer replacements on 20/07/2018 across the LU network (also mentioned throughout Sections 5.3.1, 5.3.2, and 5.3.3), so these WOs were likely artificially inflating the fault exposure rate. The one reactive WO was raised on 01/08/2018 at Piccadilly Circus, recording points failing to reverse.

### **5.5.2. Daily maximum temperature ( $t_{max}$ )**

Figure 5.23 shows the tunnel  $t_{max}$  fault exposure rates for the study period. The trends were similar between  $t_{max}$  and  $t_{mean}$ , with a peak in the Central line fault exposure rate where  $t_{max}$  is lower; and the Bakerloo, Central and Victoria line fault exposure rates exceeding one or two standard deviations at the highest temperatures. However, the Central line peak at the highest temperatures occurred at a higher  $t_{max}$  than the Bakerloo line, and the Victoria line peak only exceeded one standard deviation of the mean, not two.

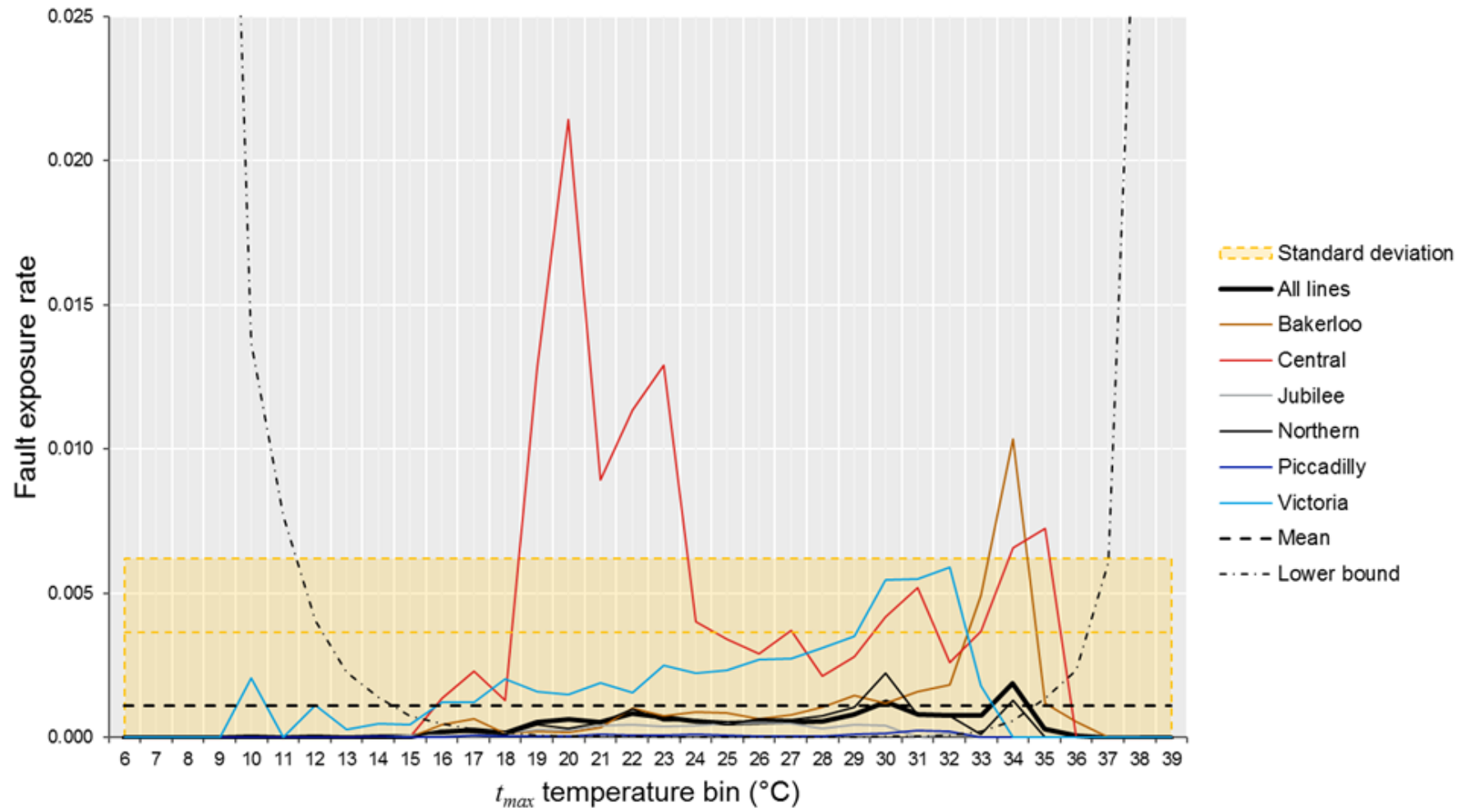


Figure 5.23 Fault exposure rates of  $t_{max}$  per LU line for the tunnel part of the LU network



The Central line  $t_{mean}$  fault exposure rate exceeded two standard deviations at two consecutive temperature bins, whereas the  $t_{max}$  fault exposure rate exceeded it across four. Many more WOs comprised these rates (109 in total: 106 corrective and three reactive) than the  $t_{mean}$  peak. They all occurred across four stations: Bethnal Green, Holborn, Liverpool Street and Queensway, primarily before April in the calendar year. These peaks highlight how infrequently tunnel temperatures observed low  $t_{max}$ , even within the lower bound range, and the proportionate impact the WOs raised at these four stations had on the fault exposure rate.

At the highest temperatures, the fault exposure rates differed across the Bakerloo, Central and Victoria lines. Firstly, the Victoria line rate gradually increased as  $t_{max}$  increased, exceeding one standard deviation at three temperature bins, between 29°C and 32°C. 92 WOs were raised: 84 corrective and eight reactive. 27 of the corrective WOs raised in July 2018 concerned point motor clip conversions and fibre washer replacements. The reactive WOs all occurred in 2017 and 2018, shown in Table 5.4. These show WOs across several stations, primarily near Seven Sisters. Most occurred during or after the extended hot period in the summer of 2018.

Table 5.4. Reactive WOs raised on the Victoria line corresponding with the highest fault exposure rates, exceeding one standard deviation

<b>Date raised</b>	<b>Nearest station</b>	<b>Equipment type</b>	<b>Fault</b>
19/06/2017	Seven Sisters	Chairlock EP points	Issue with left hand middle stretcher
16/11/2017	Finsbury Park	Chairlock EP points	Failed to reverse
02/07/2018	Seven Sisters	4' Ep (Bh) points	Air leak
26/07/2018	Seven Sisters	Chairlock EP points	Failed to normalise
20/08/2018	Victoria	Chairlock EP points	Broken signal bond
20/08/2018	Highbury & Islington	Chairlock EP points	Failed to reverse
21/08/2018	Seven Sisters	Chairlock EP points	Failed to normalise
27/08/2018	Highbury & Islington	Chairlock EP points	Failed to reverse

To review the spatial distribution of the  $t_{max}$  fault exposure rates, Figure 5.24 shows the total tunnel fault exposure rate *per* station. There were seven stations across the tunnel part of the LU network that had total fault exposure rates higher than 0.05, which are the labelled stations. The temperatures driving the fault exposure rates at these stations were in fact where lower  $t_{max}$  was observed. Across these seven stations, 91 WOs were raised where  $t_{max} < 20^{\circ}\text{C}$ . 73 were corrective and 18 were reactive. Most were raised on days that did not exceed any climate thresholds, and between January and March. Most of the reactive WOs (ten) were near Elephant & Castle station. Given its location nearest to the tunnel opening, this implies that there was a possible influence of cold surface temperatures to a certain distance within the tunnel.

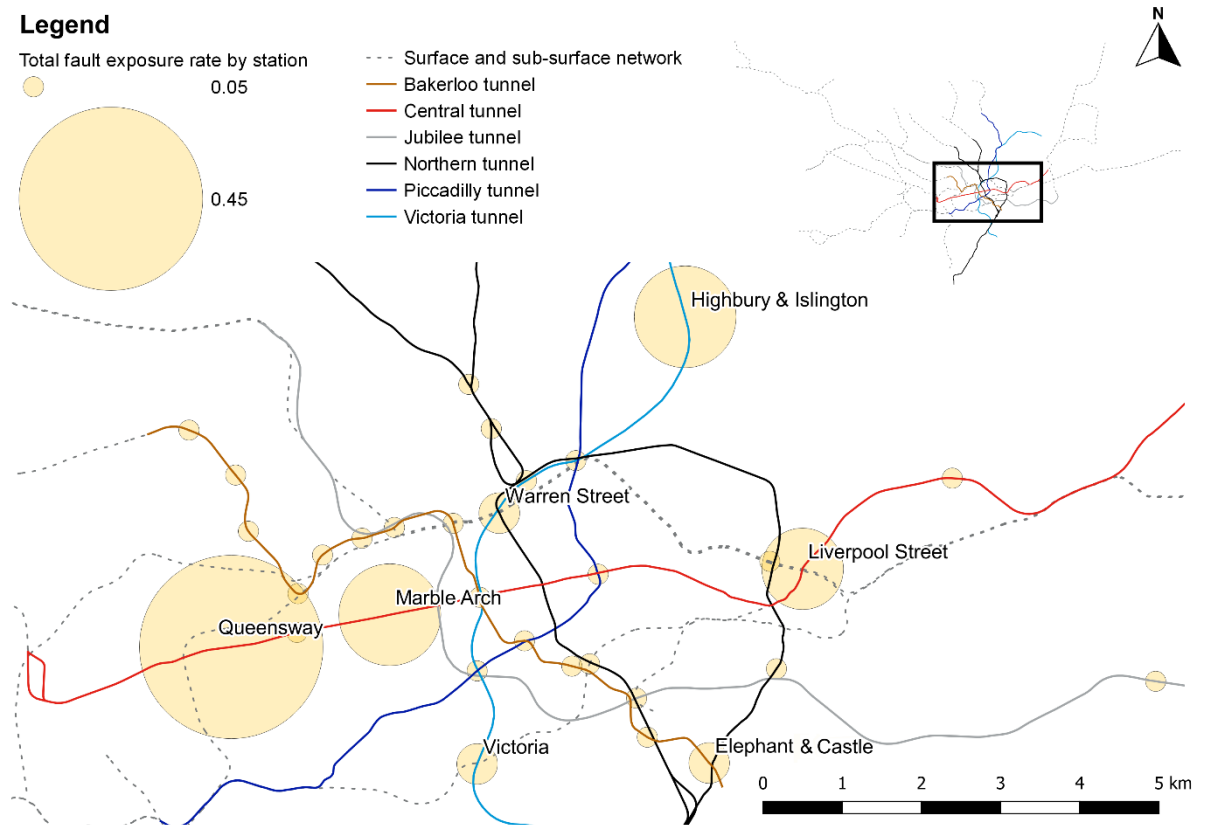


Figure 5.24 Total fault exposure rates for tunnel  $t_{max}$  by station, which is the sum of all fault exposure rates *per*  $t_{max}$  temperature bin and therefore combines rates for high and low temperature observations but does not differentiate between them

Some stations did experience high fault exposure rates at higher temperatures (greater than 0.4), particularly between 33°C and 34°C. These included Charing Cross, Oxford Circus, and Piccadilly Circus. However, the rates were offset by the normalisation process via lower fault exposure rates at other temperature bins, or a higher total asset count. Of the seven stations labelled in Figure 5.24, only Elephant & Castle station reported a high fault exposure rate at a very high  $t_{max}$ , but this was likely artificially inflated due to the previously discussed mass corrective WOs raised concerning fibre washer replacements in July 2018. Therefore, there is limited evidence to infer any spatial patterns in fault exposure rates across the tunnels under high  $t_{max}$ .

To examine the potential presence of failure harvesting across the tunnels, Figure 5.25 shows the difference in tunnel corrective and reactive fault exposure rates before and after the annual peak surface  $t_{max}$  was observed. It shows very different trends to the surface and sub-surface trends in Figure 5.10 and Figure 5.16. The corrective pre- and post-peak fault exposure rates were inverted, in that pre-peak was highest when  $t_{max}$  is high and post-peak was highest when  $t_{max}$  was low. The reactive fault exposure rates, however, showed no signal of failure harvesting. While the pre-peak reactive rate did increase slightly when tunnel  $t_{max} > 29^{\circ}\text{C}$ , the post-peak reactive rate increased at two points: once at the same point that the pre-peak began to increase, and again at a higher temperature. Therefore, the tunnel point and train stop assets were more exposed to unexpected heat-related faults after the observed annual peak surface  $t_{max}$ .

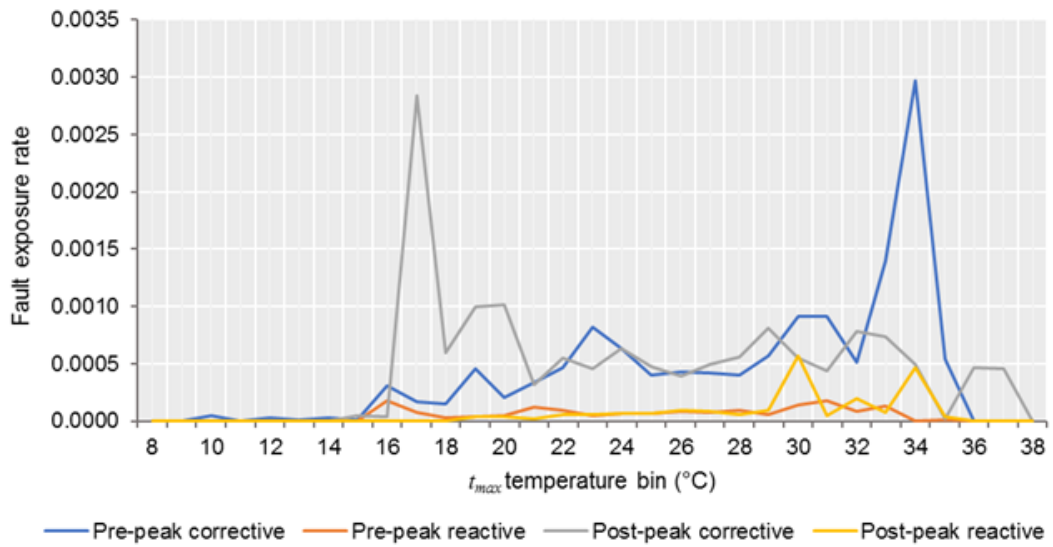


Figure 5.25 Fault exposure rates for all tunnel  $t_{max}$ , grouped by WO type; pre- and post- annual peak surface  $t_{max}$

### 5.5.3. Daily minimum temperature ( $t_{min}$ )

Figure 5.26 shows the tunnel  $t_{min}$  fault exposure rates for the study period. Trends were also similar to  $t_{mean}$  and  $t_{max}$ . The Bakerloo, Central and Victoria line rates all increased at the highest temperatures. However, only the Bakerloo and Victoria lines' fault exposure rates exceeded two standard deviations at high  $t_{min}$ .

The Central line fault exposure rate exceeded two standard deviations when  $t_{min}$  was between 15°C and 17°C. There were 35 corrective WOs, mainly at Bethnal Green, Holborn, and Liverpool Street stations, all primarily related to replacing or changing asset parts. With no reported reactive WOs, their attribution to low tunnel  $t_{min}$ , either from within the tunnels or due to the influence of the surface is limited.

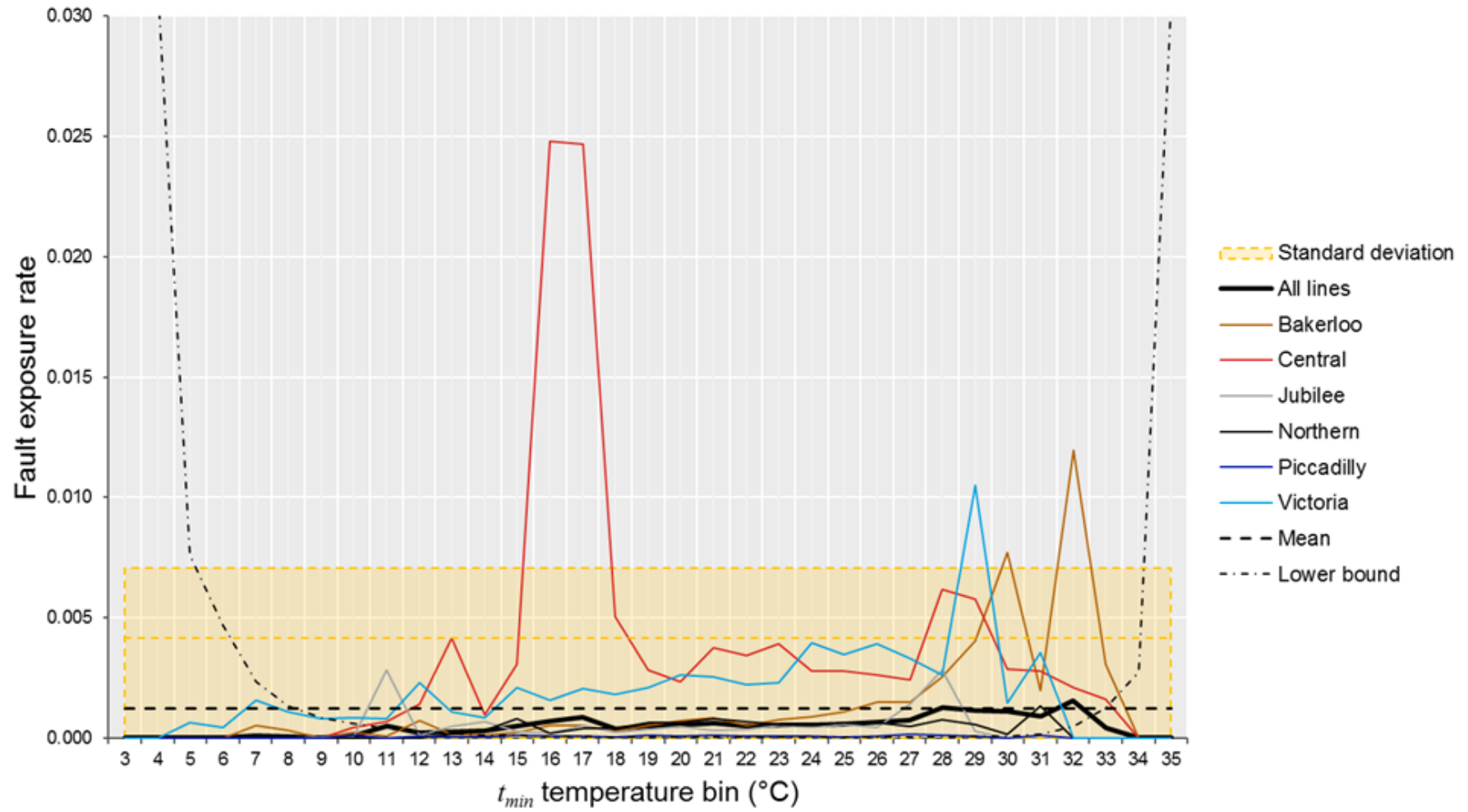


Figure 5.26 Fault exposure rates of  $t_{min}$  per LU line for the tunnel part of the LU network

At higher  $t_{min}$ , the Central line fault exposure rate exceeding one standard deviation between 27°C and 29°C. This comprised 97 WOs, all but one was corrective. Only 21 occurred on a summer day, 4 of which were also a heatwave day. The one reactive WO was raised on 20/10/2017 nearest to Marble Arch station, reporting a broken pin on a set of points.

On the Victoria line, the fault exposure rate exceeded two standard deviations between 28°C and 29°C. There were 20 corrective WOs raised, most occurring in the second half of 2018. Similarly, most of the WOs were also raised on days that did not exceed many climate thresholds. Five WOs, however, were raised on 20/07/2006, which was a heatwave day. They were concerning maintenance on gauge points to standards, occurring near Walthamstow Central station.

The Bakerloo line fault exposure rate exceeded two standard deviations between 29°C and 30°C, then again between 31°C and 32°C. The Bakerloo line recorded more WOs at higher temperatures than other LU lines, with 116 raised between 29°C and 30°C. 100 were corrective and 16 were reactive. Most of the corrective WOs also did not occur days that exceeded multiple climate thresholds. Regarding the reactive WOs, these occurred across several stations, primarily between July and August, and two in October. Seven reactive WOs were raised near Oxford Circus station between two days in late July 2016 concerning the same signalling asset, but the database did not record the specific asset description. The peak between 31°C and 32°C comprised 91 WOs, 88 corrective and three reactive. 78 of the corrective WOs were related to previously discussed mass raising of WOs, all in July and September of 2018. The three reactive WOs were raised between early July 2017 and mid-September 2018 at Paddington, Lambeth North, and Edgware Road. Only the 20/08/2018 WO at Lambeth North fell on a hot day. One fault reported a point failing to normalise, and another with an oil leak from the trip cock. One

WO description in the database could not be deciphered but reported a three-minute delay to operations as a result.

#### 5.5.4. Diurnal temperature range ( $\Delta t$ )

Figure 5.27 shows the tunnel  $\Delta t$  fault exposure rates for the study period. It shows almost no change in fault exposure rates across the tunnels, but there are three notable observations. Firstly, the Bakerloo line exceeds one standard deviation between 0 °C and 2°C. Secondly, the Central line exceeds two standard deviations between 5°C and 7°C. Finally, the Victoria line exceeds one standard deviation at two intervals: one within the lower bound range, between 14°C and 15°C, and one outside of the lower bound range, between 19°C and 20°C.

On the Bakerloo line, there were 679 WOs raised on days when  $\Delta t < 2^\circ\text{C}$ . 627 were corrective and 52 were reactive, mostly during July, September, and October. A large proportion of the WOs were at three stations: Elephant & Castle, Oxford Circus and Paddington. The high peak on the Central line was driven by 119 WOs, where 111 were corrective and eight were reactive. This peak was likely been heavily weighted by rates near Holborn station, which were 32 of the WOs, mostly during April and October. Five of the eight reactive WOs were also at Holborn, all concerning points failing to reverse or normalise. Finally, the Victoria line peak between 14°C and 15°C was due to five WOs near Seven Sisters station, on 22/11/2018. This temperature exposure frequency was unusual for this station, occurring there twice in the study period. Upon reviewing the temperature variables around that day at Seven Sisters, it was likely due to a drop in tunnel daily  $t_{min}$ , while  $t_{max}$  did not change much. Surface  $t_{min}$  also gradually decreased at this time, from 10.7°C to 0.4°C in a week, before returning to 8.0°C. The peak between 19°C and 20°C was only driven by two corrective WOs on 29/11/2017.

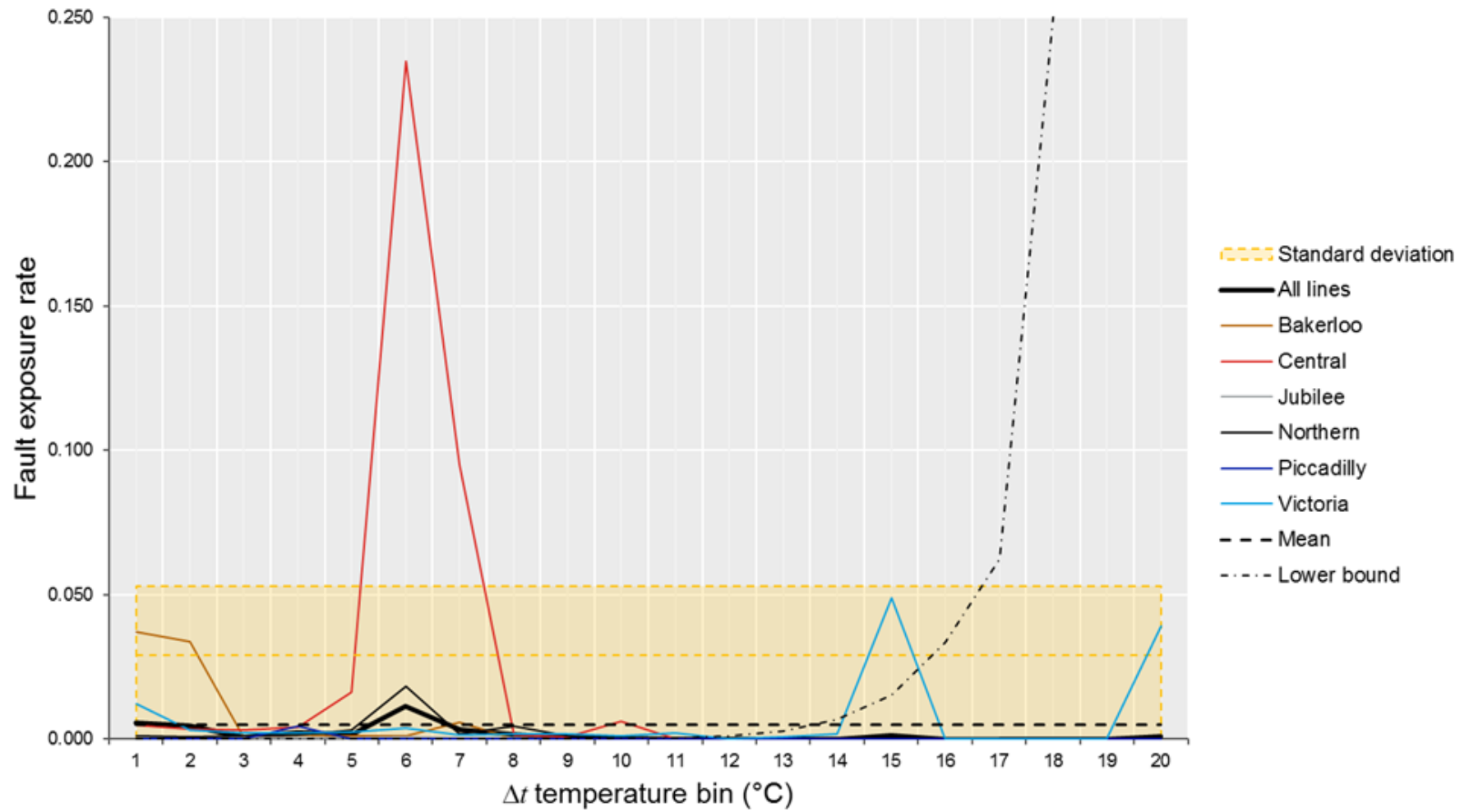


Figure 5.27 Fault exposure rates of  $\Delta t$  per LU line for the tunnel part of the LU network



## 5.6. Chapter summary

This chapter presented results on the fault exposure rates of point and train stop assets across the LU network. It used the tunnel temperature estimation model to backfill temperature data where there were observation gaps in the sub-surface and deep tube tunnel sections of the LU network, ensuring that the maximum amount of WO data provided by TfL was captured within the analysis. Grouping data by network type (*i.e.*, surface, sub-surface, deep tube tunnels) and maintenance type (*i.e.*, corrective, reactive) revealed a range of trends in fault exposure rates across the four temperature variables.

An overview analysis of the WO data within the study period showed that WOs increased since the start of the study period, and the proportion of those classified as reactive also increased. Furthermore, the share of reactive WOs across the whole study period was greater for days that exceeded the climate thresholds compared with the days where they did not exceed them.

Across the surface part of the LU network, it was clear from results such as Figure 5.4, that surface fault exposure rates increased at the highest and lowest temperature observations of the study period, with some LU lines (such as Bakerloo, Central, District, H&C and Victoria) showing higher rates than others. Fault exposure rates were highest during cold temperatures, particularly the lowest recorded temperatures between late February and early March of 2018. Moreover, there was sufficient evidence showing failure harvesting at high temperatures on the LU network, as reactive fault exposure rates increased more before annual peak surface  $t_{max}$  than afterwards. Corrective fault exposure rates increased after the annual peak surface  $t_{max}$  but could be partly attributed to WO activity on the days of annual peak surface  $t_{max}$

themselves. Surprisingly,  $\Delta t$  did not show many statistically significant relationships as the other temperature variables, even when  $\Delta t$  was high.

Within the sub-surface part of the LU network, fault exposure rates were lower than those on the surface. There was limited evidence of failure harvesting, nor divergence in fault exposure rate trends under high temperature climate thresholds. Spatial variances were apparent, as WOs at some stations repeatedly comprised the peaks across fault exposure rates by LU line. Plotting these showed that some sub-surface station clusters underpinned a large proportion of fault exposure rates. Upon inspection, these station clusters are close to intermittent tunnel openings that likely expose assets more to the surface.

In the tunnels, fault exposure rate trends differed across the six LU lines. Three LU lines (Bakerloo, Central, Victoria) showed statistically significant relationships between fault exposure rates and tunnel temperatures. However, there was also no evidence of failure harvesting. What was found instead, was that fault exposure rates often peaked after annual surface  $t_{max}$  was reached.

The next chapter takes the key findings from this chapter and Chapter Four to analyse how future climate change might affect fault exposure rates under two UKCP18 RCP scenarios recommended by the GB railway industry for strategic planning. Chapter Six approximates the change in proportion of days exceeding the climate thresholds, estimates the rate of temperature change in the sub-surface and deep tube tunnels via the tunnel temperature estimation model, and considers the change in temperature bin frequencies using the fault exposure rate. The outcome is to provide a projected range in WO rate change for the two RCP scenarios for the 2050s and the 2080s, compared with baseline data.

# Chapter Six | Future climate change

## 6.1. Chapter overview

Chapter Five presented results on the fault exposure rates *per* LU line and temperature variable across the three network types (surface, sub-surface, tunnel), and investigated how rates differed by maintenance type (corrective or reactive). The results in this chapter are split into two parts. Firstly, it presents the change in thermal environment across the different parts of the network, for the four selected climate projection scenario outcomes. Secondly, it estimates future change in corrective and reactive WOs, utilising climate thresholds, the tunnel temperature estimation model and fault exposure rates in the context of UKCP18 climate projections.

## 6.2. Change in thermal environment across the LU network

Results in Chapter Four indicated that the thermal environment varied substantially across the LU network, not least by network type. The expected changes in the thermal environment owed to future climate change are therefore likely to differ by the three network types. In line with current industrial practice, this study uses 90<sup>th</sup> percentile data from RCP 6.0 and RCP 8.5 for the 2050s and 2080s, explained in Section 3.2.4.3. As such, this chapter presents four different climate projection scenario outcomes.

Upon reviewing the results in Chapters Four and Five, this chapter focuses on the projections for  $t_{max}$ . There are several reasons for this. Firstly,  $t_{max}$  is the key variable used in most climate thresholds utilised throughout this study. Table 4.4 clearly showed change in  $t_{max}$

extremes over the study period with a sufficient proportion of observations – primarily summer days, hot days, and heatwave days. Secondly, the tunnel temperature estimation model showed the most similar degree of accuracy with surface temperatures to  $t_{mean}$ . This is particularly useful as  $t_{max}$  provides absolute peak tunnel temperatures, which is valuable information to TfL both in terms of this study and broader operational heat management on the LU network. Finally, the  $t_{max}$  fault exposure rates were similar to  $t_{mean}$ , with several instances exceeding one and two standard deviation thresholds while the  $t_{min}$  and  $\Delta t$  rates showed fewer across the network types.

### 6.2.1. Change in surface temperature

Surface temperature change can be directly inferred through UKCP18 data for this study. The temperature anomalies obtained for the selected probabilistic scenarios described in the methodology (see Section 3.2.4) were added to monthly baseline data, shown in Table 6.1. The standard deviation and relative standard deviations were calculated from all the monthly baseline observations.

Table 6.1 1981-2010 baseline monthly descriptive statistics for the Greater London administrative region (Source: Met Office, 2018c)

	Variable	J	F	M	A	M	J	J	A	S	O	N	D	Year
Baseline	$t_{max}$ (°C)	7.9	8.2	11.1	13.9	17.5	20.5	23.0	22.7	19.5	15.3	10.9	8.1	<b>14.9</b>
	$SD$ (°C)	1.9	2.3	1.5	1.5	1.6	1.4	1.8	1.7	1.4	1.4	1.3	1.7	<b>5.7</b>
	$RSD$ (%)	24%	28%	14%	11%	9%	7%	8%	7%	7%	9%	12%	20%	<b>38%</b>

$SD$  = Standard deviation

$RSD$  = Relative standard deviation

There were two obstacles regarding the monthly UKCP18 data that required addressing to apply the data appropriately for this study. Firstly, projection values obtained were single values for

Greater London, so there was no spatial variance. Hence, the UHI index (see Section 3.2.2.2; Figure 3.5 The UrbClim UHI index for London) was utilised to provide an estimated spatial distribution of  $t_{max}$ . The mean UHI intensity within the Greater London boundary was +1.14°C, and therefore is the assumed mean UHI intensity representative of the single baseline value for Greater London. When compared to the UHI intensity of all surface stations across the LU network (see Figure 6.1) +1.14°C is the 34<sup>th</sup> percentile; below the mean and median, with a distribution skewed slightly towards a higher UHI intensity.

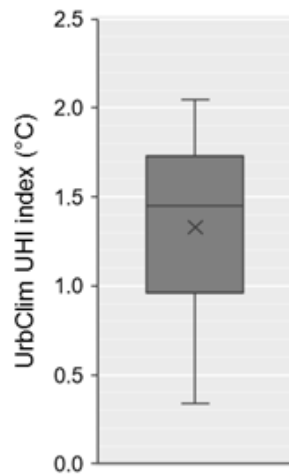


Figure 6.1 Box plot showing the spatial distribution of UHI index by surface stations across the LU network

Secondly, as the UKCP18 climate projection data are monthly, there are no extreme values to extrapolate from. This is important, as daily estimated values were critical for the fault exposure rate as they were derived from temperature exposure frequencies, which are daily observations. Table 6.2 shows the monthly projected values for Greater London *per* climate projection scenario, which are the sum of the monthly anomaly and the monthly baseline in Table 6.1. Daily estimated  $t_{max}$  values for each scenario were extrapolated by firstly calculating projected monthly standard deviations from baseline relative standard deviations, then utilising a normal distribution function to establish the % share of the month *per* 1°C temperature bin. Percentages

were converted to estimated days *per* month, then summed to provide a total estimated annual number of days *per* 1°C temperature bin for each scenario.

Table 6.2. Absolute and anomaly projected monthly  $t_{max}$  for the Greater London administrative region under each RCP scenario, 90<sup>th</sup> percentile. Values were calculated from the monthly 1981-2010 baseline values from Table 6.1

		Variable	J	F	M	A	M	J	J	A	S	O	N	D	Year
<b>RCP 6.0</b>	<b>2050s</b>	$t_{max}$ (°C)	10.0	10.6	13.1	16.2	20.1	23.8	26.5	27.3	23.1	18.4	13.1	10.0	<b>17.8</b>
		Anomaly (°C)	2.1	2.4	2.0	2.3	2.6	3.3	3.5	4.6	3.6	3.1	2.2	1.9	<b>2.9</b>
	<b>2080s</b>	$t_{max}$ (°C)	11.5	12.6	14.4	17.7	21.8	26.8	30.1	30.5	25.9	20.8	14.7	11.3	<b>20.2</b>
		Anomaly (°C)	3.6	4.4	3.3	3.8	4.3	6.3	7.1	7.8	6.4	5.5	3.8	3.2	<b>5.3</b>
<b>RCP 8.5</b>	<b>2050s</b>	$t_{max}$ (°C)	10.9	11.6	13.9	16.9	20.8	25.0	27.8	28.6	24.4	19.7	13.8	10.8	<b>18.9</b>
		Anomaly (°C)	3.0	3.4	2.8	3.0	3.3	4.5	4.8	5.9	4.9	4.4	3.0	2.7	<b>4.0</b>
	<b>2080s</b>	$t_{max}$ (°C)	12.2	13.5	16.7	18.5	22.6	26.5	31.3	32.2	30.2	23.8	18.3	13.3	<b>22.1</b>
		Anomaly (°C)	4.3	5.3	5.6	4.5	5.1	6.0	8.3	9.5	10.7	8.5	7.4	5.2	<b>7.2</b>

Figure 6.3 shows the resulting annual  $t_{max}$  frequency exposure for baseline (1981-2010) and observed (2006-2018) data, compared with the estimations from the UKCP18 climate projection data from Table 6.2. Future scenarios describe an increase in  $t_{max}$  in terms of mean and variance; with an increased distribution of frequency exposure increases in future, and to a greater extent in RCP 8.5 than RCP 6.0. The variance increase is greater at higher  $t_{max}$ , which has implications on climate thresholds – there would be a consequential increase in the summer day, hot day, and by proxy, heatwave day climate thresholds.

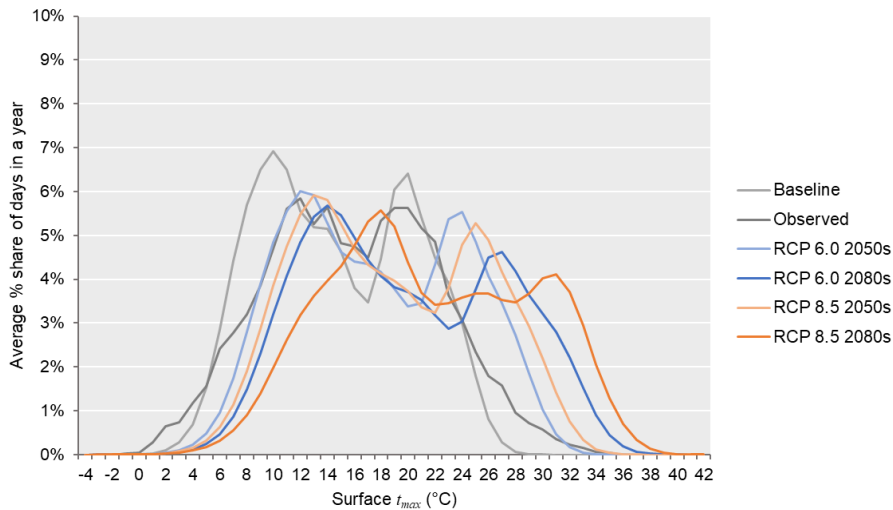


Figure 6.2 Estimated annual distributions of surface  $t_{max}$  for observed and future climate scenarios

To demonstrate the extent of the change in  $t_{max}$  variance at higher temperatures, Figure 6.3 compares present mean monthly exceedance of the summer day and hot day climate thresholds with the four climate projection scenarios. They show very large increases in such days in future. For example, where baseline and observed summer days in July are around a week of the month, in all future scenarios this is expected to increase to nearly every day of the month. Furthermore, a greater proportion of summer days and hot days in future are expected to occur in August than July, which suggests that peak summer  $t_{max}$  is more prolonged. In RCP 8.5, by the 2080s, summer days and hot days may extend into autumn months, as far as October. In the spring months, estimated increases are smaller, although the number of summer days in June by the 2080s in both scenarios increases more than triples relative to the observed data.

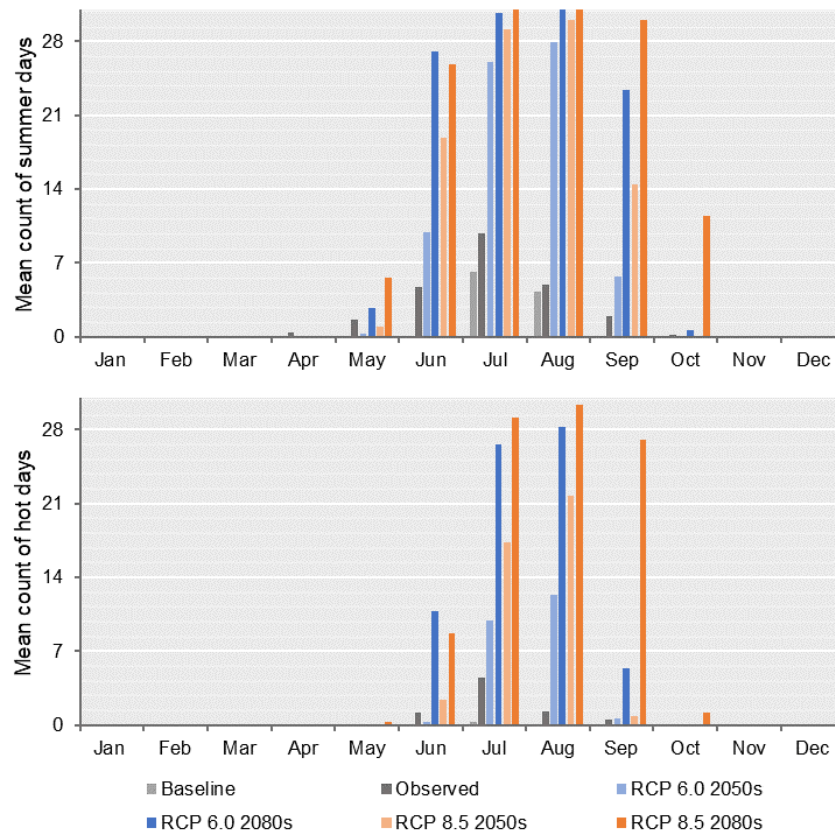


Figure 6.3 Estimated mean annual distribution of days *per* month exceeding the summer day climate threshold (top) and hot day climate threshold (bottom)

## 6.2.2. Change in sub-surface temperature

The tunnel temperature estimation model provided the basis to apply UKCP18 climate projection scenarios to estimate future station platform temperatures on the sub-surface part of the LU network. Figure 6.4 shows the distribution of present and future estimated  $t_{max}$  across the sub-surface station platforms by direction of travel. Baseline and observed  $t_{max}$  were primarily between 18°C and 19°C and increasing gradually, up to between 20°C and 21°C by the 2080s under RCP 8.5. The distribution of temperature differs between the EB/WB and IR/OR directions. The EB/WB directions show greater temperature ranges, as well as higher  $t_{max}$  in all present and projected scenarios. The observed (2006-2018)  $t_{max}$  trend suggests a recent increase in sub-surface  $t_{max}$  when compared with baseline data (1981-2010). Gradual



tunnel temperature increases continue across every LU line tunnel with each climate projection scenario.

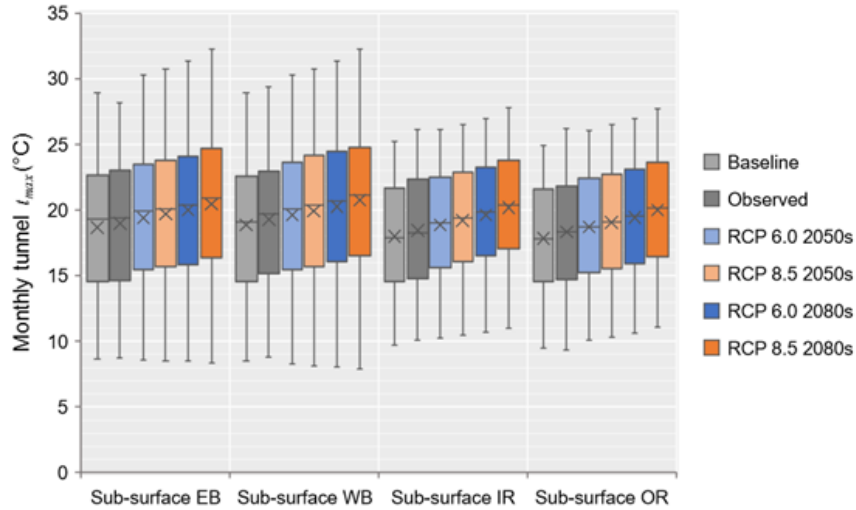


Figure 6.4 Distribution of past and projected monthly sub-surface  $t_{max}$  across each direction of travel, as calculated using station level data with the tunnel temperature estimation model

Figure 6.5 converts all the sub-surface data into mean annual present and future  $t_{max}$  frequency exposures. The distribution is a similar but simplified shape to surface  $t_{max}$  (see Figure 6.2), with two peak frequency exposures in the middle. Variance increases at higher  $t_{max}$  in projected scenarios are greater than lower  $t_{max}$ . However, recently observed (2006-2018)  $t_{max}$  recorded similar frequency exposures at the highest temperature intervals as RCP 8.5 in the 2080s. For example, both scenarios comprised two days in a year on average with a sub-surface platform  $t_{max}$  of 31°C, and one day at 32°C. This may be a symptom of the temperature estimation processes. Firstly, the tunnel temperature estimation model is not a perfect predictor of station platform temperatures – while the coefficients of determination in using surface  $t_{max}$  to predict sub-surface  $t_{max}$  was around 0.9, the residual standard errors were between 1.8°C and 2.2°C (see Section 4.3.1.2), so there is some degree of error in predictions. Secondly, the tunnel temperature estimation model is dependent on daily data, which was derived from monthly UKCP18 data in this section for the baseline and climate projection scenarios. Daily

values were therefore only representative of their time interval, implying an additional degree of error. Nevertheless, the difference in present and future  $t_{max}$  exposure frequencies in Figure 6.5 are small, so the impact these estimation errors have may not be considerable.

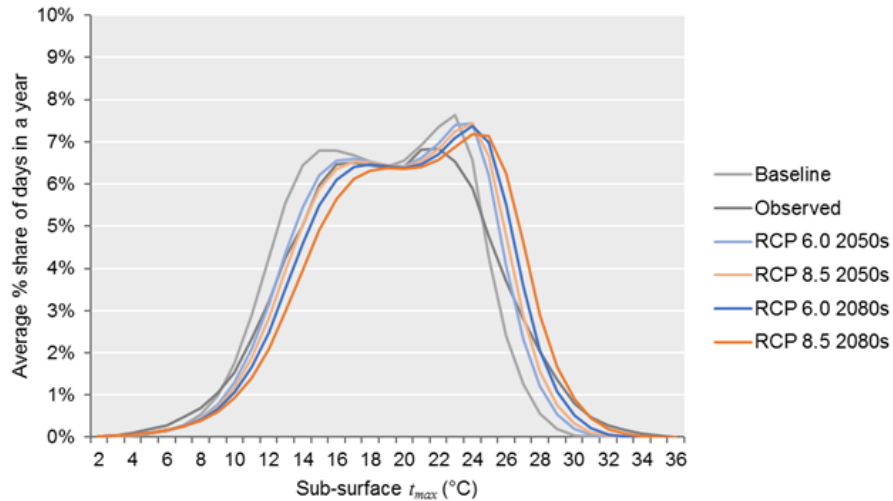


Figure 6.5 Estimated annual exposure frequency distributions of daily sub-surface  $t_{max}$  for observed and future climate scenarios

### 6.2.3. Change in tunnel temperature

Like the sub-surface part of the LU network, the tunnel temperature estimation model was used to estimate future station platform temperatures across the deep tube tunnels. Figure 6.6 shows the distribution of present and future estimated  $t_{max}$  across the tunnel station platforms by direction of travel. Recent observations, like the sub-surface, also showed an increase in temperatures compared with baseline data. It also showed gradual increases in tunnel  $t_{max}$  with each climate projection scenario. Increments in  $t_{max}$  in each scenario are greater than the sub-surface part of the LU network, suggesting that deep tube tunnel warming rates are likely to be greater than the sub-surface.

Baseline and observed mean annual  $t_{max}$  across the LU tunnels were primarily between 21°C and 27°C, depending on LU line and direction of travel. Under the RCP 6.0 scenario, annual

$t_{max}$  reaches between 24°C and 30°C by the 2050s and between 27°C and 32°C by the 2080s. In the RCP 8.5 scenario, this increases to between 25°C and 31°C by the 2050s and between 28°C and 34°C by the 2080s. The Bakerloo and Central lines remain the warmest LU tunnels. The highest reported monthly  $t_{max}$  is from June to September at Edgware Road station on the Bakerloo line, in the SB direction; between 31°C and 33°C. At this station platform, monthly  $t_{max}$  increases to 40°C in July and August under the RCP 8.5 scenario by the 2080s. The outlier values are primarily at Shepherd's Bush (Central line), Balham (Northern line), Oval (Northern line), but also Bounds Green (Piccadilly line), Brixton (Victoria line) and Victoria (Victoria line).

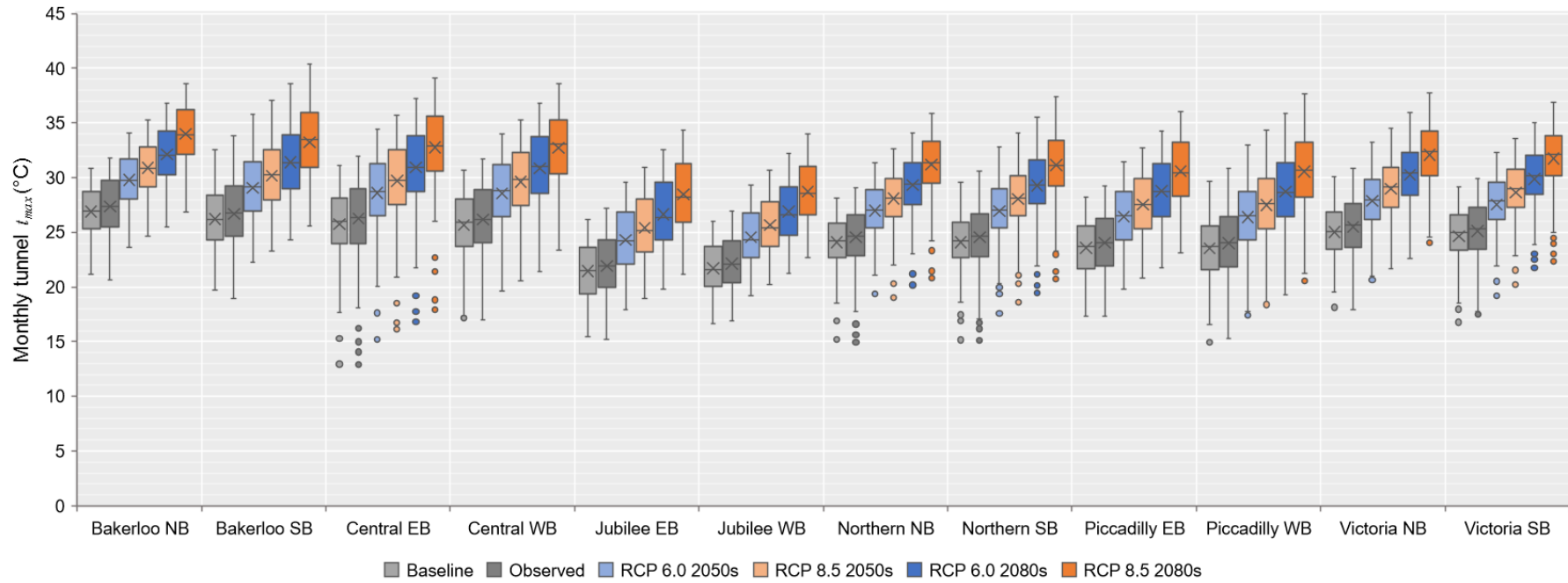


Figure 6.6 Distribution of past and projected monthly tunnel  $t_{max}$  across each LU tunnel, as calculated using station platform data with the tunnel temperature estimation model

Figure 6.7 converts all the deep tube tunnel data into mean annual present and future  $t_{max}$  frequency exposures. Present observations are similar; though observed data had a higher mean and variance to observations, which suggests that tunnel  $t_{max}$  has already been increasing. However, there is a greater increase in mean projected tunnel  $t_{max}$  than in variance. Projected increases in lower and higher  $t_{max}$  in the tunnels are proportionately similar. Additionally, to illustrate the rate of change in the future scenarios, baseline  $t_{max}$  around the upper tail end of its distribution, which is around 32°C, is around the future midpoint of the distribution of RCP 8.5 in the 2080s.

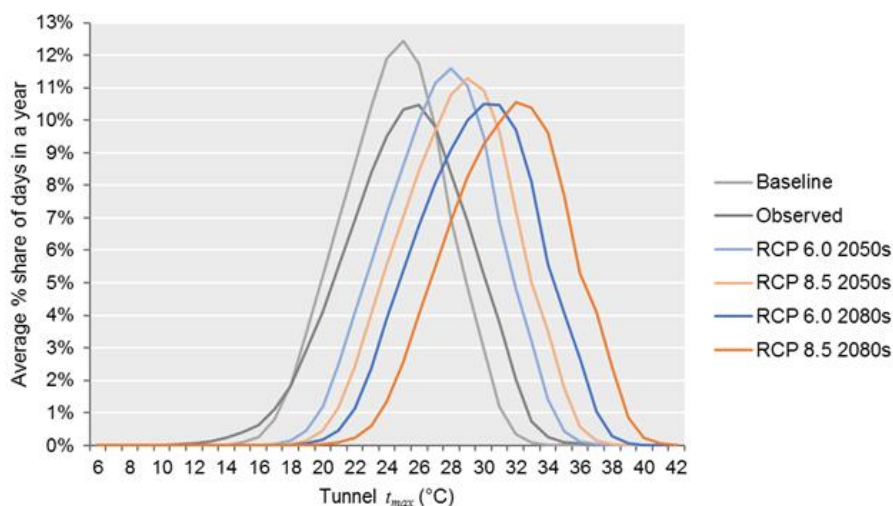


Figure 6.7 Estimated annual exposure frequency distributions of daily tunnel  $t_{max}$  for observed and future climate scenarios

### 6.3. Change in work orders across the LU network

In assessing the impacts of weather and climate on their assets and systems, infrastructure operators aim to estimate the scale of change in future infrastructure failures relative to present-day performance. Here, this section brings together all the components of this study, by using estimated future temperatures across the surface, sub-surface, and deep tube tunnels in combination with fault exposure rates from recent observations to estimate average annual WO

counts for each climate projection scenario. It is important to note that this method assumes a like-for-like network in each future scenario to the present day; that there are no significant changes to infrastructure or assets, and that its operation is similar in future.

One challenge identified in estimating future change in WOs is that future surface and tunnel temperature exposure frequencies exceed the observed temperature exposure frequencies that form the fault exposure rates in Chapter Five. Table 6.3 shows how much of an average year in each future climate scenario is outside of the range of observed  $t_{max}$  exposure frequencies *per* network type. There are no projected  $t_{max}$  increases across the sub-surface part of the LU network, a small increase in surface  $t_{max}$  in both 2080 scenarios, but large changes in tunnel  $t_{max}$  beyond current observations. These percentages therefore represent the proportion of total future WOs that the fault exposure rates cannot predict.

Table 6.3 Average annual share of each climate scenario reporting temperatures outside of the observed  $t_{max}$  exposure frequency range

	<b>RCP 6.0 2050s</b>	<b>RCP 8.5 2050s</b>	<b>RCP 6.0 2080s</b>	<b>RCP 8.5 2080s</b>
Surface $t_{max}$	0%	< 1%	0%	1%
Sub-surface $t_{max}$	0%	0%	0%	0%
Tunnel $t_{max}$	< 1%	1%	4%	13%

A second challenge in estimating future WOs involves the fault exposure rates at the highest and lowest temperatures that fall outside of the lower bound ranges. As these fault exposure rates may be artificially inflated or deflated due to the low temperature exposure frequencies, there is an implied lack of certainty in estimated WOs at these temperature bins due to the extrapolation method. There is no solution to improve the level of uncertainty, so any  $t_{max}$  fault exposure rates corresponding with a  $t_{max}$  lower bound equal or greater than 0.001 are highlighted in impending figures. Therefore, any estimated rates within these highlighted areas

include a greater level of uncertainty when interpreted. Table 6.4 shows how much of an average year in each future climate scenario is outside of the lower bound range of observed  $t_{max}$  exposure frequencies *per* network type, and therefore affected by this uncertainty in future WO estimations. All future climate scenarios are affected, with a greater share of WO estimation uncertainty in the higher emissions scenario (RCP 8.5) and the later decadal interval (2080s). More WO estimations are affected by uncertainties due to lower bounds than by temperatures outside of the observed  $t_{max}$  exposure frequencies (*i.e.*, Table 6.3).

Table 6.4 Average annual share of each climate scenario reporting lower bound temperature intervals  $\geq 0.001$

	<b>RCP 6.0 2050s</b>	<b>RCP 8.5 2050s</b>	<b>RCP 6.0 2080s</b>	<b>RCP 8.5 2080s</b>
Surface $t_{max}$	< 1%	8%	5%	15%
Sub-surface $t_{max}$	< 1%	< 1%	< 1%	1%
Tunnel $t_{max}$	2%	5%	10%	17%

### 6.3.1. Change in surface work orders

Figure 6.8 shows the rates of change in future total annual surface WOs by  $t_{max}$ , compared to the observed WO distribution. Surface WOs comprise the greatest share of observed and future estimated WOs. The trends show that increases in WOs at the highest  $t_{max}$  are greatest, as well as a decrease in WOs at lower  $t_{max}$ . Future WO counts diverge at higher  $t_{max}$  from the observed rate from approximately 24°C. Estimated WOs in both climate projection scenarios by the 2050s are high at this temperature bin, which is the current lowest temperature risk threshold for the LU Hot Weather Plan (TfL, 2022f). By the 2080s, both scenarios estimate an increase in WOs at temperatures outside of the lower bound range. Hence, while some of these rates are particularly high (*i.e.*, RCP 8.5), there is some uncertainty in their accuracy. In Figure 6.9, the data are grouped and include inferred WOs for the small percentage of WOs estimated

to occur outside of the observed  $t_{max}$  frequency exposures. It shows the scale of shift in WOs to higher temperatures, particularly increases between 25°C and 29°C, which are indicative of the effect of increased days exceeding summer day, hot day, and by proxy, heatwave day climate thresholds. The share of future estimated WOs outside the observed  $t_{max}$  are small, and only occur in the 2080s for both climate projection scenarios.

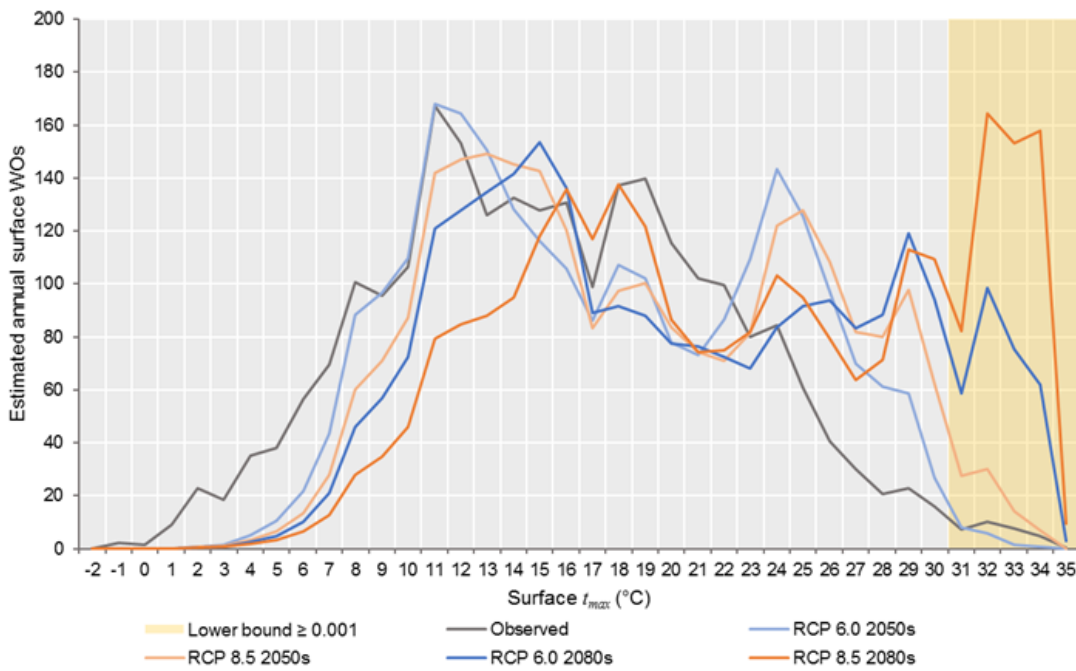


Figure 6.8 Estimated annual surface WOs for observed (2006-2018)  $t_{max}$  compared with the four selected 90<sup>th</sup> percentile climate projection scenarios

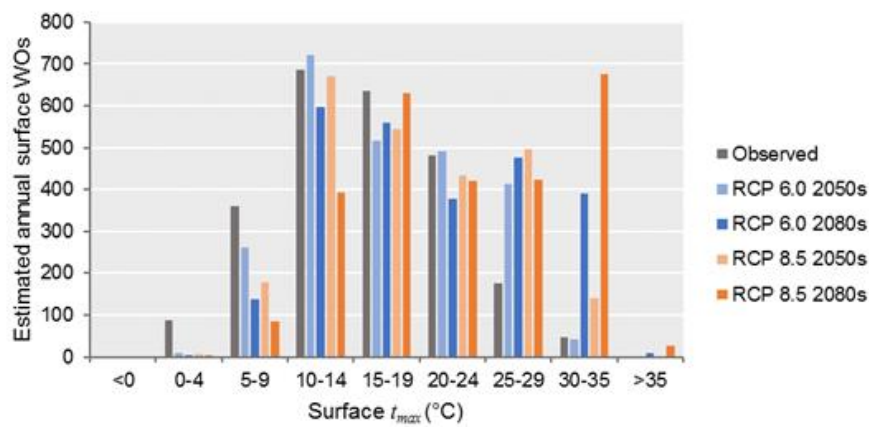


Figure 6.9 Estimated annual surface WOs, including WO estimates for upper  $t_{max}$  values outside of observations



### 6.3.2. Change in sub-surface work orders

Figure 6.10 shows very little overall change in estimated sub-surface WOs under all scenarios compared to the observed WOs. Although there are some shifts in estimations (decreased WOs at low  $t_{max}$  and increases at high  $t_{max}$ ), the actual change in overall WOs is negligible. Additionally, almost no observed or estimated future WOs extend outside the lower bound range, also shown in Figure 6.11. Therefore, the assets across the sub-surface part of the LU network are likely to be affected the least by climate change, in all scenarios.

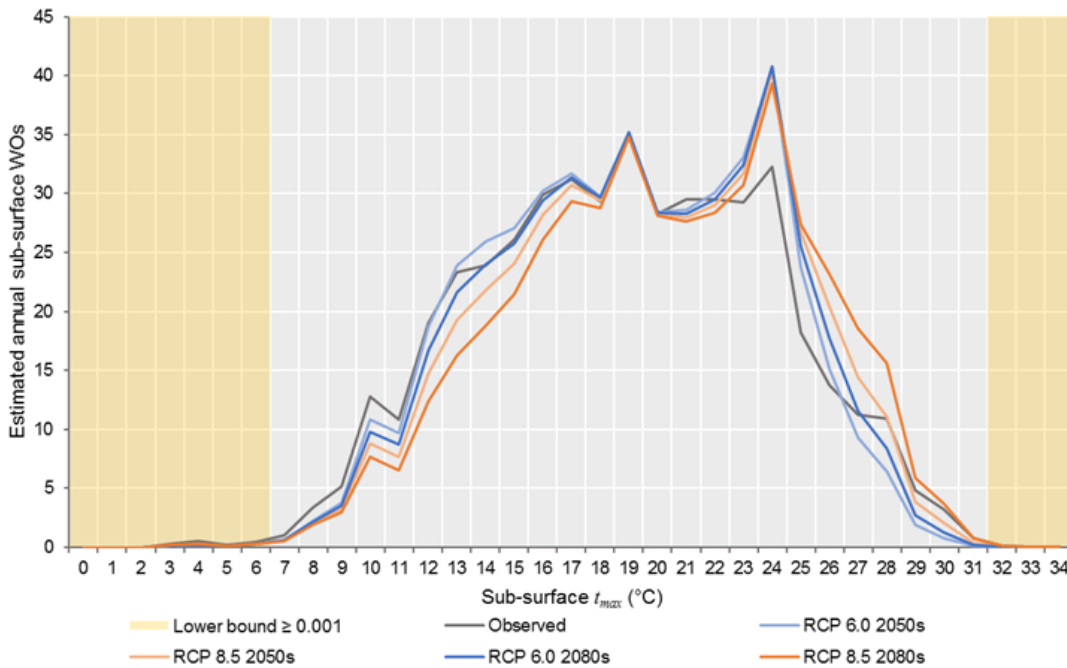


Figure 6.10 Estimated annual sub-surface WOs for observed (2006-2018)  $t_{max}$  compared with the four selected 90<sup>th</sup> percentile climate projection scenarios

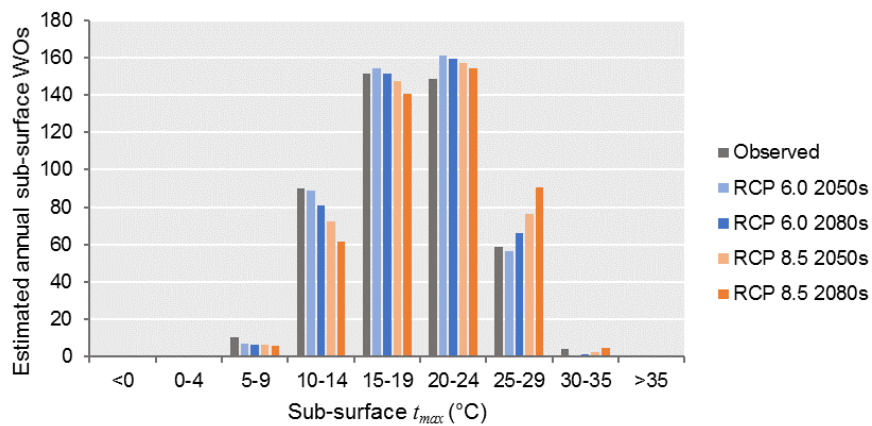


Figure 6.11 Estimated annual sub-surface WOs, including WO estimates for upper  $t_{max}$  values outside of observations

### 6.3.3. Change in deep tube tunnel work orders

The tunnel part of the LU network has the greatest proportion of the year affected by future temperatures that are either outside of the lower bound range or outside of observed  $t_{max}$  exposure frequencies. Therefore, the extrapolations undertaken to estimate future tunnel WOs likely have the most level of uncertainty of all three network types. In Figure 6.12, there are more estimated WOs at higher and  $t_{max}$ . In all the climate projection scenarios, estimated WOs at lower  $t_{max}$  decrease, and diverge from the observed rate at 30°C and above. This is also shown in Figure 6.13. The number of WOs at a tunnel  $t_{max}$  below 24°C decreases in all future scenarios and increases greatly above 30°C. Some WOs also are estimated at tunnel temperatures above 35°C. The rate of increased estimated WOs above 30°C implies the vast proportion of the tunnel part of the LU network will remain above 30°C on average throughout the year in future.

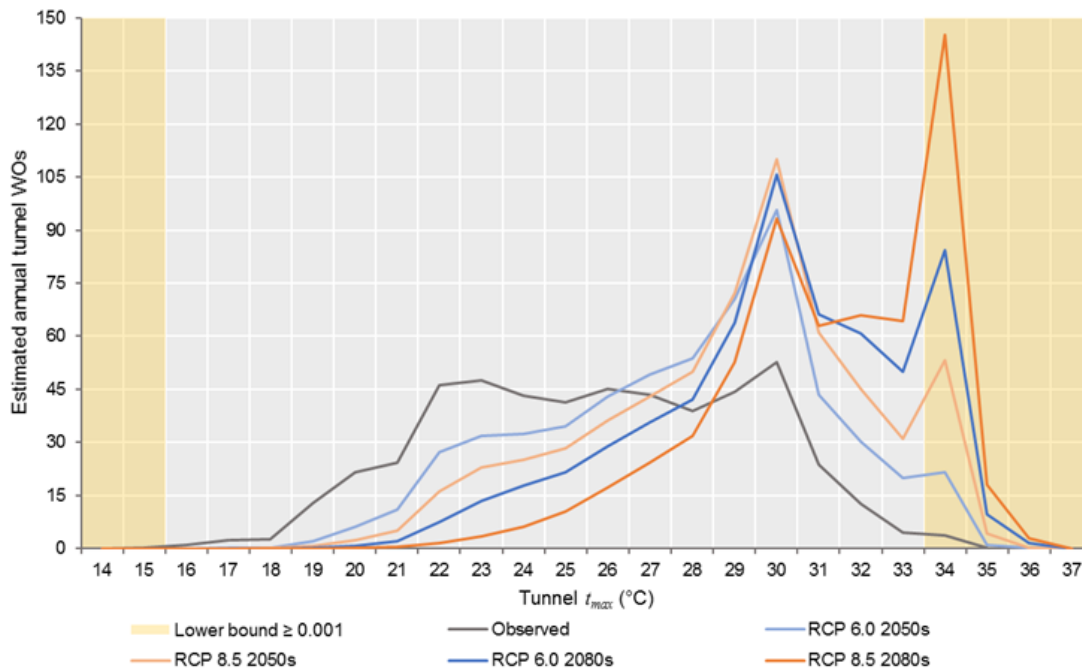


Figure 6.12 Estimated annual sub-surface WOs for observed (2006-2018)  $t_{max}$  compared with the four selected 90<sup>th</sup> percentile climate projection scenarios

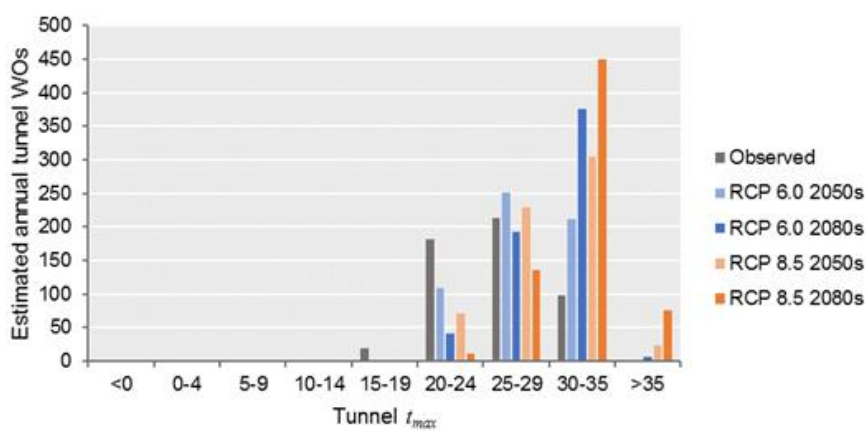


Figure 6.13 Estimated annual tunnel WOs, including WO estimates for upper  $t_{max}$  values outside of observations

### 6.3.4. Total change in work orders across the LU network

Finally, the total estimated WOs were combined to provide an estimated change in WOs due to change in temperature for point and train stop assets across the LU network. These are shown in Figure 6.14. Although there are differences in the temperatures at which these WOs occurred, the estimated annual total WOs show slight increases. Compared with the observed total WO

count, estimated WOs for RCP 6.0 in the 2050s comprise a 1% increase, and by the 2080s, a 6% increase. However, estimated WOs for RCP 8.5 in the 2050s comprise a 3% increase, and by the 2080s, a 10% increase. As mentioned in Section 6.3, these increases assume no significant changes to infrastructure or assets, and similar future operation of the LU network. Moreover, due to uncertainty and degrees of error in data and methodological approaches, there is an undefined range of confidence around these estimations; not least the chance that future WO estimations could be higher than those shown.

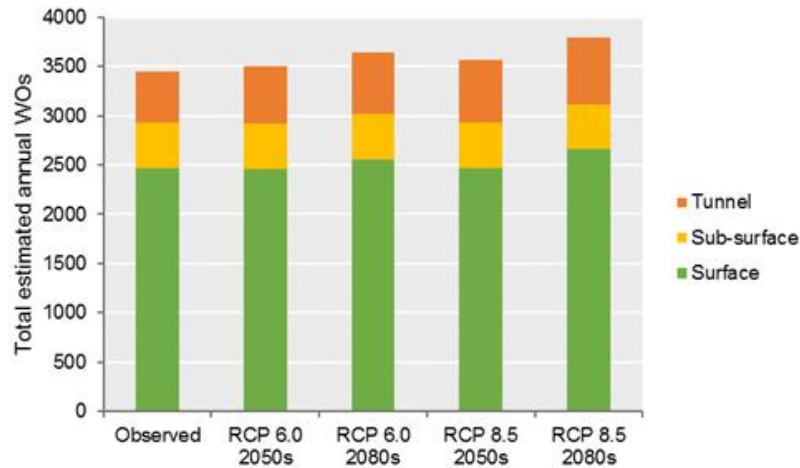


Figure 6.14. Total estimated annual WOs by network type for observed and estimated climate projection scenarios

## 6.4. Chapter summary

This chapter presented results on how four future climate change scenarios (90<sup>th</sup> percentiles of RCP 6.0 and RCP 8.5 for the 2050s and 2080s) are likely to change the thermal environment and the total estimated annual WOs for point and train stop assets by network type (*i.e.*, surface, sub-surface, deep tube tunnels). Focusing on  $t_{max}$  throughout this chapter, experimental methods were used to convert UKCP18 climate projections into future estimated  $t_{max}$  exposure frequencies. The tunnel temperature estimation model was utilised to convert the estimated exposure frequencies into platform  $t_{max}$  for the sub-surface and tunnel parts of the LU network.

Estimated temperatures across each network type were then extrapolated to network-wide reactive fault exposure rates to produce estimated annual counts of faults *per* future climate scenario.

Changes in the future thermal environment across the LU network differ by network type. On the surface, the first warm days of the year may occur earlier in the year by a month, as well as an extension of summer temperatures into autumn months. Frequency exposures of  $t_{max}$  increase in variance, particularly with increased frequencies at higher temperatures. Lower  $t_{max}$  are still likely to remain at some extent, although slightly less frequent than the present day. Across the sub-surface part of the LU network, there are slight increases in station platform temperatures, but are insignificant relative to the change on the surface. However, in the tunnels, projected station platform  $t_{max}$  increases more, varying by LU line – with observed tunnel  $t_{max}$  already shifting towards the RCP 6.0 2050s scenario.

Fault exposure rates were converted into estimated annual WOs using the estimated  $t_{max}$  exposure frequencies. However, there are limitations in the estimates for two reasons. Firstly, there is a lower confidence in fault exposure rates at the highest and lowest observed temperature intervals, where lower bound rates were high, so extrapolating from them increases the levels of certainty in estimates. Secondly, the projected  $t_{max}$  exposure frequencies often included temperatures that were not recorded in the observed data for this study, and therefore there were no fault exposure rates for them. This means that further assumptions were made to infer WO rates at temperatures beyond the observed  $t_{max}$  exposure frequencies. Nevertheless, estimated future total annual WOs showed a 1% increase in the RCP 6.0 scenario in the 2050s and a 6% increase in the 2080s; and a 3% increase in the RCP 8.5 scenario in the 2050s and a 10% increase in the 2080s.

In the next chapter, all the results from Chapters Four, Five, and Six are reviewed and discussed in the context of implications for TfL. This includes recommendations regarding the organisational procedures across the organisation to support the delivery of more climate-resilient transport for London. The methodology designed for this study is also critiqued, for the purpose of improving future analysis for London and beyond.

# Chapter Seven | Discussion

## 7.1. Chapter overview

Chapter Six presented the final set of results of this study, on how different climate projection scenarios may change the thermal environment across the three network types on the LU network. It also estimated the potential change in point and train stop asset WOs for each scenario. This chapter discusses all results from this study and their implications for TfL. It considers several strategic and organisational factors associated with adapting the LU infrastructure to climate change. Then, this chapter contextualises these factors in the wider scope of climate change adaptation on transport infrastructure. Recommendations are proposed throughout the discussion, aligned to the relevant section. The chapter is finally summarised with the Author's view on the direction TfL could take to deliver a more climate-resilient LU network in future.

## 7.2. Discussion of results chapters

The discussion of results begins with Chapter Four, which analysed the thermal environment across the LU using descriptive statistics, quantified the magnitude of recent change in the climate via climate thresholds, and finally, introduced and evaluated a tunnel temperature estimation model. This follows with discussion on Chapter Five, which utilised several of the parameters in Chapter Four to establish fault exposure rates through a robust methodological approach. The discussion of the results chapters ends with Chapter Six, which used the tools and results developed in Chapters Four and Five to estimate future WOs across the LU network in accordance with climate projections.

### **7.2.1. Thermal environment**

This section discusses the implications of the results within Chapter Four, which described and evaluated the present state of the thermal environment across the LU network. The climate is unambiguously warmer in the study period relative to the 1981-2010 baseline, and because of the variance in built form, there is a need to understand the extent of the impact of warmer temperatures on the surface upon the sub-surface and tunnel parts of the LU network.

#### **7.2.1.1. Temperature variables**

The results of this study revealed the extent of variance in thermal environments throughout the year among the surface, sub-surface, and tunnel parts of the LU network. Most notable were the differences in all temperature variables by LU line across all the deep tube tunnels, including differences between the two directions of travel on the same LU line (see Section 4.2.1).

Compared with all LU deep tube tunnels, both Jubilee line tunnels recorded considerably lower temperatures across all the variables (see Figure 4.9). This may be due to the increased ventilation capacity of the Jubilee line extension (Jones, 1999). However, it is not possible in this study to quantify the extent of the improved capacity on temperatures across the Jubilee line and compare with other LU lines. Due to security reasons, the locations of mid-tunnel ventilation shafts are not disclosed to the public (TfL, 2012), although TfL would benefit from understanding whether the ventilation capacity on the Jubilee line extension is contributing to these lower tunnel temperatures relative to the rest of the LU deep tube tunnels. By doing this, TfL could quantitatively evaluate whether ventilation capacity reduces tunnel temperatures, especially at tunnel sections where several stations do not have mid-tunnel ventilation shafts, as such analysis is not possible outside of the organisation. It is nevertheless important to note



that the Jubilee extension is only slightly over 20 years old, while the heat build-up across other LU tunnels is a result of over 100 years' activity (Botelle *et al.*, 2010). Comparisons will therefore not be like-for-like. Such results may support the business case for an evidence-based, targeted approach to climate change adaptation via greater technological advancements in cooling systems and ventilation as there are operational performance and human health co-benefits – as the low fresh air exchange also increases levels of thermal discomfort (Jenkins *et al.*, 2014) as well as reducing exposure to harmful pollutants (Kumar *et al.*, 2023).

***Recommendation 1: TfL should calculate the correlation between deep tube LU tunnel temperatures and ventilation capacities across its stations to evaluate the scale of impact of ventilation across the current network.***

#### **7.2.1.2. Climate thresholds**

This chapter reviewed the current climate of London and quantified recent change in mean and extreme temperatures using seven climate thresholds. Instances of climate threshold exceedances were conducted using surface temperature observations from the Met Office weather station at St. James's Park. Results from Table 4.4 indicate that there were more warmer days, warmer nights and WSDI days across the study period relative to the baseline period they were calculated from (see Table 3.6), which is indicative of warmer mean temperatures. For example, an average of 51% of days in the study period were considered warm nights, which would represent days higher than the 90<sup>th</sup> percentile of observed temperature within the baseline period. The remaining climate thresholds (summer days, hot days, heatwave days, tropical nights) were higher than the study period mean in the latter years, also signalling an increase in extreme heat events. Consequently, these results are indicative of the UK climate having changed in recent years.

The climate thresholds were a useful supporting reference to key points and findings throughout this study. Choice of language used to communicate climate change is extremely important (Bruine de Bruin *et al.*, 2021) and using the climate threshold terminologies would support the communication of climate change for emphasis in broader public-facing documents for TfL, such as their environmental strategies and for climate change adaptation reporting. Given that the climate threshold terminology is used by the Met Office, using them would enhance TfL's profile in terms of their understanding of climate change.

***Recommendation 2: TfL should consider the use of climate threshold definitions in relevant publications to both quantify change in weather observations relative to climate baselines while communicating an understanding of climate change in a simple way to the reader.***

Implications for this study that could not be predicted were the incidence of several extreme temperatures after the data were collected for analysis. Although this study quantitatively demonstrated warming rates and extreme heat events between 2006 and 2018 (see Table 3.6), there were few record-breaking observations in the study period. However, several occurred shortly afterwards. These include:

- Highest temperature on record for a winter month, reaching 21.2°C at Kew Gardens on 26<sup>th</sup> February 2019. These warm days occurred 21-27<sup>th</sup> February (Met Office, 2019b).
- 37.9°C recorded across London on 25<sup>th</sup> July 2019; within a heatwave event that occurred 22-26<sup>th</sup> July (Met Office, 2019c).
- Exceptionally hot day, reaching up to 37.8°C at Heathrow and 37.3°C at Kew Gardens on 31<sup>st</sup> July 2020 (Met Office, 2020b).

- An extended heatwave, reaching 36.4°C on at Heathrow on 7<sup>th</sup> August 2020. Temperatures across the southeast of England exceeded 34°C every day between 7-12<sup>th</sup> August. This included five tropical nights (Met Office, 2020a).
- A transition in temperature extremes from unusual warmth in March, where 24.5°C (a summer day) was recorded at Kew Gardens on 30<sup>th</sup> March 2021, followed by a cold plunge in April and a difference of up to 15°C reported in the space of a week (Met Office, 2021a).
- Exceptionally mild new year, reaching 16.3°C at St. James's Park on 1<sup>st</sup> January 2022 (Met Office, 2022b).
- An unprecedented hot day, reaching 40.2°C at St. James's Park on 19<sup>th</sup> July 2022 and included a record-breaking tropical night with a minimum temperature of 25.8°C at Kenley Airfield. The heatwave occurred 16-19<sup>th</sup> July (Met Office, 2022d).

These seven temperature-related extreme events since 2018 exceeded those within the study period. In terms of this study, they would add important data to the tunnel temperature estimation model, as well as additional temperature frequency exposures with the potential to affect lower bound ranges. Their inclusion could also improve future WO estimations. On the other hand, WO data from 2020 onwards would not necessarily improve fault exposure rates despite the additional temperature observations, because of reduced passenger counts and staffing due to the coronavirus pandemic.

***Recommendation 3: Future iterations of any parts of this study specifically related to climate change should include data from 2019 to 2022, capturing the increased instances of exceptional warm weather and extreme heat events that recently occurred.***

### 7.2.1.3. Tunnel temperature estimation model

Due to the importance of tunnel temperature data throughout the study, it was necessary to develop a tunnel temperature estimation model using surface temperature as a proxy value (see Section 4.3). This is because there were missing observations from the study period across the network, and to provide a means to forecast future tunnel temperatures using surface climate projections from the Met Office (see Sections 6.2.2 and 6.2.3). The tunnel temperature estimation model produced key variables that characterised the effect of surface temperature upon tunnel platform temperatures for each station, including: the mean temperature uplift in the tunnels compared to the surface; the scaling coefficient, representative of the annual fluctuation, and magnitude of the highest and lowest temperatures. The model showed a short time lag in surface temperatures affecting the deep tube tunnels, typically no more than two days. Across the sub-surface part of the LU network, the effect of surface temperature was far greater, shown by lower temperature uplift and higher scaling coefficient values.

Comparing the model results with the observations showed that there were limitations in using surface temperature as a single proxy value to estimate tunnel temperatures, based on the coefficients of determination (*e.g.*, see Table 4.5). These coefficients highlight that some of the variance in tunnel station platform temperatures can be explicitly explained by the variance in surface temperatures, as addressed in research (*e.g.*, Mortada *et al.*, 2015) and also emphasises the magnitude of other moderating factors across the deep tube tunnel part of the LU network. As the coefficients of determination also vary by LU line, it is difficult to disentangle the effect of other factors driving some of the variance in tunnel temperatures. As such, there is a degree of error in resulting tunnel temperatures from this estimation model, which likely affects the deep tube tunnel fault exposure rates (only where WOs were joined with estimated values if

there were no observed data) as well as the estimated tunnel temperatures under future climate change. The level of error is therefore a greater issue at the shorter temporal scale (*i.e.*, daily), as opposed to the longer temporal scale (*i.e.*, monthly, annual, decadal).

Nevertheless, the tunnel temperature estimation model used in this study was a useful tool to assign temperature values in the absence of observation data and updates future estimated temperatures for the deep tube part of the LU network previously estimated by Jenkins *et al.*, (2014). While the method itself has limitations, these were unavoidable because of the known varying and complex factors affecting tunnel temperature. Through this study, it was possible to demonstrate the value of estimating tunnel temperatures using a simple model, with implications for both future thermal comfort and asset performance thresholds.

***Recommendation 4: TfL should utilise a statistical method to estimate tunnel temperatures using surface temperature as a proxy, particularly to help estimate future tunnel temperatures under future climate change scenarios.***

### **7.2.2. Fault exposure rates**

This section discusses the implications of the results shown in Chapter Five on fault exposure rates of point assets by network type (surface, sub-surface, tunnel) and LU line across the LU network. Implications are focused primarily on outcomes for TfL in terms of strategic decision-making and operational planning, which underpin their response to the impacts of assets to weather and climate hazards.

### 7.2.2.1. Fault thresholds

The fault exposure rate analysis in Chapter Five built on the methodological foundation designed by Fisher (2020) and adds to the existing knowledge on frequency-related relationships between meteorological variables and asset failures on railway networks. This study showed that by synthesising several datasets, the fault exposure rate concept was applicable to the LU network and is the first ever systematic analysis that incorporates both surface and tunnel environments across a metro network.

The purpose of this analysis in Chapter Five was to identify fault thresholds in temperature whereby fault exposure rates exceed a statistically defined tolerance – in this case, exceeding one and two standard deviations. Conducting the analysis across four temperature variables ( $t_{mean}$ ,  $t_{max}$ ,  $t_{min}$ ,  $\Delta t$ ) showed varying relationships between WOs raised on the LU asset management systems and the observed (or estimated) temperature at the nearest station. Instances of threshold exceedance occurred primarily at the lowest and highest observed temperatures (*e.g.*, see Figure 5.4). As such, the fault exposure rates revealed potential upper and lower thresholds. These are summarised for daily  $t_{min}$  and  $t_{max}$  in Table 7.1, based on exceedances of one standard deviation of the mean across the 12 fault exposure rate graphs by LU line and network type presented in Chapter Five. One standard deviation was selected as there were overall very few instances exceeding two standard deviations, but several trends between one and two. It was therefore possible to include a greater proportion of results, which is important as not all LU lines reported threshold exceedances.

Table 7.1 shows emerging patterns in fault threshold exceedance. There were more fault threshold exceedances at upper than lower temperatures, implying that fault risk is greater at higher temperatures. Most fault threshold exceedances occurred at high temperatures across the

Bakerloo, Central, Victoria and H&C lines. The District line, however, only exceeded fault thresholds at low temperatures. On the surface part of the LU network, fault threshold exceedances fitted broadly into two groups. Firstly, were the Bakerloo, Central and Victoria lines, whose upper fault threshold exceedances of  $t_{max}$  were lowest but also comprised upper fault threshold exceedances for  $t_{min}$ . This is indicative of early season vulnerability to heat (low upper fault threshold exceedance of  $t_{max}$ ) and a vulnerability to persistent high temperatures with limited cooling, such as the occurrence of tropical nights (upper fault threshold exceedance of  $t_{min}$ ).

Secondly, there were lines with emerging fault threshold exceedances on hot days across the surface part of the LU network. These were on the Jubilee and H&C lines, where fault thresholds were approximately 10°C higher than the other lines, so it is likely that only instances of extreme heat affect assets in these areas.

On the sub-surface part of the LU network, few thresholds were identified. Identified upper thresholds of  $t_{min}$  were 23°C. Referring to the tunnel temperature estimation model, these upper temperature thresholds corresponded with surface temperatures indicative of or close to tropical night temperatures, further demonstrating the potential risk of continued high night-time temperatures on sub-surface infrastructure.

Table 7.1 Upper and lower fault thresholds of  $t_{min}$  and  $t_{max}$  per LU line and network type for point-related assets, derived from the fault rate analysis chapter. Fault thresholds are based on the first instance the temperature variable exceeded one standard deviation of the mean fault exposure rate at the higher and lower temperature ranges. A dash (-) indicates that no fault threshold was exceeded across the results, while N/A indicates that the respective LU line does not run through the network type, so there are no results to show.

LU line	Temp variable	First instance surface fault thresholds		First instance sub-surface fault thresholds		First instance deep tube tunnel fault thresholds	
		Lower	Upper	Lower	Upper	Lower	Upper
Bakerloo	$t_{min}$	-	18°C	N/A	N/A	-	29°C
	$t_{max}$	0°C	23°C			-	32°C
Central	$t_{min}$	- 4°C	19°C	N/A	N/A	18°C*	27°C
	$t_{max}$	2°C	24°C			23°C*	29°C
District	$t_{min}$	1°C	-	-	-	N/A	N/A
	$t_{max}$	- 1°C	-	9°C	-		
Jubilee	$t_{min}$	-	-	N/A	N /A	-	-
	$t_{max}$	-	33°C			-	-
H&C	$t_{min}$	-	-	-	23°C	N/A	N/A
	$t_{max}$	-	32°C	-	25°C*		
Metropolitan	$t_{min}$	-	-		23°C	N/A	N/A
	$t_{max}$	-	-	7°C	-		
Northern	$t_{min}$	-	-	N/A	N/A	-	-
	$t_{max}$	-	-			-	-
Piccadilly	$t_{min}$	-	-	N/A	N/A	-	-
	$t_{max}$	-	-			-	-
Victoria	$t_{min}$	-	17°C	N/A	N/A	-	28°C
	$t_{max}$	5°C	22°C			-	30°C

\* indicates the best estimated threshold interpretation due to the irregular fault exposure rate trend



On the other hand, there were fewer upper  $t_{max}$  fault thresholds identified. The lines with an upper fault threshold for  $t_{max}$  on the surface and sub-surface parts were the H&C lines. This is telling of a greater asset exposure to temperatures on these LU lines, given that the other sub-surface lines (*i.e.*, District and Metropolitan lines) did not report any upper temperature fault thresholds. On the other hand, the District and Metropolitan lines had lower temperature fault thresholds, which may be indicative of their increased exposure to the cold. One explanation could be spatial temperature variance across both the surface and sub-surface. Parts of the Metropolitan and District lines extend further out from London's centre; west and east respectively, where the UHI intensity decreases. On the other hand, the H&C lines are subjected to a greater UHI magnitude.

The deep tube tunnel thresholds in Table 7.1 show two very distinct trends: LU lines with upper temperature fault thresholds (Bakerloo, Central and Victoria lines) and those with no discernible fault thresholds (Jubilee, Northern and Piccadilly lines) and suggest that tunnel age may not be an underlying factor (see Table 1.1). The Bakerloo, Central, and Victoria lines have similar upper temperature fault thresholds. For  $t_{min}$ , these vary between 27°C and 29°C, whereas for  $t_{max}$ , these are between 29°C and 32°C. Referring to the tunnel temperature estimation model for these lines, there are a wide range of surface temperatures that can lead to these tunnel station platform temperatures being reached, depending on LU line and the time of year. For instance, before the summer peak, early warm temperatures lead to several station platform tunnel temperatures exceeding upper  $t_{min}$  fault thresholds. On the Bakerloo and Victoria lines, this is around a  $t_{min}$  of 16-17°C; whereas for the Central line it is 11-12°C. However, after the summer peak, a drop-off in upper threshold exceedance occurs when surface  $t_{min}$  decreases to 1-2°C lower than the early warm temperature range. The implications are that the interactions between surface temperature, tunnel temperatures and the impacts on assets are

extremely complex and a single level of temperature risk is not representative of the whole LU network.

In the context of the LU Hot Weather Plan (TfL, 2022f), this study challenges its existing risk thresholds. Several upper  $t_{max}$  fault thresholds from Table 7.1 fall within various stages of the Hot Weather Plan risk thresholds, with some even lower than “no risk.” Additionally, the upper  $t_{min}$  fault thresholds suggest that new risks may be emerging for LU infrastructure on the basis that assets are not sufficiently cooling down before re-exposure to daytime temperatures the following day. On the other hand, this study also identified low temperature thresholds. As snow depth is the only hazard with a risk threshold range in the LU Winter Weather Contingency Plan (TfL, 2022e), it would be beneficial to include a temperature risk threshold range to improve preparations for colder weather.

***Recommendation 5: TfL should review the current risk thresholds within the LU Hot Weather Plan, in accordance with this study’s fault exposure rates and upper  $t_{max}$  thresholds. This includes whether risk thresholds could include additional LU line- area- or station-specific foci to improve weather and climate resilience.***

***Recommendation 6: TfL should distinguish risk thresholds between surface and deep tube tunnel sections of the LU network as a minimum within the LU Hot Weather Plan and outline actions accordingly.***

***Recommendation 7: TfL should include actions within the LU hot weather plan to address the risk of continuous high  $t_{min}$  across the LU network, for all three network types.***

***Recommendation 8: TfL should incorporate low temperature risk thresholds within the LU Winter Weather Contingency Plan.***

As this study reviewed one group of assets, it would be beneficial to extend the analysis to other LU asset groups, such as track and signalling and compare the findings (such as those in Table 7.1). This is feasible as the results from this study derive from the same fault data for other asset groups. By doing this, fault exposure rates are comparable across asset groups due to the normalisation process in this methodology and as a result, can show the LU lines most at risk to temperature, establishing more robust risk thresholds.

***Recommendation 9: TfL should conduct similar fault exposure rate analyses for other asset groups at risk to temperature (e.g., track; signalling/communications) and compare the resulting temperature thresholds to those produced in this study.***

#### **7.2.2.2. Failure harvesting**

One important finding from the fault exposure rate analysis was a signal of failure harvesting of point-related assets across the LU network (see Sections 5.3.1 and 5.3.2). This is important, as it reveals a particular temporal vulnerability in the spring and early summer, emphasising that the correlation between temperature and fault exposure rates is less straightforward than the highest or lowest observed temperatures driving more failures. Validation of failure harvesting across other parts of the GB railway industry by Ferranti *et al.* (2016) suggests that this is a wider railway concern, perhaps overlooked through the lens of climate-resilient infrastructure research. Failure harvesting signals were also addressed by Oslakovic *et al.* (2013) in the winter months for the Netherlands, determining that most problems on the assessed railway section occurred during the first snowfall in the season. Though the climate in the Netherlands is not analogous to London, this highlights the extent of preparedness on the impacts of weather on infrastructure, regardless of the environment, and a particular vulnerable

point in the year being the first and earliest incident of a weather event in the year, wherever this may fall.

*Recommendation 10: TfL should extend the technique of using fault exposure rates to identify failure harvesting trend to other assets, and endeavour to identify the most vulnerable locations where early heat-related faults are occurring most frequently.*

### **7.2.3. Future climate change**

This section discusses the implications of the results presented in Chapter Six, which focused on the estimated change in  $t_{max}$  across the LU network in terms of future thermal environment by network type and future point-related WOs. Results in this chapter showed that the LU network will experience warmer temperatures in all climate projection scenarios (RCP 6.0 and RCP 8.5; 90<sup>th</sup> percentile; for the 2050s and 2080s), with consequential increase in WOs of varying rates dependent on network type and climate projection scenario, as shown in Figure 6.14.

#### **7.2.3.1. Change in thermal environment**

Estimating the future change in thermal environment across the LU network highlighted the challenges associated with the conversion of UKCP18 data to generate temperature frequency exposures. It also highlighted how necessary assumptions may have compromised accuracy in estimations by introducing additional uncertainty, alongside the assumptions associated with the tunnel temperature estimation model. These fundamental challenges arose because UKCP18 data is not provided in the relevant format required of this study, highlighting the need

for climate projection data to be produced in formats that align with the analytical approaches of organisations such as TfL. This is discussed further in Section 7.3.1.5.

Nevertheless, there were several relevant findings. Focusing on  $t_{max}$ , the rate of warming across all climate projection scenarios differs by network type. On the surface, there is an estimated increase in mean temperature and variance, especially an increase in the frequency of higher  $t_{max}$  and therefore an assumed increase in the annual percentage of exceedance in climate thresholds such as hot days, heatwave days, and tropical nights (see Section 6.2.1). Across the sub-surface part of the LU network, there is a marginal estimated change in distribution of  $t_{max}$  to slightly higher temperatures (see Section 6.2.2). However, in the deep tube tunnels, there is a bigger shift in  $t_{max}$ ; not as high as on the surface, but much higher than the sub-surface (see Section 6.2.3). These estimated future temperatures emphasise the scale of its increase as a hazard upon the overall risk to assets across the LU network, and that the scale of the increased hazard across the surface and tunnel parts of the LU network are unambiguously greater than the sub-surface. For asset managers, who are responsible for the maintenance of LU assets, this information would be extremely valuable in terms of maintenance planning, as well for longer-term strategic decisions on future asset design or renewals.

***Recommendation 11: LU asset managers should be informed of the expected rate of change in temperatures across the LU network in quantitative terms as a call to action regarding climate risk and asset management.***

### 7.2.3.2. Change in future work orders

Chapter Six also highlighted challenges with projecting future estimated WOs, particularly for infrequently observed temperatures as well as temperatures that had not yet been observed but likely to occur in the future (see Section 6.3). Even if such temperature exposure frequencies were low in future, predicting WOs with high accuracy is not possible as either the resulting fault exposure rates may be artificially inflated or deflated, or do not exist. Therefore, the results addressed where these limitations may be, and made best estimates based on the results available.

The estimates indicate there may be up to a 10% increase in point-related WOs compared to the baseline of 2006-2018 that was used for this study (see Figure 6.14). Increases vary by network type. In reviewing the change in WOs in the context of the change in thermal environment, some of the climate risk on the LU network may not necessarily be regarding the management of more WOs throughout the year but pertaining to *when* in the year the WOs may occur. For instance, increased risk may likely be when high temperatures occur early in the year. Under future climate change, these instances are likely to occur even earlier. Surface fault exposure rates before the annual peak  $t_{max}$  begin to increase from around 25°C (see Figure 5.10), coinciding with a large increase in the annual proportion of surface  $t_{max} \geq 25^\circ\text{C}$  in all climate projection scenarios (see Figure 6.2) and more estimated WOs in total (see Figure 6.8). Where such days in the baseline data only occurred around July and August, these occur as early as May in both scenarios by the 2080s. If the change in timing of such temperatures is not accounted for within heat risk management, it could lead to operational challenges at times when asset managers are potentially not prepared for the impacts of heat.

*Recommendation 12: LU asset managers should be informed of the potential change in WOs due to heat owed to climate change, including the potential for high temperature occurrence earlier in the year to improve operational responses to heat at unexpected times of the year.*

### **7.3. Increasing TfL's capacity to adapt to heat and climate change across the LU network**

Decision-makers face four key barriers that risk reducing their capacity to deliver more climate-resilient transport. These are: financial and economic; social and political; technical; and institutional and regulatory (Greenham *et al.*, 2022). Addressing these barriers via targeted actions can increase TfL's capacities. In this study, the data-driven results provided new decision-support tools, addressing the technical barrier. However, as acknowledged from the literature in Chapter Two, tacit knowledge is also extremely valuable and held across internal and external stakeholders to TfL. Engaging the relevant stakeholders would not only enhance technical, but also institutional capacities for TfL. This section discusses data and stakeholder engagement opportunities in the context of this study, and how they could drive further improvements in terms of climate change adaptation practices.

#### **7.3.1. Data**

The quality and quantity of the underpinning data were a crucial component of this study's analysis. Improving these data improves TfL's data-driven interpretation of results, which in turn enables the better planning of and response to climate risks.

### **7.3.1.1. Weather observations**

This study applied temperature data from several sources to conduct the required analyses. Doing so was necessary because as demonstrated, observed temperatures on the surface were not reflective of those in tunnels. Starting with past observed temperature data, this study oriented around data at a single-site MIDAS hourly observation weather station (St. James's Park). All derived surface temperatures for this study were calculated from data at this site. Therefore, there was a degree of error in calculated temperatures, namely the surface temperature variables *per* station adjusted for UHI that were joined to WO data for the analysis in Chapter Five. Furthermore, additional weather data available to TfL are via weather stations at LU depots and sidings managed by contractors (Vaisala), but these data are spatially biased as their locations are not uniformly distributed across the LU network.

On the other hand, a single reference point for temperature was beneficial, particularly when determining climate thresholds to evaluate the thermal environment in Chapter Four. This is because as a temporal reference, including spatial parameters to these climate thresholds or the tunnel temperature estimation model would add an unknown and uncontrolled variable to fault exposure rate analyses in Chapter Five and future climate change estimations in Chapter Six.

***Recommendation 13: Future fault exposure rate analyses should consider using gridded weather observations for temperature variables to improve accuracy of results for TfL.***

### **7.3.1.2. LU platform temperature observations**

Tunnel temperature data collected by TfL on the sub-surface and deep tube tunnel parts of the LU network were comprehensive and suitable for this study both spatially and temporally. However, large data gaps across several stations throughout the study period necessitated the



development of a tunnel temperature estimation model, which while useful, had limitations that added a degree of error to results. However, the model was essential to provide future estimations of tunnel temperatures under the selected climate projection scenarios and would improve with regular revisions with up-to-date observations, especially upon future releases of UKCP data.

***Recommendation 14: TfL should continue to update a tunnel temperature estimation model like that developed in this study with platform temperature observations to improve prediction accuracy of tunnel temperatures under future climate change scenarios.***

### **7.3.1.3. Weather forecasts**

Weather data also comprises weather forecasts. While this study did not include forecasted weather data in its methodological approach, referencing and responding to weather forecasts are a core procedure in the LU Hot Weather Plan and Winter Weather Contingency Plan. Several global weather forecasting ensemble models recently predicted very extreme weather events over two weeks before they occurred; referring to the observed 40°C across England in mid-July 2022, which was first forecast on 30<sup>th</sup> June (Lee, 2022). Considering the future increased likelihood of extreme heat of this magnitude in future (Christidis *et al.*, 2020), and that this study showed temperature risk thresholds of assets below those in the Hot Weather Plan, it would be prudent to allow for more time to prepare the LU network to impendent extreme heat events, especially where earlier forecasting allows.

***Recommendation 15: TfL should consider extending the Hot Weather Plan from a 3-day response countdown to at least a 5-day response countdown when there is a forecast of a temperatures reaching the higher risk thresholds, such as a hot day threshold (at least 28°C).***

***Recommendation 16: TfL should validate the accuracy of their forecast services to ensure that they provide sufficient forecast time should the Hot Weather Plan response countdown be increased.***

#### **7.3.1.4. Fault data**

A particular challenge when undertaking this study was joining data from two different asset management systems, and then to key asset characteristics and attributes to establish fault exposure rates. Capacity to conduct this analysis would be improved if asset data is held across one system to streamline analytical processes, as LU maintenance staff acknowledged that data collection for these systems required duplication of work in data entry, increasing the risk of data errors (Tech Monitor, 2018). This is not an issue unique to LU data; other rail networks, including Network Rail, comprise several systems that result in data gaps and ambiguities affecting fault-related analysis (*e.g.*, Ferranti *et al.* 2016).

TfL have addressed the legacy challenge of multiple systems within the organisation, by tendering out a project to migrate their systems into one integrated Asset Management Information System (AMIS) for the LU network (TfL, 2018). Data migration is underway, with completion expected in 2023 (TfL, 2022d). As the creation of fault exposure rates depend on these data and are often underutilised for weather analysis (Jaroszweski *et al.*, 2015), it is imperative that the data migration retains the spatial, temporal, and other descriptive variables mapped to assets and WOs.

***Recommendation 17: TfL should ensure that all asset and work order data is maintained and updated regularly by asset managers.***

***Recommendation 18: TfL should increase the awareness of LU asset managers and relevant operational staff on the scale of potential to apply AMIS data to other work across the organisation, such as the outcomes of this study.***

One missing data variable in the WO data that limited this study was weather condition at the time of data entry. This study therefore incorporated all WO data from the sample dataset to conduct the fault exposure rate analysis as it was not possible to filter WOs impacted by temperature. On the other hand, weather, or in the case of this study, temperature, may not necessarily be the primary cause of asset failures (Ferranti *et al.*, 2016), so the resulting dataset may not have been sufficient to conduct the scale of analysis achieved in this study.

However, there are benefits to capturing weather conditions when faults occur, because it is possible to focus in on patterns and trends surrounding underlying conditions to derive failure causality. This is especially important for reactive WOs; the “faults that find you,” as they are the occurrences more likely attributed to weather events due to their unexpected nature. Indeed, TfL’s customer delay database reports on weather events linked to delays, but the reporting process is ambiguous and there is a bias in data entry where weather attribution is more obvious, such as track flooding from heavy rain (Greenham *et al.*, 2020). It is furthermore complicated by the fact that delay attribution is not always owed to a single factor, including extreme weather events (Rail Delivery Group, 2020). Therefore, capturing real-time data by operational staff at the time of an incident or a WO would improve attribution of delays and faults to weather events. Future weather-driven analyses would then have the capability to filter explicitly by the required data. Network Rail capture some of these attributes in their fault management system and was the fundamental identification process to detect heat-related faults by Ferranti *et al.*, (2016).

***Recommendation 19: TfL should consider ways to capture observed weather at the time of entry for work order data, at least for reactive work orders as a minimum to improve weather attribution of faults for future analysis.***

A remaining challenge regarding fault data on the LU network and weather-driven analysis is to appropriately join weather observations to corrective WOs. As corrective WOs are “faults that you find,” the time they were raised would not necessarily correlate with the weather conditions that led to the fault occurrence, as it may have occurred prior to its discovery. A solution to this challenge is utilising remote condition monitoring (RCM) technology. TfL have tested RCM across some sections of the LU network, including point assets (Railway Technology, 2014) and track circuits (Etchell, 2014). Additionally, TfL recently launched a State of Good Repair (SoGR) Framework to classify and monitor asset conditions with a consistent approach (TfL, 2022i) and justifies the need for pan-LU network RCM as it would help inform SoGR scoring. Furthermore, RCM may enable TfL to transition from preventative maintenance to predictive maintenance practices on the LU network, providing effectiveness and efficiency savings (Ciocoiu *et al.*, 2017). Therefore, to address the corrective maintenance weather-driven analysis challenges, it would benefit TfL to ensure that ambient weather data is incorporated with, or possible to incorporate with RCM data to capture the relationship.

***Recommendation 20: TfL should expand its RCM capabilities across the LU network to reduce the challenges associated with weather-driven analysis regarding corrective maintenance, ensuring that RCM data is accessible and can be joined to ambient weather data for future analysis. This could begin by prioritising areas that experience the highest fault exposure rates, such as parts of the Bakerloo and Central lines.***

### 7.3.1.5. Climate data

UKCP18 data via the Met Office is currently the most appropriate data that describes future possible climate change scenarios for the UK. However, this study demonstrated that the format they are provided via the User Interface are insufficient for the quantitative methodological approach undertaken for fault exposure rate analysis. This is a known issue across the infrastructure sector, as many organisations encountered challenges making use of UKCP18 data (CCC, 2022). For instance, Network Rail commissioned research support to establish weather threshold frequencies with outcomes of varying confidence ratings (Network Rail, 2021a).

Table 7.2 shows the estimated number of days in a year likely to exceed temperature thresholds for  $t_{max}$  that affect most of Network Rail’s assets in London. The climate thresholds from this study are not directly comparable to the thresholds in Table 7.2 as their parameters fall between the below thresholds, but estimated days between both datasets are similar.

Table 7.2. Estimated frequency of days exceeding key  $t_{max}$  asset failure thresholds for Network Rail in London, compared with a 1961-1990 baseline (Source: Network Rail, 2021a)

$t_{max}$ threshold (°C)	Baseline frequency (days)	Climate change scenario*	2050s frequency (days)	2080s frequency (days)
20	75.2	Primary	142.2	166.3
		Higher	148.2	-
21	57.4	Primary	123.9	149.7
		Higher	131.9	-
26	7.3	Primary	55.8	73.4
		Higher	56.0	-
30	0.6	Primary	16.0	30.8
		Higher	18.0	-

\* Using UKCP09 climate projections. Primary = UKCP09 medium emissions scenario 90<sup>th</sup> percentile; Higher = UKCP09 high emissions scenario 90<sup>th</sup> percentile

As Network Rail continue to use UKCP09 data to establish frequency data in

Table 7.2, it highlights the limitations in UKCP18 data to meet the needs of the railways across GB. The weather generator tool from UKCP09 was not provided with UKCP18 data, opting not to use a statistical approach for climate projections. (Met Office, 2018d). However, the suggested alternative UKCP18 datasets do not provide the sufficient data resolution for RCP 6.0, leading to the resulting methodological approach used for this study, with its own limitations. Therefore, to reduce these limitations, future UKCP releases should consider the added value of re-introducing statistically derived daily data for industry purposes.

***Recommendation 21: The Met Office should consider developing or re-introducing products that meet the needs of climate projection analysis by infrastructure operators, using daily frequency data.***

Finally, as extreme heat events are inherently infrequent, TfL's capacity to quantitatively estimate the impacts of a future climate scenarios would be improved with the use of analogues. Reviewing potential analogous regions in both rail infrastructure and future climate conditions would be useful. Previously assessed analogue countries suited to the wider Great British railway network included France, the Netherlands, Belgium, Germany and Denmark (Sanderson *et al.*, 2016). However, at the city scale, a metro analogue for the LU, given its unique characteristics would need to consider the city size, form and UHI intensity, as well as the metro network size, form, and age. The metro systems in the biggest cities within the analogous countries include: the Paris Metro (France); the Berlin U-Bahn (Germany); the Rotterdam Metro (Netherlands); the Brussels Metro (Belgium); the Cologne Stadt Bahn (Germany); the Hamburg U-Bahn (Germany); the Munich U-Bahn (Germany); the Frankfurt

U-Bahn (Germany), the Amsterdam Metro (Netherlands); and the Copenhagen Metro (Denmark).

London has several networks to leverage support, and from a climate change adaptation perspective would include the C40 Cities Climate Leadership Group, which the Mayor of London currently chairs. From a transport perspective, these would include the International Association of Public Transport (UITP) and the Urban Transport Group, which are international and national organisations respectively.

***Recommendation 22: TfL should leverage its existing international networks to establish potential weather and metro network analogues for future fault estimations of the LU network.***

### **7.3.2. Stakeholder engagement**

Engaging with a wide range of internal and external stakeholders is crucial to increase TfL's capacity in delivering a more climate-resilient LU network. Different stakeholders may provide additional or new perspectives and experiences beyond the scope of TfL's current understanding of its climate challenges. Therefore, an interdisciplinary approach to climate impact analyses can broaden view horizons by considering other factors such as future socio-economic change (Jaroszweski *et al.*, 2010). The previous subsection focused on data and demonstrated the opportunities stakeholders can provide regarding improved data and provision and quality for TfL. However, stakeholders can also increase an organisation's knowledge and influence delivery mechanisms and responses to climate change in more effective and impactful ways (Allen *et al.*, 2018). This is important as there is a historic siloed approach to infrastructure management between sectors (Otto *et al.*, 2016) as well as within TfL itself (Rode, 2019).

### **7.3.2.1. Internal stakeholder engagement**

Stakeholder engagement within TfL would increase its ability to validate and respond to data-driven climate risk analyses, such as the results from this study. As previously mentioned throughout this chapter, there are limitations in the interpretation of this study's results due to data quality, methodological approach, and future climate change uncertainty. While a data-driven approach into the impact of weather and climate change on the LU network provided a more objective insight into trends and relationships, the tacit knowledge across operational disciplines within the organisation is extremely important to validate its findings; and explain possible underlying reasons for the trends, or any anomalies and outliers. Transparency between those who conduct analyses and those who work with assets would therefore reduce the risk of corporate memory loss and strengthen TfL's broader understanding of its climate risks on the LU network in the longer-term. A novel approach designed by Martello *et al.* (2022) converted expert knowledge into relationship profiles for several asset groups for a metro network, and would be an appropriate step forward in validation. As TfL recently consolidated its Asset Strategy teams (TfL, 2022i), conducting a similar exercise across several assets should be more feasible going forwards.

***Recommendation 23: TfL should solicit expert judgement across the organisation to validate the data-driven approach to fault exposure rates of asset groups on the LU network.***

### **7.3.2.2. External stakeholder engagement**

Optimising external stakeholder engagement would also improve TfL's capacity to deliver a more climate-resilient LU network, especially where there are time or financial constraints. The umbrella of external stakeholders relevant to TfL ranges from local to global (see Figure 7.1)



and it is critical that as many of these stakeholders as possible are involved in all stages of TfL's processes and procedures that result in strategic decision-making. This is because of the effect some decisions have on other stakeholders and vice versa. Some recommendations from the TRaCCA report (RSSB, 2016a) include:

- Collaborating on technical standards for infrastructure design, and sharing wider learnings on intelligent design and ICT, and building a better “system-of-systems” understanding of infrastructure networks with other national infrastructure operators.
- Engaging with key providers of weather and climate data to ensure it can be appropriately applied in a railway context.
- Sharing knowledge with overseas counterparts.
- Capturing local knowledge through local stakeholders.
- Obtaining several stakeholders' input to identify and prioritise research.

Several of these engagement activities are already addressed by TfL, as they participate in pan-stakeholder groups such as the Infrastructure Operators Adaptation Forum, the London Transport Adaptation Steering Group (chaired by TfL), the London Resilience Partnership, and the Pan-London Surface Water Flooding Task and Finish Group – created following the heavy flooding that occurred on 12<sup>th</sup> and 25<sup>th</sup> July 2021 (Gilby, 2022). These networks connect TfL with knowledge exchange opportunities, particularly in the regional and national context. Collaboration activities should continue in future, but TfL could also benefit from conducting further outreach activities for consultation specific to the organisation, such as the results of this study.

*Recommendation 24: TfL should continue to engage with external stakeholders at local, regional, national, and global scales and endeavour to consult with them regarding the outcomes and implications of fault exposure rate analyses.*

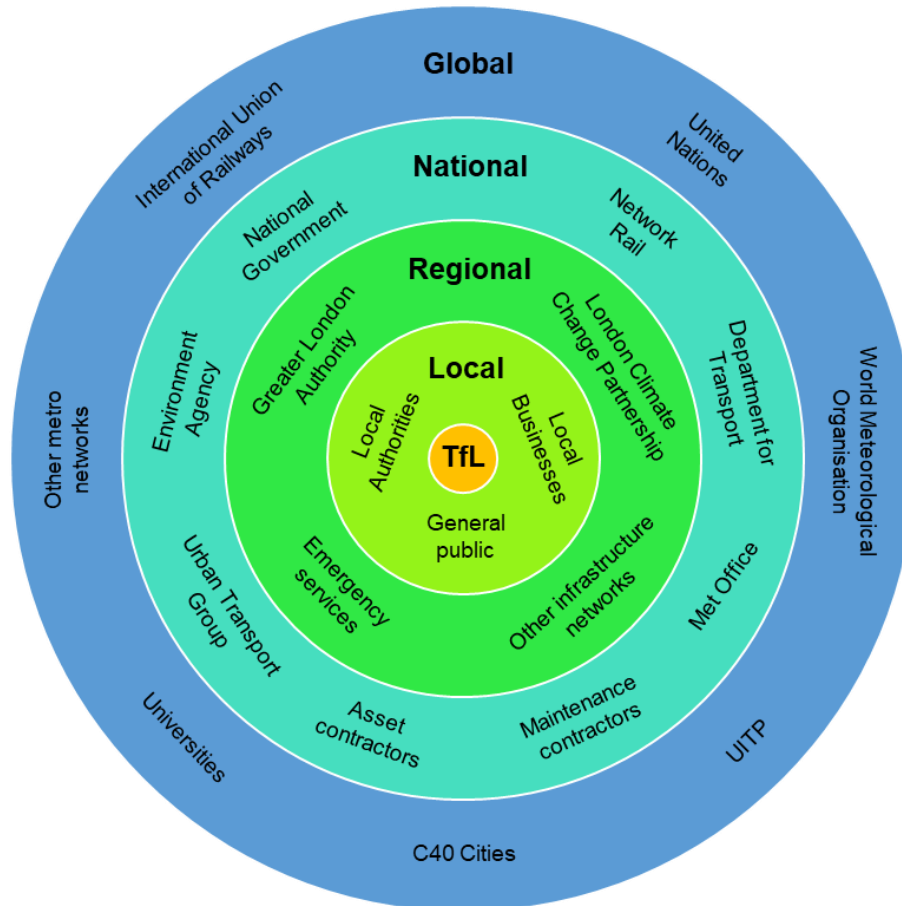


Figure 7.1. Some examples of external stakeholders relevant to TfL from a climate change adaptation perspective

### 7.3.3. The adaptation direction

Although it is outside of the scope of this study to recommend specific adaptation actions for the LU network, its findings can be reflected upon in terms of progressing from TfL’s adaptation report (TfL, 2021b) and provide guidance and direction in terms of future reporting.

Increasing climate resilience through adaptation requires looking at all possible options to address the challenges – in the case of this study, that challenge would be the threshold

exceedances of the fault exposure rates, and the consequential change in future asset failures under future climate scenarios. These could include organisational processes (*e.g.*, company policies), operations and procedures (*e.g.*, maintenance planning), ICT support, decision and risk models, and legislation (Stamos *et al.*, 2015). Reviewing a range of options is necessary as it provides a more comprehensive risk response that limits the likelihood of “maladaptation” – where actions may in fact increase the risk of climate-related outcomes, usually as an unintended consequence (IPCC, 2022). Figure 7.2 shows this risk conceptually. Each adaptation option has a potential level of effectiveness and a lifespan, but also external determinants that may not be possible to control. TfL’s capacity to deliver climate-resilient transport is dependent on the extent by which they limit the risk of maladaptation.

Echoing the recent change in asset management practices across TfL, the recently published adaptation plan takes a pan-TfL approach (TfL, 2023). It focuses on three main areas: (1) data and evidence, (2) processes and tools, and (3) collaboration and engagement. By proxy, a pan-TfL approach encourages internal and external stakeholders to work together. Through this approach, TfL can address some of the challenges identified from this study and therefore improve their capacities as there are linkages across all three categories. For example, future iterations of this study would benefit from more and improved data, which in turn could improve the efficacy and usefulness of decision-making tools as part of data utilisation. It may require stakeholders to share data or knowledge that otherwise has not been shared for adaptation purposes and will require their buy-in to the cause. Stakeholders who own or manage data with unrealised benefits for adaptation but may lack the knowledge or prior engagement on climate change challenges are a key opportunity for TfL.

**Recommendation 25:** TfL should consider all possible adaptation options for the LU network, before undertaking prioritisation, to help reduce fault exposure rates and identify the maladaptation risks to these options for decision-making purposes.

**Recommendation 26:** TfL should raise the profile of adaptation across the organisation, especially to existing and prospective stakeholders who are non-experts in the realm of climate change to increase buy-in and address actions in the pan-TfL climate change adaptation plan.

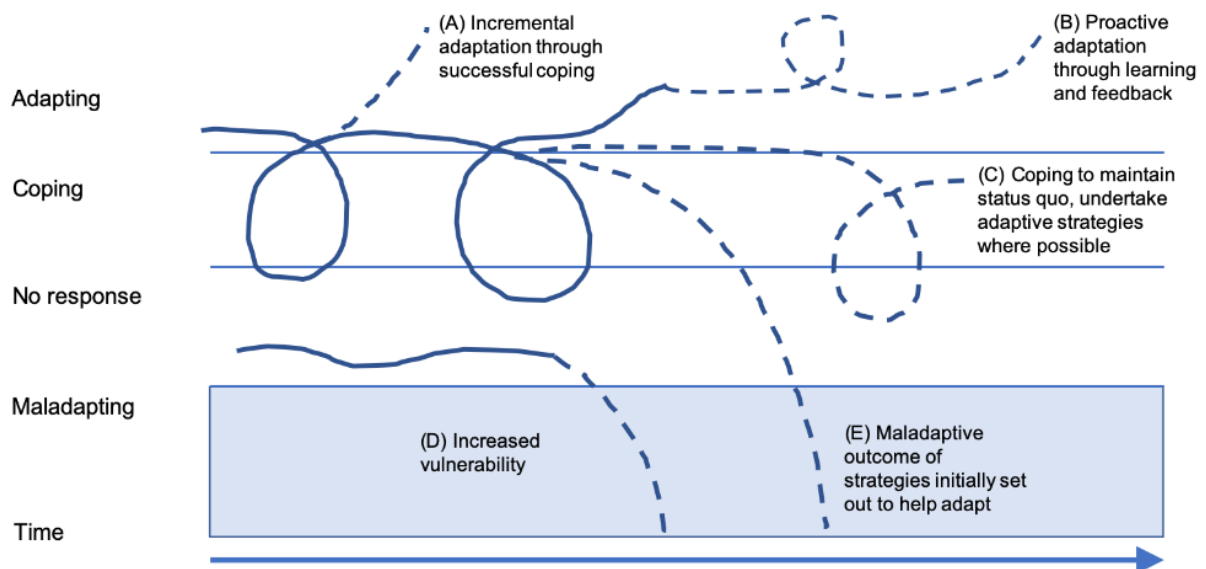


Figure 7.2. A conceptual diagram of potential adaptation outcomes over time (Source: Schipper, 2020)

Nevertheless, transport networks like the LU are constantly changing. The scale of future climate change (*i.e.*, the most likely RCP scenario) is uncertain, infrastructure and society’s resilience on ICT grows, with its own risks and interdependencies, organisational structures can change, and there will always be the chance of externalities affecting operations out of most anyone’s control (*e.g.*, the coronavirus pandemic). Adaptation plans and actions must therefore be responsive to change. This is reflected in outcome B of Figure 7.2, where learnings and feedback improve adaptative capacity and necessitates flexible planning. The pathway

approach to adaptation is appropriate in this context (Haasnoot *et al.*, 2013), as the concept enables dynamic and flexible decision-making according to pre-defined intervals such as time, extent of hazard or design parameters/thresholds. As an adaptation pathway should map several outcomes and options, it also upholds the need for stakeholder engagement to optimise the reduction of risk. Adaptation pathways also strengthen the integration of adaptation into business-as-usual practice (Quinn *et al.*, 2018), so responding to climate change becomes part of core business planning and not an additional plan or strategy.

TfL aspire to develop an adaptation pathways approach to climate change for their assets. However, a lack of data is a key barrier in achieving this to date (TfL, 2021b). Considering the iterative process implies that drafting plans with current knowledge is sufficient to begin, plans can be revisited and refined as data is improved. This is the core principle of ISO14090, the international standard on adapting to climate change (ISO, 2019), so it would be acceptable to begin designing adaptation pathways for the LU network in the near future. In the context of this study, the defined intervals for decision-making points in an adaptation pathway for point-related assets could be based on frequency of days meeting certain climate thresholds or asset temperature thresholds *per* year. As such, there would be less dependency on a temporal timeline, as the response level would be dependent on the climate change trajectory, of which frequent review cycles would facilitate the monitoring and evaluation process.

***Recommendation 27: TfL should prioritise piloting a draft adaptation pathway with knowledge to date, establishing a timeline to review and adjust them as new data and knowledge is obtained.***

## **7.4. Critique of methodology and further development**

Throughout this chapter, the discussion explicitly focuses on the results from this study and puts them into the context of TfL's current processes and procedures. Here, this chapter begins to broaden the implications of this study on infrastructure operators and stakeholders supporting the delivery of climate-resilient transport. The data-driven approach enabled the indiscriminate scrutiny of relationships between temperature and WOs across the LU network on a spatial and temporal scale. By doing this, it also enabled lesser-known relationships to be drawn out with the potential for further investigation by TfL with consideration of future climate change. Testing a tunnel temperature estimation model originally designed for Japanese railway tunnels (Kimura *et al.*, 2018) and fault exposure rate methodological principles formerly designed for a Network Rail analysis (Fisher, 2020) demonstrated their applicability to the LU network. Doing so increases the capabilities of data-driven analyses in a more standardised way that can inform decisions in adapting to climate change. Nevertheless, there are several opportunities to improve the methodology used for this study.

### **7.4.1. Joining temperature and work order data**

Due to the spatiotemporal resolution of temperature variables necessary to conduct this study, there were several options to consider when selecting the appropriate temperature data to join to the LU network WO data. Justifying a single reference point of temperature data is discussed in Section 7.3.1.1, and the reason for the method used in this study was primarily to limit the unknowns and uncontrolled variables into the analysis. Therefore, the only spatial adjustment variable was the single UHI intensity at 100m resolution, but as Chapter One described, London's UHI intensity can vary slightly throughout the day and is a likely reason for a

potential degree of error in the results. However, at the expense of resolution, the temperature data, least for fault exposure rate analysis could be substituted with 1km daily observation data by the HadUK-Grid dataset grid from the Met Office. The resolution could be increased by downscaling to 100m via resampling using mapping techniques such a bilinear interpolation; comparing results with the current study to determine which dataset is more appropriate. Similarly, this could also be evaluated for the tunnel temperature estimation model; to determine whether surface temperatures nearest to each station platform improve the estimation of tunnel temperatures.

#### **7.4.2. Prediction capabilities**

Another consideration regarding the methodological approach of this study would whether the prediction methods are fit for purpose, particularly for future iterations of this type of study. This is a particular challenge given that data in this study contained inaccuracies that could not be avoided. Centering on the WO data, there were likely human errors within the dataset, as well as the time WOs were raised likely not reflective of the actual point of failure (see Section 7.3.1.4). Asset condition is also a factor in failure rates (Dobney *et al.*, 2009), which may be intrinsically linked to maintenance activity, neither of which were within the scope of this study, but a realised potential direction of future work as a result of it.

Several of the processes undertaken for this study were manually conducted, which for an organisation like TfL, with limited human capacity to conduct manual processes could be a challenge. However, as data continues to grow and improve across TfL, and as research in analytical tools develop, there are opportunities to increase automation while also improving accuracy. Big data analysis via machine learning or artificial intelligence would be an appropriate direction for this type of data-driven approach. Once the AMIS integration is

complete for the LU network's data, it would be a timely opportunity to explore solutions to further improve accuracy. An empirical dynamic model approach is a potential option – which addresses the complexity of the relationship between asset failure and weather/climate, as well as the multiple variables upon them (Chang *et al.*, 2017). Training a model with historic temperature observations and WO data, then overlaying climate projection data could be a possible way of improving future WO estimations, especially given that fault exposure rates outside lower bound ranges were difficult to estimate. It could also have similar potential with a tunnel temperature estimation model.

***Recommendation 28: Infrastructure practitioners and researchers should consider the possibility of investigating the viability of empirical dynamic modelling to similar data used in this study to drive the future direction of this research.***

#### **7.4.3. Considerations in interpreting results**

As there are limitations to this study, it is important to take these into account when interpreting results. This is primarily an outcome of the approach in handling several datasets with different parameters and levels of quality – the interpretation of results is only as reliable as the data used to produce them. For example, threshold analyses among the fault exposure rates are based on 1°C temperature bins. As there are some variances in the accuracy of estimated or adjusted temperatures across the LU network, the defined thresholds may not be precise. This may have resulted in small degree of error in temperature variables assigned to WOs for analysis.

Specific considerations when interpreting results include: the accuracy of temperature variables from the UHI calculation and tunnel temperature estimation model; the inclusion of WO data with incomplete information (*e.g.*, missing reasons for closing WO, re-corrected locations,



WOs raised on assets that have since been removed from service); the overstating of corrective WOs affecting the fault exposure rate at specific intervals; the assumptions made in estimating projected temperature exposure frequencies; and the potential decreased accuracy in estimating future WOs at temperatures beyond the range of those observed in this study. Should TfL improve their data management practices and levels of stakeholder engagement (see Section 7.3), future iterations of this type of study would improve and the interpretation of results more reliable.

*Recommendation 29: TfL and key stakeholders should be made aware of the limitations of this study, the impact these may have on the interpretation of results, and the potential to improve the accuracy in future research based on the improvements of data and increased stakeholder engagement.*

## **7.5. Looking ahead towards more climate-resilient transport networks**

Our understanding of weather and climate risks to transport infrastructure has improved in the last 10-15 years. As a sector that was often given little explicit attention in literature (Koetse and Rietveld, 2009), there has been a significant shift in research to improve knowledge and quantify climate risk, enabling both conceptual and practical advance within the field. This section considers how the methodology designed for this study can be applied in new contexts, and how to improve it further for future utilisation by researchers, industry practitioners, and their stakeholders.

### 7.5.1. Mapping climate risk

One key finding of this study was that it is very important for metro networks to separate climate risk analysis by their different environments (*i.e.*, tunnels and surface), underpinning the need for spatial analysis. While dependent on spatial data resolution, a potential next step in improving the understanding of broader climate risk across an infrastructure network would be to layer multiple spatial data.

This study showed that spatial analysis is achievable, and while focused on the nearest station as the spatial identifier, future analysis could consider the specific location of assets within a finer resolution grid. Combining disparate hazard data (*e.g.*, temperature variables, precipitation variables, wind speed, climate projections), exposure data (*e.g.*, tree/vegetation cover, flood zones, tunnel temperature estimation model coefficients) and vulnerability data (*e.g.*, fault exposure rates, SoGR status, delay frequency, other connected infrastructure) would provide risk scores for targeted intervention and prioritisation. This method of multi-variable climate risk assessment is usually designed for plan-making, including for London (GLA, 2022) and is considered the gold standard for cities, states, public authorities and organisations alike in disclosing environmental progress transparently (CDP, 2023). Railway practitioners are interested in taking a multi-hazard approach to climate risk, though have a limited understanding of how to approach it (Green and Chmutina, 2019). Therefore, mapping climate risk is a tool that brings together several variables into a single risk outcome, while applying the methods of this study beyond its parameters and may improve practitioners' understanding of their climate risk to prioritise adaptation actions, model future climate risk, and build pathways.

*Recommendation 30: Meteorology organisations should review the appetite and benefits of improved spatial resolution of data for researchers and infrastructure practitioners.*

*Recommendation 31: TfL and other infrastructure practitioners, along with researchers should assess the viability of the tailored mapping of climate risk across their networks, using disparate data from within its organisation (which could include fault exposure rates and estimated tunnel temperature) and key stakeholders to gain a full, comprehensive overview of the infrastructure risk by compiling climate hazards, exposure, and vulnerabilities across the network.*

#### **7.5.2. Linking fault exposure rates with delay data**

This study focused on fault data that did not necessarily impact the customer, and therefore did not translate into results using delay data. This is because as *per* the review of literature in Section 2.5, customer-driven metrics risk excluding a proportion of faults that may not affect operational services, which may result in an oversight of important asset risks due to data bias. Therefore, fault-led metrics may identify faults that arise before resulting in delays that impact customers. As this study focuses on correlations and relationships between temperature and faults, it does not infer causality. However, this could be addressed with the inclusion of delay data, which TfL also collects. Joining delay data with fault data may help identify patterns regarding what type of heat-related faults lead to delays in service, helping identify potential fault causality. Conducting this analysis would be particularly beneficial using reactive WOs, which are the faults considered to cause disruption in service, although they are a smaller proportion of overall WO data collected. Nevertheless, given the increased extreme heat events that have occurred since the study period, it would be a relevant and timely development to progress this analysis further.

***Recommendation 32: TfL should consider combining LU delay data with fault exposure rate analysis results to identify any trends in faults leading to delays, in a step towards identifying heat-related causality of faults across the LU network.***

### **7.5.3. Progressing the analysis of extreme weather events**

The methodological approach for this study provided an overview of trends, however it was challenging to explore the impact of single extreme weather events. This is compounded by few extreme temperatures recorded throughout the study period, especially considering their increased frequency, intensity, and duration after the study period. Studies that look at the impacts of specific extreme weather events on transport infrastructure (*e.g.*, Ferranti *et al.*, 2018; Jaroszweski *et al.*, 2015) are useful in addressing the gap in this study's approach as they have the capability to explore site-specific failures patterns. There is perhaps an opportunity to develop the fault exposure rate for extreme weather event analysis by using hourly data with the same methodological approach. As the temperature and WO data collected for this study were hourly, it would be possible to conduct some test analyses to gain a better understanding of these infrequent events with the same approach. Furthermore, it could evaluate the efficacy of the current operational response plans. For the LU network, these are the Hot Weather Plan and the Winter Weather Contingency Plan. It could also evaluate the effectiveness of current maintenance practices, based on the SoGR status of assets going forwards.

***Recommendation 33: TfL and other infrastructure practitioners, along with researchers should assess the viability of downscaling the fault exposure rate analysis to hourly analysis days before, during and days after extreme weather events to improve understanding of weather-driven failures.***

#### **7.5.4. The international perspective**

London is a global city with substantial international interest in its activities. As home to the oldest metro network, other networks around the world have been fortunate to take learnings from the way the LU network to date has been constructed, managed, and operated. Now, during a climate emergency, the LU network faces both ongoing and new challenges in keeping London moving. Global stakeholder engagement is valuable in this case, as TfL can learn from others who once learnt from them. Benchmarking through metrics is a useful method of quantitatively evaluating climate change preparedness (Greenham *et al.*, 2020). Therefore, as the methodological approach used in this study demonstrated its applicability to other networks, there is scope for other rail and metro networks to evaluate their resilience to weather and climate change as a form of international benchmarking. Networks can then compare results, share knowledge tailored to their needs based on asset risk.

*Recommendation 34: Other metro operators should consider a quantitative, data-driven approach to evaluate climate risk for international benchmarking purposes, which provides the opportunity to tailor knowledge exchange for mutual gain in improving climate resilience.*

#### **7.6. Next steps for TfL in delivering more climate-resilient transport**

TfL, as owners and operators of the LU network is committed to ensuring that it continues to run safely. Considering future climate change, the heat-related risk to the LU network is quantifiably increasing, as the heat hazard increases. Climate risk can only be reduced, or negated, if TfL's response sufficiently limits, or reduces, the vulnerability and exposure of the LU network. Climate risk is highly variable across the LU network, as temperature thresholds

of its infrastructure – in this case, point-related assets – are affected in some parts of the LU network by temperatures below those currently not deemed a risk to operations.

The main challenge, as TfL reports, is that data is a major barrier to developing adaptation pathways for assets. To overcome this, TfL need to leverage as many stakeholders as possible to overcome this barrier and enabling the development of pathways that can be updated as improved data is available. Cross-departmental data system integration and a review of data management practices would underpin this. TfL’s AMIS project is still ongoing, and the pan-TfL adaptation plan (TfL, 2023) was published too recently to review as part of this study, but both are welcome and relevant progress in integrating practices and facilitating communication between and across the LU network and beyond.

The methodology presented in this study provides a data-led foundation to quantify and start estimating the impacts of weather events such as heat, as well as future climate change, across a metro network. It expanded initial methods across research to demonstrate flexibility and applicability to another network. The outcomes of the study should support TfL, as well as any transport network practitioner to scrutinise the relationship between weather and climate on infrastructure to begin to identify its vulnerable parts, identify key failure thresholds and begin to take appropriate action to address climate risk.

## **7.7. Chapter summary**

This chapter provided recommendations throughout aimed at TfL and other metro and railway operators and stakeholders to further develop climate-resilient transport systems, particularly to temperature hazards. These recommendations fall into three core areas: pan-organisational data management, increased internal and external stakeholder engagement, and prioritising an

iterative climate change adaptation pathways process that accommodates the growing organisational capacities. For TfL, key goals in improving the climate resilience of the LU network to heat should consider:

1. Continue to consolidate databases and data platforms; including standardising data entry practices and data variables to improve organisational transparency, increase data and analytical capacities, and streamline pan-TfL operations.
2. Improve and extend current internal and external stakeholder relationships at all stages of climate change adaptation planning. This includes at stages of scoping, collecting, and analysing data; developing and selecting adaptation options, and monitoring and evaluation activities; to improve knowledge, technical, and financial capacities.
3. Start the adaptation pathways process as soon as feasibly possible, as even where there are data or knowledge gaps, these can be added later, assuming capacity growth is achieved from points 1 and 2. This is since adaptation pathways are dynamic and the process is iterative, so failure to act risks leading to maladaptation.

# Chapter Eight | Conclusion

## 8.1. Conclusion overview

Following the discussion of results in the previous chapter, this section draws the study to a close by describing how the aim and objectives were achieved. This begins with a summary of how each objective was met, and concludes with final remarks, reflecting on this study and future implications in the context of TfL and the operation of the LU network.

## 8.2. Achievement of aims and objectives

The aim of this study was to use a systematic, data-driven approach to quantify the impact of present and future temperature-related hazards on railway assets across the LU network. This aim was achieved in stages throughout the study, with each chapter building on its previous one.

### 8.2.1. Justifying a data-driven approach

*Objective 1: Critically review the literature on delay and fault metrics that quantify the impact of weather and climate on railway infrastructure.*

The literature reviewed in this study showed several approaches to quantifying the impact of weather and climate change on railway infrastructure. A strong case was made, by reviewing the range of metrics utilised across numerous studies, to consider quantification by means of failure frequency. Although customer-driven metrics are valued by infrastructure operators, delays to customers are secondary impacts of faults on a network, therefore it is important to consider assets to improve infrastructure resilience. Frequency-based metrics were considered



most appropriate for this study, as the literature review demonstrates they correlate well with weather variables and thereby enable and justify a data-driven approach.

### **8.2.2. Demonstrating the spatial variability of temperature across metro networks**

*Objective 2: Distinguish the changes and differences in the thermal environment across the LU network.*

This study successfully demonstrated spatial and temporal variance in temperature across the LU network by evaluating the thermal environment by network type (*i.e.*, surface, sub-surface, deep tube tunnels). Moreover, the analysis determined that the climate of the study period (2006-2018) showed signals of change. Finally, the analysis demonstrated the use of surface temperature observations to estimate tunnel temperatures. All the approaches undertaken delivered quantitative evidence of variances by LU station, which is at least 270 locations – not accounting for interchange tunnel stations also, where there were additional variances among LU lines at the same location.

### **8.2.3. Quantification of the effect of temperature on infrastructure**

*Objective 3: Investigate and interrogate the relationships between LU asset faults recorded by TfL and the thermal environment.*

This study also successfully showed spatial variance in faults (corrective and reactive work orders) by LU line. By identifying one and two standard deviation thresholds, the method clearly highlighted statistically significant trends in fault exposure rates, indicating the temperatures that affect asset performance across the LU network. Fault exposure rates varied by network type and LU line for each temperature variable ( $t_{mean}$ ,  $t_{max}$ ,  $t_{min}$ ,  $\Delta t$ ). Results also

revealed failure harvesting on the surface – where early season high temperatures experienced higher fault exposure rates, which then decreased at higher summer temperatures following assets repair or replacement, thus increasing network resilience to temperature. However, the integrity of work order data affected some fault exposure rates, in some cases artificially inflating rates. TfL are in the process of improving data systems and processes. Going forward, reiterations of this type of analysis should see an improvement.

#### **8.2.4. Quantification of the effect of future climate change on infrastructure**

*Objective 4: Utilise the relationships to estimate potential change in asset failures trends on the LU network in accordance with future climate change scenarios.*

Using UKCP18 data, the tunnel temperature estimation model, and fault exposure rates, it was possible to convey change in work orders owed to increased temperature, including spatial variance by network type. Overall, there is up to a 10% estimated increase in point-related work orders across the LU network for the high emissions projection scenario (RCP 8.5), by the 2080s; assuming similar future operation of the LU network. The increase could be higher, however, as the spatial variance in estimated temperatures across some parts of London may observe some higher temperature increase due to the greater effect of the UHI. Furthermore, the estimated increases in work order rates are highest on the surface, followed by the deep tube tunnels, and then shows no discernible change across the sub-surface parts of the LU network.

#### **8.2.5. Future research development and direction**

*Objective 5: Critically evaluate the method used to produce the results, suggesting areas for future development of the approach and research direction.*

This study has demonstrated the validity of the methodology used here. The discussion of the results highlighted several opportunities to further utilise this systematic, data-driven approach. These include improved spatial methodological approaches and increasing the incorporation of mapping techniques as a tool for decision makers, as well as improving the prediction capabilities with more sophisticated statistical techniques including machine learning and artificial intelligence. Ultimately, these techniques could improve data quality, while at the same time reducing the time burden on infrastructure operators and decision-makers in conducting their own analyses and investigations.

#### **8.2.6. Practical application of the research and implications**

*Objective 6: Suggest ways that the findings can support decision-making processes for the adaptation of railway and metro networks to climate change, with recommendations for the key stakeholders involved.*

Throughout the discussion, the findings of this study identified 34 recommendations, primarily for TfL, that would improve their capacity to adapt to heat and climate change across the LU network. These are oriented around improving data, or access to data, as well as maximising stakeholder engagement opportunities. Adapting to climate change is a cross-cutting challenge, so increasing impact through utilising various data sources and consultation with a wide range of stakeholders is imperative, as it can lead to the identification of a comprehensive range of adaptation options. Furthermore, adapting to climate change requires an iterative process. Co-creating and developing adaptation pathways as new and updated data and information is continuously fed into the process is an appropriate method. This study demonstrated that this process is possible to begin now.

### **8.3. Concluding remarks**

The sections of this chapter showed how this study achieved its aim and objectives by increasing knowledge on the relationship between temperature as a hazard on assets across the LU network now and in future. It showed, for the first time, the spatial differentiation of these relationships, which is of crucial importance to TfL and will feed into their decision-making processes moving forward.

Adapting to climate change will require significant financial investment. Because of the scale of future uncertainty – in any context – there is often a reluctance by decision-makers to act (Koetse and Rietveld, 2012), but inaction is more costly in the longer-term (Bachner, 2017). This is a pertinent issue. The UK, like many countries has committed to reach Net Zero GHG emissions in the coming decades, public transport use is expected to increase, with organisations such as TfL supporting modal shift away from private car use. There are consequently co-benefits of investing in public transport networks like the LU for both climate mitigation and adaptation purposes, but finance is a key challenge. TfL’s funding model relies greatly on passenger revenue (TfL, 2022m), which was severely affected by reduced passenger counts since 2020 owed to the coronavirus pandemic. Compounded by post-Brexit challenges, the war in Ukraine and the current cost of living crisis, climate adaptation action is threatened with losing focus and priority, ultimately at a greater cost in future.

Raising the profile of climate change adaptation requires a clear understanding of climate risk. For a complex system like the LU network, this requires data-driven approaches, as well as the improved utilisation and application of tacit knowledge where appropriate. Using data to quantify climate risk may also serve as a call-to-action for investors to respond, enabling a more targeted approach to optimise and maximise future climate resilience.

## References

- Allen, S.K., Ballesteros-Canovas, J., Randhawa, S.S., et al. (2018) Translating the concept of climate risk into an assessment framework to inform adaptation planning: Insights from a pilot study of flood risk in Himachal Pradesh, Northern India. *Environmental Science & Policy*, 87: 1–10.
- Ampofo, F., Maidment, G. and Missenden, J. (2004) Underground railway environment in the UK Part 2: Investigation of heat load. *Applied Thermal Engineering*, 24 (5–6): 633–645.
- Andersson, A.K. and Chapman, L. (2011) The impact of climate change on winter road maintenance and traffic accidents in West Midlands, UK. *Accident Analysis & Prevention*, 43 (1): 284–289.
- Arnell, N.W., Kay, A.L., Freeman, A., et al. (2021) Changing climate risk in the UK: A multi-sectoral analysis using policy-relevant indicators. *Climate Risk Management*, 31: 100265.
- Athanasopoulou, A., Sousa, M.L., Dimova, S., et al. (2020) *Thermal design of structures and the changing climate*. Available at: <https://data.europa.eu/doi/10.2760/128894> (Accessed: 5 February 2023).
- Bachner, G. (2017) Assessing the economy-wide effects of climate change adaptation options of land transport systems in Austria. *Regional Environmental Change*, 17 (3): 929–940.
- Baker, L., Shaffrey, L. and Hawkins, E. (2021) Has the risk of a 1976 north-west European summer drought and heatwave event increased since the 1970s because of climate change? *Quarterly Journal of the Royal Meteorological Society*, 147 (741): 4143–4162.
- Bank of England (2023) *Inflation calculator*. Available at: <https://www.bankofengland.co.uk/monetary-policy/inflation/inflation-calculator> (Accessed: 16 March 2023).
- Bidarmaghz, A., Choudhary, R., Soga, K., et al. (2020) Large-scale urban underground hydro-thermal modelling – A case study of the Royal Borough of Kensington and Chelsea, London. *Science of The Total Environment*, 700: 134955.
- Börjesson, M. and Eliasson, J. (2011) On the use of “average delay” as a measure of train reliability. *Transportation Research Part A: Policy and Practice*, 45 (3): 171–184.
- Botelle, M., Payne, K. and Redhead, B. (2010) Squeezing the heat out of London’s Tube. *Proceedings of the Institution of Civil Engineers - Civil Engineering*, 163 (3): 114–122.
- Braganza, K., Karoly, D.J. and Arblaster, J.M. (2004) Diurnal temperature range as an index of global climate change during the twentieth century. *Geophysical Research Letters*, 31 (13): L13217.
- Brazil, W., White, A., Nogal, M., et al. (2017) Weather and rail delays: Analysis of metropolitan rail in Dublin. *Journal of Transport Geography*, 59: 69–76.

British Geological Survey (2020) *BGS Geology 625k (DiGMapGB-625) data 1: 625 000 ESRI® [Bedrock]*. Available at: <https://www.bgs.ac.uk/download/bgs-geology-625k-digmapgb-625-data-1-625-000-esri-bedrock/> (Accessed: 22 December 2022).

Bruine de Bruin, W., Rabinovich, L., Weber, K., et al. (2021) Public understanding of climate change terminology. *Climatic Change*, 167 (3–4): 37.

CDP (2023) *CDP: Who we are*. Available at: <https://www.cdp.net/en/info/about-us> (Accessed: 20 February 2023).

Chandler, T. (1965) *The Climate of London*. London, UK: Hutchinson & Co Ltd.

Chang, C.-W., Ushio, M. and Hsieh, C. (2017) Empirical dynamic modeling for beginners. *Ecological Research*, 32 (6): 785–796.

Chapman, L., Thornes, J.E., Huang, Y., et al. (2008) Modelling of rail surface temperatures: a preliminary study. *Theoretical and Applied Climatology*, 92 (1–2): 121–131.

Chapman, L., Thornes, J.E. and White, S.P. (2006) Thermal imaging of railways to identify track sections prone to buckling. *Proceedings of the Institution of Mechanical Engineers, Part F: Journal of Rail and Rapid Transit*, 220 (3): 317–327.

Chapman, S.C., Watkins, N.W. and Stainforth, D.A. (2019) Warming Trends in Summer Heatwaves. *Geophysical Research Letters*, 46 (3): 1634–1640.

Christidis, N., McCarthy, M. and Stott, P.A. (2020) The increasing likelihood of temperatures above 30 to 40 °C in the United Kingdom. *Nature Communications*, 11 (1): 3093.

Ciocioiu, L., Siemieniuch, C.E. and Hubbard, E.-M. (2017) From preventative to predictive maintenance: The organisational challenge. *Proceedings of the Institution of Mechanical Engineers, Part F: Journal of Rail and Rapid Transit*, 231 (10): 1174–1185.

Climate Action Tracker (2022) *The CAT Thermometer, November 2022*. Available at: <https://climateactiontracker.org/global/cat-thermometer/> (Accessed: 11 January 2023).

Climate Change Committee (2021a) *Independent Assessment of UK Climate Risk: Advice to Government for the UK's third Climate Change Risk Assessment (CCRA3)*. Available at: <https://www.theccc.org.uk/wp-content/uploads/2021/07/Independent-Assessment-of-UK-Climate-Risk-Advice-to-Govt-for-CCRA3-CCC.pdf>.

Climate Change Committee (2021b) *UK Climate Risk Sector Briefing: Transport*. Available at: <https://www.ukclimaterisk.org/wp-content/uploads/2021/06/CCRA3-Briefing-Transport.pdf> (Accessed: 12 January 2023).

Climate Change Committee (2022) *Understanding climate risks to UK infrastructure: Evaluation of the third round of the Adaptation Reporting Power*. Available at: <https://www.theccc.org.uk/publication/understanding-climate-risks-to-uk-infrastructure-evaluation-of-the-third-round-of-the-adaptation-reporting-power/> (Accessed: 19 October 2022).

Climate Change Committee (2023) *Progress in adapting to climate change: 2023 Report to Parliament*. Available at: <https://www.theccc.org.uk/wp-content/uploads/2023/03/WEB-Progress-in-adapting-to-climate-change-2023-Report-to-Parliament.pdf> (Accessed: 2 June 2023).

Dale, M., Shelton, K. and Dora, J. (2018) *Identifying a climate change planning scenario*.

Davis, R.E., Hondula, D.M. and Sharif, H. (2020) Examining the diurnal temperature range enigma: why is human health related to the daily change in temperature? *International Journal of Biometeorology*, 64 (3): 397–407.

Dawson, D., Shaw, J. and Roland Gehrels, W. (2016) Sea-level rise impacts on transport infrastructure: The notorious case of the coastal railway line at Dawlish, England. *Journal of Transport Geography*, 51: 97–109.

De Ridder, K., Lauwaet, D. and Maiheu, B. (2015) UrbClim – A fast urban boundary layer climate model. *Urban Climate*, 12: 21–48.

Department for Transport (2021) *Great British Railways: The Williams-Shapps Plan for Rail*.

D’Lima, M. and Medda, F. (2015) A new measure of resilience: An application to the London Underground. *Transportation Research Part A: Policy and Practice*, 81: 35–46.

Dobney, K., Baker, C.J., Chapman, L., et al. (2010) The future cost to the United Kingdom’s railway network of heat-related delays and buckles caused by the predicted increase in high summer temperatures owing to climate change. *Proceedings of the Institution of Mechanical Engineers, Part F: Journal of Rail and Rapid Transit*, 224 (1): 25–34.

Dobney, K., Baker, C.J., Quinn, A.D., et al. (2009) Quantifying the effects of high summer temperatures due to climate change on buckling and rail related delays in south-east United Kingdom. *Meteorological Applications*, 16 (2): 245–251.

Dunn, S., Wilkinson, S., Alderson, D., et al. (2018) Fragility Curves for Assessing the Resilience of Electricity Networks Constructed from an Extensive Fault Database. *Natural Hazards Review*, 19 (1): 04017019.

Ellis, I. (2019) *Ellis’ British Railway Engineering Encyclopaedia*. 4th ed.

Ellison, R., Woods, M., Allen, D., et al. (2004) *Geology of London*. Available at: <https://pubs.bgs.ac.uk/publications.html?pubID=B06069> (Accessed: 22 December 2022).

Etchell, S. (2014) *London Underground Improves Reliability for 200 Million Annual Passengers with Remote Condition Monitoring*. Available at: <https://www.ni.com/en-gb/innovations/case-studies/19/london-underground-improves-reliability-for-200-million-annual-passengers-with-remote-condition-monitoring.html> (Accessed: 16 February 2023).

European Environment Agency and Copernicus Climate Change Service (2020) *Urban Heat Island (UHI) intensity modelling*. Available at: <https://sdi.eea.europa.eu/catalogue/biodiversity9527831/api/records/45b703bb-d4f3-4eea-8b73-13fde2041f01> (Accessed: 21 April 2022).

- Falconer, J. (2008) *Brunel*. Ian Allen Publishing Ltd.
- Fankhauser, S., Smith, J.B. and Tol, R.S.J. (1999) Weathering climate change: some simple rules to guide adaptation decisions. *Ecological Economics*, 30 (1): 67–78.
- Ferranti, E., Chapman, L., Lee, S., et al. (2018) The hottest July day on the railway network: insights and thoughts for the future. *Meteorological Applications*, 25 (2): 195–208.
- Ferranti, E., Chapman, L., Lowe, C., et al. (2016) Heat-Related Failures on Southeast England’s Railway Network: Insights and Implications for Heat Risk Management. *Weather, Climate, and Society*, 8 (2): 177–191.
- Fisher, R. (2020) *Quantifying the vulnerability of GB rail to temperature and precipitation in order to improve resilience*. PhD thesis, University of Birmingham.
- Flemish Institute for Technological Research (n.d.) *Urban Climate Service Centre: Where are the hotspots in your city?* Available at: [http://www.urban-climate.be/services/eu\\_cities/](http://www.urban-climate.be/services/eu_cities/) (Accessed: 8 April 2021).
- Fu, Q. and Easton, J.M. (2016) “How does existing data improve decision making? A case study of wind-related incidents on rail network.” *In International Conference on Railway Engineering (ICRE 2016)*. Brussels, Belgium, 2016. Institution of Engineering and Technology.
- Gilbey, M. (2012) *London Underground Cooling the Tube Programme: Heat Recovery Report*.
- Gilbey, M., Duffy, S. and Thompson, J. (2011) “The Potential for Heat Recovery from London Underground Stations and Tunnels.” *In CIBSE Technical Symposium*. DeMontfort University, Leicester UK, 2011.
- Gilby, S. (2022) *Surface Water Flood Risk Management in London*. Available at: <https://www.londoncouncils.gov.uk/members-area/member-briefings/environment/surface-water-flood-risk-management-london> (Accessed: 14 March 2023).
- Golany, G. and Ojima, T. (1996) *Geo-space urban design*. New York: John Wiley.
- Greater London Authority (2011) *Managing Risks and Increasing Resilience: The Mayor’s Climate Change Adaptation Strategy*. Available at: [https://www.london.gov.uk/sites/default/files/gla\\_migrate\\_files\\_destination/Adaptation-oct11.pdf](https://www.london.gov.uk/sites/default/files/gla_migrate_files_destination/Adaptation-oct11.pdf) (Accessed: 8 April 2021).
- Greater London Authority (2022) *Climate Risk Map*. Available at: <https://www.london.gov.uk/programmes-and-strategies/environment-and-climate-change/climate-change/climate-adaptation/climate-risk-map> (Accessed: 20 February 2023).
- Green, A. and Chmutina, K. (2019) Building climate resilience of UK’s rail network through a multihazard approach. *Proceedings of the Institution of Civil Engineers - Engineering Sustainability*, 172 (8): 450–458.
- Green, O. (2019) *London’s Underground: The Story of the Tube*. White Lion.



Greenham, S., Ferranti, E., Quinn, A., et al. (2020) The impact of high temperatures and extreme heat to delays on the London Underground rail network: An empirical study. *Meteorological Applications*, 27 (3): e1910.

Greenham, S., Ferranti, E., Workman, R., et al. (2022) *Adaptation for Transport Resilience to Climate Change for LICs in Africa and South Asia: State of Knowledge Report*. Available at: <https://transport-links.com/download/state-of-knowledge-report-adaptation-for-transport-resilience-to-climate-change-aftr-cc-for-lics-in-africa-and-south-asia/> (Accessed: 14 February 2022).

Grimmond, S. (2013) *Observing London - Weather data needed for London to thrive 2013*. Available at: <http://climatelondon.org/wp-content/uploads/2017/11/Observing-London-Final.pdf> (Accessed: 24 May 2021).

Haasnoot, M., Kwakkel, J.H., Walker, W.E., et al. (2013) Dynamic adaptive policy pathways: A method for crafting robust decisions for a deeply uncertain world. *Global Environmental Change*, 23 (2): 485–498.

Halliday, S. (2013) *Underground to Everywhere*. 2nd ed. The History Press, Gloucestershire, Great Britain.

Hanlon, H.M., Bernie, D., Carigi, G., et al. (2021) Future changes to high impact weather in the UK. *Climatic Change*, 166 (3–4): 50.

Hernandez-Barrera, S., Rodriguez-Puebla, C. and Challinor, A.J. (2017) Effects of diurnal temperature range and drought on wheat yield in Spain. *Theoretical and Applied Climatology*, 129 (1–2): 503–519.

Herrick, F.C. (1926) *It is cooler below*. Available at: <https://www.ltmuseum.co.uk/collections/collections-online/posters/item/1983-4-2030> (Accessed: 22 December 2022).

Herrick, F.C. (1927) *It is warmer below*. Available at: <https://www.ltmuseum.co.uk/collections/collections-online/posters/item/1983-4-2314> (Accessed: 21 February 2023).

HM Government (2022) *Climate Change Risk Assessment 2022*. Available at: [https://assets.publishing.service.gov.uk/government/uploads/system/uploads/attachment\\_data/file/1047003/climate-change-risk-assessment-2022.pdf](https://assets.publishing.service.gov.uk/government/uploads/system/uploads/attachment_data/file/1047003/climate-change-risk-assessment-2022.pdf) (Accessed: 3 January 2023).

Holderness, T., Barr, S., Dawson, R., et al. (2013) An evaluation of thermal Earth observation for characterizing urban heatwave event dynamics using the urban heat island intensity metric. *International Journal of Remote Sensing*, 34 (3): 864–884.

Hosken, A. (2014) *BBC Today: Near disaster on the London Underground*. Available at: <https://www.bbc.co.uk/radio4/today/reports/archive/features/tube.shtml> (Accessed: 17 January 2022).

Hunt, G. (1994) *An analysis of track buckling risk, British Railways Internal Report RRTM013*.

Intergovernmental Panel on Climate Change (2013) *Climate Change 2013: The Physical Science Basis. Contribution of Working Group I to the Fifth Assessment Report of the Intergovernmental Panel on Climate Change*.

Intergovernmental Panel on Climate Change (2021) *Climate Change 2021: The Physical Science Basis. Contribution of Working Group I to the Sixth Assessment Report of the Intergovernmental Panel on Climate Change*. Available at: [https://www.ipcc.ch/report/ar6/wg1/downloads/report/IPCC\\_AR6\\_WGI\\_Full\\_Report.pdf](https://www.ipcc.ch/report/ar6/wg1/downloads/report/IPCC_AR6_WGI_Full_Report.pdf) (Accessed: 18 February 2022).

Intergovernmental Panel on Climate Change (2022) *Climate Change 2022: Impacts, Adaptation and Vulnerability. Contribution of Working Group II to the Sixth Assessment Report of the Intergovernmental Panel on Climate Change*. Available at: [https://www.ipcc.ch/report/ar6/wg2/downloads/report/IPCC\\_AR6\\_WGII\\_FullReport.pdf](https://www.ipcc.ch/report/ar6/wg2/downloads/report/IPCC_AR6_WGII_FullReport.pdf) (Accessed: 18 February 2022).

International Standards Organization (2019) *ISO 14090:2019 Adaptation to climate change - Principles, requirements and guidelines*. Available at: <https://www.iso.org/standard/68507.html> (Accessed: 14 July 2021).

International Transport Forum (2021) *Data-driven Transport Infrastructure Maintenance*. Available at: <https://www.oecd-ilibrary.org/docserver/alcc71cc-en.pdf?expires=1675632949&id=id&accname=guest&checksum=B31F9C393EF67EB6A09BB053191E61BB> (Accessed: 5 February 2023).

Jaroszweski, D., Chapman, L. and Petts, J. (2010) Assessing the potential impact of climate change on transportation: the need for an interdisciplinary approach. *Journal of Transport Geography*, 18 (2): 331–335.

Jaroszweski, D., Fu, Q. and Easton, J. (2019) “A data model heat-related rail buckling: implications for operations, maintenance and long-term adaptation.” *In World Congress on Railway Research*. Tokyo, Japan, 2019.

Jaroszweski, D., Hooper, E., Baker, C., et al. (2015) The impacts of the 28 June 2012 storms on UK road and rail transport: Impacts of the 28 June 2012 storms on UK transport. *Meteorological Applications*, 22 (3): 470–476.

Jelle, B.P. (2012) Accelerated climate ageing of building materials, components and structures in the laboratory. *Journal of Materials Science*, 47 (18): 6475–6496.

Jenkins, K., Gilbey, M., Hall, J., et al. (2014) Implications of climate change for thermal discomfort on underground railways. *Transportation Research Part D: Transport and Environment*, 30: 1–9.

Jones, I. (1999) Trains and electrical and mechanical equipment for the Jubilee Line extension. *Proceedings of the Institution of Civil Engineers - Civil Engineering*, 132 (6): 65–71.

Kendon, M., McCarthy, M., Jevrejeva, S., et al. (2022) State of the UK Climate 2021. *International Journal of Climatology*, 42 (S1): 1–80.

- Kennedy, R.P., Cornell, C.A., Campbell, R.D., et al. (1980) Probabilistic seismic safety study of an existing nuclear power plant. *Nuclear Engineering and Design*, 59 (2): 315–338.
- Kennedy-Asser, A.T., Andrews, O., Mitchell, D.M., et al. (2021) Evaluating heat extremes in the UK Climate Projections (UKCP18). *Environmental Research Letters*, 16 (1): 014039.
- Kimura, K., Shibata, K., Sato, M., et al. (2018) Simple estimation formula of air temperature in tunnels: Estimation method for cooling load caused by train wind in an underground station: part 2. *Journal of Environmental Engineering (Transactions of AIJ)*, 83 (749): 607–613.
- Koetse, M.J. and Rietveld, P. (2009) The impact of climate change and weather on transport: An overview of empirical findings. *Transportation Research Part D: Transport and Environment*, 14 (3): 205–221.
- Koetse, M.J. and Rietveld, P. (2012) Adaptation to Climate Change in the Transport Sector. *Transport Reviews*, 32 (3): 267–286.
- Kolokotroni, M. and Giridharan, R. (2008) Urban heat island intensity in London: An investigation of the impact of physical characteristics on changes in outdoor air temperature during summer. *Solar Energy*, 82 (11): 986–998.
- Kumar, P., Zavala-Reyes, J.C., Kalaiarasan, G., et al. (2023) Characteristics of fine and ultrafine aerosols in the London underground. *Science of The Total Environment*, 858: 159315.
- Lauwaet, D., Hooyberghs, H., Maiheu, B., et al. (2015) Detailed Urban Heat Island Projections for Cities Worldwide: Dynamical Downscaling CMIP5 Global Climate Models. *Climate*, 3 (2): 391–415.
- Lee, S. (2022) *40°C in the UK?* Available at: <https://www.rmets.org/metmatters/40-degc-uk> (Accessed: 12 February 2023).
- Lee, W., Bell, M.L., Gasparri, A., et al. (2018) Mortality burden of diurnal temperature range and its temporal changes: A multi-country study. *Environment International*, 110: 123–130.
- Liu, W., Liang, S., Huang, Q., et al. (2022a) Estimation of thermal hazards in surrounding rock of subway tunnel under dual periodic temperature boundaries: a case study. *Environmental Science and Pollution Research*, 29 (44): 67063–67075.
- Liu, W., Liang, S. and Shi, C. (2022b) Risk modelling and simulation of thermal safety in underground railway tunnel surrounding. *Accident Analysis & Prevention*, 168: 106620.
- London Assembly (2020) *The Climate Emergency: Extreme Weather and Emissions*. Available at: [https://www.london.gov.uk/sites/default/files/london\\_assembly\\_environment\\_committee\\_-\\_climate\\_emergency\\_report\\_final.pdf](https://www.london.gov.uk/sites/default/files/london_assembly_environment_committee_-_climate_emergency_report_final.pdf) (Accessed: 21 January 2023).
- Lowe, J.A., Bernie, D., Bett, P., et al. (2019) *UKCP18 Science Overview Report*. Available at: <https://www.metoffice.gov.uk/pub/data/weather/uk/ukcp18/science-reports/UKCP18-Overview-report.pdf> (Accessed: 9 February 2022).

Manoli, G., Fatichi, S., Schläpfer, M., et al. (2019) Magnitude of urban heat islands largely explained by climate and population. *Nature*, 573 (7772): 55–60.

Martello, M.V., Whittle, A.J. and Lyons-Galante, H.R. (2022) Depth-damage curves for rail rapid transit infrastructure. *Journal of Flood Risk Management*, 16 (1): e12856.

Martinović, K., Reale, C. and Gavin, K. (2018) Fragility curves for rainfall-induced shallow landslides on transport networks. *Canadian Geotechnical Journal*, 55 (6): 852–861.

McKenna, C. (2005) *Paddington Circle-District station [Photograph]*. Available at: [https://commons.wikimedia.org/wiki/File:Paddington\\_Circle-District\\_station.jpg](https://commons.wikimedia.org/wiki/File:Paddington_Circle-District_station.jpg) (Accessed: 27 February 2023).

Met Office (2012) *Hot Spell August 1990*. Available at: <https://www.metoffice.gov.uk/binaries/content/assets/metofficegovuk/pdf/weather/learn-about/uk-past-events/interesting/1990/hot-spell-august-1990---met-office.pdf> (Accessed: 11 October 2022).

Met Office (2015) *Heatwave 1 July 2015*. Available at: <https://www.metoffice.gov.uk/binaries/content/assets/metofficegovuk/pdf/weather/learn-about/uk-past-events/interesting/2015/heatwave-1-july-2015---met-office.pdf> (Accessed: 6 March 2023).

Met Office (2018a) *Snow and low temperatures February to March 2018*. Available at: <https://www.metoffice.gov.uk/binaries/content/assets/metofficegovuk/pdf/weather/learn-about/uk-past-events/interesting/2018/snow-and-low-temperatures-february-to-march-2018---met-office.pdf> (Accessed: 23 August 2022).

Met Office (2018b) *State of the UK Climate 2017: Supplementary report on Climate Extremes*. Available at: [https://www.metoffice.gov.uk/binaries/content/assets/metofficegovuk/pdf/weather/learn-about/uk-past-events/state-of-uk-climate/soc\\_supplement-002.pdf](https://www.metoffice.gov.uk/binaries/content/assets/metofficegovuk/pdf/weather/learn-about/uk-past-events/state-of-uk-climate/soc_supplement-002.pdf) (Accessed: 14 January 2022).

Met Office (2018c) *UK Climate Projections User Interface*. Available at: <https://ukclimateprojections-ui.metoffice.gov.uk/ui/home> (Accessed: 3 February 2022).

Met Office (2018d) *UKCP18 Guidance: UKCP18 for UKCP09 users*. Available at: <https://www.metoffice.gov.uk/binaries/content/assets/metofficegovuk/pdf/research/ukcp/ukcp18-guidance-ukcp18-for-ukcp09-users.pdf> (Accessed: 17 February 2023).

Met Office (2019a) *Dataset Record: MIDAS Open: UK hourly weather observation data, v201908*. Available at: <http://dx.doi.org/10.5285/6c441aea187b44819b9e929e575b0d7e> (Accessed: 3 December 2019).

Met Office (2019b) *Exceptional warmth February 2019*. Available at: [https://www.metoffice.gov.uk/binaries/content/assets/metofficegovuk/pdf/weather/learn-about/uk-past-events/interesting/2019/2019\\_002\\_february\\_warmspell.pdf](https://www.metoffice.gov.uk/binaries/content/assets/metofficegovuk/pdf/weather/learn-about/uk-past-events/interesting/2019/2019_002_february_warmspell.pdf) (Accessed: 13 February 2023).

Met Office (2019c) *Record breaking heat-wave July 2019*. Available at: [https://www.metoffice.gov.uk/binaries/content/assets/metofficegovuk/pdf/weather/learn-about/uk-past-events/interesting/2019/2019\\_007\\_july\\_heatwave.pdf](https://www.metoffice.gov.uk/binaries/content/assets/metofficegovuk/pdf/weather/learn-about/uk-past-events/interesting/2019/2019_007_july_heatwave.pdf) (Accessed: 6 December 2022).

Met Office (2019d) *UKCP18 Factsheet: Temperature*. Available at: <https://www.metoffice.gov.uk/binaries/content/assets/metofficegovuk/pdf/research/ukcp/ukcp18-fact-sheet-temperature.pdf> (Accessed: 25 February 2023).

Met Office (2020a) *August heat-wave*. Available at: [https://www.metoffice.gov.uk/binaries/content/assets/metofficegovuk/pdf/weather/learn-about/uk-past-events/interesting/2020/2020\\_06\\_august\\_heatwave.pdf](https://www.metoffice.gov.uk/binaries/content/assets/metofficegovuk/pdf/weather/learn-about/uk-past-events/interesting/2020/2020_06_august_heatwave.pdf) (Accessed: 13 February 2023).

Met Office (2020b) *Exceptionally hot day, 31 July 2020*. Available at: [https://www.metoffice.gov.uk/binaries/content/assets/metofficegovuk/pdf/weather/learn-about/uk-past-events/interesting/2020/2020\\_05\\_july\\_temperature.pdf](https://www.metoffice.gov.uk/binaries/content/assets/metofficegovuk/pdf/weather/learn-about/uk-past-events/interesting/2020/2020_05_july_temperature.pdf) (Accessed: 13 February 2023).

Met Office (2021a) *Extremes of temperature, March and April 2021*. Available at: [https://www.metoffice.gov.uk/binaries/content/assets/metofficegovuk/pdf/weather/learn-about/uk-past-events/interesting/2021/2021\\_03\\_high\\_temperatures.pdf](https://www.metoffice.gov.uk/binaries/content/assets/metofficegovuk/pdf/weather/learn-about/uk-past-events/interesting/2021/2021_03_high_temperatures.pdf) (Accessed: 13 February 2023).

Met Office (2021b) *Synoptic and climate stations*. Available at: <https://www.metoffice.gov.uk/research/climate/maps-and-data/uk-synoptic-and-climate-stations> (Accessed: 25 May 2021).

Met Office (2022a) *127 years since UK's joint-lowest temperature... will we see it again?* Available at: <https://blog.metoffice.gov.uk/2022/02/11/127-years-since-uks-joint-lowest-temperature-will-we-see-it-again/> (Accessed: 22 February 2023).

Met Office (2022b) *Exceptionally mild New Year, 2021/2022*. Available at: [https://www.metoffice.gov.uk/binaries/content/assets/metofficegovuk/pdf/weather/learn-about/uk-past-events/interesting/2021/2021\\_09\\_high\\_temperatures.pdf](https://www.metoffice.gov.uk/binaries/content/assets/metofficegovuk/pdf/weather/learn-about/uk-past-events/interesting/2021/2021_09_high_temperatures.pdf) (Accessed: 13 February 2023).

Met Office (2022c) *Past weather events*. Available at: <https://www.metoffice.gov.uk/weather/learn-about/past-uk-weather-events> (Accessed: 30 December 2022).

Met Office (2022d) *Unprecedented extreme heatwave, July 2022*. Available at: [https://www.metoffice.gov.uk/binaries/content/assets/metofficegovuk/pdf/weather/learn-about/uk-past-events/interesting/2022/2022\\_03\\_july\\_heatwave.pdf](https://www.metoffice.gov.uk/binaries/content/assets/metofficegovuk/pdf/weather/learn-about/uk-past-events/interesting/2022/2022_03_july_heatwave.pdf) (Accessed: 13 September 2022).

Met Office (2022e) *What is the definition for a UK heatwave?* Available at: <https://www.metoffice.gov.uk/weather/learn-about/weather/types-of-weather/temperature/heatwave> (Accessed: 15 April 2022).

Met Office (2023a) *Prolonged spell of low temperatures, December 2022*. Available at: [https://www.metoffice.gov.uk/binaries/content/assets/metofficegovuk/pdf/weather/learn-about/uk-past-events/interesting/2022/2022\\_04\\_december\\_low\\_temperatures\\_v1.pdf](https://www.metoffice.gov.uk/binaries/content/assets/metofficegovuk/pdf/weather/learn-about/uk-past-events/interesting/2022/2022_04_december_low_temperatures_v1.pdf) (Accessed: 22 February 2023).

Met Office (2023b) *UK Climate Projections News*. Available at: <https://www.metoffice.gov.uk/research/approach/collaboration/ukcp/about/project-news> (Accessed: 25 February 2023).

Mortada, A., Choudhary, R. and Soga, K. (2015) Thermal Modeling and Parametric Analysis of Underground Rail Systems. *Energy Procedia*, 78: 2262–2267.

Mozer, V., Osvald, A., Lovecek, T., et al. (2013) “Fire safety in tunnels forming part of critical infrastructure.” *In 2013 47th International Carnahan Conference on Security Technology (ICCST)*. Medellin, Colombia, October 2013. IEEE. pp. 1–5.

National Academies of Sciences, Engineering, and Medicine (U.S.) (ed.) (2016) *Attribution of extreme weather events in the context of climate change*. Washington, DC: The National Academies Press.

National Oceanic & Atmospheric Administration (2022) *Trends in Atmospheric Carbon Dioxide*. Available at: <https://www.esrl.noaa.gov/gmd/ccgg/trends/global.html> (Accessed: 28 December 2022).

Network Rail (2014) *Route Weather Resilience and Climate Change Adaptation Plans: Western*. Available at: <https://www.networkrail.co.uk/wp-content/uploads/2019/05/Western-Route-WRCCA-Plan.pdf> (Accessed: 5 August 2022).

Network Rail (2020) *Route weather resilience plans 2019-2024*. Available at: <https://www.networkrail.co.uk/sustainability/climate-change/climate-change-adaptation/> (Accessed: 7 February 2022).

Network Rail (2021a) *Climate Change Projections Guidance Note: Weather Resilience and Climate Change Adaptation*. Available at: <https://safety.networkrail.co.uk/wp-content/uploads/2019/09/Climate-change-projections-Guidance-Note.pdf> (Accessed: 31 January 2022).

Network Rail (2021b) *Network Rail Third Adaptation Report*. Available at: <https://www.networkrail.co.uk/wp-content/uploads/2022/01/Network-Rail-Third-Adaptation-Report-December-2021.pdf> (Accessed: 5 January 2023).

Network Rail (2023a) *Looking after the railway: Track*. Available at: <https://www.networkrail.co.uk/running-the-railway/looking-after-the-railway/track/> (Accessed: 17 January 2023).

Network Rail (2023b) *Payments for disruption on the railway*. Available at: <https://www.networkrail.co.uk/industry-and-commercial/information-for-operators/payments-for-disruption-on-the-railway/> (Accessed: 5 January 2023).

- Nguyen, M.N., Wang, X. and Wang, C.-H. (2012) A reliability assessment of railway track buckling during an extreme heatwave. *Proceedings of the Institution of Mechanical Engineers, Part F: Journal of Rail and Rapid Transit*, 226 (5): 513–517.
- Nieto, N., Chamorro, A., Echaveguren, T., et al. (2022) Fragility curves for road embankments exposed to adjacent debris flow. *Progress in Physical Geography: Earth and Environment*, 47 (1): 030913332211114.
- Oke, T.R. (1973) City size and the urban heat island. *Atmospheric Environment*, 7: 769–779.
- Oslakovic, I.S., ter Maat, H., Hartmann, A., et al. (2012) Climate Change and Infrastructure Performance: Should We Worry About? *Procedia - Social and Behavioral Sciences*, 48: 1775–1784.
- Oslakovic, I.S., ter Maat, H., Hartmann, A., et al. (2013) “Risk Assessment Of Climate Change Impacts On Railway Infrastructure.” *In Engineering Project Organization Conference*. Devil’s Thumb Ranch, Colorado, 2013.
- Otto, A., Hall, J.W., Hickford, A.J., et al. (2016) A Quantified System-of-Systems Modeling Framework for Robust National Infrastructure Planning. *IEEE Systems Journal*, 10 (2): 385–396.
- Palin, E.J., Stipanovic Oslakovic, I., Gavin, K., et al. (2021) Implications of climate change for railway infrastructure. *WIREs Climate Change*, 12 (5): e728.
- Palin, E.J., Thornton, H.E., Mathison, C.T., et al. (2013) Future projections of temperature-related climate change impacts on the railway network of Great Britain. *Climatic Change*, 120 (1–2): 71–93.
- Pan, S., Fan, L., Liu, J., et al. (2013) A Review of the Piston Effect in Subway Stations. *Advances in Mechanical Engineering*, 5: 950205.
- Pant, R., Hall, J.W. and Blainey, S.P. (2016) *Vulnerability assessment framework for interdependent critical infrastructures: case-study for Great Britain’s rail network.*, p. 21.
- Paul, J.D. (2016) High-resolution geological maps of central London, UK: Comparisons with the London Underground. *Geoscience Frontiers*, 7 (2): 273–286.
- Pescaroli, G. and Alexander, D. (2018) Understanding Compound, Interconnected, Interacting, and Cascading Risks: A Holistic Framework: A Holistic Framework for Understanding Complex Risks. *Risk Analysis*, 38 (11): 2245–2257.
- Preston, J., Wall, G., Batley, R., et al. (2009) Impact of Delays on Passenger Train Services: Evidence from Great Britain. *Transportation Research Record: Journal of the Transportation Research Board*, 2117 (1): 14–23.
- Quinn, A., Ferranti, E., Hodgkinson, S., et al. (2018) Adaptation Becoming Business as Usual: A Framework for Climate-Change-Ready Transport Infrastructure. *Infrastructures*, 3 (2): 10.

Race to Resilience (2021) *Race to Resilience: Metrics Framework*. Available at: [https://racetozero.unfccc.int/wp-content/uploads/2021/11/202111\\_R2R\\_Metrics\\_framework.pdf](https://racetozero.unfccc.int/wp-content/uploads/2021/11/202111_R2R_Metrics_framework.pdf) (Accessed: 28 January 2023).

Race to Resilience (2022) *Adaptation and Resilience Breakthroughs: The global transformation towards resilient development ahead of COP27*. Available at: <https://climatechampions.unfccc.int/wp-content/uploads/2022/09/Adaptation-and-Resilience-Breakthroughs.pdf> (Accessed: 28 January 2023).

Rail Delivery Group (2020) *Delay Attribution Review. A report to ORR*. Available at: <https://www.orr.gov.uk/sites/default/files/2020-09/rdg-delay-attribution-review-report-2020-09-28.pdf> (Accessed: 26 July 2022).

Rail Safety and Standards Board (2016a) *Tomorrow's Railway and Climate Change Adaptation: Final Report*. Available at: <https://www.rssb.co.uk/en/research-catalogue/CatalogueItem/T1009> (Accessed: 25 August 2017).

Rail Safety and Standards Board (2016b) *Tomorrow's Railway and Climate Change Adaptation: Work Package 1 Summary Report*. Available at: <https://www.rssb.co.uk/en/research-catalogue/CatalogueItem/T1009> (Accessed: 14 August 2021).

RailSystem (n.d.) *Turnouts*. Available at: <https://railsystem.net/turnouts/> (Accessed: 17 January 2023).

Railway Technology (2014) *Strukton Rail installs POSS monitoring system on London Underground*. Available at: <https://www.railway-technology.com/news/newsstrukton-rail-installs-poss-monitoring-system-on-london-underground-4317180/> (Accessed: 16 February 2023).

Ricke, K.L. and Caldeira, K. (2014) Maximum warming occurs about one decade after a carbon dioxide emission. *Environmental Research Letters*, 9 (12): 124002.

Rode, P. (2019) Urban planning and transport policy integration: The role of governance hierarchies and networks in London and Berlin. *Journal of Urban Affairs*, 41 (1): 39–63.

Ryan, M. and Hunt, G. (2005) *Stress free temperature and stability of continuous welded rail: A report produced for Rail Safety & Standards Board*.

Sanderson, M.G., Hanlon, H.M., Palin, E.J., et al. (2016) Analogues for the railway network of Great Britain: Analogues for the railway network of Great Britain. *Meteorological Applications*, 23 (4): 731–741.

Schipper, E.L.F. (2020) Maladaptation: When Adaptation to Climate Change Goes Very Wrong. *One Earth*, 3 (4): 409–414.

Simpson, N.P., Mach, K.J., Constable, A., et al. (2021) A framework for complex climate change risk assessment. *One Earth*, 4 (4): 489–501.



- Singhal, A., Kamga, C. and Yazici, A. (2014) Impact of weather on urban transit ridership. *Transportation Research Part A: Policy and Practice*, 69: 379–391.
- Skarova, A., Harkness, J., Keillor, M., et al. (2022) Review of factors affecting stress-free temperature in the continuous welded rail track. *Energy Reports*, 8: 769–775.
- Stamos, I., Mitsakis, E. and Grau, J.M.S. (2015) Roadmaps for Adaptation Measures of Transportation to Climate Change. *Transportation Research Record: Journal of the Transportation Research Board*, 2532 (1): 1–12.
- Stott, P.A., Stone, D.A. and Allen, M.R. (2004) Human contribution to the European heatwave of 2003. *Nature*, 432 (7017): 610–614.
- Sun, T., Luo, Z. and Chay, T. (2021) An analytical model to predict the temperature in subway-tunnels by coupling thermal mass and ventilation. *Journal of Building Engineering*, 44: 102564.
- Sun, X., Ren, G., You, Q., et al. (2019) Global diurnal temperature range (DTR) changes since 1901. *Climate Dynamics*, 52: 3343–3356.
- Taha, H. (1997) Urban climates and heat islands: albedo, evapotranspiration, and anthropogenic heat. *Energy and Buildings*, 25 (2): 99–103.
- Tang, A.M., Hughes, P.N., Dijkstra, T.A., et al. (2018) Atmosphere–vegetation–soil interactions in a climate change context; impact of changing conditions on engineered transport infrastructure slopes in Europe. *Quarterly Journal of Engineering Geology and Hydrogeology*, 51 (2): 156–168.
- Tech Monitor (2018) *TfL Offers £186 Million to Simplify Asset Management Software*. Available at: <https://techmonitor.ai/technology/software/tfl-contract-amis> (Accessed: 15 February 2023).
- The Climate Change Act 2008, c.27* (n.d.). Available at: <https://www.legislation.gov.uk/ukpga/2008/27/contents> (Accessed: 12 September 2021).
- The Evening Standard (2017) *London weather: thermal camera captures heat of Tube on hottest June day since 1976*. Available at: <https://www.standard.co.uk/news/transport/thermal-camera-captures-heat-of-tube-on-hottest-june-day-since-1976-a3570956.html> (Accessed: 22 March 2022).
- The Expert Team on Climate Change Detection and Indices (2009) *Climate Change Indices: Definitions of the 27 core indices*. Available at: [http://etccdi.pacificclimate.org/list\\_27\\_indices.shtml](http://etccdi.pacificclimate.org/list_27_indices.shtml) (Accessed: 6 April 2023).
- The Independent (2019) *London weather: Central Line found to be hotter than body temperature*. Available at: <https://www.independent.co.uk/travel/news-and-advice/london-underground-tube-temperature-central-line-heat-a9021236.html> (Accessed: 22 March 2022).
- Tinytag (2019) *Data sheet: Tinytag Plus 2 Dual Channel Temperature/Relative Humidity TGP-4500*. Available at: <http://gemini2.assets.d3r.com/pdfs/original/3751-tgp-4500.pdf> (Accessed: 21 May 2021).

Transport for London (2012) *Location of Mid Tunnel Vent Shafts & Intervention Points*. Available at: [https://www.whatdotheyknow.com/request/location\\_of\\_mid\\_tunnel\\_vent\\_shaf](https://www.whatdotheyknow.com/request/location_of_mid_tunnel_vent_shaf) (Accessed: 12 February 2023).

Transport for London (2016a) *Category 1 Standard SI067 A3: Tunnel and public area cooling and ventilation*.

Transport for London (2016b) *LU Asset Management Strategy Summary*. Available at: <https://content.tfl.gov.uk/lu-asset-management-strategy.pdf> (Accessed: 15 February 2023).

Transport for London (2017a) *FOI request detail - Axonometric drawings of every single station on the London Transport network*. Available at: <https://tfl.gov.uk/corporate/transparency/freedom-of-information/foi-request-detail?referenceId=FOI-1216-1718> (Accessed: 15 January 2022).

Transport for London (2017b) *Tube map with tunnels*. Available at: <https://content.tfl.gov.uk/tube-map-with-tunnels.pdf> (Accessed: 23 March 2022).

Transport for London (2018) *Contract notice: Software package and information systems 2018/S 238-544050*. Available at: <https://ted.europa.eu/udl?uri=TED:NOTICE:544050-2018:TEXT:EN:HTML&tabId=1> (Accessed: 15 February 2023).

Transport for London (2020a) *Excess Journey Time Guidance Notes*. Available at: <https://content.tfl.gov.uk/excess-journey-time-guidance-notes.pdf> (Accessed: 26 January 2023).

Transport for London (2020b) *Lost Customer Hours Guidance Notes*. Available at: <https://content.tfl.gov.uk/lost-customer-hours-guidance-notes.pdf> (Accessed: 26 July 2022).

Transport for London (2021a) *London Underground - Transport for London*. Available at: <https://tfl.gov.uk/corporate/about-tfl/culture-and-heritage/londons-transport-a-history/london-underground> (Accessed: 6 June 2021).

Transport for London (2021b) *TfL Adaptation Reporting Power Submission 2021*. Available at: <https://tfl.gov.uk/corporate/about-tfl/sustainability> (Accessed: 8 April 2022).

Transport for London (2021c) *Working Timetables of the Tube network*. Available at: <https://tfl.gov.uk/corporate/publications-and-reports/working-timetables> (Accessed: 26 July 2022).

Transport for London (2022a) *2023 Business Plan, 2022/23 - 2025/26*. Available at: <https://content.tfl.gov.uk/2023-business-plan-acc.pdf> (Accessed: 20 January 2023).

Transport for London (2022b) *Asset Performance Managers Handbook: Seasonal Maintenance*.

Transport for London (2022c) *Ellipse Maintenance Types (Standard Jobs)*.

Transport for London (2022d) *Investment programme report 26 June 2022 - 17 September 2022*. Available at: <https://content.tfl.gov.uk/tfl-investment-programme-report-13-december-2022-acc.pdf> (Accessed: 15 February 2023).

Transport for London (2022e) *London Underground Winter Weather Contingency Plan*.

Transport for London (2022f) *Network Hot Weather Plan: Summer 2021*.

Transport for London (2022g) *Public Transport Journeys by Type of Transport*. Available at: <https://data.london.gov.uk/dataset/public-transport-journeys-type-transport> (Accessed: 20 November 2022).

Transport for London (2022h) *Reference R0111: Signal maintenance regime*.

Transport for London (2022i) *Standard S1158: Track - Inspection and Maintenance*.

Transport for London (2022j) *Status definitions*. Available at: <https://tfl.gov.uk/status-updates/status-definitions> (Accessed: 26 July 2022).

Transport for London (2022k) *TfL advises customers to only travel if essential on Monday 18 and Tuesday 19 July, due to very high temperatures*. Available at: <https://tfl.gov.uk/info-for/media/press-releases/2022/july/tfl-advises-customers-to-only-travel-if-essential-on-18-and-19-july-due-to-very-high-temperatures-being-forecast> (Accessed: 23 September 2022).

Transport for London (2022l) *TfL Asset Renewals: February 2022*. Available at: <https://board.tfl.gov.uk/documents/s17438/pic-20220302-item09b-asset-renewals-app1.pdf> (Accessed: 16 February 2023).

Transport for London (2022m) *TfL Mayor's Budget 2023/24 (draft)*. Available at: <https://content.tfl.gov.uk/tflbudget2324acc2.pdf> (Accessed: 21 January 2023).

Transport for London (2022n) *Transport for London quarterly performance report Q2 2022/23*. Available at: <https://content.tfl.gov.uk/tfl-quarterly-performance-report-q2-2022-23.pdf> (Accessed: 21 December 2022).

Transport for London (2023) *Climate Change Adaptation Plan 2023*. Available at: <https://content.tfl.gov.uk/tfl-climate-change-adaptation-plan.pdf> (Accessed: 15 March 2023).

Tsapakis, I., Turner, J., Cheng, T., et al. (2012) Effects of Tube Strikes on Journey Times in Transport Network of London. *Transportation Research Record: Journal of the Transportation Research Board*, 2274 (1): 84–92.

Union Internationale des Transports Publics (International Association of Public Transport) (2022) *World Metro Figures 2021: Statistics Brief*. Available at: <https://cms UITP.org/wp/wp-content/uploads/2022/05/Statistics-Brief-Metro-Figures-2021-web.pdf> (Accessed: 21 December 2022).

United Nations Department of Economic and Social Affairs (2021) *SDG Goal 9: Build resilient infrastructure, promote inclusive and sustainable industrialization and foster innovation*. Available at: <https://sdgs.un.org/goals/goal9> (Accessed: 21 July 2021).

United Nations Framework Convention on Climate Change (2015) *The Paris Agreement*. Available at: [https://unfccc.int/sites/default/files/english\\_paris\\_agreement.pdf](https://unfccc.int/sites/default/files/english_paris_agreement.pdf) (Accessed: 8 April 2021).

United Nations Framework Convention on Climate Change (2022) *What is the Race to Resilience?* Available at: <https://climatechampions.unfccc.int/what-is-the-race-to-resilience/> (Accessed: 28 January 2023).

Vasilyev, G.P., Peskov, N.V. and Lysak, T.M. (2022) Heat balance model for long-term prediction of the average temperature in a subway tunnel and surrounding soil. *International Journal of Thermal Sciences*, 172: 107344.

Wen, Y., Leng, J., Shen, X., et al. (2020) Environmental and Health Effects of Ventilation in Subway Stations: A Literature Review. *International Journal of Environmental Research and Public Health*, 17 (3): 1084.

World Meteorological Organisation (2017) *WMO Guidelines on the Calculation of Climate Normals*. Available at: [https://library.wmo.int/doc\\_num.php?explnum\\_id=4166](https://library.wmo.int/doc_num.php?explnum_id=4166) (Accessed: 4 February 2022).

Wu, J. and Liao, H. (2020) Weather, travel mode choice, and impacts on subway ridership in Beijing. *Transportation Research Part A: Policy and Practice*, 135: 264–279.

Zachariah, M., Vautard, R., Schumacher, D.L., et al. (2022) *Without human-caused climate change temperatures of 40°C in the UK would have been extremely unlikely*. Available at: <https://www.worldweatherattribution.org/wp-content/uploads/UK-heat-scientific-report.pdf> (Accessed: 2 January 2023).

Zhang, X., Manzanedo, R.D., Lv, P., et al. (2022) Reduced diurnal temperature range mitigates drought impacts on larch tree growth in North China. *Science of The Total Environment*, 848: 157808.

Zhang, Y. and Li, X. (2019) Response-surface-model based on influencing factor analysis of subway tunnel temperature. *Building and Environment*, 160: 106140.

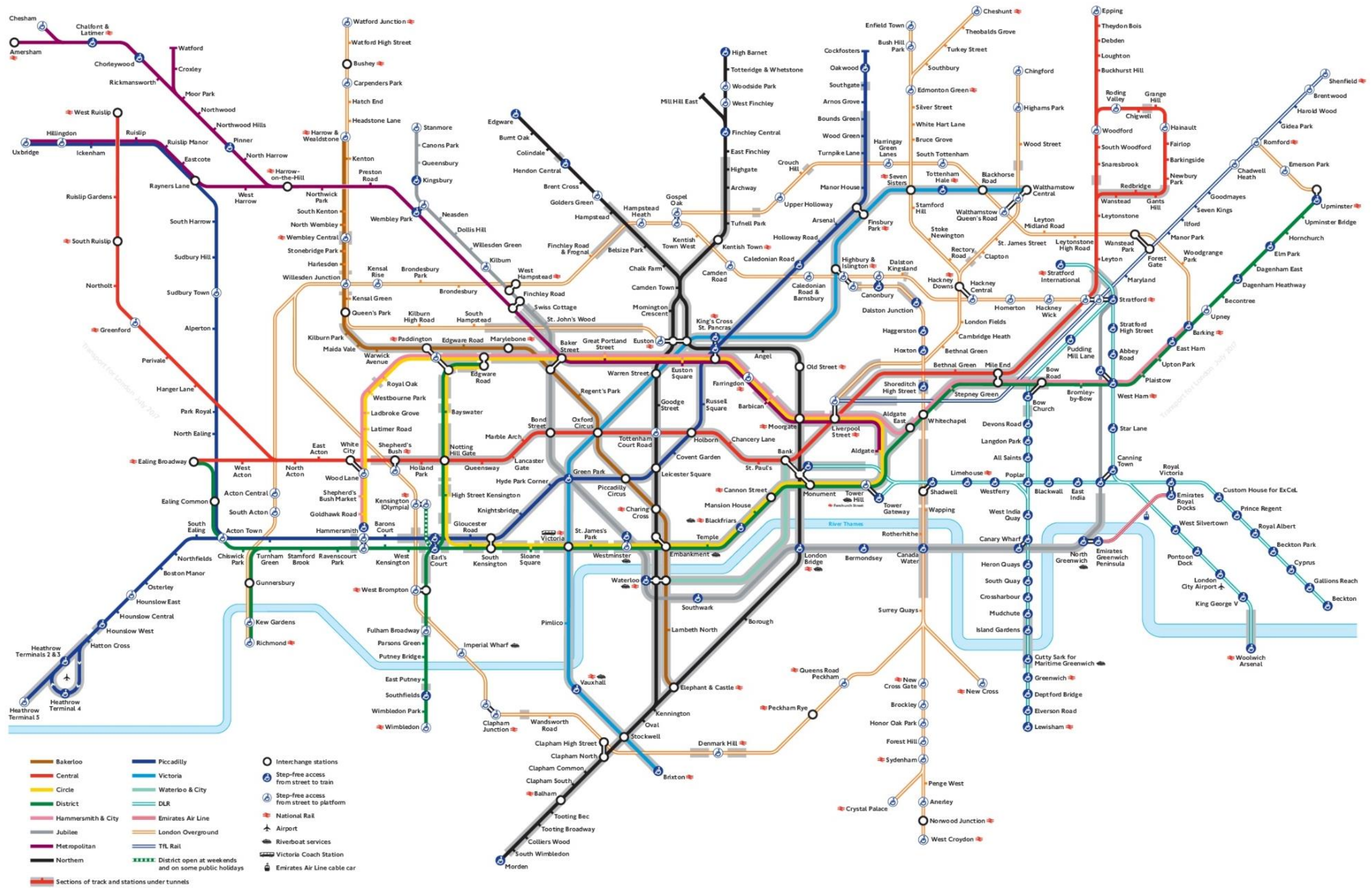
Zhang, Y., Peng, M., Wang, L., et al. (2018) Association of diurnal temperature range with daily mortality in England and Wales: A nationwide time-series study. *Science of The Total Environment*, 619–620: 291–300.

Zhao, L., Lee, X., Smith, R.B., et al. (2014) Strong contributions of local background climate to urban heat islands. *Nature*, 511 (7508): 216–219.

# Appendices

<b>Appendix A</b>	Map of the London Underground network, showing tunnel parts
<b>Appendix B</b>	R code sample to build the tunnel temperature estimation model
<b>Appendix C</b>	Tunnel temperature model equation variables
<b>Appendix D</b>	R code sample to join temperature data to work orders
<b>Appendix E</b>	R code sample to estimate future tunnel temperatures

Appendix A: Map of the London Underground network, showing tunnel parts (Source: TfL, 2017b)





## Appendix B: R code sample to build the tunnel temperature estimation model

```
#packages utilised throughout R code build
library(tidyverse)
library(scales)
library(dplyr)#also plyr where required
library(runner)
library(lubridate)
library(TSA)
library(reshape2)
library(data.table)

##Sample code: tmean/Paddington/SB/Bakerloo line##

#Step 1. cross-correlation#

#load data - tunnel observations
Bakerloo <-
  list.files(path = "/*REDACTED*/Bakerloo",
            pattern = ".*csv",
            full.names = TRUE)
Tube_temperature_humidity_Bakerloo <- lapply(Bakerloo, read.csv)
names(Tube_temperature_humidity_Bakerloo) <-
  c(
    "2006",
    "2007",
    "2008",
    "2009",
    "2010",
    "2011",
    "2012",
    "2013",
    "2014",
    "2015",
    "2016",
    "2017",
    "2018"
  )
Bakerloo <-
  rbind(
    Tube_temperature_humidity_Bakerloo$`2006`,
    Tube_temperature_humidity_Bakerloo$`2007`,
    Tube_temperature_humidity_Bakerloo$`2008`,
    Tube_temperature_humidity_Bakerloo$`2009`,
    Tube_temperature_humidity_Bakerloo$`2010`,
    Tube_temperature_humidity_Bakerloo$`2011`,
    Tube_temperature_humidity_Bakerloo$`2012`,
    Tube_temperature_humidity_Bakerloo$`2013`,
    Tube_temperature_humidity_Bakerloo$`2014`,
    Tube_temperature_humidity_Bakerloo$`2015`,
    Tube_temperature_humidity_Bakerloo$`2016`,
    Tube_temperature_humidity_Bakerloo$`2017`,
    Tube_temperature_humidity_Bakerloo$`2018`
  )

#load data - Met office observations
weather_obs_St_James <-
```



```

list.files(path = "/*REDACTED*/Met Office/Weather observations/St
Jamess Park",
           pattern = ".*csv",
           full.names = TRUE)
Met_Office_weather_observations_St_Jamess_Park <-
  lapply(weather_obs_St_James, read.csv)
names(Met_Office_weather_observations_St_Jamess_Park) <-
  c(
    "2006",
    "2007",
    "2008",
    "2009",
    "2010",
    "2011",
    "2012",
    "2013",
    "2014",
    "2015",
    "2016",
    "2017",
    "2018"
  )
weather_obs_St_James <-
  rbind(
    Met_Office_weather_observations_St_Jamess_Park$`2006`,
    Met_Office_weather_observations_St_Jamess_Park$`2007`,
    Met_Office_weather_observations_St_Jamess_Park$`2008`,
    Met_Office_weather_observations_St_Jamess_Park$`2009`,
    Met_Office_weather_observations_St_Jamess_Park$`2010`,
    Met_Office_weather_observations_St_Jamess_Park$`2011`,
    Met_Office_weather_observations_St_Jamess_Park$`2012`,
    Met_Office_weather_observations_St_Jamess_Park$`2013`,
    Met_Office_weather_observations_St_Jamess_Park$`2014`,
    Met_Office_weather_observations_St_Jamess_Park$`2015`,
    Met_Office_weather_observations_St_Jamess_Park$`2016`,
    Met_Office_weather_observations_St_Jamess_Park$`2017`,
    Met_Office_weather_observations_St_Jamess_Park$`2018`
  )
weather_obs_St_James = weather_obs_St_James %>% drop_na("id")

#conversion of data to daily mean
POSIXct_St_Jamess_Park <-
  as.POSIXct(weather_obs_St_James$ob_time, format = "%d/%m/%Y %H:%M")
Time_St_Jamess_Park <-
  as.data.frame(format(POSIXct_St_Jamess_Park, "%H:%M"))
Date_St_Jamess_Park <-
  as.data.frame(format(POSIXct_St_Jamess_Park, "%d/%m/%Y"))
Time_Date_St_Jamess_Park <-
  as.data.frame(
    cbind(
      Time_St_Jamess_Park$`format(POSIXct_St_Jamess_Park, "%H:%M")`,
      Date_St_Jamess_Park$`format(POSIXct_St_Jamess_Park, "%d/%m/%Y")`,
      weather_obs_St_James
    )
  )
colnames(Time_Date_St_Jamess_Park)[1] <- "Hour"
colnames(Time_Date_St_Jamess_Park)[2] <- "Date"
Average_daily_St_Jamess_Park <-
  as.data.frame(ddply(

```

```

    Time_Date_St_Jamess_Park,
    .(Date),
    summarize,
    air_temperature = mean(air_temperature, na.rm = TRUE)
  ))
Average_daily_St_Jamess_Park$Date =
(as.POSIXct(Average_daily_St_Jamess_Park$Date, format =
            "%d/%m/%Y"))
Average_daily_St_Jamess_Park <-
as.data.frame(Average_daily_St_Jamess_Park[order(Average_daily_St_Jamess_Pa
rk$Date), , drop =
                                                    FALSE])
Average_daily_St_Jamess_Park <-
as.data.frame(Average_daily_St_Jamess_Park[complete.cases(Average_daily_St_
Jamess_Park),])
week_rolling_Average_St_Jamess_Park <-
  as.data.frame(
    mean_run(
      x = Average_daily_St_Jamess_Park$air_temperature,
      k = 7,
      lag = 0,
      idx = as.Date(Average_daily_St_Jamess_Park$Date)
    )
  )
colnames(week_rolling_Average_St_Jamess_Park)[1] <- "rollingmean"
Average_daily_St_Jamess_Park <-
  as.data.frame(
    cbind(
      Average_daily_St_Jamess_Park,
      week_rolling_Average_St_Jamess_Park$rollingmean
    )
  )
colnames(Average_daily_St_Jamess_Park)[3] <- "Outside rolling mean"
Average_daily_St_Jamess_Park <-
as.data.frame(Average_daily_St_Jamess_Park[complete.cases(Average_daily_St_
Jamess_Park),])

#extract Paddington SB data and convert to 7-day rolling average
Tube_temperature_humidity_Bakerloo_Paddington_SB <-
  as.data.frame(filter(Bakerloo, Station == "Paddington", Direction ==
"SB"))

POSIXct_Tube_temperature_humidity_Bakerloo_Paddington_SB <-
  as.POSIXct(Tube_temperature_humidity_Bakerloo_Paddington_SB$InsideDate,
            format = "%d/%m/%Y %H:%M")
Time_Tube_temperature_humidity_Bakerloo_Paddington_SB <-
  as.data.frame(format(
    POSIXct_Tube_temperature_humidity_Bakerloo_Paddington_SB,
    "%H:%M"
  ))
Date_Tube_temperature_humidity_Bakerloo_Paddington_SB <-
  as.data.frame(format(
    POSIXct_Tube_temperature_humidity_Bakerloo_Paddington_SB,
    "%d/%m/%Y"
  ))
Time_Date_Tube_temperature_humidity_Bakerloo_Paddington_SB <-

```

```

as.data.frame(
  cbind(

Time_Tube_temperature_humidity_Bakerloo_Paddington_SB$`format(POSIXct_Tube_
temperature_humidity_Bakerloo_Paddington_SB, "%H:%M")`,

Date_Tube_temperature_humidity_Bakerloo_Paddington_SB$`format(POSIXct_Tube_
temperature_humidity_Bakerloo_Paddington_SB, "%d/%m/%Y")`,
  Tube_temperature_humidity_Bakerloo_Paddington_SB
)
)
colnames(Time_Date_Tube_temperature_humidity_Bakerloo_Paddington_SB)[1] <-
"Hour"
colnames(Time_Date_Tube_temperature_humidity_Bakerloo_Paddington_SB)[2] <-
"Date"
Average_daily_Bakerloo_Paddington_SB <-
as.data.frame(
  ddply(
    Time_Date_Tube_temperature_humidity_Bakerloo_Paddington_SB,
    .(Date),
    summarize,
    AvgTemp = mean(AvgTemp, na.rm = TRUE)
  )
)
Average_daily_Bakerloo_Paddington_SB$Date =
(as.POSIXct(Average_daily_Bakerloo_Paddington_SB$Date, format =
"%d/%m/%Y"))
Average_daily_Bakerloo_Paddington_SB <-

as.data.frame(Average_daily_Bakerloo_Paddington_SB[order(Average_daily_Bake
rloo_Paddington_SB$Date), , drop =
FALSE])
week_rolling_Average_Bakerloo_Paddington_SB <-
as.data.frame(
  mean_run(
    x = Average_daily_Bakerloo_Paddington_SB$AvgTemp,
    k = 7,
    lag = 0,
    idx = as.Date(Average_daily_Bakerloo_Paddington_SB$Date)
  )
)
colnames(week_rolling_Average_Bakerloo_Paddington_SB)[1] <-
"rollingmean"
Average_daily_Bakerloo_Paddington_SB <-
as.data.frame(
  cbind(
    Average_daily_Bakerloo_Paddington_SB,
    week_rolling_Average_Bakerloo_Paddington_SB$rollingmean
  )
)
colnames(Average_daily_Bakerloo_Paddington_SB)[3] <- "SB rolling mean"
Average_daily_Bakerloo_Paddington_SB <-

as.data.frame(Average_daily_Bakerloo_Paddington_SB[complete.cases(Average_d
aily_Bakerloo_Paddington_SB),])
Average_daily_Bakerloo_Paddington_SB$Date =
(as.POSIXct(Average_daily_Bakerloo_Paddington_SB$Date, format =
"%d/%m/%Y"))
Bakerloo_Paddington_SB <-

```

```

merge(Average_daily_St_Jamess_Park,
      Average_daily_Bakerloo_Paddington_SB,
      by = "Date")

#run cross-correlation and identify highest correlation coefficient
ccf(
  Bakerloo_Paddington_SB$`Outside rolling mean`,
  Bakerloo_Paddington_SB$`SB rolling mean`,
  plot = FALSE
)
Bakerloo_Paddington_SB_ccf <-
  ccf(
    Bakerloo_Paddington_SB$`Outside rolling mean`,
    Bakerloo_Paddington_SB$`SB rolling mean`,
    main = " ",
    ylab = 'Cross correlation',
    lag.max = 100,
    ylim = c(-0.5, 1)
  )
cor = Bakerloo_Paddington_SB_ccf$acf[, , 1]
lag = Bakerloo_Paddington_SB_ccf$lag[, , 1]
res = data.frame(cor, lag)
res.max = res[which.max(res$cor), ]$lag
res.max

#Step 2. Identify values of a and b via regression#

Surface = read.csv("/**REDACTED**/Analysis/Descriptive statistics/St.
James's Park/St. James's Park daily mean.csv")

Bakerloo_SB = read.csv("/**REDACTED**/Bakerloo/Station and
direction/Bakerloo SB daily mean.csv")
Bakerloo_SB=full_join(Surface,Bakerloo_SB,by="Date")
Bakerloo_SB=Bakerloo_SB[-c(3)]
colnames(Bakerloo_SB)[2]<-"Surface"

Bakerloo_SB_td = Bakerloo_SB
mean_air_temperature <-
  mean(as.numeric(Bakerloo_SB$Surface), na.rm = TRUE)

#use time lag delay from step 1
Bakerloo_SB_td$Paddington = shift(
  Bakerloo_SB_td$Surface,
  n = 5,
  fill = NA,
  type = "lag"
) - mean_air_temperature

Bakerloo_SB$Paddington = Bakerloo_SB$Paddington - mean_air_temperature

#run linear model regression
Bakerloo_SB_lm <-
  lm(Bakerloo_SB$Paddington ~ Bakerloo_SB_td$Paddington)
Bakerloo_SB_lm

#Step 3. Test model fit#
Model_tmean_Bakerloo_SB = read.csv(

```

```

    "/*REDACTED*/Analysis/Descriptive statistics/St. James's Park/St.
James's Park daily mean.csv"
)
colnames(Model_tmean_Bakerloo_SB)[2] <- "Surface"
Model_tmean_Bakerloo_SB$Date = as.Date(Model_tmean_Bakerloo_SB$Date,
"%d/%m/%Y")
Model_tmean_Bakerloo_SB$Surface =
as.numeric(as.character(Model_tmean_Bakerloo_SB$Surface))
mean_tmean <-
  mean(as.numeric(as.character(Model_tmean_Bakerloo_SB$Surface)), na.rm =
TRUE)

#add each station's variables for that time period (a,b,td); per direction
Model_tmean_Bakerloo_SB$"Paddington" <-
  ((mean_tmean + 15.9727) + ((
    shift(
      Model_tmean_Bakerloo_SB$Surface,
      n = 5,
      fill = NA,
      type = "lag"
    ) - mean_tmean
  ) * 0.3726))

#run linear model to compare estimations to observations (combines all
Bakerloo SB line)

#Load measured data and convert date type
Bakerloo_measured_SB <-
  read.csv(
    "/*REDACTED*/Analysis/Descriptive statistics/Bakerloo/Station and
Direction/Bakerloo SB daily mean.csv"
  )
Bakerloo_measured_SB <- Bakerloo_measured_SB[-c(1)]

#Rename Stations
colnames(Bakerloo_measured_SB)[2] <- "Baker Street"
colnames(Bakerloo_measured_SB)[3] <- "Charing Cross"
colnames(Bakerloo_measured_SB)[4] <- "Edgware Road"
colnames(Bakerloo_measured_SB)[5] <- "Elephant & Castle"
colnames(Bakerloo_measured_SB)[6] <- "Embankment"
colnames(Bakerloo_measured_SB)[7] <- "Kilburn Park"
colnames(Bakerloo_measured_SB)[8] <- "Lambeth North"
colnames(Bakerloo_measured_SB)[9] <- "Maida Vale"
colnames(Bakerloo_measured_SB)[10] <- "Marylebone"
colnames(Bakerloo_measured_SB)[11] <- "Oxford Circus"
colnames(Bakerloo_measured_SB)[12] <- "Paddington"
colnames(Bakerloo_measured_SB)[13] <- "Piccadilly Circus"
colnames(Bakerloo_measured_SB)[14] <- "Regents Park"
colnames(Bakerloo_measured_SB)[15] <- "Warwick Avenue"
colnames(Bakerloo_measured_SB)[16] <- "Waterloo"

#Gather columns - wide format to long format
Bakerloo_measured_SB <-
  gather(Bakerloo_measured_SB,
    "Station",
    "Mean daily measured temp",
    2:16)

```

```

#Load model fit data and convert date type
Bakerloo_model_SB <-
  read.csv(
    "///REDACTED//Analysis/Tunnel temp model/tmean/3. Tunnel model
fit/Bakerloo/Bakerloo daily Mean model values SB.csv"
  )

#Delete unnecessary columns
Bakerloo_model_SB <- Bakerloo_model_SB[-c(1, 3)]

#Rename Stations
colnames(Bakerloo_model_SB)[2] <- "Kilburn Park"
colnames(Bakerloo_model_SB)[3] <- "Maida Vale"
colnames(Bakerloo_model_SB)[4] <- "Warwick Avenue"
colnames(Bakerloo_model_SB)[5] <- "Paddington"
colnames(Bakerloo_model_SB)[6] <- "Edgware Road"
colnames(Bakerloo_model_SB)[7] <- "Marylebone"
colnames(Bakerloo_model_SB)[8] <- "Baker Street"
colnames(Bakerloo_model_SB)[9] <- "Regents Park"
colnames(Bakerloo_model_SB)[10] <- "Oxford Circus"
colnames(Bakerloo_model_SB)[11] <- "Piccadilly Circus"
colnames(Bakerloo_model_SB)[12] <- "Charing Cross"
colnames(Bakerloo_model_SB)[13] <- "Embankment"
colnames(Bakerloo_model_SB)[14] <- "Waterloo"
colnames(Bakerloo_model_SB)[15] <- "Lambeth North"
colnames(Bakerloo_model_SB)[16] <- "Elephant & Castle"

#Gather columns - wide format to long format
Bakerloo_model_SB <-
  gather(Bakerloo_model_SB, "Station", "Mean daily model temp", 2:16)

#Merge model and measured data to one dataframe
Bakerloo_SB <-
  left_join(Bakerloo_measured_SB,
            Bakerloo_model_SB,
            by = c("Date", "Station"))

#linear model regression
Bakerloo_SB_lm <-
  lm(Bakerloo_SB$`Mean daily measured temp` ~ Bakerloo_SB$`Mean daily model
temp`)
Bakerloo_SB_lm
summary(Bakerloo_SB_lm)

#residual density plot
res <- resid(Bakerloo_SB_lm)
plot(
  density(res),
  main = "Bakerloo SB",
  xlim = c(-15, 15),
  ylim = c(0.00, 0.30)
)

```

## Appendix C: Tunnel temperature model equation variables

LU tunnel	Station	$t_{mean}$			$t_{min}$			$t_{max}$		
		$t_d$	$a$	$b$	$t_d$	$a$	$b$	$t_d$	$a$	$b$
Bakerloo NB	Baker Street	3	14.28	0.42	2	16.05	0.47	3	11.70	0.35
Bakerloo NB	Charing Cross	3	13.95	0.46	1	14.62	0.55	4	11.68	0.36
Bakerloo NB	Edgware Road	2	15.58	0.38	1	16.29	0.43	3	13.24	0.31
Bakerloo NB	Elephant & Castle	2	11.71	0.61	1	12.53	0.67	2	9.84	0.51
Bakerloo NB	Embankment	5	14.95	0.37	3	17.14	0.41	6	12.18	0.31
Bakerloo NB	Kilburn Park	3	15.11	0.43	2	15.50	0.56	4	12.95	0.34
Bakerloo NB	Lambeth North	6	14.82	0.39	4	16.40	0.45	21	12.37	0.31
Bakerloo NB	Maida Vale	6	16.11	0.34	5	18.81	0.36	22	13.18	0.28
Bakerloo NB	Marylebone	3	13.70	0.44	2	15.94	0.45	3	10.97	0.36
Bakerloo NB	Oxford Circus	3	15.18	0.32	3	17.50	0.33	4	12.45	0.26
Bakerloo NB	Paddington	9	16.68	0.33	9	19.22	0.35	19	13.70	0.28
Bakerloo NB	Piccadilly Circus	3	13.78	0.42	2	15.78	0.46	4	11.15	0.34
Bakerloo NB	Regents Park	3	13.81	0.40	1	14.58	0.50	4	11.50	0.32
Bakerloo NB	Warwick Avenue	2	15.84	0.37	1	16.63	0.45	21	13.43	0.29
Bakerloo NB	Waterloo	5	12.72	0.42	4	14.94	0.45	5	9.99	0.34
Bakerloo SB	Baker Street	2	13.55	0.51	1	11.90	0.67	3	12.14	0.39
Bakerloo SB	Charing Cross	4	15.54	0.40	1	15.94	0.51	6	13.37	0.30
Bakerloo SB	Edgware Road	3	17.60	0.38	3	20.21	0.39	5	15.09	0.31
Bakerloo SB	Elephant & Castle	1	10.18	0.67	1	9.61	0.77	1	8.99	0.55
Bakerloo SB	Embankment	3	13.44	0.46	2	15.51	0.52	3	10.75	0.38
Bakerloo SB	Kilburn Park	3	10.74	0.47	2	12.95	0.52	3	7.84	0.40
Bakerloo SB	Lambeth North	2	9.76	0.53	1	10.92	0.59	3	7.76	0.42
Bakerloo SB	Maida Vale	4	14.17	0.25	3	16.31	0.46	4	11.38	0.36
Bakerloo SB	Marylebone	3	14.69	0.46	2	14.77	0.61	4	12.64	0.34
Bakerloo SB	Oxford Circus	3	15.11	0.36	2	17.16	0.35	4	12.42	0.30
Bakerloo SB	Paddington	5	15.97	0.37	5	18.38	0.39	5	13.27	0.31
Bakerloo SB	Piccadilly Circus	3	15.16	0.46	2	16.70	0.53	3	12.76	0.37
Bakerloo SB	Regents Park	2	12.05	0.48	1	12.47	0.58	3	9.93	0.38
Bakerloo SB	Warwick Avenue	2	12.67	0.49	1	13.02	0.58	3	10.56	0.38
Bakerloo SB	Waterloo	4	13.18	0.46	3	14.49	0.52	4	10.89	0.37
Central EB	Bank	3	15.84	0.43	3	18.53	0.43	3	12.91	0.37
Central EB	Bethnal Green	2	12.54	0.54	1	12.91	0.64	2	11.20	0.44
Central EB	Bond Street	3	15.24	0.45	2	17.26	0.48	2	12.51	0.39
Central EB	Chancery Lane	2	14.16	0.48	2	16.40	0.49	2	11.54	0.42
Central EB	Holborn	2	13.72	0.45	1	13.91	0.58	3	11.72	0.35
Central EB	Holland Park	3	12.67	0.48	3	15.22	0.50	2	9.76	0.42
Central EB	Lancaster Gate	2	12.82	0.49	1	12.52	0.60	2	10.85	0.41

LU tunnel	Station	$t_{mean}$			$t_{min}$			$t_{max}$		
		$t_d$	$a$	$b$	$t_d$	$a$	$b$	$t_d$	$a$	$b$
Central EB	Liverpool Street	2	12.12	0.53	1	13.59	0.63	2	9.95	0.43
Central EB	Marble Arch	3	15.48	0.46	1	16.82	0.56	3	12.94	0.38
Central EB	Mile End	2	11.33	0.54	2	12.53	0.61	3	9.39	0.44
Central EB	Notting Hill Gate	3	13.16	0.49	3	15.33	0.51	2	10.39	0.43
Central EB	Oxford Circus	3	15.56	0.42	3	18.09	0.42	2	12.67	0.37
Central EB	Queensway	3	12.96	0.49	2	15.55	0.50	3	10.17	0.40
Central EB	Shepherd's Bush	0	4.67	0.86	0	5.23	0.92	0	3.50	0.78
Central EB	St. Paul's	2	12.48	0.52	1	10.61	0.69	2	11.24	0.41
Central EB	Tottenham Court Road	3	15.86	0.42	3	17.50	0.46	2	13.26	0.36
Central WB	Bank	3	15.94	0.39	4	18.60	0.39	3	12.99	0.34
Central WB	Bethnal Green	1	9.83	0.60	0	10.57	0.69	1	7.94	0.50
Central WB	Bond Street	2	14.18	0.47	2	15.82	0.54	2	11.81	0.39
Central WB	Chancery Lane	2	13.89	0.48	1	15.39	0.63	3	11.25	0.40
Central WB	Holborn	3	13.04	0.44	2	15.29	0.48	3	10.24	0.38
Central WB	Holland Park	3	14.03	0.45	3	16.11	0.47	3	11.32	0.38
Central WB	Lancaster Gate	2	14.29	0.45	1	13.05	0.60	3	12.69	0.35
Central WB	Liverpool Street	2	11.00	0.61	2	12.82	0.67	2	8.84	0.50
Central WB	Marble Arch	3	15.55	0.43	2	17.37	0.50	4	12.87	0.36
Central WB	Mile End	2	10.18	0.57	2	12.24	0.60	2	7.63	0.49
Central WB	Notting Hill Gate	3	13.66	0.49	2	15.11	0.54	3	11.28	0.41
Central WB	Oxford Circus	3	15.56	0.38	2	18.10	0.39	3	12.60	0.33
Central WB	Queensway	5	15.72	0.37	5	18.62	0.38	5	12.62	0.32
Central WB	Shepherd's Bush	1	8.18	0.70	1	8.85	0.76	1	6.52	0.60
Central WB	St. Paul's	2	12.89	0.51	1	13.70	0.55	2	10.74	0.43
Central WB	Tottenham Court Road	2	13.56	0.46	2	14.59	0.55	2	11.33	0.38
Jubilee EB	Baker Street	1	8.00	0.70	1	7.83	0.81	1	6.43	0.57
Jubilee EB	Bermondsey	2	9.09	0.35	2	11.20	0.38	2	6.30	0.32
Jubilee EB	Bond Street	1	6.25	0.71	1	6.42	0.81	1	4.79	0.57
Jubilee EB	Canada Water	2	9.58	0.57	2	10.98	0.71	2	7.14	0.46
Jubilee EB	Canary Wharf	1	7.48	0.56	0	9.36	0.62	1	5.25	0.48
Jubilee EB	Green Park	2	10.09	0.54	1	12.09	0.58	2	7.56	0.46
Jubilee EB	London Bridge	2	9.31	0.36	1	11.52	0.40	2	6.53	0.31
Jubilee EB	North Greenwich	2	10.43	0.40	1	12.52	0.44	2	7.77	0.34
Jubilee EB	Southwark	1	8.97	0.39	1	10.21	0.52	1	6.66	0.33
Jubilee EB	St Johns Wood	2	10.24	0.51	2	12.84	0.52	2	7.35	0.44
Jubilee EB	Swiss Cottage	2	7.20	0.62	2	9.61	0.63	2	4.41	0.54
Jubilee EB	Waterloo	1	10.36	0.34	1	12.23	0.34	1	7.78	0.30
Jubilee EB	Westminster	2	9.70	0.39	1	11.31	0.40	2	7.32	0.33
Jubilee WB	Baker Street	3	10.83	0.43	2	12.76	0.47	3	8.12	0.37



LU tunnel	Station	$t_{mean}$			$t_{min}$			$t_{max}$		
		$t_d$	$a$	$b$	$t_d$	$a$	$b$	$t_d$	$a$	$b$
Jubilee WB	Bermondsey	1	7.15	0.47	1	8.89	0.54	1	4.65	0.41
Jubilee WB	Bond Street	2	10.15	0.46	1	10.52	0.60	3	8.12	0.37
Jubilee WB	Canada Water	2	8.80	0.44	1	11.14	0.52	2	5.91	0.37
Jubilee WB	Canary Wharf	1	9.30	0.46	1	11.52	0.51	2	6.66	0.39
Jubilee WB	Green Park	1	7.60	0.58	1	7.81	0.78	1	8.00	0.37
Jubilee WB	London Bridge	2	9.12	0.37	1	11.60	0.36	2	6.22	0.33
Jubilee WB	North Greenwich	2	9.82	0.46	2	12.15	0.49	2	7.06	0.39
Jubilee WB	Southwark	2	10.11	0.42	1	11.37	0.60	2	6.36	0.32
Jubilee WB	St Johns Wood	2	10.36	0.49	2	12.68	0.52	2	7.63	0.41
Jubilee WB	Swiss Cottage	3	9.45	0.50	2	11.30	0.55	3	6.96	0.43
Jubilee WB	Waterloo	1	8.90	0.35	1	10.70	0.34	1	7.25	0.29
Jubilee WB	Westminster	2	10.00	0.32	1	12.27	0.34	2	5.65	0.45
Northern NB	Angel	1	8.25	0.49	1	7.27	0.65	2	6.95	0.35
Northern NB	Archway	3	11.10	0.40	2	12.34	0.44	3	8.67	0.33
Northern NB	Balham	1	5.49	0.67	0	4.98	0.84	1	4.18	0.55
Northern NB	Bank	5	13.33	0.32	6	15.71	0.22	4	10.49	0.28
Northern NB	Belsize Park	20	14.13	0.31	19	16.78	0.32	25	11.07	0.26
Northern NB	Borough	3	12.10	0.37	2	13.15	0.47	5	9.82	0.27
Northern NB	Camden Town - Hampstead	6	14.07	0.28	5	16.86	0.28	16	10.97	0.24
Northern NB	Camden Town - Highgate	2	13.35	0.31	1	14.80	0.40	5	10.66	0.25
Northern NB	Chalk Farm	4	14.05	0.32	3	16.31	0.37	4	11.15	0.26
Northern NB	Charing Cross	4	13.67	0.37	4	16.23	0.40	5	10.73	0.30
Northern NB	Clapham Common	2	12.03	0.48	1	14.08	0.53	2	9.62	0.40
Northern NB	Clapham North	1	8.04	0.64	1	6.01	0.82	1	7.10	0.48
Northern NB	Clapham South	3	11.54	0.40	2	13.96	0.44	4	8.78	0.31
Northern NB	Colliers Wood	1	8.09	0.55	1	6.71	0.72	1	6.69	0.43
Northern NB	Elephant & Castle	5	12.29	0.32	4	15.07	0.34	5	9.23	0.28
Northern NB	Embankment	5	12.56	0.32	3	15.04	0.37	6	9.54	0.26
Northern NB	Euston (City)	5	12.13	0.34	4	14.90	0.36	5	9.10	0.29
Northern NB	Euston (CX)	2	11.46	0.44	1	12.39	0.54	2	9.18	0.36
Northern NB	Goodge Street	4	12.41	0.40	3	14.39	0.48	4	9.67	0.32
Northern NB	Hampstead	21	14.50	0.28	20	17.38	0.28	22	11.35	0.24
Northern NB	Highgate	5	9.99	0.37	3	11.98	0.42	5	7.19	0.30
Northern NB	Kennington (City)	5	12.56	0.29	5	15.30	0.30	6	9.59	0.26
Northern NB	Kennington (CX)	4	13.16	0.34	3	15.27	0.36	4	10.32	0.29
Northern NB	Kentish Town	3	11.31	0.37	1	11.38	0.52	4	9.24	0.29
Northern NB	Kings Cross	2	11.07	0.45	1	12.22	0.58	3	8.83	0.34
Northern NB	Leicester Square	3	13.09	0.39	2	15.36	0.43	3	10.40	0.32
Northern NB	London Bridge	2	10.06	0.42	1	10.19	0.57	3	8.09	0.32

LU tunnel	Station	$t_{mean}$			$t_{min}$			$t_{max}$		
		$t_d$	$a$	$b$	$t_d$	$a$	$b$	$t_d$	$a$	$b$
Northern NB	Moorgate	3	11.24	0.37	2	13.68	0.40	3	8.52	0.30
Northern NB	Mornington Crescent	5	12.51	0.35	3	15.10	0.39	5	9.51	0.29
Northern NB	Old Street	3	12.83	0.35	1	13.47	0.53	4	10.46	0.26
Northern NB	Oval	5	11.90	0.32	4	14.39	0.34	4	8.96	0.27
Northern NB	South Wimbledon	4	9.93	0.39	2	12.27	0.43	4	7.05	0.32
Northern NB	Stockwell	3	11.35	0.39	1	11.35	0.57	4	9.39	0.29
Northern NB	Tooting Bec	3	11.50	0.37	2	12.61	0.46	4	8.95	0.30
Northern NB	Tooting Broadway	4	11.90	0.30	2	13.98	0.38	20	9.11	0.25
Northern NB	Tottenham Court Road	3	12.86	0.39	2	14.92	0.43	4	10.12	0.32
Northern NB	Tufnell Park	5	12.18	0.34	4	14.93	0.36	6	9.12	0.28
Northern NB	Warren Street	6	13.49	0.32	5	16.29	0.34	6	10.41	0.27
Northern NB	Waterloo	4	12.21	0.38	3	14.97	0.41	4	9.14	0.32
Northern SB	Angel	3	9.94	0.37	1	10.14	0.53	4	7.78	0.28
Northern SB	Archway	2	9.34	0.49	2	11.31	0.53	3	6.89	0.39
Northern SB	Balham	3	12.16	0.39	1	13.33	0.52	4	9.65	0.30
Northern SB	Bank	4	13.55	0.33	4	16.07	0.35	4	10.83	0.27
Northern SB	Belsize Park	4	12.81	0.37	3	14.51	0.44	4	10.14	0.31
Northern SB	Borough	5	12.52	0.30	4	15.33	0.31	5	9.41	0.25
Northern SB	Camden Town - Hampstead	2	11.94	0.43	1	10.85	0.61	2	10.07	0.34
Northern SB	Camden Town - Highgate	3	10.53	0.46	1	10.61	0.62	2	8.51	0.37
Northern SB	Chalk Farm	2	11.74	0.43	2	13.77	0.47	2	9.11	0.36
Northern SB	Charing Cross	4	14.63	0.38	2	15.76	0.46	4	12.18	0.30
Northern SB	Clapham Common	3	12.39	0.43	3	14.68	0.46	3	9.71	0.37
Northern SB	Clapham North	1	7.05	0.65	1	5.63	0.78	1	6.25	0.51
Northern SB	Clapham South	5	13.96	0.31	4	16.56	0.33	6	10.99	0.25
Northern SB	Colliers Wood	3	11.85	0.37	2	13.07	0.49	5	9.38	0.28
Northern SB	Elephant & Castle	3	13.86	0.40	2	15.05	0.50	4	11.72	0.32
Northern SB	Embankment	3	11.54	0.44	2	11.87	0.61	3	9.43	0.33
Northern SB	Euston (City)	2	10.85	0.42	1	12.88	0.45	2	8.15	0.36
Northern SB	Euston (CX)	2	10.82	0.46	1	12.23	0.57	2	8.46	0.36
Northern SB	Goodge Street	4	12.37	0.37	3	14.47	0.46	4	9.50	0.30
Northern SB	Hampstead	4	12.82	0.35	4	15.32	0.36	4	9.96	0.28
Northern SB	Highgate	3	8.25	0.46	3	10.67	0.49	3	5.36	0.40
Northern SB	Kennington (City)	4	12.96	0.33	3	15.23	0.36	3	10.10	0.28
Northern SB	Kennington (CX)	4	13.42	0.30	4	16.18	0.31	4	10.34	0.26
Northern SB	Kentish Town	3	11.07	0.45	1	12.10	0.59	3	8.57	0.36
Northern SB	Kings Cross	2	10.65	0.46	1	11.24	0.62	3	8.44	0.35
Northern SB	Leicester Square	3	13.50	0.34	3	15.98	0.36	3	10.57	0.29
Northern SB	London Bridge	3	12.52	0.36	1	13.59	0.47	4	10.08	0.28

LU tunnel	Station	$t_{mean}$			$t_{min}$			$t_{max}$		
		$t_d$	$a$	$b$	$t_d$	$a$	$b$	$t_d$	$a$	$b$
Northern SB	Moorgate	4	13.56	0.30	4	16.33	0.32	5	10.53	0.24
Northern SB	Mornington Crescent	4	14.04	0.38	3	16.39	0.43	4	11.21	0.31
Northern SB	Old Street	2	10.23	0.46	1	11.47	0.60	2	7.93	0.36
Northern SB	Oval	1	5.40	0.67	0	4.80	0.86	0	4.25	0.57
Northern SB	South Wimbledon	4	12.64	0.34	2	14.53	0.40	5	9.83	0.28
Northern SB	Stockwell	1	7.45	0.58	1	8.59	0.64	1	5.62	0.48
Northern SB	Tooting Bec	5	13.10	0.34	5	15.98	0.35	5	9.99	0.29
Northern SB	Tooting Broadway	4	12.88	0.33	2	14.07	0.41	6	10.33	0.27
Northern SB	Tottenham Court Road	2	12.90	0.42	1	14.73	0.47	2	10.28	0.36
Northern SB	Tufnell Park	2	10.85	0.44	1	12.21	0.50	2	8.38	0.37
Northern SB	Warren Street	4	11.43	0.36	3	14.21	0.38	4	8.42	0.30
Northern SB	Waterloo	4	13.05	0.36	4	15.80	0.37	5	10.02	0.30
Piccadilly EB	Arsenal	3	11.41	0.45	2	13.60	0.50	3	8.59	0.37
Piccadilly EB	Bounds Green	3	11.04	0.46	3	13.06	0.48	4	8.33	0.37
Piccadilly EB	Caledonian Road	4	13.26	0.37	4	15.59	0.39	4	10.36	0.31
Piccadilly EB	Covent Garden	2	11.80	0.45	2	13.66	0.53	2	9.16	0.38
Piccadilly EB	Earls Court	2	10.56	0.53	2	12.77	0.59	2	7.84	0.46
Piccadilly EB	Finsbury Park	2	10.93	0.42	2	11.18	0.47	2	8.94	0.34
Piccadilly EB	Gloucester Road	3	11.92	0.45	2	14.69	0.47	3	8.99	0.37
Piccadilly EB	Green Park	3	11.76	0.40	3	14.46	0.41	3	8.84	0.35
Piccadilly EB	Holborn	4	13.84	0.37	4	16.70	0.38	5	10.86	0.30
Piccadilly EB	Holloway Road	3	11.63	0.44	2	12.45	0.54	3	9.25	0.36
Piccadilly EB	Hyde Park Corner	1	7.51	0.64	0	6.48	0.82	1	6.18	0.51
Piccadilly EB	Kings Cross	2	10.76	0.54	1	12.24	0.62	2	8.59	0.44
Piccadilly EB	Knightsbridge	3	11.57	0.45	3	14.25	0.47	3	8.68	0.39
Piccadilly EB	Leicester Square	2	12.24	0.45	2	14.36	0.49	2	9.57	0.38
Piccadilly EB	Manor House	2	9.60	0.54	1	9.41	0.69	2	7.87	0.42
Piccadilly EB	Piccadilly Circus	3	12.70	0.40	2	15.23	0.43	3	9.77	0.35
Piccadilly EB	Russell Square	2	11.92	0.46	2	13.64	0.53	2	9.31	0.38
Piccadilly EB	South Kensington	2	9.94	0.54	1	10.40	0.68	2	7.83	0.41
Piccadilly EB	Turnpike Lane	2	7.50	0.62	1	7.67	0.78	2	5.86	0.49
Piccadilly EB	Wood Green	3	11.26	0.47	2	12.51	0.54	3	8.72	0.39
Piccadilly WB	Arsenal	2	8.30	0.56	1	7.09	0.74	2	6.93	0.43
Piccadilly WB	Bounds Green	2	6.38	0.64	1	8.65	0.67	2	3.86	0.54
Piccadilly WB	Caledonian Road	3	11.45	0.43	3	13.77	0.46	4	8.54	0.36
Piccadilly WB	Covent Garden	3	14.11	0.46	2	15.43	0.54	3	11.73	0.38
Piccadilly WB	Earls Court	4	13.07	0.39	3	15.36	0.41	4	10.21	0.33
Piccadilly WB	Finsbury Park	1	9.85	0.53	1	9.11	0.70	2	8.20	0.41
Piccadilly WB	Gloucester Road	3	11.78	0.45	3	14.34	0.48	4	9.07	0.36

LU tunnel	Station	$t_{mean}$			$t_{min}$			$t_{max}$		
		$t_d$	$a$	$b$	$t_d$	$a$	$b$	$t_d$	$a$	$b$
Piccadilly WB	Green Park	3	13.30	0.38	2	15.38	0.40	3	10.54	0.33
Piccadilly WB	Holborn	2	12.77	0.46	1	13.11	0.63	3	10.55	0.36
Piccadilly WB	Holloway Road	3	10.19	0.48	2	11.76	0.51	3	7.56	0.40
Piccadilly WB	Hyde Park Corner	2	9.16	0.55	1	9.38	0.72	3	7.19	0.42
Piccadilly WB	Kings Cross	2	11.89	0.45	1	13.26	0.59	3	9.37	0.35
Piccadilly WB	Knightsbridge	2	10.86	0.51	2	13.23	0.54	2	8.07	0.44
Piccadilly WB	Leicester Square	2	12.80	0.44	1	15.08	0.48	3	10.00	0.37
Piccadilly WB	Manor House	2	8.62	0.57	1	8.97	0.72	2	6.73	0.46
Piccadilly WB	Piccadilly Circus	2	11.01	0.45	2	12.27	0.52	2	8.73	0.37
Piccadilly WB	Russell Square	4	13.25	0.39	3	15.54	0.44	5	10.33	0.32
Piccadilly WB	South Kensington	2	12.30	0.46	1	12.38	0.63	3	10.13	0.35
Piccadilly WB	Turnpike Lane	2	9.41	0.55	1	9.92	0.70	2	7.19	0.44
Piccadilly WB	Wood Green	2	9.95	0.52	1	10.75	0.63	2	7.75	0.42
Sub-surface EB	Baker Street	1	5.57	0.73	1	7.41	0.77	1	3.19	0.63
Sub-surface EB	Bank	2	10.65	0.59	1	12.65	0.64	2	8.22	0.48
Sub-surface EB	Cannon Street	0	5.13	0.87	0	9.39	0.92	1	3.45	0.73
Sub-surface EB	Embankment	1	5.95	0.76	0	6.17	0.90	1	4.23	0.68
Sub-surface EB	Gloucester Road	0	5.30	0.74	1	6.89	0.79	2	2.91	0.62
Sub-surface EB	Liverpool Street	0	4.43	0.81	0	5.52	0.82	0	3.36	0.83
Sub-surface EB	Mile End	2	8.92	0.62	2	10.49	0.65	1	9.60	0.54
Sub-surface EB	Moorgate	1	4.65	0.74	0	6.89	0.77	1	2.27	0.66
Sub-surface EB	Notting Hill Gate	0	1.48	1.00	0	2.24	0.97	0	1.01	1.03
Sub-surface EB	Paddington	0	2.14	1.00	0	2.83	0.97	0	2.50	1.14
Sub-surface EB	South Kensington	0	1.40	1.04	0	1.41	0.99	1	1.74	1.00
Sub-surface EB	Victoria	1	4.97	0.77	0	6.19	0.85	1	3.08	0.71
Sub-surface IR	Aldgate	0	2.10	0.93	0	2.91	0.95	0	0.89	0.84
Sub-surface IR	Baker Street	1	5.79	0.76	1	7.53	0.81	1	3.47	0.66
Sub-surface IR	Bayswater	1	4.12	0.84	0	6.20	0.88	1	1.76	0.74
Sub-surface IR	Blackfriars	1	7.94	0.81	1	6.29	0.88	1	2.94	0.70
Sub-surface IR	Euston Square	2	7.97	0.65	2	10.65	0.67	2	5.12	0.57
Sub-surface IR	Gloucester Road	0	2.07	0.90	0	3.31	0.92	0	0.47	0.81
Sub-surface IR	Great Portland Street	2	6.15	0.68	1	8.25	0.72	2	3.66	0.59
Sub-surface IR	Kings Cross	1	5.08	0.81	1	5.56	0.88	1	3.26	0.68
Sub-surface IR	Mansion House	1	5.50	0.73	1	7.48	0.76	2	2.96	0.61
Sub-surface IR	St. James's Park	1	6.44	0.80	1	8.31	0.81	1	4.26	0.70
Sub-surface IR	Temple	1	7.25	0.79	1	9.40	0.81	1	4.75	0.69
Sub-surface IR	Tower Hill	1	5.45	0.84	1	6.76	0.87	1	3.53	0.73
Sub-surface OR	Aldgate	0	2.21	0.87	0	3.23	0.86	0	0.86	0.82
Sub-surface OR	Baker Street	1	5.79	0.76	1	7.53	0.81	1	3.47	0.66

LU tunnel	Station	$t_{mean}$			$t_{min}$			$t_{max}$		
		$t_d$	$a$	$b$	$t_d$	$a$	$b$	$t_d$	$a$	$b$
Sub-surface OR	Bayswater	1	2.18	0.88	0	4.03	0.93	1	0.06	0.78
Sub-surface OR	Blackfriars	1	4.22	0.81	1	5.56	0.86	1	2.33	0.71
Sub-surface OR	Euston Square	2	7.67	0.69	2	10.03	0.69	2	5.06	0.61
Sub-surface OR	Gloucester Road	0	2.07	0.90	0	3.31	0.92	0	0.47	0.81
Sub-surface OR	Great Portland Street	0	4.09	0.84	0	5.23	0.86	1	2.68	0.72
Sub-surface OR	Kings Cross	2	6.45	0.68	1	7.68	0.79	2	4.12	0.59
Sub-surface OR	Mansion House	1	6.71	0.75	1	8.07	0.78	1	4.70	0.66
Sub-surface OR	St. James's Park	1	6.15	0.80	1	7.63	0.82	1	4.18	0.71
Sub-surface OR	Temple	1	6.21	0.80	1	8.34	0.82	1	3.83	0.70
Sub-surface OR	Tower Hill	2	6.05	0.80	1	8.09	0.84	2	3.61	0.69
Sub-surface WB	Baker Street	1	5.57	0.73	1	7.41	0.77	1	3.19	0.63
Sub-surface WB	Bank	2	10.66	0.68	2	13.09	0.70	2	7.96	0.59
Sub-surface WB	Cannon Street	1	8.59	0.72	1	10.94	0.76	2	5.97	0.64
Sub-surface WB	Embankment	1	5.29	0.83	0	6.17	0.90	1	4.23	0.68
Sub-surface WB	Gloucester Road	0	5.30	0.74	1	6.89	0.79	2	2.91	0.62
Sub-surface WB	Liverpool Street	0	4.43	0.81	0	5.52	0.82	0	3.36	0.83
Sub-surface WB	Mile End	2	8.92	0.62	2	10.49	0.65	1	9.60	0.54
Sub-surface WB	Moorgate	1	4.65	0.74	0	6.89	0.77	1	2.27	0.66
Sub-surface WB	Notting Hill Gate	0	4.03	0.88	0	4.71	0.90	0	2.50	0.79
Sub-surface WB	Paddington	0	1.23	1.00	0	1.79	0.97	0	1.19	1.08
Sub-surface WB	South Kensington	0	1.40	1.04	0	1.41	0.99	0	1.74	1.00
Sub-surface WB	Victoria	0	4.25	0.89	0	5.35	0.89	0	2.57	0.80
Victoria NB	Blackhorse Road	4	12.42	0.33	2	13.37	0.46	20	10.19	0.25
Victoria NB	Brixton	1	8.00	0.57	1	8.24	0.64	1	6.49	0.46
Victoria NB	Euston	2	12.78	0.41	1	14.15	0.53	3	10.57	0.32
Victoria NB	Finsbury Park	4	13.15	0.35	2	13.83	0.42	4	11.02	0.28
Victoria NB	Green Park	4	15.41	0.28	3	17.67	0.30	5	12.63	0.24
Victoria NB	Highbury	4	12.79	0.28	3	14.49	0.28	4	10.48	0.24
Victoria NB	Kings Cross	2	11.48	0.51	2	12.45	0.60	3	9.66	0.38
Victoria NB	Oxford Circus	5	16.19	0.29	4	18.87	0.30	6	13.22	0.24
Victoria NB	Pimlico	3	12.53	0.36	1	12.96	0.53	4	10.42	0.27
Victoria NB	Seven Sisters	1	10.68	0.50	1	9.38	0.69	2	9.73	0.34
Victoria NB	Stockwell	3	13.18	0.31	1	12.69	0.46	4	11.50	0.23
Victoria NB	Tottenham Hale	2	9.31	0.44	1	10.08	0.59	3	7.23	0.33
Victoria NB	Vauxhall	1	10.05	0.44	1	9.08	0.58	2	8.93	0.32
Victoria NB	Victoria	2	12.97	0.43	1	14.71	0.54	3	10.53	0.33
Victoria NB	Walthamstow	3	10.79	0.30	2	13.11	0.33	18	8.41	0.22
Victoria NB	Warren Street	1	11.79	0.47	1	9.98	0.68	2	11.03	0.33
Victoria SB	Blackhorse Road	2	9.44	0.49	1	9.58	0.65	3	7.90	0.35

LU tunnel	Station	$t_{mean}$			$t_{min}$			$t_{max}$		
		$t_d$	$a$	$b$	$t_d$	$a$	$b$	$t_d$	$a$	$b$
Victoria SB	Brixton	1	7.71	0.53	0	8.29	0.63	1	6.15	0.44
Victoria SB	Euston	3	13.99	0.35	2	15.60	0.37	4	11.46	0.29
Victoria SB	Finsbury Park	3	13.11	0.40	1	12.19	0.60	4	11.74	0.28
Victoria SB	Green Park	3	14.22	0.31	2	16.35	0.34	3	11.60	0.26
Victoria SB	Highbury	2	9.36	0.42	2	9.83	0.46	2	7.74	0.34
Victoria SB	Kings Cross	2	12.22	0.39	1	11.79	0.52	3	10.85	0.29
Victoria SB	Oxford Circus	4	14.96	0.30	3	17.19	0.32	5	12.22	0.25
Victoria SB	Pimlico	2	12.12	0.39	1	12.17	0.53	4	10.41	0.28
Victoria SB	Seven Sisters	3	11.15	0.35	2	12.86	0.42	4	8.65	0.28
Victoria SB	Stockwell	3	12.60	0.30	1	13.42	0.37	5	10.51	0.23
Victoria SB	Tottenham Hale	3	12.34	0.35	1	13.44	0.50	5	9.95	0.26
Victoria SB	Vauxhall	4	13.88	0.33	2	15.83	0.42	5	11.17	0.26
Victoria SB	Victoria	1	6.85	0.70	0	6.73	0.82	1	5.90	0.57
Victoria SB	Walthamstow	4	13.94	0.33	3	16.11	0.35	5	11.70	0.27
Victoria SB	Warren Street	2	10.24	0.52	1	11.18	0.63	2	8.28	0.42

## Appendix D: R code sample to join temperature data to work orders

#See Appendix B for packages loaded and tested throughout R code build

##Sample code: tmean/surface##

```
#Step 1. Combine WO data from Ellipse and Maximo with asset data
#Ellipse load
points <-
  read.csv(file = "/*REDACTED*/Ellipse/Points & Trainstops 2006-
2018/20201002_points.csv")
trainstops <-
  read.csv(file = "/*REDACTED*/Ellipse/Points & Trainstops 2006-
2018/20201002_trainstops.csv")
E_WOs <-
  read.csv(file = "/*REDACTED*/Ellipse/Points & Trainstops 2006-
2018/20201002_works.csv")
pandt <- rbind.fill(points, trainstops)
join1_E <-
  inner_join(E_WOs, pandt, by = c("EQUIPMENT_NO" = "PARENT_EQUIP_NO"))
join2_E <-
  inner_join(E_WOs, pandt, by = c("EQUIPMENT_NO" = "CHILD_EQUIP_NO"))
Ellipse_WOs <- rbind.fill(join1_E, join2_E)
#remove duplicate WOs in the join
Ellipse_WOs = Ellipse_WOs[!duplicated(Ellipse_WOs$WONUM), ]

#Maximo load
pandc <-
  read.csv(file = "/*REDACTED*/Maximo/Points & Crossings 2006-
2018/maximo_master_pandc.csv")
M_WOs <-
  read.csv(file = "/*REDACTED*/Maximo/Points & Crossings 2006-
2018/maximo_signals_wos.csv")
join1_M <- inner_join(M_WOs, pandc, by = c("location" = "assetnum"))
join2_M <- inner_join(M_WOs, pandc, by = c("equip_no" = "location"))
Maximo_WOs <- rbind.fill(join1_M, join2_M)

#remove duplicate WOs in the join
Maximo_WOs = Maximo_WOs[!duplicated(Maximo_WOs$wonum), ]

#changing column names in maximo to match those in ellipse that can be
joined
colnames(Maximo_WOs)[1] <- "WONUM"
colnames(Maximo_WOs)[3] <- "MAINT_TYPE"
colnames(Maximo_WOs)[4] <- "EQUIPMENT_NO"
colnames(Maximo_WOs)[7] <- "CLOSED_DATETIME"
colnames(Maximo_WOs)[8] <- "CLOSED_DATE"
colnames(Maximo_WOs)[9] <- "CLOSED_TIME"
colnames(Maximo_WOs)[12] <- "RAISED_DATE"
colnames(Maximo_WOs)[13] <- "RAISED_TIME"
colnames(Maximo_WOs)[14] <- "RAISED_DATETIME"
colnames(Maximo_WOs)[15] <- "TRUNCATED_DESCRIPTION"
colnames(Maximo_WOs)[23] <- "LCS"
colnames(Maximo_WOs)[27] <- "OWNING_LINE"
colnames(Maximo_WOs)[39] <- "M_START"
colnames(Maximo_WOs)[40] <- "M_STOP"
colnames(Maximo_WOs)[41] <- "PARENT_STATUS_DESCRIPTION"
```

```

colnames(Maximo_WOs)[42] <- "PARENT_TYPE"

#a few columns needed correcting in format as they did not match before
joining
Ellipse_WOs$EQUIPMENT_NO = as.character(Ellipse_WOs$EQUIPMENT_NO)
Ellipse_WOs$M_START = as.integer(Ellipse_WOs$M_START)
Maximo_WOs$M_START = as.integer(Maximo_WOs$M_START)

#Join filtered Ellipse and Maximo files
Ellipse_Maximo_WOs <- full_join(Ellipse_WOs, Maximo_WOs)

#Step 2. load combined Ellipse and Maximo WOs
WOs <-
  read.csv(file = "/*REDACTED*/Ellipse & Maximo combined/WOs_all.csv")

#join surface daily means per station with UHI adjustment
dailymean_temp <-
  read.csv(file = "/*REDACTED*/Analysis/Descriptive statistics/St.
James's Park/UHI adjusted/Observations/St James Park daily mean UHI
adjusted per station.csv", check.names =
  FALSE)
dailymean_temp <-
  gather(dailymean_temp, "Station", "Mean daily surface temp", 2:271)
colnames(WOs)[10] <- "Date"
colnames(WOs)[90] <- "Station"
WOs$Date = as.POSIXct(as.character(WOs$Date), format = "%d/%m/%Y")
dailymean_temp$Date = as.POSIXct(as.character(dailymean_temp$Date), format
=
  "%d/%m/%Y")
WOs$Station = (as.character(WOs$Station))
dailymean_temp$Station = as.character(dailymean_temp$Station)
WOs <- left_join(WOs, dailymean_temp, by = c("Date", "Station"))

write.csv(WOs, file = "/*REDACTED*/Analysis/Faults/Fault rate
analysis/Surface tmean/WOs surface tmean.csv")
#need to do a separate vlookup for Paddington (H&C)

```



## Appendix E: R code sample to estimate future tunnel temperatures

```
#See Appendix B for packages loaded and tested throughout R code build

##Sample code: tmean/Paddington/SB/Bakerloo line/RCP8.5/2080s##

#Load monthly met data

St_James_monthlymean <-
  read.csv(
    "/*REDACTED*/Analysis/Climate projections/UKCP18 1981-2010 baseline
monthly mean.csv"
  )

#calculate annual mean - taken from the overall mean of UKCP18 monthly
values
St_James_annualmean <-
  mean(as.numeric(St_James_monthlymean$Mean), na.rm = TRUE) + 6.67057382

#Bakerloo SB station estimation
St_James_monthlymean_Bakerloo_SB <- St_James_monthlymean
St_James_monthlymean_Bakerloo_SB$"Paddington" <-
  ((St_James_annualmean + 15.9727) +
((St_James_monthlymean_Bakerloo_SB$X2080s.8.5.mean) -
  St_James_annualmean
  ) * 0.3726)
```